Exploring Kinase Function in Planar Polarity in *Drosophila*

Hongyu Shao

Submitted for the degree of Doctor of Philosophy

the University of Sheffield

Faculty of Science

School of Biosciences

December 2022

Abstract

Planar polarity is a conserved phenomenon in metazoans such that cells in epithelial sheets obtain the same orientation in the plane of the sheet. There is a set of proteins, the so-called ‘‘core planar polarity proteins’’, that specify planar polarity in the *Drosophila* pupal wing by being sorted to opposite cell ends forming “distal” and “proximal” protein complexes. The mechanism for this planar polarity establishment is still unclear.

Several lines of evidence show that kinases regulate planar polarity in various model systems. Elucidating which kinases regulate planar polarity in the simple model, the single-layer epithelium of *Drosophila* pupal wings, will provide insights into mechanisms of planar polarity establishment.

By first screening a set of candidate kinases, I provide evidence supporting the planar polarity regulation role of atypical Protein Kinase C (aPKC), and evidence partly supporting those of Abelson (Abl), Misshapen (Msn), and Nemo (Nmo), but not that of Par-1.

The role of Discs Overgrown (Dco, Casein Kinase Iε in vertebrates) kinase in regulating planar polarity in *Drosophila* wings has been previously investigated. In this work, I show that acute knock-down of Dco affects planar polarity, and chemical inhibition of Dco destabilises Dishevelled (a distal protein) and stabilises Strabismus (a proximal protein). My data also show that Dco is localised asymmetrically on distal ends in *Drosophila* pupal wing cells, supporting a model where Dco localises on distal cell ends and locally stabilises Dishevelled and mobilises Strabismus, thus enhancing the sorting of core planar polarity proteins to opposite cell edges.

The most promising candidate kinase showing a regulatory role in planar polarity in pupal wings, aPKC, is also further investigated. Here I showed that aPKC positively regulates planar polarity in *Drosophila* pupal wings, although the mechanism remains unclear.

Declaration

I, Hongyu Shao, certify that the work described here is, to the best of my knowledge and belief, original, the product of my own investigations, except those acknowledged and referenced, and has not previously been submitted in whole or in part for a degree, diploma, or other qualification at this or any other university or institution of higher learning.

December 2022

Contents

List of Figures

Chapter 4

List of Tables

Acknowledgment

As this moment of this Thesis is about to finish, I cannot wait to express my gratitude to my advisor, Professor David Strutt. Before I became his student, I wrote in an email to him, "it is the opportunity I valued", and now I think it is true. Thanking him for giving me the opportunity to do such an interesting and challenging planar polarity research. Looking back on these four years of study, David has always supported my wild ideas and guided me the way to carefully validate my ideas. Without David's guidance, this Thesis would not have been possible.

I would like to thank Helen Strutt for her support. It was Helen who gave me guidance on the experimental operations that allowed me to carry out my research work smoothly. I would also like to thank Helen for her valuable comments on the first draft of this thesis.

I would also like to thank Samantha J Warrington for her support on microscopic imaging techniques and for her comments on the draft of this Thesis. Also thank lab members Alexandre CARAYON, Carl L Harrison, and Larra MP Trinidad for their comments on the Thesis draft. Of course, I am grateful to every lab member for their help with my studies and life.

I would like to thank the University of Sheffield for funding my PhD studies so that I can focus on my research without worrying about the financial problems living in the UK.

Finally, I would like to express my gratitude (and apologies) to my parents who are more than 8,000 km away from me. I have not been able to return home since four years ago. Missing and love you.

Salutations

CHAPTER 1

General Introduction

The subject of this thesis consists of three concepts, 1) kinases, 2) planar polarity, and 3) *Drosophila*. To explain these concepts, I am going to discuss in this chapter why *Drosophila* is used as the model system, what planar polarity is, and what kinases are.

1.1 Drosophila as a model animal

Drosophila melanogaster (*D. melanogaster*, also known as fruit fly, or fly, or *Drosophila* in short in this thesis) is a widely used model animal. The easy husbandry, short generation time, and the high potential in genetic manipulation of *Drosophila* have attracted a huge society of scientists from a vast range of biomedical research fields. Up to the time of writing, six Nobel Prices have been awarded to *Drosophila* related research (in the year 1933, 1946, 1995, 2004, 2011, and 2017).

Drosophila has a small genome size. It has only four pairs of chromosomes: one pair of sex chromosomes (XY) and three pairs of autosomal chromosomes (II/2, III/3, IV/4). To map the exact loci of genes or insertions, the chromosomes are also labelled as X, 2L, 2R, 3L, 3R, and 4. The L and R here refer to the left arm and the right arm of the chromosome, respectively. The X and the 4 chromosomes have long left arms and tiny right arms. See (Hafen, 1997; Hales et al., 2015) for more information.

1.1.1 *Drosophila* life cycle

Drosophila can be kept in a range of temperatures from 18°C to 29°C. The lower the temperature is, the slower the generation time would be. *Drosophila* has the highest reproductive yield and best viability at 25°C and 60% relative humidity.

The generation time at 25°C is approximately 10 days from eggs to adult (Figure 1.1, reviewed in (Hales *et al.*, 2015)). During the one-day egg stage, embryogenesis establishes the segmentation of the body before hatching. The newly hatched larvae reach a stage called 1st instar. The 1st instar larva takes one day to grow into the 2nd

instar larva, which grows into the 3rd instar larva another day later. After about two days of 3rd instar larva stage, the larva stops growing and wanders to find an appropriate site for pupariation. The start time of the pupating process is marked as 0 hours after puparium formation (APF), when the pupa is still white before the cuticle starts to get tanned and harden. The larva undergoes metamorphosis during an approximately four-day pupal stage after puparium formation, before emergence (eclosion) of the adult fly. The female fly becomes sexually mature 8 to 12 hours after emergence.

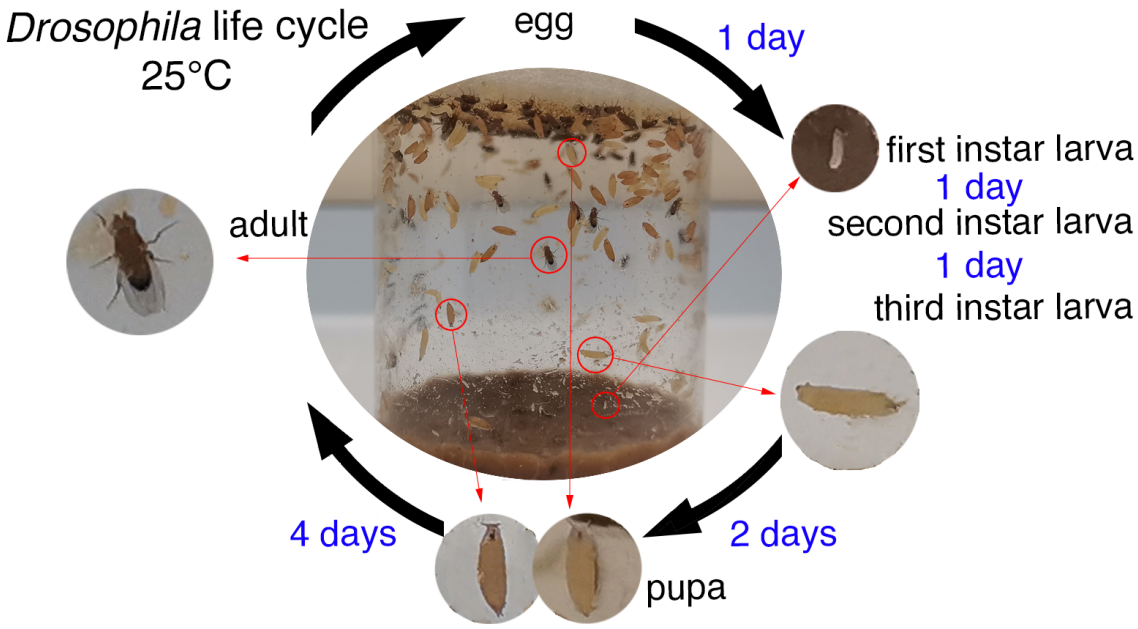

Figure 1.1 *Drosophila* life cycle

Schematic showing *Drosophila* life cycle at 25°C. The 1st instar larva takes one day to grow into the 2nd instar larva, and another day to grow into the 3rd instar larva. The 3rd instar larva takes two days to form pupa. The newly formed pupa is white, whose cuticle gets tanned and harden in pupal stage. The adult fly emerges from pupa cuticle four days after puparium formation. The female fly becomes sexually mature 8 to 12 hours after emergence, then mates and lays eggs to start a new life cycle.

1.1.2 *Drosophila* wing development

Drosophila is an excellent model animal in planar polarity research not only due to its short generation time but also the easily observable epithelial patterning phenotype in this system, including ommatidia in the eye, and hairs and bristles on the wing, abdomen, leg, and notum. In this thesis, the wings are used as the model system.

The *Drosophila* wing derives from the larval wing imaginal disc. The larval wing imaginal disc ('wing disc' in short) is specified during embryogenesis and grows in size during the growth of larva.

The wing discs undergo a series of major morphogenetic transformations after the formation of the pupa. During the larval stages the wings disc has two layers: the future wing tissue and a peripodial membrane. In early pre-pupal morphogenesis at end of 3rd instar stage, the peripodial membrane disintegrates and the wing tissue everts (Aldaz et al., 2010; 2013). The pouch region of the apical-outside wing disc then elongates into a flat double-layer epithelial wing blade (Aldaz *et al.*, 2010; 2013; Fristrom et al., 1993).

The wing blade undergoes a series of morphogenetic transformations to form the adult wing (Figure 1.2). After the eversion and elongation, at about 6 h APF, the pupal cuticle is secreted (Waddington, 1939). The wing then flattens (Fristrom *et al.*, 1993; Waddington, 1939). The wing hinge, developed from the hinge region of wing disc, anchoring the wing blade to the pupal cuticle, begins to contract at about 16 h APF. Such contraction applies a force on the wing blade that regulates wing morphogenesis (Aigouy et al., 2010; Etournay et al., 2015; Ray et al., 2015). During hinge contraction, the poorly packed wing blade cells transform into hexagonal shapes (16-30 h APF, Aigouy *et al.*, 2010; Classen et al., 2005), simultaneous to the establishment of the asymmetric localisation of the core planar polarity proteins (16-32 h APF, Aigouy *et al.*, 2010; Axelrod, 2001; Bastock et al., 2003; Usui et al., 1999). See **Section 1.2.2 and 1.2.3**). Subsequently, the trichomes emerge apico-distally (32 h APF). After 46 h APF,

the wing continues growing and folds in the pupal cuticle (Fristrom *et al.*, 1993). Folded wings get unfolded after eclosion by pumping hemolymph into the adult wing through wing veins (Johnson and Milner, 1987; Togel et al., 2008).

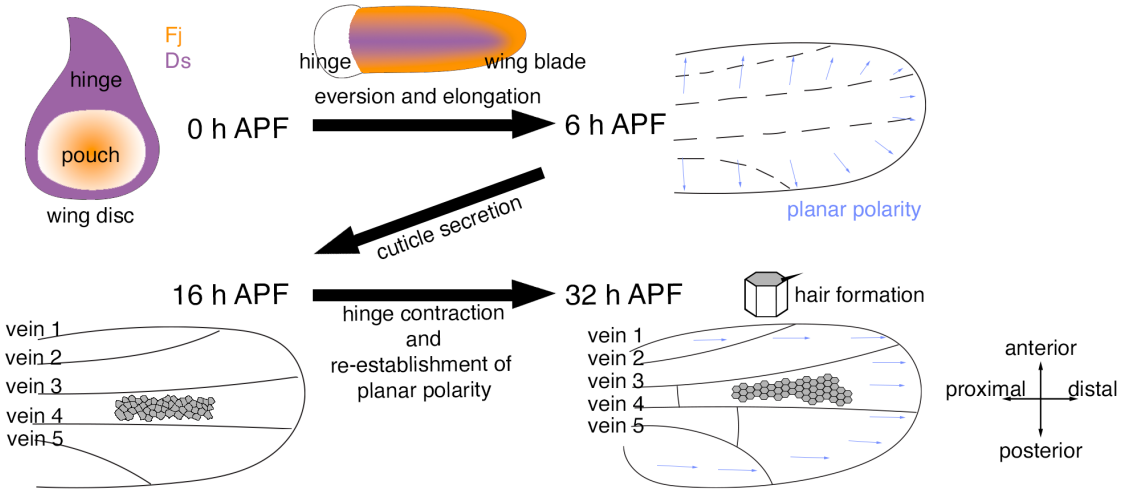

Figure 1.2 *Drosophila* wing development

Schematic showing *Drosophila* wing development. In early pre-pupal morphogenesis at end of the 3rd instar stage, the wing disc everts and then elongates into the wing blade. In the wing disc, Fj is expressed higher distally and lower proximally (shown in orange), while Ds is expressed proximally in the hinge region (shown in purple); in the pupal wing, the expression of Fj is higher at the wing margin (shown in orange), while Ds is expressed along the centre stripe of the wing (shown in purple). In this stage, the core planar polarity is oriented in a radial pattern (indicated by blue arrows). At about 6 h APF, the pupal cuticle is secreted. At about 16 h APF the wing hinge begins to contract. During hinge contraction, the poorly packed wing blade cells transform into hexagonal shapes, simultaneous to the re-establishment of the proximodistal core pathway planar polarity (indicated by blue arrows). The trichomes emerge apico-distally at 32 h APF, which then grow into wing hairs in adult wings.

1.2 The axes of polarity in epithelial tissue

The presence of epithelial tissue is conserved in all metazoans and is evolutionarily crucial for metazoans. The sponge-like simple metazoans have an epithelium separating the organism from its the feeding chamber and absorbing nutrients from the seawater in the chamber (Leys and Hill, 2012).

A similar function of the epithelium is also present in morphologically complex animals like mammals. For most of the organs in mammals, the structure is defined by and the main functions are performed by the epithelia. For instance, the outer layer of the skin is a stratified epithelium that separates the body interior from the outside environment; the one-cell thick simple epithelium of the small intestine borders the gut and absorbs nutrients from it; lung epithelium is directly exposed to air and performs inhalation and exhalation. Epithelia are also crucial in blood vessels, renal tubules, etc.

1.2.1 The polarity in the apicobasal axis

The function of the epithelium requires the cells to coordinate into a specific structure. Take the widely studied columnar shape epithelial cells of the mammalian intestine as an example (Klunder et al., 2017). There are three compartments categorised by their position: the ‘apical surface’ is the free surface facing the intestine lumen, specialised for absorbing nutrients from the intestine; the ‘lateral surface’ contacts and binds to adjacent cells; and the ‘basal surface’ contacts the basement membrane, extracellular matrix and blood vessels. Furthermore, the basal and lateral surfaces are often collectively referred to as the basolateral surface because they share a similar composition (Figure 1.3 A).

Between the distinct apical and basolateral surface of the cell lies the apical junctional complexes that mediate the adhesion between adjacent epithelial cells and recruit proteins to different membrane domains, reviewed in (Buckley and St Johnston, 2022;

Nelson, 2003). The separation of the apical surface and the basolateral surface indicates the anisotropy of the epithelial cells. This kind of anisotropy of the cell is referred to as 'apicobasal polarity', involving the asymmetry of the cell surface, the directional intracellular vesicle trafficking, and the polarised cytoskeleton, reviewed in (Bryant and Mostov, 2008; Li and Gundersen, 2008; Mellman and Nelson, 2008; Nelson, 2003). The apicobasal polarity regulates cell proliferation, differentiation, migration, adhesion, and death (Tepass, 2012).

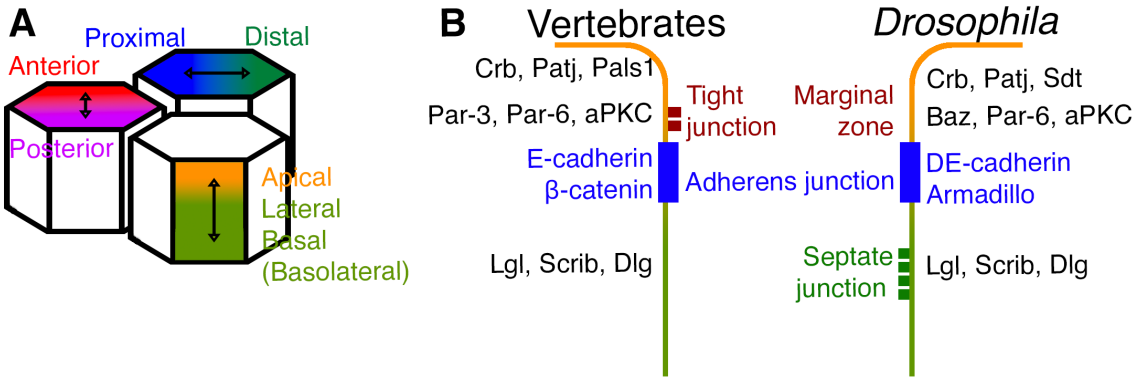

Figure 1.3 Polarity axis and apicobasal polarity

(A) Schematic showing three axes of polarities in hexagonal cells.

(B) Schematic showing relative spatial relations of cell junctions and apicobasal polarity components in typical *Drosophila* (left) and vertebrate (right) epidermal cells. Apical side is on the top.

1.2.1.1 the apical junctional complexes

Regulating apicobasal polarity, there are three protein complexes localised asymmetrically on cell membranes. To demonstrate the spatial pattern of these complexes, I will first describe the apicobasal structure of the apical junctional complex.

Epithelial cells in both *Drosophila* and vertebrates have a structure called the adherens junctions (AJ) below the apical surface. Apical to the AJ, vertebrate epithelial cells have a tight junction (TJ) forming an impermeable barrier, whereas in *Drosophila* epithelial cells, there is no TJ structure but a sub-apical region called the marginal zone (MZ). In addition, a septate junction (SJ) localised basal to the AJ is present in the *Drosophila* epithelial cells to perform the barrier function (Figure 1.3, B). In the following of this section, I will focus on *Drosophila* epithelial cells.

The AJ is an adhesive structure that mediates cell-cell contacts and associates with the actin cytoskeleton, consisting of DE-cadherin (the homologue of E-cadherin in vertebrates), Armadillo (β-catenin in vertebrates), α-catenin, *etc*.

DE-cadherin belongs to the cadherin protein superfamily. The extracellular cadherin repeat domains (CADs) of cadherin protein superfamily members mediate cell-cell contacts via trans interactions between neighbouring cells (Boggon et al., 2002). The cytoplasmic domain of cadherins binds to catenins (including α-catenin, Armadillo, and p120-catenin, reviewed in (Shapiro and Weis, 2009)) and transduces extracellular force to the actin cytoskeleton (Borghi et al., 2012; Yonemura et al., 2010). p120-catenin interacts with Rho GTPases which mediates cytoskeletal dynamics and cadherin endocytosis (Pieters et al., 2012). Armadillo binds to α-catenin (a filamentous-actin-binding protein, Rimm et al., 1995) and links cadherin-mediated cell-cell contacts to the actomyosin cytoskeleton (Desai et al., 2013). The linkage via AJs transduces mechanical forces to the actomyosin cytoskeleton and regulates tissue morphogenesis (reviewed in (Pannekoek et al., 2019)). Besides, the actin and microtubule

cytoskeletons are rearranged in response to cell-cell contact, facilitating polarised vesicle trafficking, and maintaining cell shape, reviewed (Mellman and Nelson, 2008).

1.2.1.2 the apicobasal polarity determinants

Above the AJ, in the MZ and the apical surface of the cell membrane, localise a set of proteins that define apicobasal polarity (Figure 1.3, B). Specifically, 1) the Crumbs complex: consisting of Crumbs (Crb) (Tepass, 1996), Pals-associated tight-junction protein (Patj; PATJ and MUPP1 in vertebrates) (Bhat et al., 1999; Pielage et al., 2003; Zhou and Hong, 2012), and Stardust (Sdt; PALS1/MPP5 in mammals) (Tepass and Knust, 1993); 2) the Par (partition defective) complex (Goldstein and Macara, 2007; Suzuki and Ohno, 2006): consisting of the Rho family GTPase Cdc42, Bazooka (Baz; Par-3 in vertebrates), Par-6, and atypical protein kinase C (aPKC, Harris and Peifer, 2005; Hutterer et al., 2004; Wodarz et al., 2000); 3) other proteins: e.g. PTEN, Moesin, and Yurt (reviewed in (Tepass, 2012)). Note that the protein listed above are categorised into complexes for historical reasons. These proteins function as a whole network rather than independent protein complexes. For instance, Baz recruits apical Crb (Bilder et al., 2003) and also interacts with Sdt (Krahn et al., 2010); aPKC stabilises apical Crb (Sotillos et al., 2004), and Crb, in turn, stabilises apical Baz (Harris and Peifer, 2004); PAR-6 interact and recruit apical Patj (Hutterer *et al.*, 2004), and also interact with Crb, enhancing the apical recruitment of Par6/aPKC (Walther and Pichaud, 2010).

Besides the apical polarity proteins, there is also a series of proteins defining basolateral polarity (Figure 1.3, B): the Scribble module (consisting of Lethal giant larvae (Lgl), Scribble (Scrib), and Disc large (Dlg), reviewed in (Carmena, 2020)); Par-1 and Par-5 serine/threonine kinases, reviewed in (Goldstein and Macara, 2007); FERM proteins Yurt (Yrt) and Coracle (Cora) (Laprise et al., 2009); Rac GTPase (Couto et al., 2017), *etc*.

The basolateral polarity proteins and the apical polarity proteins are mutually antagonistic to ensure the apical/basolateral localisation of the polarity proteins (Benton and St Johnston, 2003; Bilder *et al.*, 2003; Chartier et al., 2011; Hutterer *et al.*, 2004; Laprise *et al.*, 2009; Tanentzapf and Tepass, 2003; Ventura et al., 2020), reviewed in (Buckley and St Johnston, 2022; Flores-Benitez and Knust, 2016). For instance, Dlg and Scrib repress aPKC ectopic localisation and aPKC restricts Lgl on basolateral surface (Ventura *et al.*, 2020). The correct localisation of apical polarity proteins helps the AJs to be limited at apical-lateral surface boarder, for instance, Baz is required for apical DE-cadherin complex formation (Harris and Peifer, 2004), reviewed in (Buckley and St Johnston, 2022).

1.2.2 The core planar polarity pathway - polarity in the plane of epithelial sheets

The epithelium is a 3-D structure with not only one axis of polarity (Figure 1.3 A). In the plane orthogonal to the axis of apicobasal polarity, there is another axis of polarity, planar polarity, or planar cell polarity (PCP). Planar polarity is the focus of this thesis.

Planar polarity is well characterised by the conserved phenotype among metazoans, where cells in the plane of the epithelial sheets are coordinated and aligned in the same direction. As a consequence, structures in the epithelium can serve as a readout for planar polarity. In *Drosophila*, planar polarity can be observed in the orientation of hairs in adult wings (Figure 1.4), of ommatidia in the eye, and of the bristles on the thorax and abdomen. In vertebrates, many developmental processes of vertebrates have been shown to be regulated by planar polarity genes, for instance, vertebrate gastrulation (Heisenberg et al., 2000; Tada et al., 2002; Wallingford et al., 2000); neural tube closure (Kibar et al., 2001; Murdoch et al., 2001), mammalian inner ear development (Copley et al., 2013; Curtin et al., 2003; Montcouquiol et al., 2006); oriented cell divisions (Segalen et al., 2010); left/right patterning (Song et al., 2010);

kidney (Yates et al., 2010a) and lung (Yates et al., 2010b) branching, reviewed in (Butler and Wallingford, 2017). Consistently, planar polarity is also observable in the orientation of hair bundles in inner ear sensory cells (Etheridge et al., 2008; Montcouquiol *et al.*, 2006; Wang et al., 2005; Wang et al., 2006c) and the orientation of hair on the skin (Devenport and Fuchs, 2008; Guo et al., 2004; Wang et al., 2006b), reviewed in (Butler and Wallingford, 2017; Devenport, 2014; Goodrich and Strutt, 2011).

There is a set of proteins named 'core planar polarity proteins' (or 'core proteins' in short in this thesis) that specify cell polarity by being sorted to opposite cell edges in the *Drosophila* wings. The earliest asymmetric localisation of core proteins observed in *Drosophila* wing development is in late third instar wing discs and prepupal wings (Classen *et al.*, 2005). From this stage to about 15 h APF, the core proteins are localised in a radial polarity pointing to the vein 3 (Aigouy *et al.*, 2010; Classen *et al.*, 2005)(blue arrows in Figure 1.2 indicate the axis of planar polarity). After 18 h APF, when pupal wings undergo the hinge contraction process, the alignment of the planar polarity decreases and reaches the nadir at about 20 h APF (Aigouy *et al.*, 2010), during which the localisations of the core proteins are largely symmetric (Axelrod, 2001; Usui *et al.*, 1999). Then, the planar polarity gets re-established after hinge contraction in the proximodistal axis, followed by the strongest asymmetric localisation of the core proteins at 32 h APF, just before the emergence of the trichome (Aigouy *et al.*, 2010; Axelrod, 2001; Bastock *et al.*, 2003; Strutt, 2001; Tree et al., 2002; Usui *et al.*, 1999)(Figure 1.2, blue arrows indicate the axis of planar polarity).

In this thesis, the term 'establishment of planar polarity' refers to the re-establishment process of planar polarity from 24 h to 32 h APF. Actually, the planar polarity was believed to be established only in this stage, until it is observed in wing discs and 6 h APF prepupal wings (Classen *et al.*, 2005). However, unlike the planar polarity throughout the whole tissue in 24 h to 32 h APF, the polarity of the core proteins in early pupal wings is only observed in part of the cells (Classen *et al.*, 2005). Consistent

with this, localisation of Dsh and Pk is reported to be symmetric in about 2 - 2.5 h (2h for Dsh; 2.5 h for Pk) APF pre-pupal wings (Axelrod, 2001; Tree *et al.*, 2002). The re-establishment of planar polarity regulates the downstream effectors (see **Section 1.2.4**) and positions the trichome emerges at 32 h APF (Strutt, 2001).

1.2.2.1 Core planar polarity proteins

In 24 h to 32 h APF stage pupal wings, the proximodistal sorted core proteins are clustered into 'distal complex' and 'proximal complex', named after their subcellular localisation. Specifically, the 'distal complex' consists of Frizzled (Fz), Dishevelled (Dsh; Dvl1-3 in mammals), Diego (Dgo; Inversin/Diversin in vertebrates), and Flamingo (Fmi; also known as Starry night/ Stan in *Drosophila*; Celsr in mammals); while the 'proximal complex' consists of Strabismus (Stbm; also known as Van Gogh/Vang; Vang-like/Vangl in vertebrates), Prickle (Pk), and also Fmi (Axelrod, 2001; Bastock *et al.*, 2003; Das et al., 2004; Feiguin et al., 2001; Shimada et al., 2001; Strutt, 2001; Tree *et al.*, 2002; Usui *et al.*, 1999), reviewed in (Goodrich and Strutt, 2011)(Figure 1.5, A).

In the field of planar polarity research, the ommatidia in the *Drosophila* eye are another major multicellular level readout system. Similar to the distribution of core proteins in the wing, the core proteins are accumulated along the R3/R4 photoreceptor cell boundary and localised asymmetrically in the developing *Drosophila* ommatidia. Specifically, Fz is localised to the R3 side while Stbm to the R4 side (Das et al., 2002; Rawls and Wolff, 2003; Strutt and Strutt, 2002)(Figure 1.5, A).

Besides *Drosophila*, the vertebrate homologues are also asymmetrically localised and regulate planar polarity via a similar mechanism. For instance, in the sensory hair cells of the inner ear (Etheridge *et al.*, 2008; Montcouquiol *et al.*, 2006; Wang *et al.*, 2005; Wang *et al.*, 2006c) and mouse skin (Devenport and Fuchs, 2008; Guo *et al.*, 2004; Wang *et al.*, 2006b).

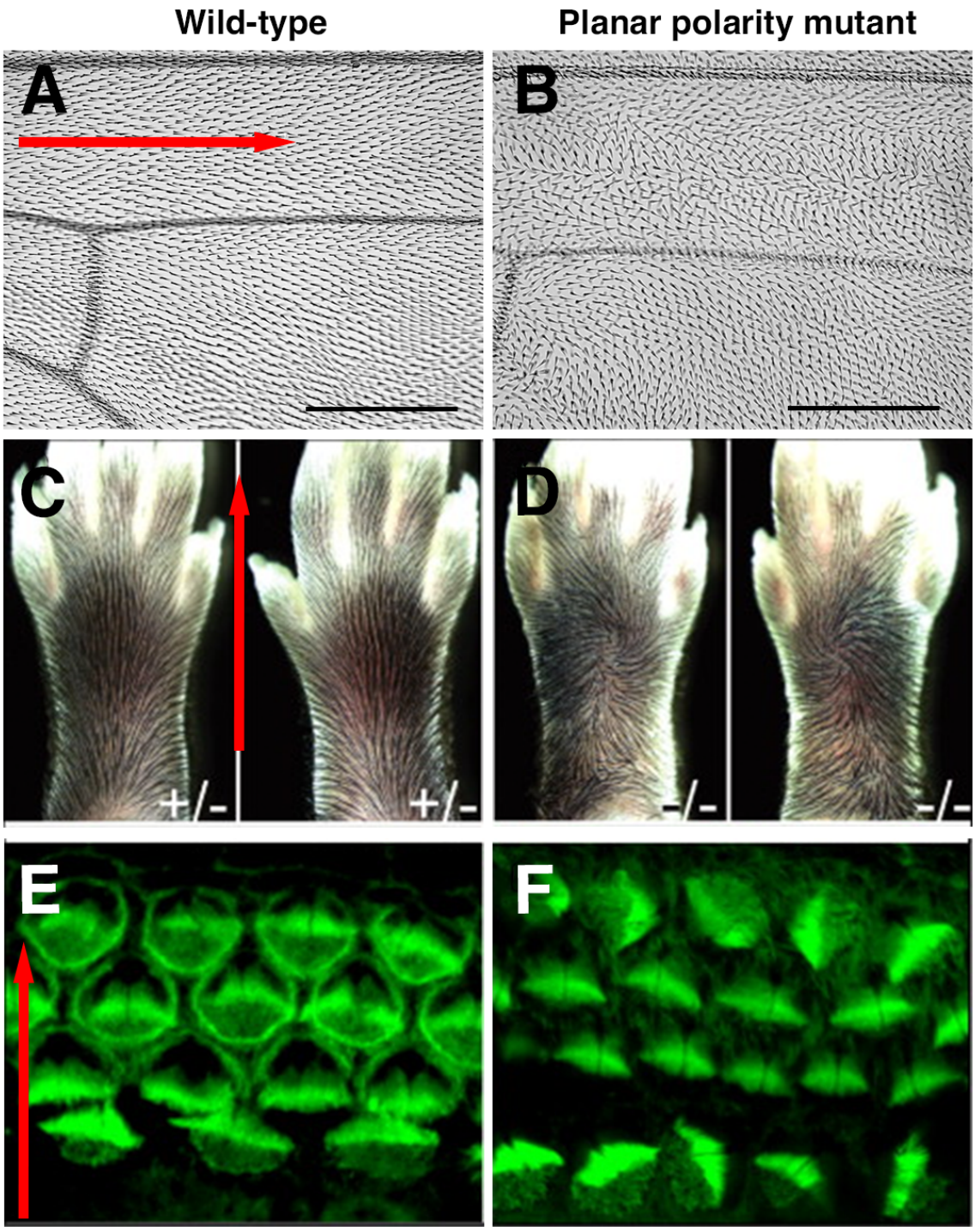

Figure 1.4 Example phenotypes of core planar polarity gene mutant

Figure legends in next page

Figure 1.4 Example phenotypes of core planar polarity gene mutant

(A) The pattern of the adult wing hairs in *w[1118]* wild-type *Drosophila* wing. The red arrow indicates the distal-pointing direction of wing hairs. Scale bar 200 μm.

(B) The pattern of the adult wing hairs in *fz[P21]* mutant *Drosophila* wing. The proximodistal alignment of wing hairs is no observed. Scale bar 200 μm.

(C) The pattern of hairs on paw in *Frizzled6* heterozygotes mouse. The red arrow indicates the distal-pointing direction of hairs.

(D) The pattern of hairs on paw in *Frizzled6* homozygotes mouse.

(E) The pattern of sensory receptor cells in the mouse cochlea. The red arrow indicates the actin-rich stereocilia face to the cochlear lumen.

(F) The pattern of sensory receptor cells in the mouse cochlea is disrupted in *Vangl2* mutant mouse.

Images in (E) and (F) were reused with permission from (Zallen, 2007).

Images in (C) and (D) were reused with permission from (Guo *et al.*, 2004) Copyright (2004) National Academy of Sciences, U.S.A.

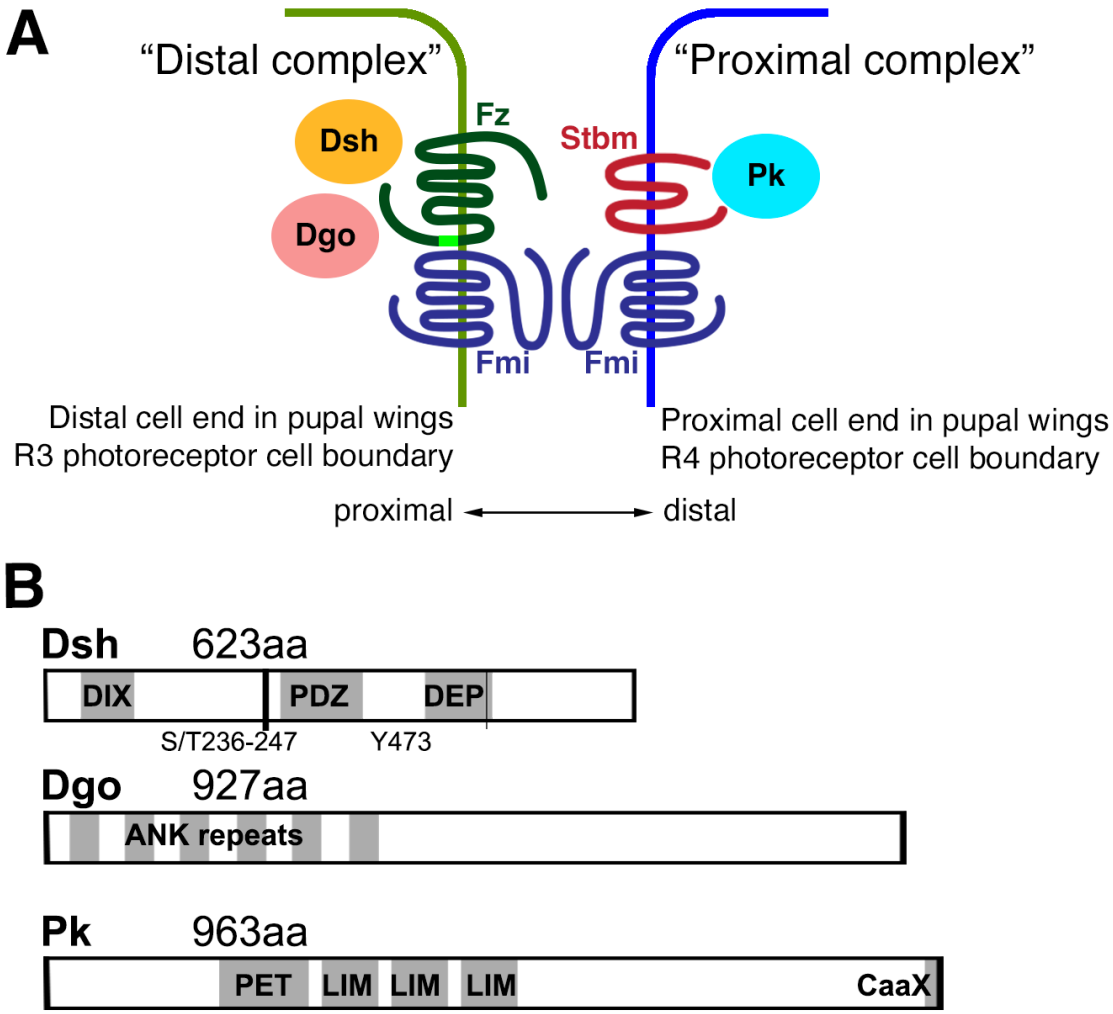

Figure 1.5 Core planar polarity protein complex

(A) Schematic showing core planar polarity protein forming intercellular complex. Fmi, Fz, Dsh, and Dgo localise on the distal cell end of the cell on the proximal side or on the R3 photoreceptor cell boundary (shown on the left); Fmi, Stbm, and Pk localise on the proximal cell end of the cell on the distal side or on the R4 photoreceptor cell boundary (shown on the right). The light green box region on Fz indicates the KTxxxW motif.

(B) Schematic showing three cytoplasm core planar polarity proteins. Dsh is consisting of 623 amino acids, with three major conserved domains: DIX, PDZ, and DEP. Locations of S/T236-247 and Y473 are also indicated. Dgo is consisting of 927 amino acids, containing six ankyrin (ANK) repeats on its N terminus. Pk is consisting of 963 amino acids, containing a PET domain, three LIM domains, and a C-terminal prenylation motif (CaaX).

Frizzled (Fz)

The 7-pass transmembrane protein Frizzled, consisting with 581 amino acids (aa), obtains distal cell localisation in planar polarity re-establishment.

As well as acting in planar polarity, Fz also is involved in an evolutionarily conserved canonical Wnt signalling pathway (also known as Wingless (Wg) signalling pathway in *Drosophila*, Chen and Struhl, 1999). For this reason, the planar polarity pathway is sometimes referred to as a 'non-canonical Wnt pathway', or Wnt/PCP pathway (Goodrich and Strutt, 2011).

In Wnt/Wg signalling pathway, Fz acts as a receptor for Wnt ligands. Wnt ligands bind to the N-terminal extracellular domain of Fz family receptors (Bhanot et al., 1996; Cong et al., 2004b; Hsieh et al., 1999). After Wnt binding, Fz recruits Dsh and triggers the nuclear localisation of Armadillo/β-Catenin, thus, activating Wnt/Wg target gene expression (Cong et al., 2004a; b; Povelones et al., 2005; Umbhauer et al., 2000), reviewed in (MacDonald et al., 2009).

The recruitment of Dsh is mediated by the C-terminal tail and the intracellular loops in the transmembrane region:

The transmembrane region consists of seven transmembrane domains and the associated intracellular loops and extracellular loops. The intracellular loops regulate canonical Wnt pathway in vertebrates (Cong *et al.*, 2004b); and both canonical Wnt pathway and planar polarity in *Drosophila* (Jones et al., 1996; Povelones *et al.*, 2005; Strutt et al., 2012; Wu et al., 2008).

On the C-terminal side of the transmembrane region is the C-terminal tail which contains a "KTxxxW" motif (Fz residues 557–561 in *Drosophila*, light green box region in Figure 1.5 A indicates the KTxxxW motif on Fz). Mutations in the "KTxxxW" motif reveal its importance in canonical Wnt pathway in vertebrates (Cong *et al.*, 2004b;

Umbhauer *et al.*, 2000) and both canonical Wnt pathway and core planar polarity pathway in *Drosophila* (Strutt *et al.*, 2012; Wu *et al.*, 2008).

Mutations in the intracellular loops and the C-terminal tail of vertebrate Fz block its binding to Dsh (Cong *et al.*, 2004b; Tauriello et al., 2012; Umbhauer *et al.*, 2000; Wong et al., 2003). Reduced or lost Dsh membrane localisation is also reported when these two regions in *Drosophila* Fz are mutated (Strutt *et al.*, 2012).

There are four Frizzled family receptors in *Drosophila*, Fz, Fz2, Fz3, and Fz4. While the function of Fz3 and Fz4 is less well studied, Fz and Fz2 are redundant receptors for Wg (Bhanot et al., 1999; Bhat, 1998; Chen and Struhl, 1999). Fz2 does not regulate planar polarity, thus for planar polarity only Fz is involved. The pathway specificity may be due to their subcellular localisation mediated by cytoplasmic tail. Fz has a shorter cytoplasmic tail which localises it to the subapical region of cells, while Fz2 has a longer cytoplasmic tail which localises it to the basolateral surface (Boutros et al., 2000; Wu et al., 2004).

Dishevelled (Dsh)

Dsh is a cytoplasmic protein consisting of 623 aa, of which three homologs exist in vertebrates (Dvl1, Dvl2, and Dvl3).

In the context of planar polarity, Dsh is recruited to the distal complex by Fz (Axelrod, 2001; Shimada *et al.*, 2001).

Similar to Fz, Dsh also participates in both Wg signalling pathway and core planar polarity. If Fz is overexpressed in the wing, an increased level of Dsh is recruited to and trapped in the distal subapical junctional region by Fz, which causes a reduction in Wg signalling (Wu *et al.*, 2004). Sharing between distinct pathways, there must be a mechanism of Dsh that transduce signals selectively.

Dsh has a delicate mechanism of transducing signals via binding to distinct downstream components with distinct domains. Widely accepted, there are three major conserved domains on Dsh: DIX (Dishevelled and Axin), PDZ (Post-synaptic density protein-95, Disc large tumor suppressor, Zonula occludens-1) and DEP (Dishevelled, EGL-10 and Pleckstrin)(Figure 1.5 B). All three domains have been implicated in protein-protein interactions. Having no catalytic activity reported, Dsh might serve as an adaptor or scaffold molecule (Boutros and Mlodzik, 1999; Wallingford and Habas, 2005).

The DIX domain undergoes head-to-tail multimerization of Dsh (Schwarz-Romond et al., 2007). The DEP domain is bound to Frizzled (Gammons et al., 2016; Tauriello *et al.*, 2012), and is essential to rescue planar polarity defects (Boutros et al., 1998) and for Dsh to be recruited by Fz (Axelrod et al., 1998). Historically, The DIX and PDZ domains are found essential for Wnt/Wg signalling, while The PDZ and DEP domains participate in planar polarity signalling, reviewed in (Wallingford and Habas, 2005). Recent publications point out that the PDZ domain is not required in canonical Wg signalling in flies (Mieszczanek et al., 2022) and in vertebrates (Gammons *et al.*, 2016). Also, the DEP domain is found required for canonical signalling in vertebrates (Gammons *et al.*, 2016). Thus, to summarise, the DIX domain function is restricted in canonical Wnt/Wg signalling and interacts with itself via homodimerization; the PDZ domain function is restricted in non-canonical Wnt/Wg signalling planar polarity pathway; while the DEP domain regulates the binding to Fz and participates in both canonical and non-canonical Wnt/Wg signalling.

Diego (Dgo)

Dgo is a cytoplasmic protein with 927 amino acids containing six ankyrin (ANK) repeats on its N terminus (Figure 1.5 B). Dgo is a member of distal complex binds to Dsh (Jenny et al., 2005), whose junctional localisation requires Fz (Das *et al.*, 2004; Feiguin *et al.*, 2001) and partially dependent on Dsh (Wu *et al.*, 2008).

Notably, Dgo participate in Dsh recruitment by Fz. In Dgo overexpressed wing discs, Dsh-GFP is relocalised into subapical regions instead of cytoplasmic and basolateral regions in a Fz-dependent manner (Wu *et al.*, 2008).

Strabismus (Stbm)

The proximal complex protein Stbm is a transmembrane protein, consisting with 608 aa, with 4 transmembrane domains and a C-terminal PDZ-binding motif (Wolff and Rubin, 1998). To date, no function of Stbm other than regulating planar polarity has been reported. In the context of planar polarity, Stbm is asymmetrically localised to proximal cell edges and recruits Pk (Bastock *et al.*, 2003).

Prickle (Pk)

Pk[Pk], Pk[Sple], and Pk[M] are three isoforms of the *Prickle* gene in *Drosophila*, only differing in their N-terminal. Pk is the dominant isoform in the wing and notum, while Sple dominantly functions in the legs, abdomen and eye (Gubb et al., 1999). The balance of Pk/Sple isoform is crucial for planar polarity (Collu et al., 2018; Gubb *et al.*, 1999). Pk[M] is only expressed in embryo and has no phenotype in adults, whose function is also unknown (Gubb *et al.*, 1999).

Pk contains a PET domain (Prickle, Espinas, and Testin), three LIM domains (Gubb *et al.*, 1999), and a C-terminal prenylation motif (Figure 1.5 B). The proximal protein Pk is reported to bind to Stbm (Bastock *et al.*, 2003; Jenny et al., 2003). Such binding is likely mediated by LIM domain as the LIM domain is usually involved in protein binding via the two zinc-finger motifs. The prenylation motif, which mediates the membrane localisation of cytoplasmic proteins via prenylation (Maurer-Stroh et al., 2007), is also required for the normal localisation and function of Pk in planar polarity pathway (Lin and Gubb, 2009; Strutt et al., 2013b; Veeman et al., 2003). The prenylation of Pk promotes its interaction with Stbm (Strutt *et al.*, 2013b).

Flamingo (Fmi)

The atypical cadherin Fmi is a large protocadherin with about 3,600 amino acids, contains seven transmembrane domains and a large extracellular domain, which consists of nine cadherin motifs, four EGF-like motifs, and two laminin G motifs (Chae et al., 1999; Usui *et al.*, 1999). Unlike the classical cadherins, Fmi lacks catenin binding site, suggesting that it is not directly linked to the cytoskeleton mediated cell adhesion (Chae *et al.*, 1999; Usui *et al.*, 1999). Instead, Fmi may be involved in intercellular adhesion as it undergoes homophilic interactions *in vitro* (Usui *et al.*, 1999).

Although it is previously noted that Fmi is also known as Stan, Fmi and Stan are two isoforms of the *fmi* gene. The more common Stan isoform has a PDZ-binding motif on its C-terminal, which is absent in Fmi isoform (Wasserscheid et al., 2007).

1.2.3 The mechanisms of planar polarity

As stated above, the planar polarity is re-established before 32 h APF (Aigouy *et al.*, 2010; Axelrod, 2001; Bastock *et al.*, 2003; Strutt, 2001; Tree *et al.*, 2002; Usui *et al.*, 1999). Dsh and Pk are found recruited to apical junctional region symmetrically at early pupal stage (Axelrod, 2001; Tree *et al.*, 2002). Subsequently, at 18-24 h APF, Fz and Dsh obtain distal localisation, which peaks at 30 h APF just before the emergence of the trichomes (Axelrod, 2001; Strutt, 2001; Tree *et al.*, 2002).

There are three levels of mechanism required in the establishment process of the tissue scale planar polarity: 1) The molecular-scale local sorting and feedback, 2) The cell-scale sorting to opposite cell ends, and 3) tissue level upstream signals.

1.2.3.1 The molecular scale mechanisms

The molecular scale mechanisms describe the formation of the core planar polarity protein complex at cell junctions. Because the formation of the intercellular complex

involves the complexes forming within cells and the intercellular binding of the transmembrane proteins, I would describe these two processes separately.

Intercellular recognition and binding

One of the features of the planar polarity is the non-autonomous signalling between adjacent cells, which depends on the intercellular interactions of core proteins (Figure 1.6). When Fz is absent within a clone, Stbm within the clone localises to the clone boundary where it can interact with Fz in the neighbouring wild type cells; Fz protein of the neighbouring wild-type cells accumulates on the clone boundary (Figure 1.6 A, Chen et al., 2008; Strutt and Strutt, 2007; Strutt, 2001). Also, trichomes of surrounding wild-type cells point towards the *fz-* clone (Adler et al., 2000; Gubb and Garcia-Bellido, 1982; Lawrence et al., 2004; Struhl et al., 2012; Vinson and Adler, 1987). Such non-autonomy can be propagated over several rows of cells (Vinson and Adler, 1987). Similarly, at the edge of the *stbm-* clone, wild-type cells localise their proximal complex at the clone boundary and thus reorient trichomes away from the clone (Figure 1.6 B, Chen *et al.*, 2008; Lawrence *et al.*, 2004; Strutt and Strutt, 2007; Taylor et al., 1998). Unlike *fz-* or *stbm-* clones, clones of *fmi-* mutation have no non-autonomous changes in trichome direction (Chen *et al.*, 2008; Lawrence *et al.*, 2004; Struhl *et al.*, 2012; Strutt and Strutt, 2007), and co-mutant of *fmi-* and *fz-/stbm-* abolishes the change in trichome direction in *fz-* and *stbm-* clones (Strutt and Strutt, 2007). The loss of non-autonomy suggests that Fmi is required for coordinating intercellular planar polarity formation at both sides of cell boundaries.

The non-autonomous signalling requires the recognition and binding between the distal complex proteins and the proximal complex proteins in their intercellular domains:

Fmi can interact homophilically between adjacent cells via its extracellular cadherin repeats (Usui *et al.*, 1999). Fmi:Fmi (":" represents intercellular binding) homodimers are asymmetrically distributed, recruiting Fz and Stbm at each side of the cell boundary,

where it serves as an intercellular bridge (Chen *et al.*, 2008; Struhl *et al.*, 2012; Strutt and Strutt, 2007). Comparing to Stbm, Fz is preferred to be recruited to the clone border by Fmi:Fmi, suggesting that Fmi has higher affinity for Fz than Stbm (Chen *et al.*, 2008; Strutt and Strutt, 2008). Furthermore, The Fz-Fmi:Fmi complex is necessary and sufficient to polarise trichomes in cells, in the absence of Stbm (Struhl *et al.*, 2012).

The formation of the Fz-Fmi:Fmi complex is crucial for the planar polarity establishment. The mutation of either component largely disrupts the apical junctional localisation of other core proteins (Struhl *et al.*, 2012; Strutt and Strutt, 2007; Strutt, 2001). The correct localisation of Fz-Fmi:Fmi complex might be the first step of the planar polarity establishment, as it recruits Stbm of neighbouring cells (Chen *et al.*, 2008), which in turn stabilises Fmi (Strutt and Strutt, 2008) and Fz (Warrington et al., 2017) on membrane (Figure 1.7). Despite the colocalisation and the mutual recruitment between Fz and Stbm (Chen *et al.*, 2008; Strutt and Strutt, 2007), whether Fz and Stbm physically bind to each other is unclear. (Wu and Mlodzik, 2008) report the physical interaction in *in vitro* pull-down experiments and in *ex vivo* cell interaction experiments; while (Chen *et al.*, 2008) show that there is no direct evidence for the physical interaction, in this case, the recruitment and the stabilising function of Stbm is likely via cis- binding to Fmi.

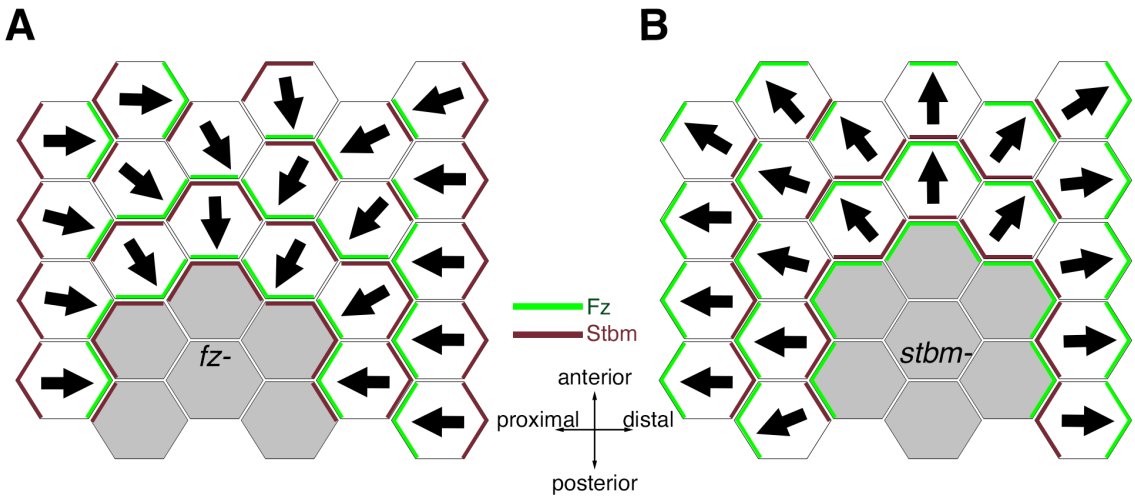

Figure 1.6 Non-autonomous effect of *fz-* and *stbm-* mutant clones

Schematics showing the non-autonomous effect of *fz-* (A) and *stbm-* (B) mutant clones. Fz cell membrane localisation is represented by green lines; Stbm cell membrane localisation is represented by red lines.

(A) *fz-* clone alters Fz and Stbm localisation and trichome direction in neighbouring wild-type cells. Black arrows indicate the orientation of trichomes in neighbouring wild-type cells point towards the *fz-* clone.

(B) *stbm-* clone alters Fz and Stbm localisation and trichome direction in neighbouring wild-type cells. Black arrows indicate the orientation of trichomes in neighbouring wild-type cells point away from the *stbm-* clone.

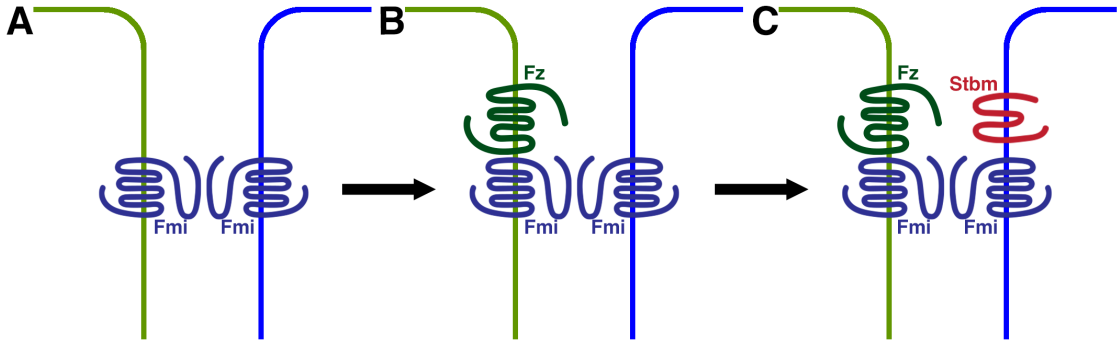

Figure 1.7 Fz-Fmi:Fmi:Stbm bridge

(A) Fmi can interact homophilically between adjacent cells, and recruits Fz and Stbm.

(B) Fz is preferred to be recruited to Fmi:Fmi.

(C) Fz-Fmi:Fmi complex recruits Stbm and forming the intercellular Fz-Fmi:Fmi:Stbm bridge

Formation of the distal and proximal complex

After the formation of the intercellular bridge of Fmi, cytoplasmic core proteins accumulate and form highly dense structure described as puncta, where asymmetry is greater and core proteins are highly stable with lower turnover rates (Figure 1.8 A, red arrows indicate puncta)(Brittle et al., 2022; Cho et al., 2015a; Strutt et al., 2011).

The formation of puncta results from the networks of interactions within the distal complex components and within the proximal complex components, respectively. Within the distal complex, Fz recruits Dsh (Shimada *et al.*, 2001; Strutt *et al.*, 2012)(see **Section 1.2.2.1-Frizzled (Fz)**) and may also recruit Dgo (Wu *et al.*, 2008); while Dsh recruits Dgo (Wu *et al.*, 2008). Within the distal complex, Stbm recruits Pk (Bastock *et al.*, 2003; Strutt *et al.*, 2013b). Evidence in physical interactions also supports the view of the networks of interactions, summarised in Table 1.1 and reviewed in (Harrison et al., 2020).

Cytoplasmic core proteins in the puncta contribute to stabilising the core proteins. The stability of Fz in puncta is weakened in the absence of cytoplasmic Dsh, Dgo, and Pk, as well as reduced polarity (Strutt *et al.*, 2011; Warrington *et al.*, 2017); the overexpression of these cytoplasmic core proteins, in contrast, leads to the formation of larger puncta (Cho et al., 2015b; Feiguin *et al.*, 2001; Tree *et al.*, 2002). Besides, Pk localises symmetrically on cell membrane in both *fz*- and *dsh*- tissue (Tree *et al.*, 2002) and the acute sequestration of Dsh weakens the membrane localisation of Pk in the adjacent cell (Ressurreicao et al., 2018), suggesting a stabilisation function of Dsh across junctions. Also, the absence of Pk reduces Dsh distal membrane localisation in adjacent cells (Tree *et al.*, 2002). However, aside from stabilising core proteins, cytoplasmic proteins Dsh and Pk are not required for intercellular signalling as *dsh*- or *pk*- mutant clones still exhibit non-autonomous Fmi localisation in adjacent cells (Strutt and Strutt, 2007).

Cloud model and feedback

The previous two sections introduce the local intracellular interactions and the intercellular binding of core proteins. Such multiple binding suggests that the core proteins stabilise into a signalosome-like complex in a mutual binding manner (Strutt et al., 2016). However, mutual bindings cannot explain the alignment of complexes within the puncta. How the core proteins complex establishes its asymmetricity is still unclear. Here, I will introduce a molecular level 'feedback' model.

The basic principle of the 'feedback' model is that complexes with the same orientation will be stabilised in the puncta, while complexes of the opposite orientation will be destabilised (Figure 1.8 B). Specifically, distal complexes stabilise other distal complexes and destabilise proximal complexes on cell junctions; while proximal complexes stabilise other proximal complexes and destabilise distal complexes.

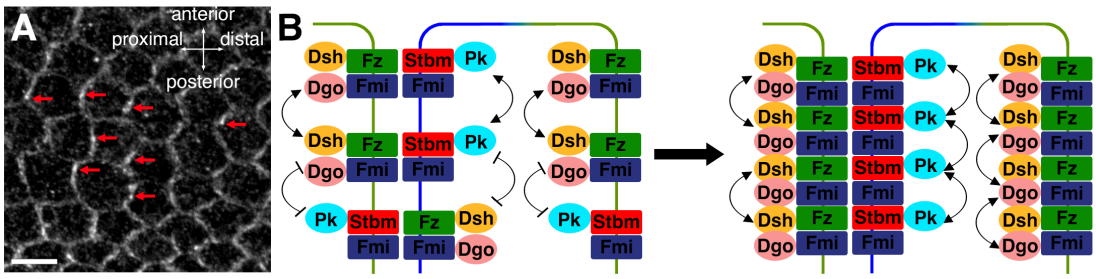

Figure 1.8 Feedback model

(A) Fmi immunolabelling in 28 h APF *w[1118]* wild-type pupal wings. Red arrows indicate Fmi puncta with high intensity. Scale bar 5 μm.

(B) Schematic showing the feedback model where distal complexes stabilise other distal complexes and destabilise proximal complexes; while proximal complexes stabilise other proximal complexes and destabilise distal complexes. Thus, two sets of proteins localise to opposite cell ends.

Table 1.1 Direct interactions between core proteins

Direct interaction		distal complex			Both complex	Proximal complex	
		Fz	**Dsh**	**Dgo**	**Fmi**	**Stbm**	**Pk**
distal complex	**Fz**		/	/	/	/	/
	Dsh	PEPSCAN-based ELISA * (Tauriello *et al.*, 2012)		/	/	/	/
	Dgo		Co-IP GST (Jenny *et al.*, 2005)		/	/	/
Both complex	**Fmi**	Co-IP (Chen *et al.*, 2008)				/	/
Proximal complex	**Stbm**	Co-IP ** (Montcouquiol *et al.*, 2006)	Co-IP (Bastock *et al.*, 2003) GST (Jenny *et al.*, 2003)	GST (Das *et al.*, 2004)	Co-IP *** (Devenport and Fuchs, 2008)	GST (Jenny *et al.*, 2003) Co-IP, yeast two-hybrid (Belotti et al., 2012)	/
	Pk		GST Tree et al., 2002 (Jenny *et al.*, 2005)	GST (Das *et al.*, 2004)		Co-IP (Bastock *et al.*, 2003) GST (Jenny *et al.*, 2003)	GST (Jenny *et al.*, 2003)

* Mouse Fzd5 binds to Dvl1

** Mouse Fzd3 binds to Vangl2

*** Mouse Celsr1 binds to Vangl2

One example of feedback is between Pk and Fz/Dsh. On the one hand, Pk localisation is regulated by the distal Fz/Dsh complex as Pk localises symmetrically in both *fz*- and *dsh*- tissue (Tree *et al.*, 2002). On the other hand, the distal complex is also regulated by Pk as the *pk*- mutant experiments show that the proximal localisation of Pk is required for the correct distal localisation of Fz (Strutt, 2001) and Dsh (Tree *et al.*, 2002), and for the overexpression phenotype of Dsh and Fz (Tree *et al.*, 2002). Besides, induced expression of Pk in *pk*- mutant background decreases Fz-EGFP stable amount on cell junctions (Warrington *et al.*, 2017). The decreasing effect of induced Pk on Fz is Dsh dependent, as induction of Pk in *pk-,dsh*- double mutant background increases Fz-EGFP stable amount instead (Warrington *et al.*, 2017). This suggests a model where when Pk mis-localises distally it interacts with Fz-Dsh complex and destabilise Fz/Dsh complex from the distal cell junction. Supporting this model, Pk is reported to bind to Dsh (Jenny *et al.*, 2005; Tree *et al.*, 2002) and block Dsh membrane localisation when co-transfected in human cells (Tree *et al.*, 2002). An *in vitro* experiment also shows that Pk competes with Dgo for Dsh binding (Jenny *et al.*, 2005). This can be the mechanism for the decreasing effect of Pk on Fz-EGFP in (Warrington *et al.*, 2017) where induced Pk mis-localises distally and binds to Dsh to reduce its membrane localisation, thus, destabilises the distal complex.

Another example of feedback model is that overexpression of Pk induces Fmi/Vang/Pk complex internalisation in pupal wings (Cho *et al.*, 2015b). Interestingly, such internalisation requires the presence of Fz (Cho *et al.*, 2015b), suggesting a negative feedback model where overexpressed Pk mis-localises Fmi/Vang/Pk complex to distal cell ends thus being internalised in a Fz dependent manner. Supporting this, core protein puncta are larger and less asymmetric in Pk overexpressed tissue (Bastock *et al.*, 2003; Cho *et al.*, 2015b), suggesting a mis-localisation of Fmi/Vang/Pk complex.

Other than the internalisation of Fmi/Vang/Pk complex stated above (Cho *et al.*, 2015b), Fz (Warrington *et al.*, 2017) and Fmi (Strutt and Strutt, 2008) are also found to be endocytosed. Fmi and Fz are proposed to be co-trafficked as blocking trafficking to

late endosomes leads to early endosomes accumulation of Fmi and Fz (Strutt and Strutt, 2008). In addition, the loss of Rabenosyn-5 (Rbsn-5), an evolutionarily conserved effector of the small GTPase Rab5, results in intracellular accumulation of the recycling Fmi fraction (Mottola et al., 2010), suggesting recycling of Fmi. Interestingly, Fmi directly associates with Snx27 *in vitro*, a retromer-associated cargo adaptor which controls endosomal recycling, and loss of Snx27 reduces Fmi and Stbm junctional levels in pupal wings clones, suggesting a Fmi mediated endosomal recycling of Fmi and Stbm back to the plasma membrane (Strutt et al., 2019b). Also, Rbsn-5 is found distributed in proximodistal axis in a Fmi-dependent manner (Mottola *et al.*, 2010), and the exocyst component Sec5, whose mutation tissue accumulates Cadherin in internal vesicles, is also recruited by Fmi (Classen *et al.*, 2005), suggesting Fmi regulates vesicles recycle. Thus, these examples suggest that the internalised vesicles may get recycled back onto the cell junction in a feedback manner.

Another piece of evidence supporting the feedback model is the mutual interaction between distal components and proximal components (summarised in Table 1.1). The physical interactions suggest the possibly destabilising interaction between the oppositely oriented complex and the correctly oriented complex. However, there is no direct evidence showing the existence of the mixed opposite oriented complex in physiological conditions (Brittle *et al.*, 2022), presumably because the feedback is active.

Multiple evidence shows that Post-Translational Modification (PTM) regulates core protein localisation on the membrane, which may be involved in the feedback mechanism. Dsh is a target for Cullin3-Diablo/Kelch E3 ubiquitin ligase complex mediated ubiquitylation and is targeted for proteasomal degradation, which results in a reduction in Dsh level at cell junctions (Angers et al., 2006; Strutt et al., 2013a). Besides, Pk is a target for Cullin1(Cul1)/SkpA/Supernumerary limbs (Slimb) complex mediated ubiquitylation (Cho *et al.*, 2015b). While the prenylation of Pk promotes its recruitment to Stbm(Strutt *et al.*, 2013b), Stbm reversely promotes the degradation of

excess Pk via Cullin1 complex (Cho *et al.*, 2015b; Nagaoka et al., 2019; Strutt *et al.*, 2013b). Also, deubiquitylation is reported to regulate the core protein recycling and membrane localisation as the deubiquitinase Fat facets (Faf) promotes the junctional localisation of internalised Fmi (Strutt *et al.*, 2013a). In addition, the phosphorylation of kinases, the main topic of this thesis, is also found to regulate planar polarity and may be important for feedback, see **Introduction 1.3**, reviewed in (Harrison *et al.*, 2020).

1.2.3.2 Upstream signals

In **Section 1.2.3.1**, I described mutual interactions among core proteins which lead to positive and negative feedback. Computational models have shown that positive and negative feedback interactions are sufficient to establish the asymmetric localisation of core proteins via amplifying an initial slight bias (Amonlirdviman et al., 2005; Burak and Shraiman, 2009; Fisher and Strutt, 2019; Le Garrec et al., 2006; Schamberg et al., 2010). The question now is, is there an initial bias? What is the initial slight bias? Is it provided by a long-range upstream signal cue? What is this upstream signal?

The identification of a long-range upstream signal cue is controversial. There are two signalling pathways that have been proposed to act upstream of core planar polarity pathway: 1) Fat-Dachsous (Ft-Ds) pathway and 2) Wg signalling pathway. Also, there are other possible mechanisms, e.g., hinge contraction.

Ft-Ds pathway

The Ft-Ds pathway consists of four major components: two atypical cadherins Fat (Ft)(Mahoney et al., 1991) and Dachsous (Ds)(Clark et al., 1995), the atypical myosin Dachs (D)(Mao et al., 2006), and the Golgi-localized kinase Four-jointed (Fj)(Brodsky and Steller, 1996; Villano and Katz, 1995).

Ft contains 34 cadherin repeats (Mahoney *et al.*, 1991) and Ds contains 27 cadherin repeats (Clark *et al.*, 1995). Ft and Ds localise asymmetrically in *Drosophila* epithelial

tissues and form heterophilic intercellular complexes between adjacent cells (Ambegaonkar et al., 2012; Brittle et al., 2012; Ma et al., 2003; Matakatsu and Blair, 2004). The heterophilic binding is regulated by the phosphorylation on the extracellular cadherin repeats by Fj (Ishikawa et al., 2008). The phosphorylation promotes the binding of Ft to Ds but inhibits binding of Ds to Ft (Brittle et al., 2010; Hale et al., 2015; Ishikawa *et al.*, 2008; Simon et al., 2010; Strutt et al., 2004).

The expressions of Fj and Ds present gradients. In the wing disc, Fj is expressed higher distally and lower proximally, while Ds is expressed proximally in the hinge region; in the pupal wing, the expression of Fj is higher at the wing margin, while Ds is expressed along the centre stripe of the wing (Figure 1.2)(Hale *et al.*, 2015; Matakatsu and Blair, 2004; Strutt *et al.*, 2004; Strutt and Strutt, 2002). This leads to a model where the asymmetry of Ft and Ds is driven by the gradient of Fj: the cells with higher Fj activity promote Ft binding to Ds of the lower Fj activity cells. Although Ft appears to be uniformly expressed, the expression gradients of Fj and Ds lead to a preferred proximally subcellular localisation of Ft. Thus, Ds localises to distal cell edges and Ft localises to proximal cell edges in the wing disc (Ambegaonkar *et al.*, 2012; Brittle *et al.*, 2012), reviewed in (Strutt and Strutt, 2021; Thomas and Strutt, 2012). In addition, D colocalises with Ds at distal cell junctions and transduces Ft-Ds signalling via 1) binding and inhibiting Warts (Wts, a component of the Hippo signalling pathway), and 2) orienting spindle affecting cell division (reviewed in (Thomas and Strutt, 2012)).

Several lines of evidence suggest that Ft-Ds signalling is required for core planar polarity pathway. The core protein Fmi and Dsh localisation is observed to be mis-oriented in *ft-* clones in *Drosophila* pupal wings (Ma *et al.*, 2003; Strutt and Strutt, 2002). Loss of *ft* or *ds* correspondingly induces swirling wing hair pattern (Matakatsu and Blair, 2004; Strutt and Strutt, 2002). Also, when Ds is induced to mis-express, the core protein Fz in pupal wing stage get mis-oriented, the wing hairs in adult wings are also in a swirling pattern (Matakatsu and Blair, 2004).

There is also evidence denying a direct link between the core pathway and the Ft-Ds pathway in the wing. Loss of the Ft-Ds gradient by uniform expression rescues the swirling wing hair phenotype in majority compartment of wings (Brittle *et al.*, 2012; Sagner et al., 2012; Simon, 2004), suggesting that Ft-Ds gradient is not the direct long-range cue. Nevertheless, expression of Ft lacking extracellular domain still rescues *ft* mutant phenotype, suggesting the asymmetrical localisation driven by the Ft/Ds interaction is not essential (Matakatsu and Blair, 2006; 2012; Pan et al., 2013).

Albeit there is evidence supporting the role of Ft-Ds pathway in regulating planar polarity, the evidence against it is stronger in the pupal wing. Thus, the Ft-Ds pathway may serve as a redundant regulator or only functions via affecting wing morphology. Supporting the indirection role, the effect of Ft-Ds on regulating planar polarity is proposed to be due to change in wing growth, given the fact that Ft and D are also Hpo/Wts pathway components (Brittle *et al.*, 2012; Feng and Irvine, 2007; Mao *et al.*, 2006; Matakatsu and Blair, 2006). Also, Cell packing is proposed to regulate planar polarity, which is disrupted in *ft* clones (Ma et al., 2008). Tissue flow is also proposed to regulate planar polarity, which is disrupted in *ft*- or *ds*- pupal wings (Aigouy *et al.*, 2010). As the hinge contraction (see **Section Hinge Contraction**) generates tissue flow, the Ft-Ds pathway may indirectly regulate planar polarity via affecting hinge contraction. For more information, please see Review (Strutt and Strutt, 2021).

Wnt/Wg signalling

The core planar polarity proteins Fz and Dsh are also two conserved members of the Wnt/Wg signalling pathway. For this reason, whether Wnt ligands regulate planar polarity and how different outputs are specified are two important questions in the field.

There is evidence showing Wnt5a, Wnt7a, and Wnt11 ligands are required for planar polarity in specific vertebrate tissues, reviewed in (Gao and Yang, 2013; Rogers and Scholpp, 2022; Seifert and Mlodzik, 2007). For instance, given that the convergent

extension is regulated by planar polarity pathway (Jessen et al., 2002; Wang et al., 2006a; Yin et al., 2008), Wnt5 and Wnt11 have been shown to be required for convergent extension in vertebrates (Heisenberg *et al.*, 2000; Lele et al., 2001; Tada and Smith, 2000; Westfall et al., 2003). Recent publications also support that Wnt signalling is required for planar polarity in vertebrates. Research in alveolar formation showed an essential role of Vangl2 in Wnt5a-mediated alveologenesis in mice (Zhang et al., 2020). Besides, loss of Wnt5a in mice causes defects in heart formation and can be rescued by expressing a planar polarity effector Daam1, a Dvl-binding protein (Li et al., 2019), providing new evidence for Wnt5a act upstream of planar polarity.

The role of Wnt signalling in planar polarity in vertebrates is suggested to be instructive. In chick embryo development, WNT11 mediates orientational myocyte, the primitive muscle fibres, elongation through planar polarity pathway, and the ectopic source of WNT11 changes the orientation of myocytes (Gros et al., 2009). Wnt5a exhibits a gradient in developing vertebrates, which induces Vangl2 Thr/Ser phosphorylation by Ror2 (Gao et al., 2011) or CK1ε/δ (Yang et al., 2017) in a Wnt5a dose-dependent manner. In *Xenopus* early ectoderm, Vangl2/Prickle3 complex is polarised to the anterior cell end whose polarity can be disrupted by Wnt antagonists (Chu and Sokol, 2016). Such polarity of Vangl2/Prickle3 complex is oriented by Wnt5a, Wnt11, and Wnt11b as the Vangl2/Prickle3 complexes localise away from ectopic Wnts sources (Chu and Sokol, 2016). Similarly, the polarity of Vangl2 in the neuroectoderm can also be re-oriented by ectopic Wnts source (Chu and Sokol, 2016). Also, in node cells of mouse embryos, loss of anterior-posteriorly distributed Wnt5 and Sfrps (secreted Frizzled-related proteins, a Wnt antagonist) results in mis-localisation of its Basal Body, which requires Prickle 1 and Prickle 2 (Minegishi et al., 2017). Similar loss of polarity phenotype is also present in the even distribution of Wnt5a or Sfrp1 (Minegishi *et al.*, 2017).

Although vertebrate research links downstream planar polarity effectors to Wnt ligands, evidence supporting Wg signalling regulating planar polarity in *Drosophila* is

insufficient. Unlike in vertebrates, mutants lacking Wg, DWnt-2, DWnt-4, D-Wnt-6, and D-Wnt-10 show no planar polarity defects in wings (Chen *et al.*, 2008). In addition, CRISPR-based Wnt/Wg knock-outs and Wg RNAi experiments produce no planar polarity defects and blocking Wg ligand secretion does not produce detectable planar polarity phenotypes (Ewen-Campen et al., 2020; Yu et al., 2020).

Hinge Contraction

As stated above, the planar polarity gets rearranged from the radial axis to the proximodistal axis during hinge contraction (Figure 1.2)(Aigouy *et al.*, 2010; Classen *et al.*, 2005). The hinge contraction is also considered to regulate planar polarity.

Supporting this, the planar polarity re-establishment is disrupted when the hinge contraction is disrupted by severing the wing hinge (Aigouy *et al.*, 2010; Etournay *et al.*, 2015). The hinge contraction may result in diverse effects, including cell elongation, directional mechanical forces, and cell rearrangement (Aigouy *et al.*, 2010). Although the hinge contraction does not explain how the initial bias is formed, it provides a view of how global alignment of planar polarity is formed.

Since the identification of the upstream clue in *Drosophila* wings is controversial, these mechanisms may function redundantly, or there could be other unknown signals serving as the global upstream clue.

1.2.3.3 The cell-scale sorting to opposite cell ends

So far, I have described the feedback model where an initial bias is needed, and the possible upstream clue which may provide such an initial bias. However, these models fail to explain the observation where the induced expression of Fz in *fz*- background at 24 h APF leads to a swirling pattern of wing hairs (Strutt and Strutt, 2002). In this case, on the one hand, as the putative global tissue-scale signal results in a proximodistal

polarity, the swirling pattern should not be the direct result of it. On the other hand, since the wing is initially lacking Fz, there is not an initial bias to be amplified by feedback. Therefore, there shall be a cell-scale mechanism breaking the symmetry (Fischer et al., 2013). One possible mechanism that localises core protein complexes to opposite cell ends is discussed in **Discussion 5.2.1**.

1.2.4 Downstream of planar polarity

Trichome orientation is the main readout of planar polarity in *Drosophila* pupal wings. The trichomes are actin-rich hairs that grow from the distal cell edge of *Drosophila* pupal wing cells at about 32h APF (Figure 1.2), which develop into wing hairs in adult wings. The distal localisation of the trichome is regulated by planar polarity core proteins, whose absence leads trichomes to initiate from the centre of the cell (Strutt, 2001; Wong and Adler, 1993).

Although the mechanism is still unclear, the 'planar polarity effector (PPE) proteins' act downstream of core planar polarity proteins to regulate trichome localisation and direction. Three planar polarity effector proteins: Inturned (In), Fritz (Frtz), and Fuzzy (Fy), are localised to the proximal cell ends in core protein-dependent manner (Adler et al., 2004; Collier and Gubb, 1997; Collier et al., 2005; Gubb and Garcia-Bellido, 1982; Park et al., 1996; Strutt and Warrington, 2008; Wong and Adler, 1993). The core proteins and the PPE proteins act with Rab23 (Gerondopoulos et al., 2019) to localise an actin cytoskeleton inhibitor Multiple wing hair (Mwh) to the proximal side, thus, inhibiting the trichome forming proximally (Adler *et al.*, 2004; Lu et al., 2015; Lu et al., 2010; Strutt and Warrington, 2008).

1.3 Overview of kinases

'Kinase' is a term used to describe a group of enzymes that transfer phosphate groups to their substrates. Categorising by its substrates, there are protein kinases, lipid kinases, carbohydrate kinases, etc. In this thesis, I focus on protein kinases and the term 'kinase' narrowly refers to 'protein kinase'.

The transfer process of phosphate groups is called phosphorylation. The protein kinases transfer one phosphate group from the high energy ATP to the amino acid side chain to form a reversible covalent bond, and meanwhile produce an ADP.

Serine (Ser, S), threonine (Thr, T), and tyrosine (Tyr, Y) are the three most widely studied phosphorylatable amino acids. All these three amino acids contain hydroxyl group (-OH) on their side chain and form phosphoester (P-O) bonds after phosphorylation. Categorising by the substrate amino acid, there are serine/threonine (S/T) kinases and tyrosine kinases. Note, but irrelevant to this thesis, Histidine can also be phosphorylated and form phosphoramidate (P-N) bonds, which are less stable than P-O bonds.

The kinases are well conserved from bacteria to animals and plants. There are more than 500 protein kinases encoded by the human genome, whose phosphorylation activity regulates a vast range of biochemical processes. For instance, they can activate or deactivate a protein, stabilise or destabilise a protein, and associate or dissociate a protein with others. These activities make kinases excellent candidates for mediating feedback between the core proteins. Specifically, kinase may promote physical interactions between core proteins, stabilise core proteins into puncta or destabilise the mis-localised core protein from the puncta. In following sections, I will introduce some candidate kinases involve in regulating planar polarity (also reviewed in (Harrison *et al.*, 2020)).

1.3.1 aPKC

Atypical Protein Kinase C (aPKC) is a crucial apicobasal polarity regulator localised to the apical marginal region (**Section 1.2.1.2,** reviewed in (Goldstein and Macara, 2007; Suzuki and Ohno, 2006)). It is also reported to regulate planar polarity in *Drosophila* eyes (Djiane et al., 2005).

Djiane et al. proposed that aPKC is recruited to Fz via dPatj which binds the cytoplasmic tail of Fz (Djiane *et al.*, 2005). In addition, aPKC is reported to phosphorylate Fz *in vitro* on S554 and S560 residues in the C-terminal tail (Figure 1.5 A, light green box region indicates the KTxxxW motif on Fz)(Djiane *et al.*, 2005). While overexpression of Fz or phosphomutant form of Fz induces chirality defects in ommatidia, overexpression of phosphomimetic form of Fz provides relatively normal phenotype (Djiane *et al.*, 2005), suggesting aPKC phosphorylates and inhibits Fz in eyes.

Whether aPKC regulates planar polarity in the wing and the mechanism of how such phosphorylation alters the planar polarity is currently unknown. A possible model is that the Fz phosphorylation inhibits Dsh binding thus downregulates planar polarity. Two putative phosphorylation sites S554 and S560 are previously shown to be involved in Dsh recruitment. Fz[S554>F] mutant fails to recruit Dsh (Strutt *et al.*, 2012) and S560 lies within the conserved KTxxxW motif, which is also required for Dsh binding in *Xenopus* (Umbhauer *et al.*, 2000), *in vitro* (Wong *et al.*, 2003), and in *Drosophila* wing discs (Wu *et al.*, 2008).

The function of aPKC in planar polarity in the wing is further examined in **Chapter 2** and **Chapter 4**.

1.3.2 Par-1

Based on mass-spectrometry analysis data, Yanfeng *et al.* identified multiple phospho-residues of Dsh *in vivo* (Yanfeng et al., 2011). Although this study surprisingly claims that all conserved serines/threonines residues are non-essential for planar polarity (Yanfeng *et al.*, 2011), lines of evidence show serines/threonines kinases Par-1 and Casein Kinase Iε (CKIε, also known as Discs Overgrown, Dco, in flies) phosphorylate Dsh and regulate planar polarity (Klein et al., 2006; Penton et al., 2002; Strutt et al., 2019a; Strutt et al., 2006). Such a conflict may be due to the redundancy between sites. Yanfeng *et al.*, in their rescue screening, only tested cluster mutations within DEP domain or C-terminal of Dsh, while the clusters reported in other publications (S/T236-247, upstream of PDZ domain, Figure 1.5 B) were only screened in single mutations.

Drosophila PAR-1 is a conserved member of the PAR-1 kinase family, which is the homolog of *C. elegans* PAR-1 and the mammalian MARKs. Par-1 was previously shown to be required for convergent extension in *Xenopus* (Ossipova et al., 2005). Par-1 binds to and phosphorylates an S/T rich region of Dsh (S/T236-247) in *Xenopus* embryo, thus positively regulating the Wnt signalling pathway and inhibiting Jun-N-terminal kinase (JNK) pathway (Sun et al., 2001). Mutations in these residues reduce the Fz-dependent Dsh membrane localisation (Ossipova *et al.*, 2005).

Studies in *Drosophila* also found that mutations in S/T236-247 do not rescue the planar polarity defect in *dsh[1]* mutant in *Drosophila* (Penton *et al.*, 2002). However, whether Par-1 directly phosphorylates Dsh *in vivo* in the *Drosophila* pupal wing model, and whether it regulates Dsh localisation remains unknown.

The function of Par-1 in *Drosophila* wings is examined in **Chapter 2**.

1.3.3 CKIε/Dco

CKIε/Dco is a highly conserved Ser/Thr protein kinase which is also known as Doubletime (Dbt) as it was independently identified in studies in *Drosophila* circadian rhythm (Ko et al., 2002). In the regulation of the circadian phenotype, Dco phosphorylates and promotes the turnover of the circadian protein Period (Kloss et al., 1998).

Dco is reported to affect planar polarity. Wing hairs are found to be mis-orientated in *dco*- mutant clones (Klein *et al.*, 2006), *dco*- mutant whole wings, dominant-negative Dco expressed tissue, and Dco RNAi expressed tissue (Strutt *et al.*, 2006). Dco overexpression also leads to a wing hair mis-orientation phenotype (Strutt *et al.*, 2019a; Strutt and Strutt, 2020). Besides in adult wings, in *dco*- mutants clones in pupal wings, Dsh is found to be localised in puncta that are uniformly distributed around the cell edge (Strutt *et al.*, 2006). It is also shown that dominant-negative form of Dco destabilises Dsh from the membrane (Strutt *et al.*, 2019a).

The function of Dco on planar polarity is likely due, in part, to its phosphorylation activity on Dsh. First of all, Dco binds and phosphorylates Dsh in Wnt/Wg signalling pathway (Bernatik et al., 2014; Cong *et al.*, 2004a; Gao et al., 2002; Kishida et al., 2001; Klein *et al.*, 2006; McKay et al., 2001; Peters et al., 1999; Sakanaka et al., 1999; Zhang et al., 2006). In *Drosophila* wing tissue, *dco*- mutant reduces Dsh phosphorylation level (Strutt *et al.*, 2006). Expression of dominant-negative forms of Dco in pupal wings also reduces Dsh phosphorylation *in vivo* (Klein *et al.*, 2006; Strutt *et al.*, 2006). *In vitro* kinase assay shows that the mutation on residue S236 in the PDZ domain blocks the phosphorylation of Dsh by vertebrate Dco homologue CKIε (Klein *et al.*, 2006). S236 lies within S/T236-247, suggesting CKIε/Dco shares the possible phosphorylation site with Par-1 (Strutt *et al.*, 2006). Furthermore, loss of two newly found regulators of Dco/CKIε activity, DAnkrd49 (an ankyrin repeat protein) or Bdbt (Bride of Doubletime, a non-canonical FK506 binding protein family member) results in a reduction in Dsh phosphorylation, decreased Dsh levels at cell junctions and in the cytoplasm, and a

reduction in core protein asymmetry in pupal wing cells (Strutt and Strutt, 2020). Research in vertebrate provides a possible mechanism for the regulation on Dsh, where CK1ε regulate DVL conformational dynamics and DVL with an open conformation shows less cytoplasmically punctate and more efficient membrane recruitment by Fz (Harnos et al., 2019).

However, mutation of 5 S/T residues in S/T236-247 region rescue *dsh*- mutant adult wing trichome phenotype (Strutt *et al.*, 2006), and the mass-spectrometry analyses failed to detect phosphorylation in S/T236-247 (Yanfeng *et al.*, 2011). These results contradict the result where 8 S/T residues mutation does not rescue *dsh*- mutant trichome phenotype (Strutt *et al.*, 2006). The contradiction may be due to either the redundancy or conformation change of multiple mutations, which raises the question of whether Dco directly phosphorylates and regulates Dsh. In fact, more than 100 S/T residues and 11 conserved Tyrosines are present among 623 amino acids in *Drosophila* Dsh, suggesting that more than 1/6 amino acids have the potential to be phosphorylated. Thus, it is hard to identify the kinases phosphorylating Dsh and functional phosphorylation sites in Dsh.

Besides the function on Dsh, evidence for Dco/CKIε phosphorylating Stbm is more robust. Two conserved N-terminal clusters of serine and threonine residues in vertebrate Vangl2 are phosphorylated in tissue culture (Gao *et al.*, 2011; Yang *et al.*, 2017). Residues in these clusters in *Drosophila* Stbm are reported to be phosphorylated in S2 cells (Kelly et al., 2016) and pupal wings (Strutt *et al.*, 2019a). Furthermore, CK1 inhibitor D4476 (Rena et al., 2004) and kinase-dead Dco abolishes Stbm phosphorylation in S2 cells (Kelly *et al.*, 2016). Also, Stbm and Dco physically interact in a co-immunoprecipitation experiment (Kelly *et al.*, 2016). These results strongly suggest that Stbm is a direct substrate of Dco.

The phosphorylation of Stbm by Dco regulates planar polarity. In the *Drosophila* eye, removing one copy of *dco*- enhances Stbm overexpression phenotype (Kelly *et al.*,

2016), suggesting Dco negatively regulates Stbm. In the wing, phosphomutant and phosphomimetic Stbm do not rescue the trichome orientation phenotype of *stbm*- mutants (Strutt *et al.*, 2019a).

Membrane localisation of Stbm is affected by the phosphorylation by Dco. Stbm-GFP membrane intensity is decreased in *dco*- clones in 30 h APF pupal wing (Kelly *et al.*, 2016). In addition, phosphomimetic Stbm forms fewer puncta and a greater population is observed in non-puncta compartment on cell membrane, whereas in phosphomutant Stbm, core proteins cluster into puncta but loss their asymmetry as complexes in both orientations are observed (Strutt *et al.*, 2019a). Phosphomutant Stbm results suggest that the phosphorylation by Dco helps remove the complex of the wrong orientation. Kelly *et al*., used a different phosphomutant Stbm construct but got a similar result that Stbm and Fmi reduce their polarity and distribute randomly on cell membrane (Kelly *et al.*, 2016).

Being a possible mechanism for the change in membrane localisation, Stbm stabilisation at cell junctions is affected by Dco. The phosphomutant Stbm is more stable at cell junctions while the phosphomimetic Stbm is less stable observed (Strutt *et al.*, 2019a). Expression of a kinase-dead dominant-negative form of Dco has no further effect on such stability change observed (Strutt *et al.*, 2019a), implying these two clusters of S/T residues are the only functional phosphorylation sites of Dco.

The phosphorylation of Stbm by Dco is regulated by Fz and/or Pk. Firstly, Stbm-3xFlag increases its gel mobility in *fz*- mutant larval lysate, showing reduced phosphorylation (Kelly *et al.*, 2016). GFP-tagged Stbm decreases its gel mobility in S2 cells transfected with Fz (Kelly *et al.*, 2016). These results show that Fz promotes the phosphorylation of Stbm. Fz is likely to regulate phosphorylation within the cell as Fz lacking the proposed Stbm binding extracellular region still induces Stbm phosphorylation (Kelly *et al.*, 2016). However, a pupal wing lysate Western Blot experiment contradicted these results, in which the endogenous Stbm did not show change in gel migration observed

(Strutt *et al.*, 2019a). The contradiction may be due to the C-terminal tagging affecting its function or the phosphorylation event being regulated differently between developing stages. The presumable stage specificity can be: Fz does promote the phosphorylation of Stbm, but as the sorting is active in pupal wing stage the endogenous Stbm does not physically close to Fz, thus, Fz cannot promote Stbm phosphorylation. Secondly, as for Pk, *pk*- mutation increases while Pk overexpression decreases Stbm phosphorylation level in pupal wings (Strutt *et al.*, 2019a). Therefore, the distally localised Fz promotes Stbm phosphorylation while proximally localised Pk negatively regulates and stabilises Stbm on cell membrane, suggesting the phosphorylation of Stbm is regulated in the core protein complex on cell junctions. Indeed, a Stbm mutant which is unable to transport to cell membranes is not phosphorylated in S2 cells and *in vivo* (Kelly *et al.*, 2016).

To sum up, Dco is proposed to phosphorylate Dsh and Stbm. The effect of these two phosphorylation events is the opposite: Dsh gets stabilised while Stbm gets destabilised. Since Dsh and Stbm are on opposite ends of the cell, Dco may be involved in feedback stabilising Dsh and destabilising Stbm at distal cell junctions. This is further examined in **Chapter 3**.

1.3.4 Abl

Abelson nonreceptor tyrosine kinase (Abl) has also been reported to regulate planar polarity. Both *abl*- alleles and overexpression of Abl leads to planar polarity defect phenotype in the *Drosophila* eye (Singh et al., 2010). In addition, Abl genetically interacts with core planar polarity proteins as removing one copy of *Abl* gene suppresses Fz or Dsh overexpression phenotypes in eyes (Singh *et al.*, 2010).

Abl may regulate planar polarity via phosphorylating Dsh. Abl binds and phosphorylates Dsh on its C-terminal residue *in vitro* (Singh *et al.*, 2010). The

conserved residue DshY473 within the DEP domain is identified as the phosphorylation site (Singh *et al.*, 2010, Figure 1.5 B), whose phosphorylation is essential for Dsh function in planar polarity (Yanfeng *et al.*, 2011). Furthermore, the DEP domain is crucial for the membrane recruitment of Dsh (Axelrod *et al.*, 1998; Gammons *et al.*, 2016; Tauriello *et al.*, 2012). These results support a hypothesis that the kinase Abl phosphorylates Dsh on Y473 and regulates Dsh membrane localisation.

The role of the reported phosphorylation site DshY473 in planar polarity is examined in **Chapter 2**.

1.3.5 Msn

The Ste20 kinase Misshapen (Msn, vertebrates homologue called Misshapen-like kinase 1, Mink1) was reported to physically interact with *Drosophila* Pk[Pk] and Pk[Sple] *in vitro* (Daulat et al., 2012).

Msn was also reported to regulate the planar polarity pathway. In the *Drosophila* eye, loss-of-function alleles of *msn* suppress the Dsh overexpression phenotype (Paricio et al., 1999), and *msn* RNAi knock-down enhances Pk[Sple] overexpression phenotype (Daulat *et al.*, 2012). However, in the wing, loss-of-function *msn*- induces no canonical planar polarity defects but missing or defective hairs, suggesting Msn acts downstream of core protein pathway (Paricio *et al.*, 1999). The difference between eyes and wings may be due to the Pk isoform specificity.

In vertebrates, MINK1 (Msn in human) phosphorylates PRICKLE1 on a vertebrate conserved threonine residue, thus regulating Rab5-dependent endosomal trafficking (Daulat *et al.*, 2012), which can be essential for core protein sorting and membrane localisation. Indeed, the PRICKLE1 membrane localisation is increased in MINK1 overexpressed HEK293T cells and decreased in morpholino oligonucleotide (MO)-xMink1 knock-down in *Xenopus* embryos (Daulat *et al.*, 2012).

Whether Pk membrane localisation is regulated by Msn is unknown in *Drosophila* wings. In **Chapter 2**, experiments checking the role of Msn in *Drosophila* pupal wings are described.

1.3.6 Nmo

Nemo (Nmo) kinase, a member of the MAPK family, was previously found to regulate ommatidia rotation in *Drosophila* eyes (Choi and Benzer, 1994; Collu *et al.*, 2018; Mirkovic et al., 2011). Loss of *nmo* enhances *pk[sple1] mutant* phenotype in *Drosophila* eyes (Collu *et al.*, 2018) and enhances *pk[sple1] mutant* phenotype and Pk[Pk] overexpression phenotype in *Drosophila* legs (Collu *et al.*, 2018).

As described in **Section 1.2.2.1**, Pk[Pk] and Pk[Sple] are two antagonistic isoforms of the prickle gene. Pk[Pk] is the dominant isoform in the wings, while Pk[Sple] is the major functional isoform in the eye. (Collu *et al.*, 2018) found that Nmo down regulates the *act-* driven Pk[Pk] levels but not Pk[Sple] in *Drosophila* eyes via proteasome-mediated degradation. The regulation on Pk[Pk] is likely due to the phosphorylation on two clusters of potential MAPK phosphorylation sites as the *Act5C* induced phosphomutant Pk has higher protein level in eye discs (Collu *et al.*, 2018). Thus, Nmo may serve as a repressor for Pk[Pk] to ensure the dominancy of Pk[Sple] in eyes.

nmo- mutant leads to wing hair oriental change (Verheyen et al., 2001), but the mechanism is unclear. To test whether Nmo regulates planar polarity via regulating Pk[Pk] protein level in wing, the function of the putative phosphorylation sites was examined in **Chapter 2**.

1.4 Aims of the project

In this thesis, I focus on the role of kinases in planar polarity in *Drosophila* wing model. The candidate kinases listed above were screened (**Chapter 2**). Then I investigated the kinases that regulate planar polarity in the wing and tried to examine the mechanism for the local sorting and feedback (**Chapter 3 Dco, Chapter 4 aPKC**). My main hypothesis is that the kinases can act as switches to promote core planar polarity protein sorting by locally controlling their stability in core protein complexes.

CHAPTER 2

Screening of candidate kinases

2.1 Introduction - Aims of this Chapter

Chapter 1 has summarised published data on a series of kinases reported to phosphorylate core planar polarity proteins and affect planar polarity in different models ranging from invertebrate *Drosophila* eyes to vertebrates. Compared to vertebrates and *Drosophila* eyes, the *Drosophila* wing has its unique advantages. First of all, the planar polarity is most well-studied in *Drosophila* wings (Goodrich and Strutt, 2011; Maung and Jenny, 2011; Strutt and Strutt, 2021; Thomas and Strutt, 2012). Secondly, the readout of the planar polarity is clear and simple in *Drosophila* pupal wing cells, which establishes the asymmetrical proximodistal localisation of core planar polarity proteins after 24 h APF (Aigouy *et al.*, 2010; Axelrod, 2001; Bastock *et al.*, 2003; Strutt, 2001; Tree *et al.*, 2002; Usui *et al.*, 1999). The asymmetric localisation of core proteins is easily accessible in the flat monolayer epithelium pupal wings. Unlike in *Drosophila* eyes, where protein asymmetry is harder to assess due to the presence of multiple cell types and the more indirect read-out of ommatidial rotation is generally used. The ommatidia pattern is also indirectly regulated by Epidermal Growth Factor Receptor (EGFR) and Notch signalling pathway (Brown and Freeman, 2003; Das *et al.*, 2002; O'Keefe et al., 2009; Strutt and Strutt, 2003; Weber et al., 2008), most likely through effects on photoreceptor identity and number. As for vertebrates, cost of the animal husbandry and difficulties of analysing planar polarity in vertebrates, e.g., the genetic redundancy in the planar polarity genes (Goodrich and Strutt, 2011) and relative difficulty accessing tissues in the embryo, make them less efficient models in the planar polarity research. Also, Wnt signalling regulates planar polarity in vertebrates (Chu and Sokol, 2016; Gao *et al.*, 2011; Gros *et al.*, 2009; Minegishi *et al.*, 2017; Yang *et al.*, 2017)(See **Introduction 1.2.3.2**).

The aim of this chapter is to identify the role of kinases in the core planar polarity pathway in one model. The *Drosophila* pupal wing is used as a simple model system to judge the effects of each kinase on core planar polarity. The distribution of the core proteins was measured in pupal wing epithelia at 28 h APF. Different genetically

manipulated conditions were examined to test whether specific kinases affect planar polarity.

2.2 Results

2.2.1 aPKC

aPKC affects planar polarity in *Drosophila* eyes (Djiane *et al.*, 2005) (**Introduction 1.3.1)**. However, the aPKC function in ommatidia pattern was only examined by overexpressing aPKC (Djiane *et al.*, 2005). Thus, I want to use multiple genetic tools to check whether and how aPKC affects planar polarity in pupal wings in this section.

2.2.1.1 The quantification of aPKC clones in the Drosophila wing

***aPKC*- amorphic allele clones**

The first approach I used is to check if *aPKC*- mutant allele affects planar polarity in clones, where the clear boundaries of clones of cells with different genotypes can be observed. *aPKC*- mutant twin-clones were generated using FLP/FRT system (Xu and Rubin, 1993). In the clonal approach, FLP recombinase induced the recombination of *FRT* element in the heterozygous genotype cells, thus generating two distinct heterozygous cell types after mitosis. In this way, patches of cells that are genetically different from their neighbours were generated, which facilitates comparison within the same wing. The clonal approach is a powerful method in the field of planar polarity where the clear clone boundary is crucial for analysing protein polarised localisation (Chen *et al.*, 2008; Strutt and Strutt, 2007; Strutt, 2001; Strutt and Strutt, 2008).

The planar polarity is represented by the polarised localisation of the core proteins, which is detected by quantifying the asymmetric localisation of the core protein (see **Materials and Methods 6.2.6**). The asymmetric localisation was calculated by comparing the immunolabelled or fluorescent-tagged core protein signal along cell edges, thus, generating the ‘single cell polarity’, the magnitude and the direction of the

‘single cell polarity’ were then averaged over a three-cell size to generate the ‘Coarse-Grain polarity’ (Tan et al., 2021).

In this experiment, the asymmetric localisation of Fmi is measured and compared. Note that it is Fz that was previously reported to be phosphorylated by aPKC, so it is Fz in theory a better reporter for checking the role of aPKC. However, the immunolabeling against Fz is not of the ideal quality in practice, so I used immunolabeling against Fmi in this experiment, whose staining is better in quality (compare Figure 2.1 A’ to Figure 2.2 A’ and F’).

Clones of a strong *aPKC*- allele (*aPKC[k06403]*) were first tested in 28 h APF pupal wings cultured at 25°C. However, all the *aPKC*- homozygous clones are overall small in size with only one row of cells (Figure 2.1 A, clones marked by red arrows). The reason for the small clone size can be that the *aPKC[k06403]* amorphic allele strongly affects cell viability or proliferation. Indeed, this amorphic allele is found homozygous and hemizygous lethal, and no protein is detectable in cells (Guilgur et al., 2012; Rolls et al., 2003; Wodarz *et al.*, 2000). Also note that as most wings do not have *aPKC[k06403]* clones, the best example image to show carries holes, as indicated by yellow dots in (Figure 2.1 A)

Given that the homozygous *aPKC[k06403]* clones are small, heterozygous *aPKC[k06403]/+* cells were also quantified. Among the three types of cells, there is not any obvious observable change in Fmi polarity orientation (shown by nematics in Figure 2.1 B-D, blue lines represent single cell polarity nematics), polarity strength (Figure 2.1 F), or membrane intensity (Figure 2.1 E). As both the heterozygous *aPKC*- cells and wild-type cells have aPKC copy(ies) in their genome, the only conclusion I can draw is the removal of one copy of aPKC does not affect Fmi polarity in pupal wings. The only genotype in absence of aPKC only produces small clone size, which also has no difference in polarity compared to clones of other genotypes either (Figure 2.1 F).

Note that the small size of homozygous *aPKC[k06403]* clones makes the polarity unable to be decently quantified due to the nonautonomous feature of planar polarity where the polarity of the cell on the edge of the clone, sharing boundaries with wild-type neighbours, is affected by its neighbouring cells. For this reason, I cannot make a solid conclusion based on this experiment. So another method, a weaker temperature-sensitive aPKC allele, was used to alter aPKC expression.

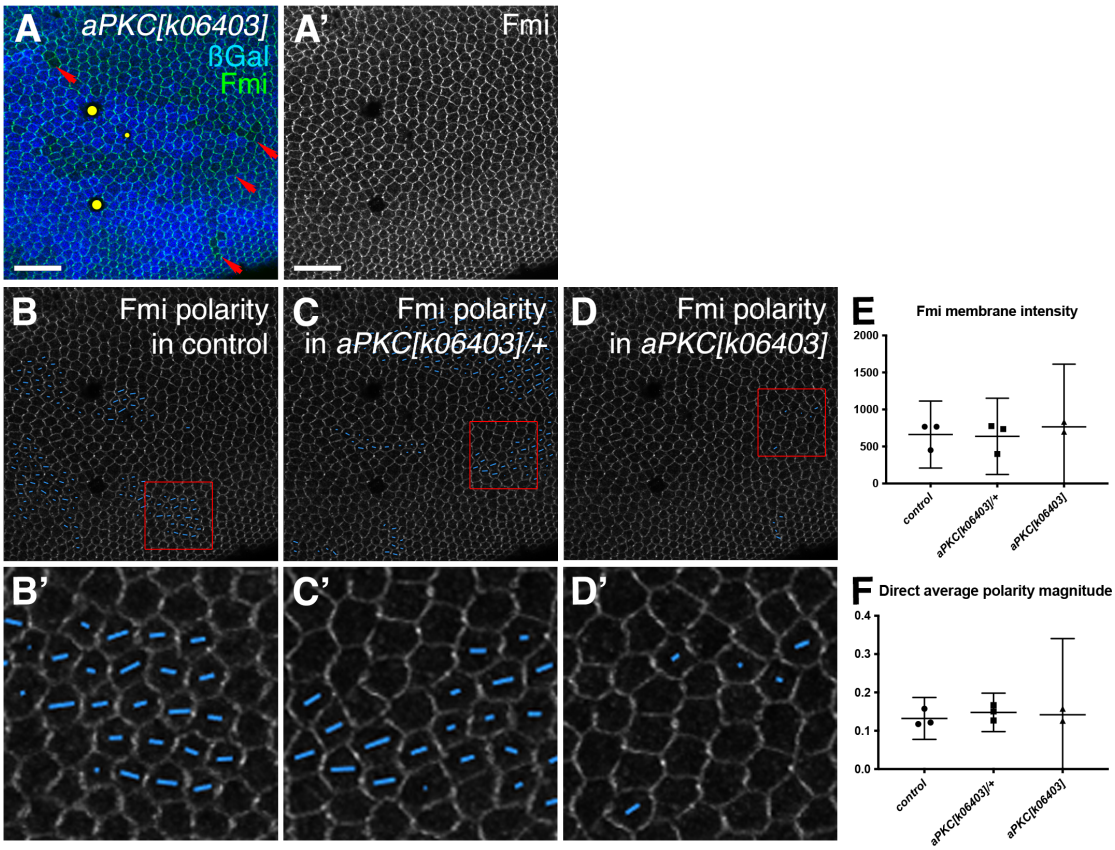

Figure 2.1 Fmi in *aPKC[k06403]* amorphic allele clones

(A,A') 28 h APF pupal wing aged at 25°C, carrying small twin clones of *aPKC[k06403]* (homozygous *aPKC[k06403]* tissue is indicated by the loss of blue β-gal immunolabelling and red arrows); yellow dots in penal A indicate holes of dissecting damage. β-gal is immunolabelled in blue (A); Fmi is immunolabelled in green (A) or grey (A'). Scale bar 20 μm.

(B-D') Blue lines represent single cell polarity nematics of Fmi in penal A in *arm-LacZ/arm-LacZ* control tissue (B), *aPKC[k06403]/arm-LacZ* heterozygous tissue (C), and homozygous *aPKC[k06403]* tissue (D). Regions in red boxes are zoomed-in in panel (B'-D').

(E-F) Comparison of Fmi intensity on the cell membrane (E) and Fmi polarity (F) among control tissue (N = 3 wings), heterozygous *aPKC[k06403]/+* tissue (N = 3 wings), and homozygous *aPKC[k06403]* tissue (N = 2 wings). Error bar: 95% confidence interval.

(E) No significant difference on Fmi membrane intensity is shown in the ANOVA test. p-value ANOVA results for comparisons between the control and *aPKC[k06403]/+* = 0.9846; control and *aPKC[k06403]* = 0.8098; *aPKC[k06403]/+* and *aPKC[k06403]* = 0.7289.

(F) No significant difference on Fmi direct average polarity is shown in the ANOVA test. p-value ANOVA results for comparisons between the control and *aPKC[k06403]/+* = 0.6566; control and *aPKC[k06403]* = 0.8774; *aPKC[k06403]/+* and *aPKC[k06403]* = 0.9449.

Clones of a temperature sensitive allele of aPKC

In order to quantify planar polarity in absence of aPKC activity in pupal wing cells, a temperature-sensitive form of aPKC is used to avoid the long-term poor viability and/or proliferation effect of strong *aPKC*- mutant.

Guilgur *et al.* isolated *aPKC[ts, temperature sensitive]* allele to study aPKC function in mitotic spindle orientation in larval wing discs (Guilgur *et al.*, 2012). In (Guilgur *et al.*, 2012), hemizygous (*aPKC[ts]/Df(2R)l4*) and heterozygous (*aPKC[ts]/aPKC[k06403]*) larvae were viable and morphologically normal at 25°C (described as permissive temperature); viable but morphologically abnormal at 27-28°C (described as semi-permissive temperature); the majority of pupae failed to emerge from the pupal case at 30°C (described as restrictive temperature), resembling the hemizygous mutant (*aPKC[k06403]/Df(2R)l4*) phenotype.

As shown in (Figure 2.2 A and F), in pupal wings aged at 25°C and 29°C, the *aPKC[ts]* clone size is reasonably big but no polarity change is observed. At a permissive temperature 25°C, immunolabelling of endogenous Fz shows no significant difference in polarity or membrane intensity among the homozygous, heterozygous, and wild-type cells (Figure 2.2 A-E), as expected. However, in the restrictive temperature 29°C, there is no significant difference as well (Figure 2.2 F-J), possibly due to retained kinase activity *in vivo*. Indeed, 27-28°C is considered as the semi-permissive temperature *in vivo* (Guilgur *et al.*, 2012), suggesting *aPKC[ts]* retains a considerable level of kinase activity at 29°C as it does not reach the 30°C restrictive temperature. Nevertheless, even *aPKC[ts]* at the 30°C restrictive temperature does not affect the apical localisation of Baz nor the phosphorylation of Baz (Guilgur *et al.*, 2012). The correct localisation of Baz depends on the phosphorylation by aPKC (Krahn *et al.*, 2010; Morais-de-Sa et al., 2010). These results suggest aPKC[ts] is still functional at 29°C in the pupal wing experiment. The retained kinase activity is possibly sufficient to maintain normal planar polarity.

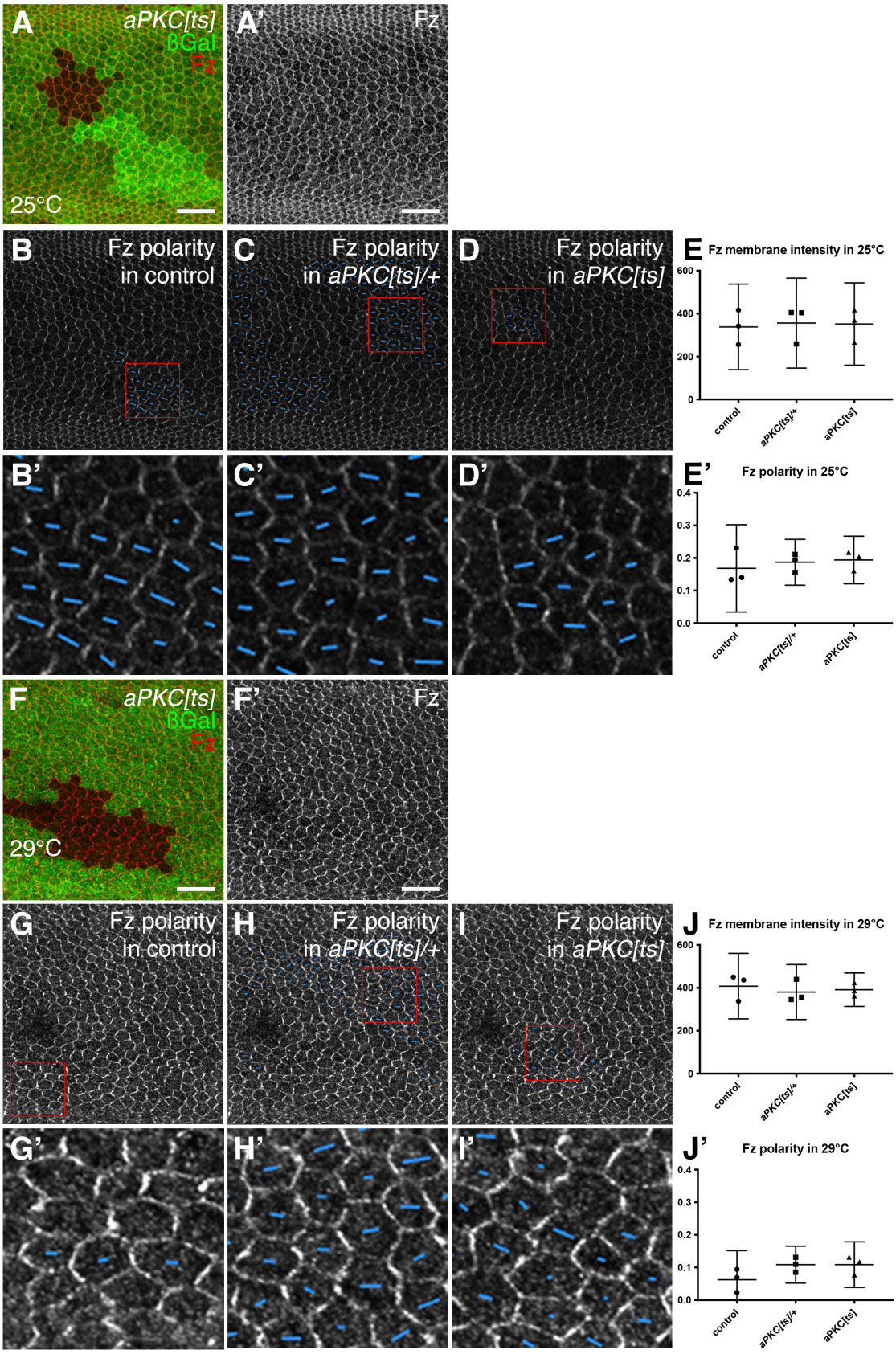

Figure 2.2 Fz in *aPKC[ts]* clones Figure legends in next page

Figure 2.2 Fz in *aPKC[ts]* clones

(A-A') APF Pupal wings aged at 25°C for 28 h, carrying twin clones of *aPKC[ts]* (homozygous *aPKC[ts]* tissue is indicated by the loss of green β-gal immunolabelling); β-gal is immunolabelled in green (A); Fz is immunolabelled in red (A) or grey (A'). Scale bar 20 μm.

(B-D') Blue lines represent single cell polarity nematics of Fz in 28 h APF Pupal wings aged at 25°C in panel A, in *arm-LacZ/arm-LacZ* control tissue (B), *aPKC[ts]/arm-LacZ* heterozygous tissue (C), and *aPKC[ts]/aPKC[ts]* tissue (D). Regions in red boxes are zoomed-in in panel (B'-D').

(E-E') Comparison of Fz intensity on the cell membrane (E) and Fz direct average polarity (E'). N = 3 wings, Error bar: 95% confidence interval.

(E) No significant difference in Fz membrane intensity is shown in the ANOVA test. p-value ANOVA results for comparisons between the control and *aPKC[ts]/+* = 0.9610; control and *aPKC[ts]* = 0.9770; *aPKC[ts]/+* and *aPKC[ts]* = 0.9978.

(E') No significant difference in Fz polarity is shown in the ANOVA test. p-value ANOVA results for comparisons between the control and *aPKC[ts]/+* = 0.8341; control and *aPKC[ts]* = 0.7147; *aPKC[ts]/+* and *aPKC[ts]* = 0.9736.

(F-F') Pupal wings aged at 29°C for 24 h, carrying twin clones of *aPKC[ts]* (homozygous *aPKC[ts]* tissue is indicated by the loss of green β-gal immunolabelling); β-gal is immunolabelled in green (F); Fz is immunolabelled in red (F) or grey (F'). Scale bar 20 μm.

(G-I') Blue lines represent single cell polarity nematics of Fz in 28 h APF Pupal wings aged at 29°C in panel F, in *arm-LacZ/arm-LacZ* control tissue (G), *aPKC[ts]/arm-LacZ* heterozygous tissue (H), and *aPKC[ts]/aPKC[ts]* tissue (I). Regions in red boxes are zoomed-in in panel (G'-I').

(J-J') Comparison of Fz intensity on the cell membrane (J) and Fz direct average polarity (J'). N = 3, Error bar: 95% confidence interval.

(J) No significant difference in Fz membrane intensity is shown in the ANOVA test. p-value ANOVA results for comparisons between the control and *aPKC[ts]/+* = 0.7833; control and *aPKC[ts]* = 0.9136; *aPKC[ts]/+* and *aPKC[ts]* = 0.9604.

(J') No significant difference in Fz polarity is shown in the ANOVA test. p-value ANOVA results for comparisons between the control and *aPKC[ts]/+* = 0.2103; control and *aPKC[ts]* = 0.2107; *aPKC[ts]/+* and *aPKC[ts]* > 0.9999.

Conditional expression of dominant-negative aPKC induces polarity swirls

Previous sections show that clonal analysis of a strong allele resulted in the generation of tiny clones that could not be sufficiently analysed while a temperature sensitive allele is suggested to be insufficient to induce polarity change. Therefore, in this section, other methods perturbing aPKC activity shall be examined.

A dominant-negative form of aPKC (aPKC[DN], containing a mutation (K293W) in the ATP binding site and a membrane-targeting CaaX motif (Gao et al., 2009)) has been reported to disrupt apicobasal polarity (Sotillos *et al.*, 2004). This can be used to manipulate aPKC activity in pupal wings to examine planar polarity change.

The Gal4/UAS system (Brand et al., 1994; Brand and Perrimon, 1993) is used to temporally express aPKC[DN]. When the Gal4 coding sequence is inserted downstream of a promoter (*engrailed(en)*(Johnson et al., 1995) or *patched(ptc)*(Hinz et al., 1994), in this experiment), the yeast transcriptional activator GAL4 can be expressed in the certain region of the wing where the promoter is functioning. The *aPKC[DN]* sequence was inserted downstream of the Upstream Activation Sequence (UAS), which can be bound by Gal4 and activates downstream gene expression. In this experiment, aPKC[DN] is spatial-temporally expressed in either the posterior of the wing (*en-Gal4* expression, yellow line on the left of Figure 2.4 A indicates the approximate *en-Gal4* expression region), or between veins 3-4 of the pupal wing (*ptc-Gal4* expression, yellow line on the left of Figure 2.5 indicates the approximate *ptc-Gal4* expression region) to examine if the polarity direction and polarity magnitude are altered relative to neighbouring wild-type tissue. Every wing is double-immunolabelled with Fmi and Stbm.

The wild-type wing stained for Fmi and Stbm is first examined as a control for conditional expression experiments. As expected, Fmi is asymmetrically localised on the proximal-distal cell junctions and polarity is also aligned along the proximal-distal axis (Figure 2.3, A-C).

Conditional expression of the dominant-negative form of aPKC changes the direction of polarity manifested as mis-localised core protein puncta. When aPKC[DN] was induced to express using *en-Gal4* in the posterior region of the wing, nemetics of the Fmi polarity was observed to change orientation (Figure 2.4, comparing B-B'' and C-C''). The same was observed in the *ptc* expression domain (Figure 2.5, comparing B-B'' and C-C''), showing the expression of aPKC[DN] affects planar polarity orientation in pupal wing cells. Notably, near the estimated *en*- and *ptc*- expression border, Fmi mis-localised to the anteroposterior cell membranes (Figure 2.4 A'' and Figure 2.5 A'', red arrows indicate the anteroposterior cell membranes localised Fmi), showing the expression of aPKC[DN] causes a non-autonomous effect near the expression border.

The expression of the dominant-negative form of aPKC also decreases the strength of polarity. Both Fmi (Figure 2.4 D, p-value < 0.0001) and Stbm (Figure 2.4 A',F, p-value = 0.0002; Figure 2.5 A',F p-value = 0.0012) polarity in the aPKC[DN] expressed tissue has a lower polarity magnitude than that of the internal-control wild-type tissue, showing a weaker asymmetrical localisation of the core proteins. However, Fmi polarity in *ptc*>aPKC[DN] tissue and control tissue show weak/no statistical difference (Figure 2.5 D, p-value = 0.0701). This may also support a change in polarity as the immunolabelled Stbm in the same wings show a significant difference in polarity (Figure 2.5 F). Thus, the expression of aPKC[DN] reduces planar polarity.

Besides the asymmetric localisation, the membrane intensity of Fmi and Stbm is also compared among wing regions with or without aPKC[DN] expression. Only subtle increase of Fmi membrane intensity in aPKC[DN] expression is observed (Figure 2.4 E, p-value = 0.0093; Figure 2.5 E, p-value = 0.0312). As the change in membrane intensity of Fmi is mild, and the immunolabelled Stbm in the same wings show no significant difference in membrane intensity (Figure 2.5 F), the role of aPKC in regulating core protein membrane level is needed to be further confirmed. At this stage, data shown here suggest that aPKC[DN] does not or only mildly increases core protein membrane levels.

Taken together my results in this section, strong *aPKC* allele twin-clones were generated but only small clones were found; clones of a temperature sensitive allele were then generated, which might be too weak to change planar polarity; the conditionally expressed dominant-negative form of aPKC finally provides evidence for aPKC regulating planar polarity in *Drosophila* pupal wings.

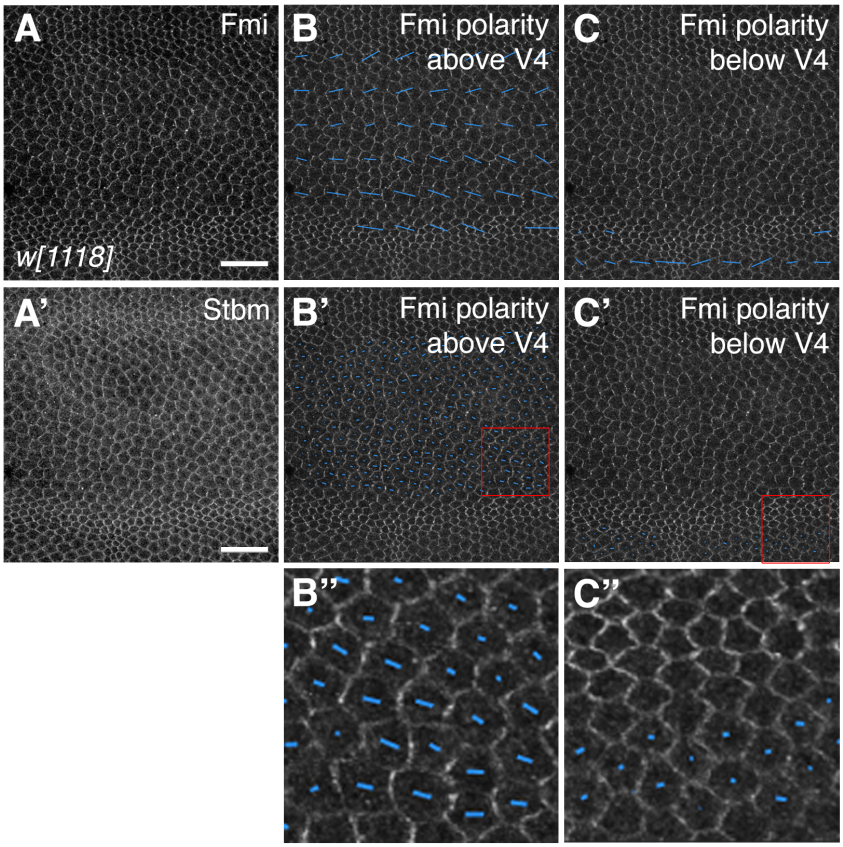

Figure 2.3 Core planar polarity protein polarity and intensity in *w[1118]* pupal wings

(A-A') Fmi (A) or Stbm (A') immunolabelling in 28h APF *w[1118]* wild-type pupal wings. Vein 3 is on the top and vein 4 is on the bottom. Scale bar 20 μm.

(B-C'') Blue lines represent polarity nematics of Fmi in panel A in the region between vein 3 and vein 4 (B) or below vein 4 (C). (B,C) Coarse-Grain polarity nematics averaged over a 3-cell size. (B',C') Single cell polarity nematics (B'',C'') zoomed-in of red box region.

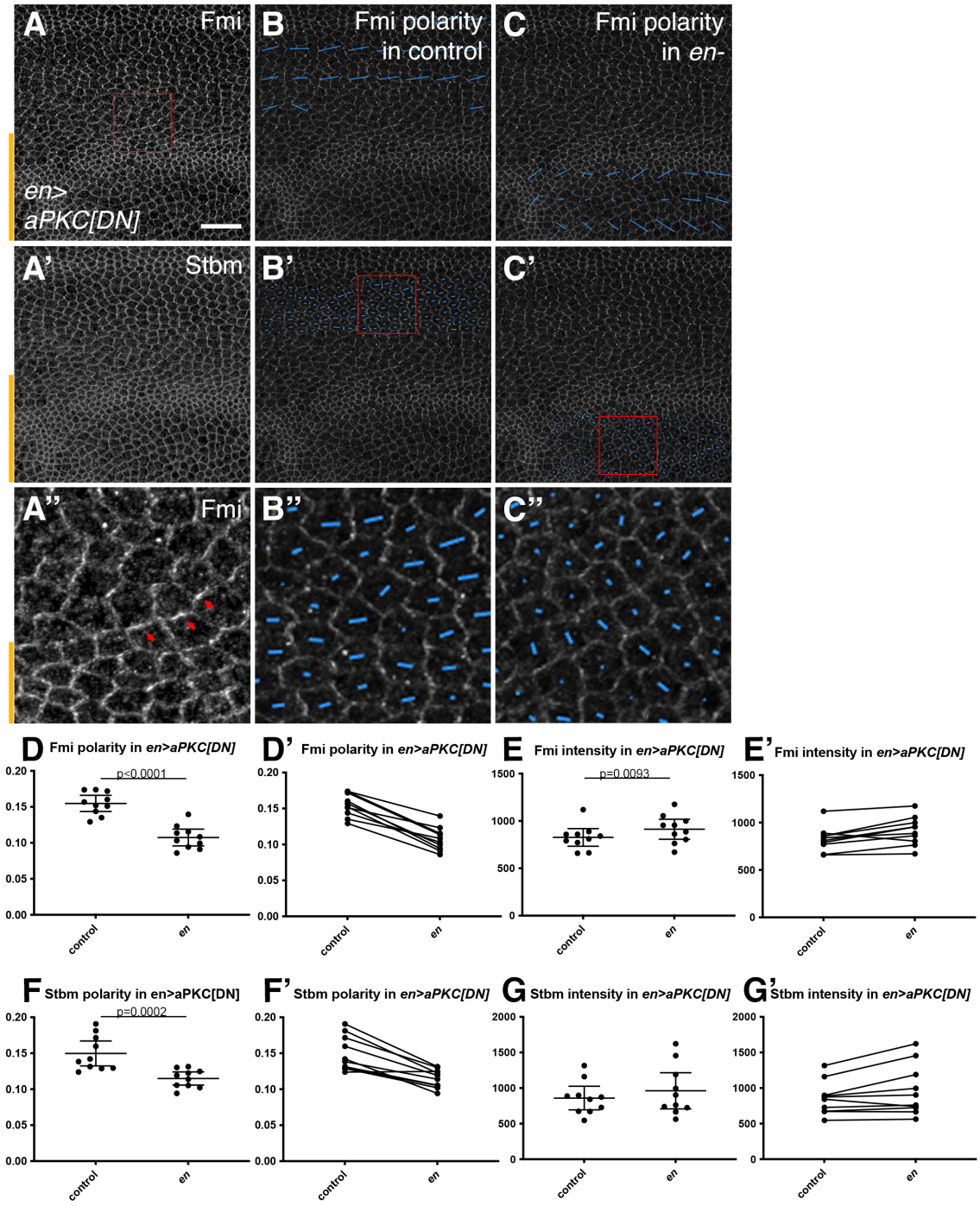

Figure 2.4 Core planar polarity protein polarity and intensity in *en>aPKC[DN]* pupal wings

(A-A'') Fmi (A) or Stbm (A') immunolabelling in 28h APF *en>aPKC[DN]* pupal wings aged at 25°C. The approximate *en* expression region is indicated by the yellow line on the left. (A'') Zoom-ed in of red box region in panel A, red arrows indicate mis-localised Fmi puncta localising to horizontal cell junctions near to the expression boundary. Scale bar 20 μm.

(B-C'') Blue lines represent polarity nematics of Fmi in panel A in control region

without *en* expression (B), *en* expression region (C). (B-C) Coarse-Grain polarity nematics averaged over a 3-cell size. (B'-C') Single cell polarity nematics (B''-C'') zoomed-in of red box region.

(D-D') Comparison of Fmi direct average polarity in *en>aPKC[DN]* pupal wings. Fmi polarity is lower in *en* expression region, p-value in two-tail two-sample Student's paired t-test < 0.0001, N = 10 wings. Error bar: 95% confidence interval. (D') Lines link polarity data points from the same wing.

(E-E') Comparison of Fmi membrane intensity in *en>aPKC[DN]* pupal wings. Fmi membrane intensity is slightly higher in *en* expression region, p-value in two-tail two-sample Student's paired t-test = 0.0093, N = 10 wings. Error bar: 95% confidence interval. (E') Lines link polarity data points from the same wing.

(F-F') Comparison of Stbm direct average polarity in *en>aPKC[DN]* pupal wings. Stbm polarity is lower in *en* expression region, p-value in two-tail two-sample Student's paired t-test = 0.0002, N = 10 wings. Error bar: 95% confidence interval. (F') Lines link polarity data points from the same wing.

(G-G') Comparison of Stbm membrane intensity in *en>aPKC[DN]* pupal wings. No significant difference in two-tail two-sample Student's paired t-test, p-value = 0.0538, N = 10 wings. Error bar: 95% confidence interval. (G') Lines link polarity data points from the same wing.

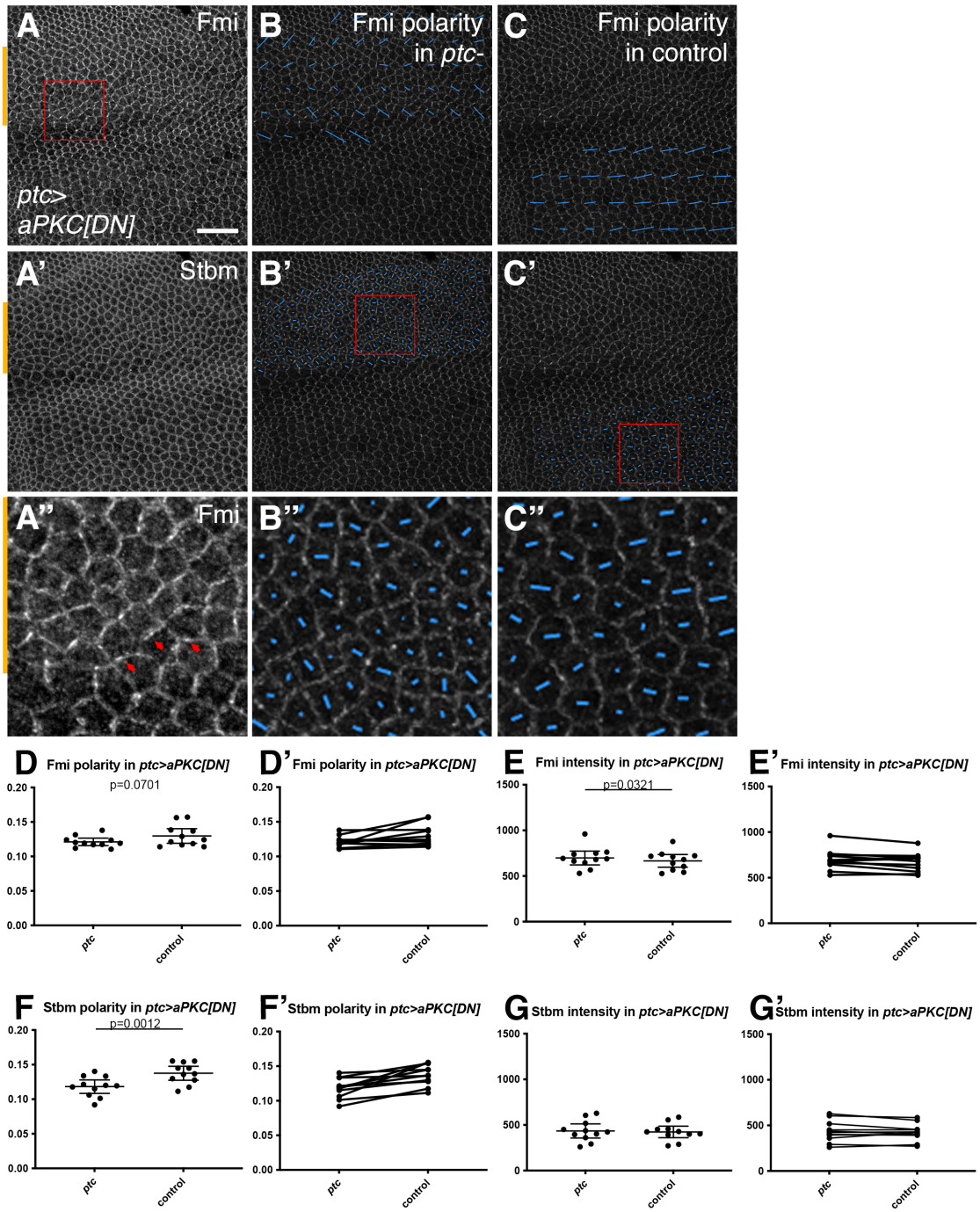

Figure 2.5 Core planar polarity protein polarity and intensity in *ptc>aPKC[DN]* pupal wings

(A-A'') Fmi (A) or Stbm (A') immunolabelling in 28h APF *ptc>aPKC[DN]* pupal wings aged at 25°C. The approximate *ptc* expression region is indicated by the yellow line on the left. (A'') Zoom-ed in of red box region in panel A, red arrows indicate mis-localised Fmi puncta localising to horizontal cell junctions near to the expression boundary. Scale bar 20 μm.

(B-C'') Blue lines represent polarity nematics of Fmi in panel A in *ptc* expression

region (B), control region without *ptc* expression (C). (B-C) Coarse-Grain polarity nematics averaged over a 3-cell size. (B'-C') Single cell polarity nematics (B''-C'') zoomed-in of red box region.

(D-D') Comparison of Fmi direct average polarity in *ptc>aPKC[DN]* pupal wings. No significant difference in two-tail two-sample Student's paired t-test, p-value = 0.0701, N = 11 wings. Error bar: 95% confidence interval. (D') Lines link polarity data points from the same wing.

(E-E') Comparison of Fmi membrane intensity in *ptc >aPKC[DN]* pupal wings. Fmi membrane intensity is slightly higher in *ptc* expression region, p-value in two-tail two-sample Student's paired t-test = 0.0321, N = 11 wings. Error bar: 95% confidence interval. (E') Lines link polarity data points from the same wing.

(F-F') Comparison of Stbm direct average polarity in *ptc >aPKC[DN]* pupal wings. Stbm polarity is lower in *ptc* expression region, p-value in two-tail two-sample Student's paired t-test = 0.0012, N = 11 wings. Error bar: 95% confidence interval. (F') Lines link polarity data points from the same wing.

(G-G') Comparison of Stbm membrane intensity in *ptc >aPKC[DN]* pupal wings. No significant difference in two-tail two-sample Student's paired t-test, p-value = 0.3790, N = 11 wings. Error bar: 95% confidence interval. (G') Lines link polarity data points from the same wing.

2.2.2 Kinases phosphorylating Dsh - Par-1

Par-1 was previously shown to be required for convergent extension in *Xenopus* (Ossipova *et al.*, 2005). Par-1 binds to and phosphorylates the S/T236-247 regions of Dsh in *Xenopus* embryo (Sun *et al.*, 2001) and mutations in these residues reduce the Fz-dependent Dsh membrane localisation (Ossipova *et al.*, 2005). Studies in *Drosophila* also found that mutations in S/T236-247 do not rescue the planar polarity defect in *dsh[1]* mutant in *Drosophila* (Penton *et al.*, 2002). However, whether Par-1 directly phosphorylates Dsh *in vivo* in the *Drosophila* pupal wing model, and whether it regulates Dsh localisation remains unknown. Thus, the role of Par-1 in planar polarity in *Drosophila* pupal wings is going to be tested here.

2.2.2.1 Par-1 hypomorphic allele clones show normal polarity

Par-1[k05603] is a hypomorphic allele previously used to study the polarity establishment in oocytes (Shulman et al., 2000; Tomancak et al., 2000). *Par-1[k05603]* clones marked by loss of ß-gal immunolabelling were generated to compare homozygous *par-1[k05603]* cells to wild-type control cells (Figure 2.6). No significant change in Dsh polarity was observed comparing homozygous *par-1[k05603]* clones to control tissue (Figure 2.6E, comparing B-B' to C'C'). Note that although the red box marked region in *par-1[k05603]* clones appear to have less bright membrane puncta (Figure 2.6, comparing B' to C'), the quantification shows no significant difference in membrane intensity of Dsh on the cell membrane (Figure 2.6 D). Thus, Dsh, the putative phosphorylation substrate of Par-1 (Ossipova *et al.*, 2005; Sun *et al.*, 2001), show normal asymmetric localisation on the cell membrane in *Par-1[k05603]* clones.

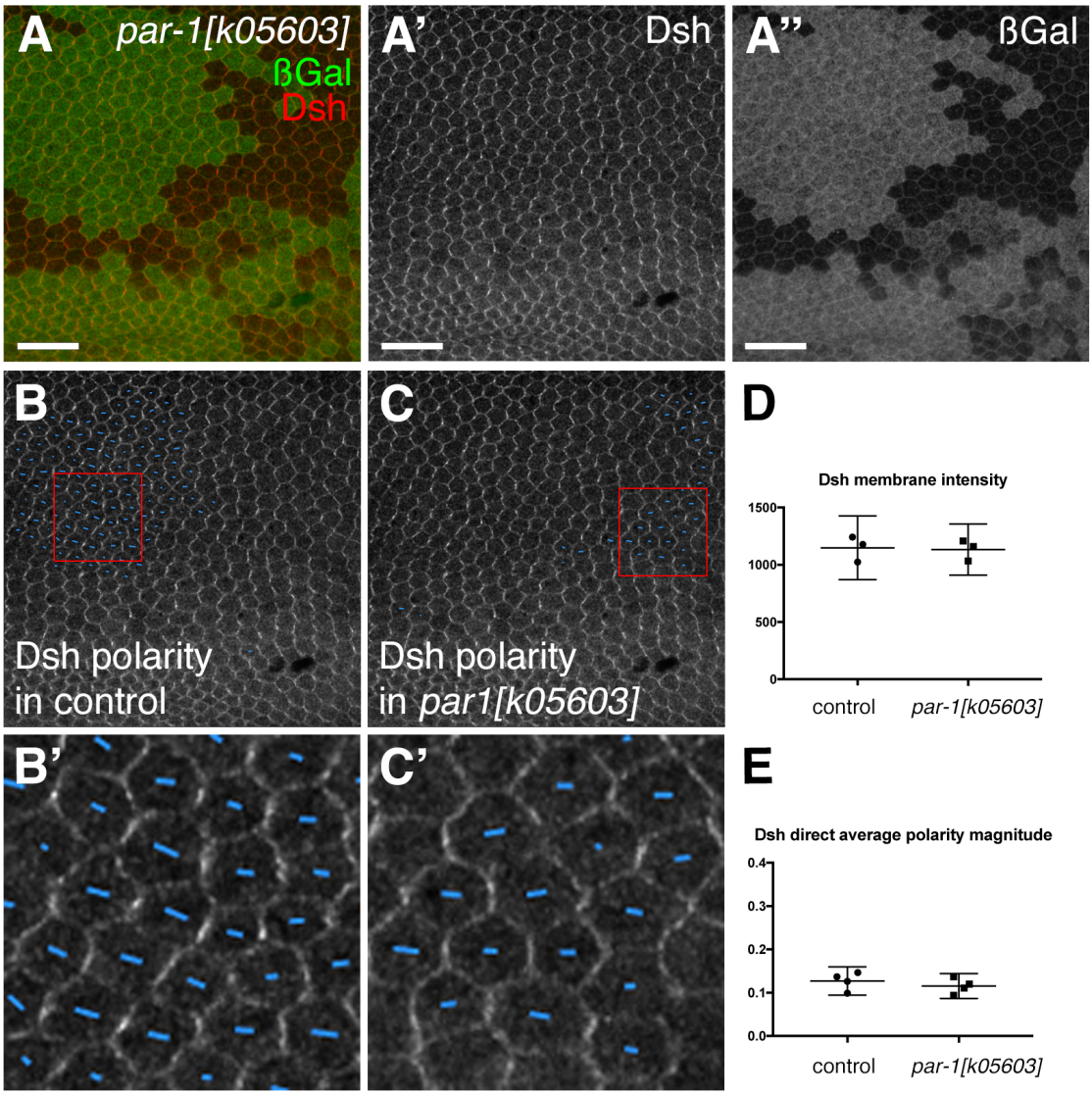

Figure 2.6 Dsh in *par-1[k05603]* allele clones

(A-A'') 28 h APF pupal wing, carrying twin clones of *par-1[k05603]* (homozygous *aPKC[k06403]* tissue is indicated by the loss of green β-gal immunolabelling (A'')); β-gal is immunolabelled with a secondary antibody cross-reaction to Rat anti-Ecad, in green (A) or grey (A''); Dsh is immunolabelled in red (A) or grey (A'). Scale bar 20 μm.
(B-C') Blue lines represent single cell polarity nematics of Dsh in panel A in *arm-LacZ/arm-LacZ* control tissue (B) and homozygous *par-1[k05603]* tissue (C). Regions in red boxes are zoomed-in in panel (B'-C').
(D-E) Comparison of Dsh membrane intensity (D) and polarity (E). No significant difference in membrane intensity (N = 3 wings) or polarity (N = 4 wings) between the control tissue and homozygous *par-1[k05603]* clones in two-tail two-sample Student's paired t-test. Error bar: 95% confidence interval.

2.2.2.2 Par-1 RNAi conditional expressions show normal polarity

Another attempt to examine the function of Par-1 is to knock-down its activity via RNAi. Operated by *Gal4*, cells with transgenic RNAi insertion express short hairpin RNA (shRNA), which via the endogenous microRNA pathway produces the small interfering RNA (siRNA) against its target mRNA, thus decreasing the expression of the target protein (Perkins et al., 2015). In the RNAi experiment described in this section, when RNAi against Par-1 (*TRiP.HMS00405*, see M&M) was expressed under *en-Gal4*, the planar polarity and the membrane intensity of Dsh and Fmi show no difference to its internal wild-type control (Figure 2.7, example image for Fmi not shown). This experiment, consistent with the *par-1[k05603]* hypomorphic allele clone experiment, does not support the conclusion that Par-1 regulates planar polarity in *Drosophila* pupal wings.

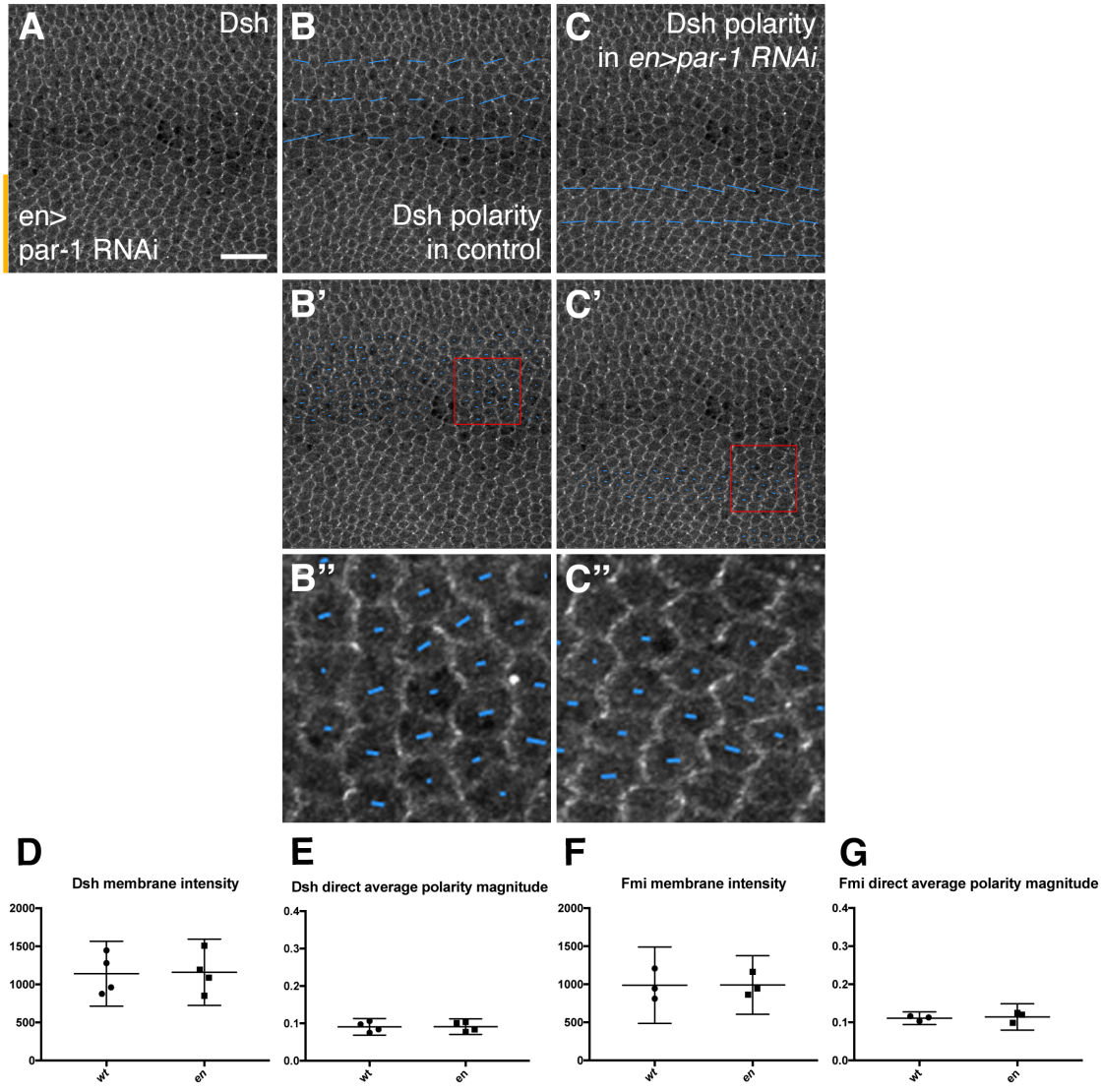

Figure 2.7 Core planar polarity protein polarity and intensity in *en>par-1 RNAi* pupal wings

(A) Dsh immunolabelling in 28h APF *en>par-1 RNAi* pupal wings. The approximate *en* expression region is indicated by the yellow line on the left. Scale bar 20 μm.

(B-C'') Blue lines represent polarity nematics of Dsh in panel A in control region without *en* expression (B), *en* expression region (C). (B-C) Coarse-Grain polarity nematics averaged over a 3-cell size. (B'-C') Single cell polarity nematics (B''-C'') zoomed-in of red box region.

(D-E) Comparison of membrane intensity (D) and polarity (E) of Dsh in *en>par-1 RNAi* pupal wings. N = 4 wings, no significant difference in two-tail two-sample Student's paired t-test. Error bar: 95% confidence interval.

(F-G) Comparison of membrane intensity (F) and polarity (G) of Fmi in *en>par-1 RNAi* pupal wings. N = 3 wings, no significant difference in two-tail two-sample Student's paired t-test. Error bar: 95% confidence interval.

2.2.2.3 Mutation on candidate phosphorylation site S/T236-247

As result in *Xenopus* supporting Par-1 regulates planar polarity via phosphorylation on Dsh in S/T236-247 region and reduces the Fz-dependent Dsh membrane localisation (Ossipova *et al.*, 2005). Studies in *Drosophila* found that mutations in S/T236-247 do not rescue the planar polarity defect in *dsh[1]* mutant in *Drosophila* (Penton *et al.*, 2002). Thus, I next want to check whether the phosphorylation site reported is also regulating planar polarity *in vivo* in *Drosophila* pupal wings. Note that there is no direct evidence showing S/T236-247 residues in Dsh can be directly phosphorylated by Par-1 or Dco *in vivo*, so the reported S/T236-247 residues are only putative Dco/CKIε phosphorylation sites.

Strutt et al. generated an Enhanced GFP (EGFP) tagged Dsh transgene, which rescues *dsh-* in pupal wings (Strutt *et al.*, 2016), by inserting the EGFP sequence into a *P[acman]* transgene covering the Dsh genomic region (Venken et al., 2009) on the N-terminal of unmutated *Dsh* coding sequence (marked as *EGFP-Dsh[wt]*)(Strutt *et al.*, 2016). Phosphomutant *Dsh[S/T236-247>A]*, mimicking a phosphor-inhibited status, and phosphomimetic *Dsh[S/T236-247>E]*, mimicking a permanently phosphorylated status, mutants were generated by mutating the reported phosphorylation site to Alanine (A) or Glutamic acid (E) in *EGFP-Dsh[wt]*. Thus, three transgenes, *EGFP-Dsh[wt]*, *EGFP-Dsh[S/T236-247>A]* (marked as *EGFP-Dsh[A]*) and *EGFP-Dsh[S/T236-247>E]* (marked as *EGFP-Dsh[E]*), were generated (Figure 2.8 A), see **Materials and Methods 6.1.3**.

By using a genomic rescue strategy where *P[acman]* transgenes express wild-type or mutated EGFP-Dsh in *dsh-* mutant background, whether S/T236-247 are possible phosphorylation sites was tested and the possible effect of phosphorylation on these sites is examined.

The phenotype in adult wings was first checked. As shown in **Table 2.1**, neither EGFP-Dsh[A] nor EGFP-Dsh[E] fully rescues the planar polarity defect phenomenon in adult

Drosophila notum and wing, consistent with a previous publication where EGFP-Dsh[A] cannot rescue the wing hair swirling phenotype (Strutt *et al.*, 2019a). These results show S/T236-247 residues affect the Dsh function in planar polarity.

As *dsh[V26]* allele is lethal, clones of *dsh[V26]* were generated to compare EGFP-Dsh[wt], EGFP-Dsh[A], and EGFP-Dsh[E] in *dsh*- mutant background in pupal wings. EGFP-Dsh[wt] localises asymmetrically while both phosphomutant (p-value < 0.0001) and phosphomimetic (p-value < 0.0001) forms of EGFP-Dsh have weaker asymmetrical localisation than wild-type EGFP-Dsh (Figure 2.8. B, C-E), suggesting compromised Dsh activity. The membrane intensity of EGFP-Dsh[A] (p-value = 0.0004) and phosphomimetic EGFP-Dsh[E] (p-value < 0.0001) is also lower than that of EGFP-Dsh[wt] (Figure 2.8 B'). The reduction in membrane intensity can be a consequence of either reduction in Dsh protein level or a reduction of Dsh localisation on the plasma membrane. As the Western Blot for pupal wing lysate showing the overall protein level in pupal wing cells is relatively equal (Figure 2.8 F), mutations in S/T236-247 residues are likely to affect Dsh localisation on the cell membrane. These results suggesting the phosphorylation in S/T236-247 residues regulate Dsh protein sorting to the cell membrane and affect its asymmetric localisation. However, it is noticed that the EGFP-Dsh[A] and EGFP-Dsh[E] have a similar extent of reduction in membrane intensity and asymmetrical localisation in pupal wings.

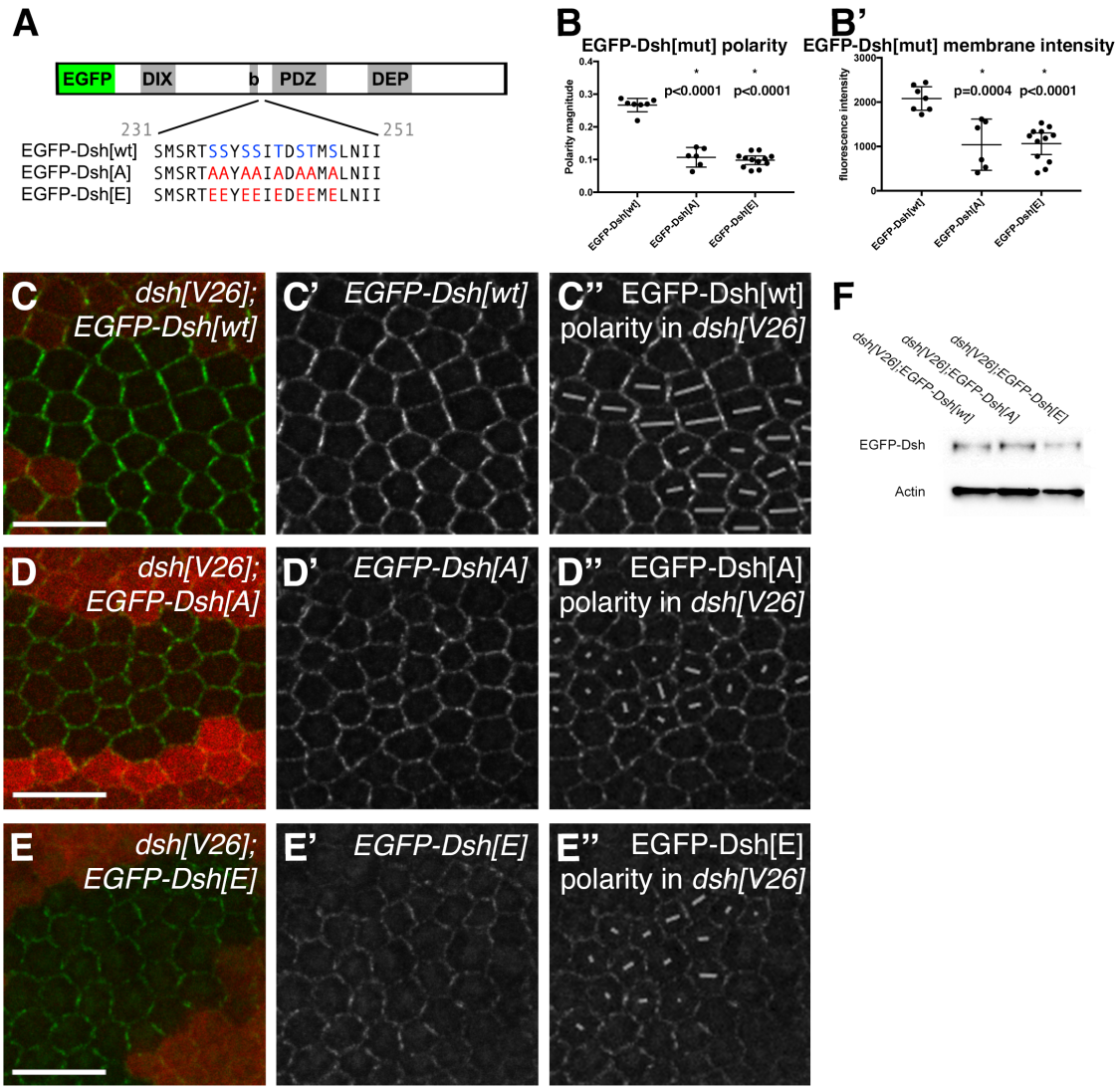

Figure 2.8 Phosphorylation site mutations in Dsh affect its membrane localisation and polarity

(A) Schematic for the amino acid sequence of Serine/Threonines rich basic region in EGFP-Dsh. Putative Serine/Threonines kinases phosphorylation sites on Dsh are marked in blue. Mutated amino acids to either Alanine (A) or Glutamic acid (E) are shown in red.

(B-B') Comparison of EGFP-Dsh mutant (EGFP-Dsh[mut]) polarity (B) and membrane intensity (B'). Error bars: 95% confidence intervals.

(B) Both EGFP-Dsh[A] (N = 6 wings) and EGFP-Dsh[E] (N = 12 wings) show weaker polarity comparing to EGFP-Dsh[wt] (N = 7 wings). p-value ANOVA results for comparisons between EGFP-Dsh[wt] and EGFP-Dsh[A] < 0.0001; EGFP-Dsh[wt] and EGFP-Dsh[E] < 0.0001. No significant difference between EGFP-Dsh[A] and EGFP-Dsh[E], p-value ANOVA = 0.7231.

(B') Both EGFP-Dsh[A] (N = 6 wings) and EGFP-Dsh[E] (N = 12 wings) show lower

membrane intensity comparing to EGFP-Dsh[wt] (N = 7 wings). p-value ANOVA results for comparisons between EGFP-Dsh[wt] and EGFP-Dsh[A] = 0.0004; EGFP-Dsh[wt] and EGFP-Dsh[E] < 0.0001. No significant difference between EGFP-Dsh[A] and EGFP-Dsh[E], p-value ANOVA = 0.9926.

(C-E'') 28 h APF pupal wing, carrying twin clones of *EGFP-Dsh[wt]* (C-C''), *EGFP-Dsh[A]* (D-D''), or *EGFP-Dsh[E]* (D-D'') in *dsh[V26]* background. Homozygous *EGFP-Dsh[mut]* clones are indicated by the loss of red β-gal immunolabelling in (C-E). Scale bar 10 μm. (C''-E'') Grey lines represent polarity nematics of EGFP-Dsh[wt] (C''), EGFP-Dsh[A] (D''), or EGFP-Dsh[E] (E'').

(F) Western blot probed with Dsh antibody of extracts from 28 h APF pupal wings from *dsh[V26];EGFP-Dsh[wt]*, *dsh[V26];EGFP-Dsh[A]*, or *dsh[V26];EGFP-Dsh[E]* flies. Actin is used as loading control.

Table 2.1 Adult phenotypes of flies carry S/T236-247 mutated or Y473>F mutated EGFP-Dsh in *dsh-* background

Genotype	Notum	Leg joint	Wing hair	Pupal wing
dsh[1]/Y	Strong hair swirling phenotype	Ectopic joint	Strong hair swirling phenotype	-
dsh[1]/Y; EGFP-Dsh[ST236-247>A]/+	Partly rescue	No ectopic joint	No rescue	Symmetrical localisation
dsh[1]/Y; EGFP-Dsh[ST236-247>E]/+	Partly rescue	No ectopic joint	No rescue	Symmetrical localisation
dsh[1]/Y;EGFP-Dsh[wt]/+	Fully rescue	No ectopic joint	Fully rescue	Asymmetrical localisation
dsh[1]/Y; EGFP-Dsh[Y473>F]/+	Strong hair swirling phenotype	Ectopic joint	No rescue	Weak membrane localisation
dsh[V26]/Y; EGFP-Dsh[ST236-247>A]	-	No ectopic joint	Shrunk wings	-
dsh[V26]/Y; EGFP-Dsh[ST236-247>E]	-	No ectopic joint	No rescue	-

dsh[1] is a planar polarity-specific mutant allele

dsh[V26] is an amorphic allele

Another method used to test the possible effect of phosphorylation is the Fluorescence Recovery After Photobleaching (FRAP) approach. FRAP is a method for quantifying the protein dynamics and stability on the cell junctions (Strutt *et al.*, 2011; Warrington *et al.*, 2017). By bleaching fluorescent-protein-tagged protein on the chosen region along cell junctions (Figure 2.9 A-A'), the recovery fluorescent signal is expected to be recovered (Figure 2.9 A'') due to the turnover of proteins. The more stable the protein is, the less recovery signal would be detected as there is a smaller mobile fraction (Figure 2.9 B), also see **Materials and Methods 6.2.7**. Both EGFP-Dsh[A] (p-value = 0.0020) and EGFP-Dsh[E] (p-value = 0.0005) mutants show higher fluorescence recovery compared to wild-type EGFP-Dsh, while the fluorescence recovery of EGFP-Dsh[A] and EGFP-Dsh[E] is not statically different (p-value = 0.0819)(Figure 2.9 C).

In summary, results in this section show that reducing Par-1 activity does not affect Dsh polarity and membrane intensity, in the hypomorphic allele clones and in RNAi knock-down tissue. Thus, the regulatory role of Par-1 in planar polarity in *Drosophila* wings is not supported. I also mutated the putative Par-1 and/or Dco phosphorylation sites in Dsh, where both phosphomutant and phosphomimetic EGFP-Dsh exhibit reduced polarity strength, Dsh membrane level, and Dsh mobility, showing these residues are important for Dsh function. It is worth noticing that an online tool predicting kinase specific phosphorylation sites, NetPhos ((Blom et al., 1999), https://services.healthtech.dtu.dk/service.php?NetPhos-3.1), predicts that the S/T236-247 region shown in (Figure 2.8 A) is phosphorylated by multiple serine/threonine protein kinases other than Par-1 and Dco. Thus, the effects of the mutations on putative phosphorylation sites can be redundant by multiple kinases. However, it is still unclear whether the phosphorylation on these residues is important as no opposite effects were observed between phosphomutant and phosphomimetic. Lack of an opposite effect leaves the question open, as the phosphomimetic mutations might not be sufficiently charged to mimic phosphorylated serine and threonine.

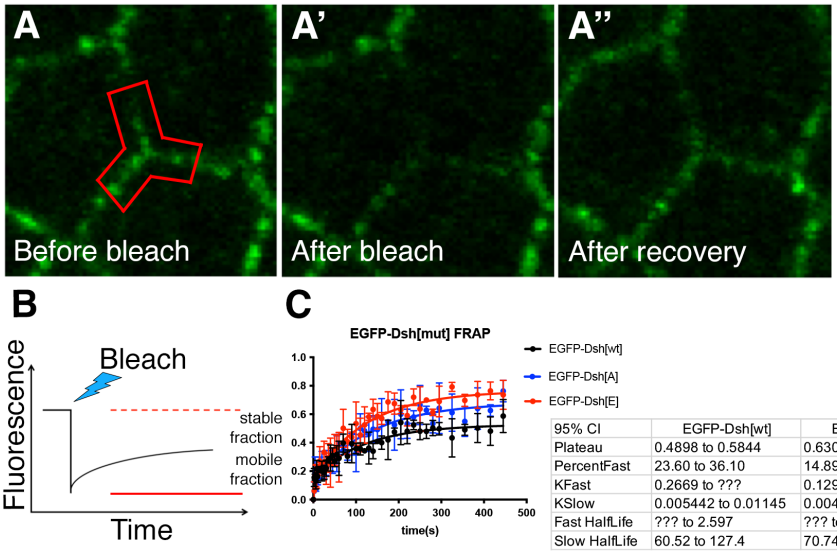

95% CI	EGFP-Dsh[wt]	EGFP-Dsh[A]	EGFP-Dsh[E]
Plateau	0.4898 to 0.5844	0.6301 to 0.7652	0.7151 to 0.8359
PercentFast	23.60 to 36.10	14.89 to 28.11	13.78 to 26.37
KFast	0.2669 to ???	0.1293 to ???	0.1473 to ???
KSlow	0.005442 to 0.01145	0.004846 to 0.009798	0.005731 to 0.01029
Fast HalfLife	??? to 2.597	??? to 5.362	??? to 4.705
Slow HalfLife	60.52 to 127.4	70.74 to 143.0	67.33 to 120.9

Figure 2.9 Phosphorylation site mutations in Dsh affect its mobility

(A-A'') Example images showing EGFP-Dsh[wt] fluorescent proteins on cell junctions before bleaching (A), after bleaching (A'), and after 595 seconds recovery (A''). The bleached region is marked in red. The example images were taken in a 6 h APF *y w dsh[V26]; P[acman]-EGFP-Dsh* prepupal wing treated with a chemical Dco inhibitor.

(B) Example curve shows the fluorescence recovery after bleaching. The ed dotted line represents the initial fluorescence before bleaching and 100% relative recovery (1.0 in a FRAP); the red line represents the fluorescence after bleaching and 0% relative recovery (0.0 in a FRAP).

(C) FRAP analysis on 28h APF pupal wings of genotype *dsh[V26]/Y;EGFP- Dsh[wt]* (n=3), *dsh[V26]/Y;EGFP-Dsh[A]* (n=3), and *dsh[V26]/Y;EGFP-Dsh[E]* (n=3). Error bar: standard deviation. Curves are fitted in two-phase exponential association, parameters in fitted curves are summarised in the table on the right, the '???' in the table indicate the curve fitting that is uncertain. Curves for EGFP-Dsh[wt] is in black, for EGFP-Dsh[A] is in blue, and for EGFP-Dsh[E] is in red. The recovery plateau of EGFP-Dsh[A] (p-value = 0.0020) and EGFP-Dsh[E] (p-value = 0.0005) is higher than that of EGFP-Dsh[wt]. The recovery plateau of EGFP-Dsh[A] and EGFP-Dsh[E] is not statically different (p-value = 0.0819). Statistical significance calculated by extra sum-of-squares F test.

2.2.3 Abl

2.2.3.1 Dsh[Y473>F] doesn't rescue adult phenotype

DshY473 residue is found to be phosphorylated by Abl *in vitro* and in transfected HEK293T cells, and is essential for Dsh function in planar polarity in *Drosophila* wings and eyes (Singh *et al.*, 2010; Yanfeng *et al.*, 2011). To dissect whether the phosphorylation of the Y473 residue is crucial for Dsh phosphorylation and membrane localisation, a *P[acman]-EGFP-Dsh[Y473>F]* construct was made, which carries the Y473>F mutation preventing Dsh phosphorylation (**Materials and Methods 6.1.3**).

In *dsh[1]* mutant *Drosophila*, wing hairs exhibited swirling patterns and ectopic joints were observed as shown in (Figure 2.10 F-F'). In the presence of EGFP-Dsh[wt], those phenotypes were rescued such that wing hairs aligned in the proximodistal axis, and no ectopic joint was found (Figure 2.10 D-D'), similar to the wild-type control (Figure 2.10 C-C'). However, the *P[acman]-EGFP-Dsh[Y473>F]* insertion cannot rescue the planar polarity phenotype (Figure 2.10 E-E', Table 2.1), showing Y473>F mutation disrupts Dsh function in planar polarity.

Supporting this, the membrane localisation of EGFP-Dsh[Y473>F] protein was significantly reduced in a *dsh[V26]* amorphic mutant background (Figure 2.10 A-B, comparing A'' to B''). This data shows that Y473 residue is essential for Dsh recruitment.

In contrast to the Y473>F phosphomutant, a phosphomimetic mutation is also wanted on the DshY473. However, there is no phosphomimetic mutant for Tyr, so this experiment cannot be performed.

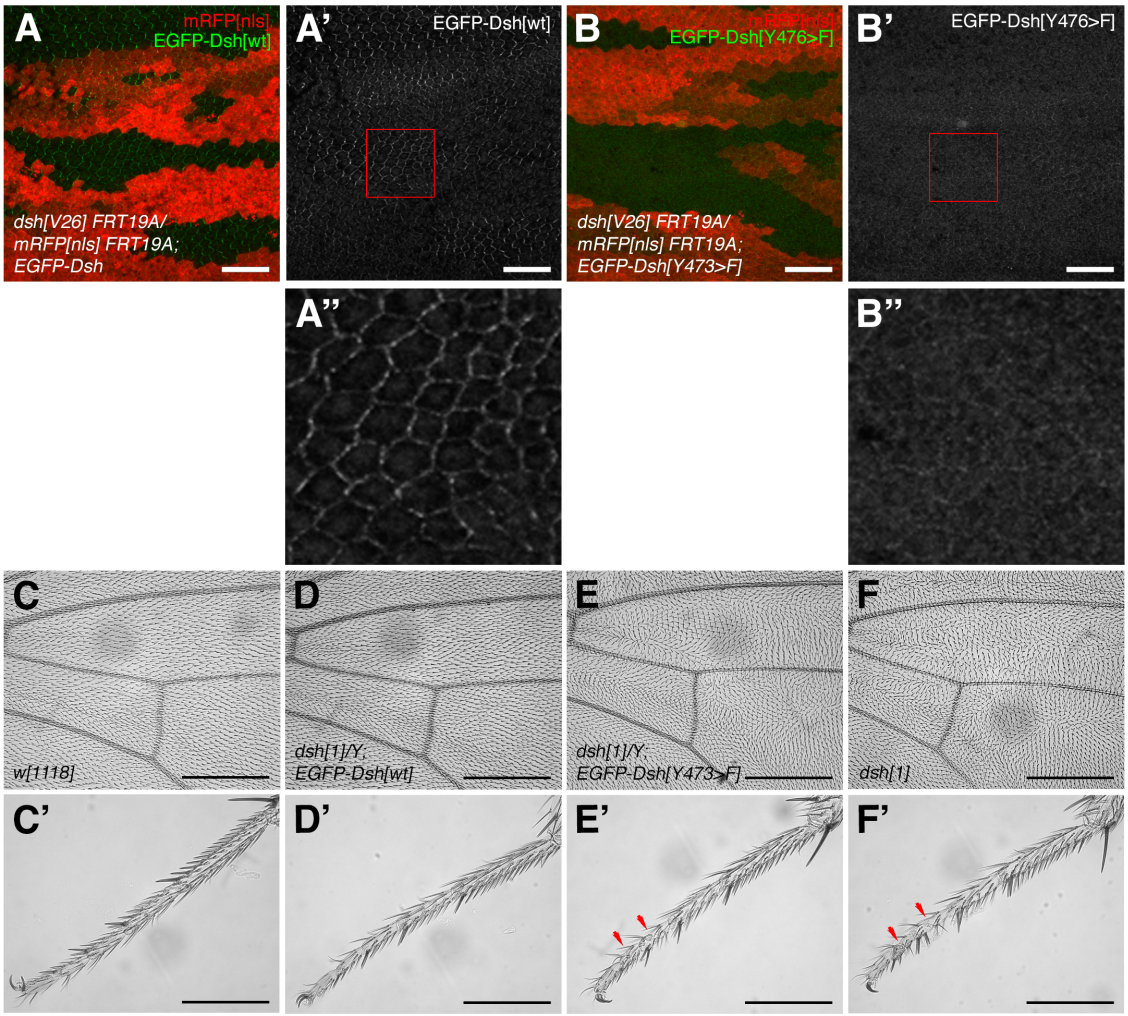

Figure 2.10 Dsh[Y473>F] shows poor membrane localisation and does not rescue *dsh[V26]* phenotype

(A-B'') 28 h APF pupal wing expressing EGFP-Dsh[wt] (A-A'') or EGFP-Dsh[Y473>F] (B-B''), carrying twin clones of *dsh[V26]* (homozygous *dsh[V26]* tissue is indicated by the loss of red mRFP signals). EGFP-Dsh[wt] or Dsh[Y473>F] is shown in green (in A or B, respectively) or grey (in A' or B', respectively). (A'',B'') Zoomed-in of red box region in *dsh[V26]* clones show Dsh[Y473>F] (B'') show weaker membrane localisation compared to EGFP[wt] (A''). Scale bar 20 µm.

(C-F') Wings (C-F) and legs (C'-F') from *w[1118]* (C,C'), *dsh[1]/Y;EGFP-Dsh* (D,D'), *dsh[1]/Y;EGFP-Dsh[Y473>F]* (E,E'), or *dsh[1]* (F,F') adults. Wing hairs point distally in (C,D) but no distal alignment in (E,F); no ectopic leg joint in (C',D'), red arrows indicate ectopic leg joints in (E',F'). Scale bar 200 µm.

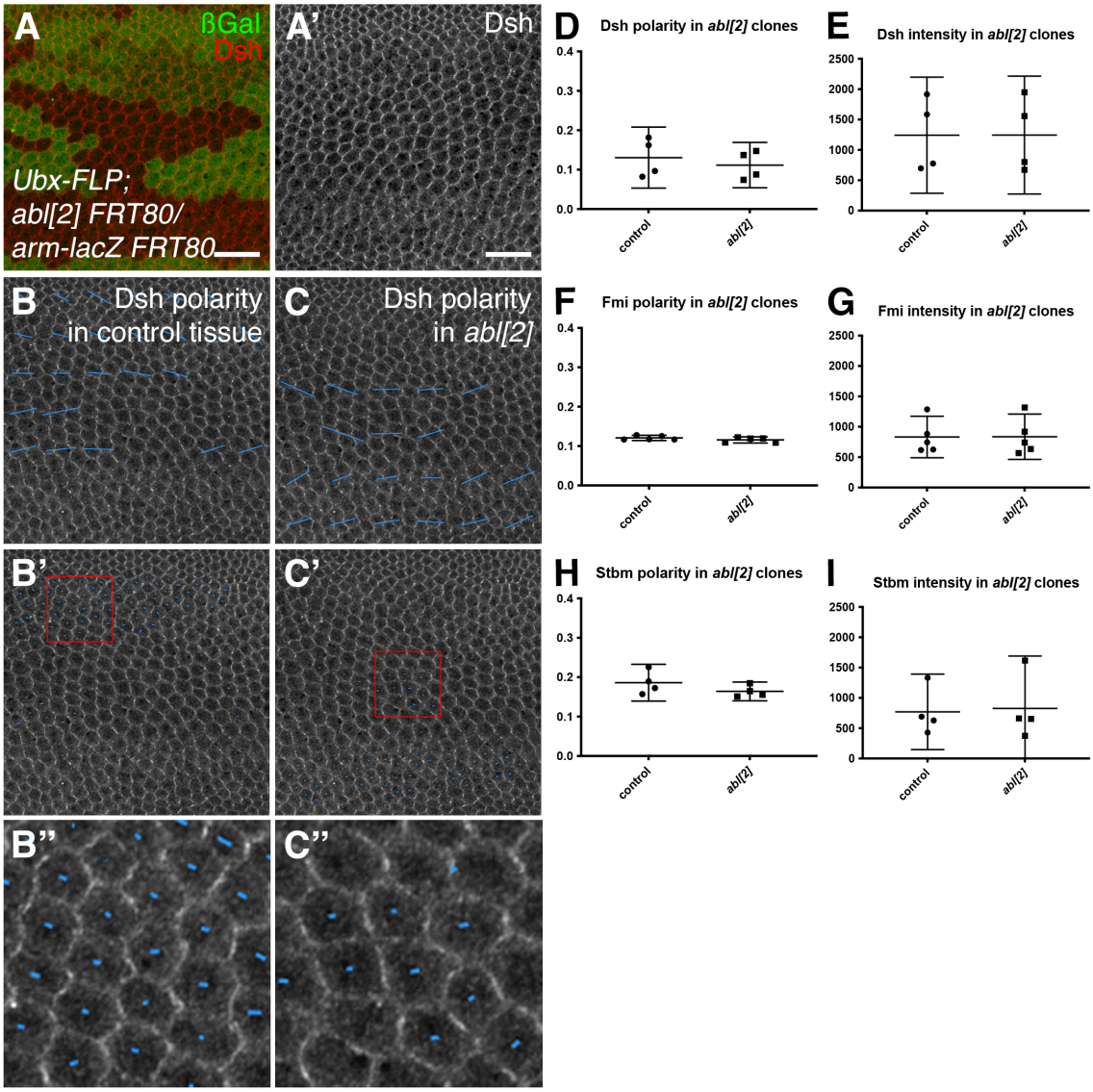

Figure 2.11 *abl[2]* allele clones show no change in core planar polarity protein localisation and polarity

(A,A') 28 h APF pupal wing, carrying twin clones of *abl[2]* (homozygous *abl[2]* tissue is indicated by the loss of green β-gal immunolabelling); Dsh is immunolabelled in green (A) or grey (A'). Scale bar 20 μm.

(B-C'') Blue lines represent polarity nematics of Dsh in panel A in *arm-LacZ/arm-LacZ* control tissue (B), and homozygous *abl[2]* tissue (C). (B-C) Coarse-Grain polarity nematics averaged over a 3-cell size. (B'-C') Single cell polarity nematics (B''-C'') zoomed-in of red box region.

(D,F,H) Comparison of the polarity of Dsh (D), Fmi (F), or Stbm (H) comparing control tissue to *abl[2]* clones. No significant difference in two-tail two-sample Student's paired t-test, (D) p-value = 0.1167, N = 4 wings; (F) p-value = 0.2569, N = 5 wings; (H) p-value = 0.0695, N = 4 wings. Error bar: 95% confidence interval.

(E,G,I) Comparison of membrane intensity of Dsh (E), Fmi (G), or Stbm (I) comparing

control tissue to *abl[2]* clones. No significant difference in two-tail two-sample Student's paired t-test, (E) p-value = 0.8895, N = 4 wings; (G) p-value =0.8047, N = 5 wings; (I) p-value =0.5236, N = 4 wings. Error bar: 95% confidence interval.

2.2.3.2 Abl amorphic allele *abl[2]* clones show normal polarity

As the DshY473 residue is shown to be important for Dsh membrane localisation, the next question is whether Abl kinase plays a role in pupal wing cells. If Abl phosphorylates Dsh on Y473 residue, a weaker Dsh membrane localisation is expected when Abl activity is reduced.

To test this, *abl[2]* amorphic allele, which has a nonsense mutation in its kinase domain (Smith and Liebl, 2005), twin-clones were generated. However, no significant change in protein level on cell membrane is observed in immunolabelled Dsh (Figure 2.11 E), Fmi (Figure 2.11 G), and Stbm (Figure 2.11 I), comparing homozygous *abl[2]* cells to control cells (Figure 2.11 comparing B-B'' to C-C''). In addition, core protein polarity was not affected (Figure 2.11 D,F,H). Hence, the reduced Dsh membrane localisation phenotype, as shown in DshY473>F phosphomutant (Figure 2.10), is not observed in *abl-* mutant tissue, suggesting that Abl phosphorylation is not crucial for Dsh membrane localisation.

2.2.3.3 Conditional Abl overexpression and Abl RNAi

As a supplementary to the *abl[2]* mutant clonal experiment, Abl was overexpressed and Abl RNAi was expressed under the control of *ptc-Gal4* (Figure 2.12) or *en-Gal4* (Figure 2.13), Fmi and Stbm were stained to check if the core protein localisation is affected.

Consistent with the twin-clone results described in **Section 2.2.3.2** (Figure 2.11), no obvious difference was observed in membrane protein level in immunolabelled Fmi (Figure 2.12 H,J; Figure 2.13 H,J) or Stbm (Figure 2.12 L,N; Figure 2.13 L). These results suggest that Abl phosphorylation is not crucial for core protein membrane level.

It is noticed that the polarity strength of Fmi (Figure 2.12 I, p-value = 0.0066) and Stbm (Figure 2.12 M, p-value = 0.0302) has a minor but statistically significant increase in *ptc>Abl RNAi* tissue compared to control tissue. This is not observed in *en>Abl RNAi* expressed wings (Figure 2.13 I,K) and *abl[2]* mutant clones (Figure 2.11 D,F,H). Also, comparing Abl overexpression tissue to control tissue, the strength of planar polarity of Fmi (Figure 2.12 G, Figure 2.13 G) and Stbm (Figure 2.12 K) is not significantly affected. Hence, no robust conclusion can be drawn on whether Abl affects planar polarity. However, cells near *ptc*- expression region boundary appear to be irregular and core protein puncta was observed to be mis-localised (Figure 2.12 A,B'', red arrows). As Abl has been reported to regulate epithelial morphogenesis via regulating adherens junctions and cytoskeleton (Fox and Peifer, 2007; Grevengoed et al., 2001), the effect of Abl overexpression in core protein mis-localisation can be indirect via affecting pupal wings cell shape.

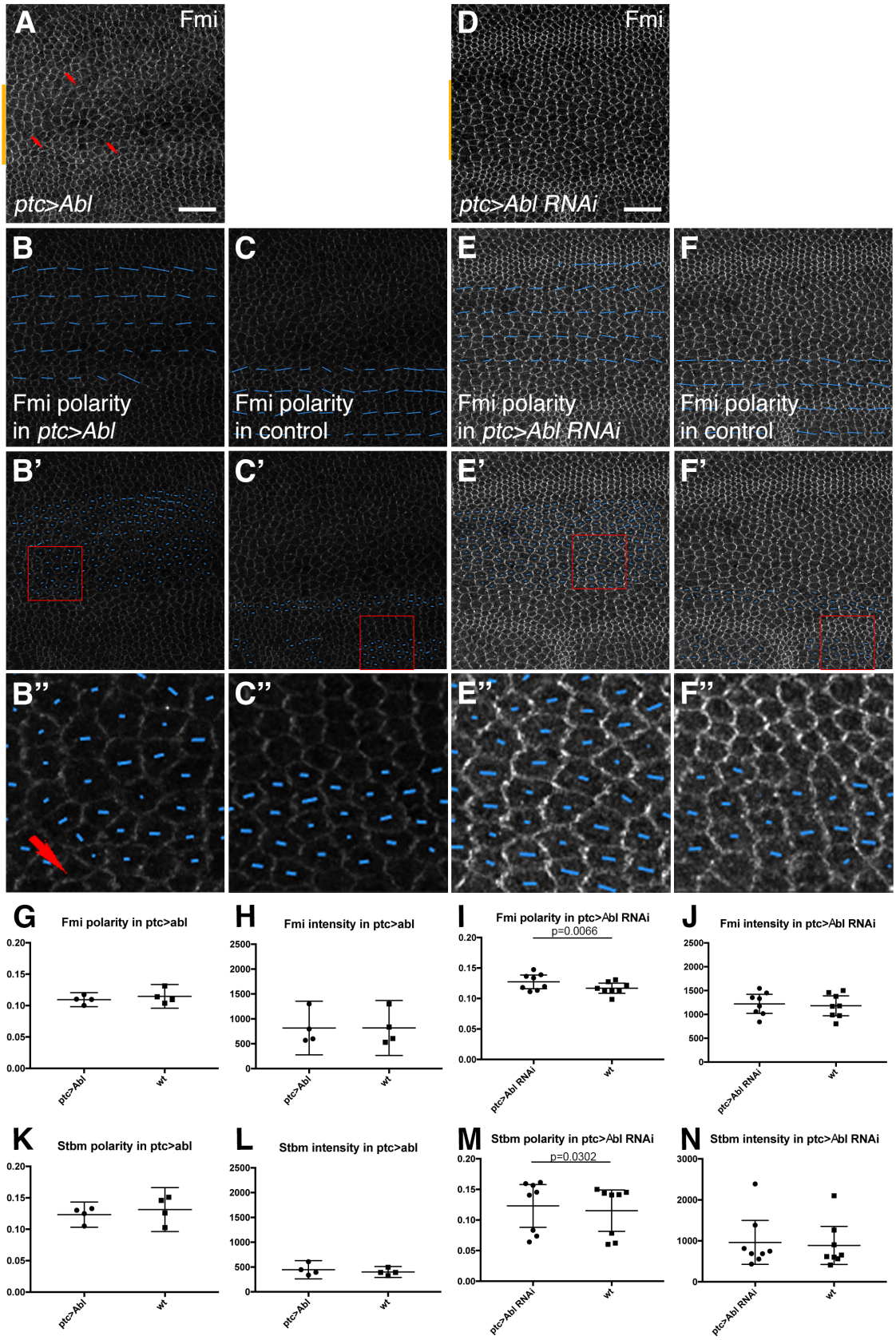

Figure 2.12 Core planar polarity protein polarity and intensity in *ptc>Abl* and *ptc>Abl RNAi* pupal wings Figure legends in next page

Figure 2.12 Core planar polarity protein polarity and intensity in *ptc>Abl* and *ptc>Abl RNAi* pupal wings

(A,D) *ptc>Abl* (A) or *ptc>Abl RNAi* (D) expressing 28h APF pupal wings. Fmi is immunolabelled in grey. The *ptc* expression region is indicated by the yellow line on the left. (A) Red arrows indicate mis-localised Fmi puncta. Scale bar 20 μm.

(B-C'') Blue lines represent polarity nematics of Fmi in panel A in *ptc>Abl* expressed region (B) and no *ptc* expression control region (C). (B-C) Coarse-Grain polarity nematics averaged over a 3-cell size. (B'-C') Single cell polarity nematics (B''-C'') zoomed-in of red box region. Red arrow in (B'') indicate mis-localised Fmi puncta as shown in panel A.

(E-F'') Blue lines represent polarity nematics of Fmi (in D) in *ptc>Abl RNAi* expressed region (E) and no *ptc* expression control region (F). (E-F) Coarse-Grain polarity nematics averaged over a 3-cell size. (E'-F') Single cell polarity nematics (E''-F'') zoomed-in of red box region.

(G-H) Comparison of Fmi polarity (G) and membrane intensity (H) comparing *ptc>Abl* expressed tissue to control tissue. No significant difference in polarity (G, N = 4 wings, p-value = 0.1822) or membrane intensity (H, N = 4 wings, p-value = 0.9296) in two-tail two-sample Student's paired t-test. Error bar: 95% confidence interval.

(I-J) Comparison of Fmi polarity (I) and membrane intensity (J) comparing *ptc>Abl RNAi* expressed tissue to control tissue. Fmi polarity is higher in *ptc>Abl RNAi* expressed tissue (I, N = 8 wings, p-value = 0.0066). No significant difference in membrane intensity (J, N = 8 wings, p-value = 0.1322) in two-tail two-sample Student's paired t-test. Error bar: 95% confidence interval.

(K-L) Comparison of Stbm polarity (K) and membrane intensity (L) comparing *ptc>Abl* expressed tissue to control tissue. No significant difference in polarity (K, N = 4 wings, p-value = 0.2132) or membrane intensity (L, N = 4 wings, p-value = 0.1649) in two-tail two-sample Student's paired t-test. Error bar: 95% confidence interval.

(M-N) Comparison of Stbm polarity (M) and membrane intensity (N) comparing *ptc>Abl RNAi* expressed tissue to control tissue. Fmi polarity is higher in *ptc>Abl RNAi* expressed tissue (M, N = 8 wings, p-value = 0.0302). No significant difference in membrane intensity (N, N = 8 wings, p-value = 0.1093) in two-tail two-sample Student's paired t-test. Error bar: 95% confidence interval.

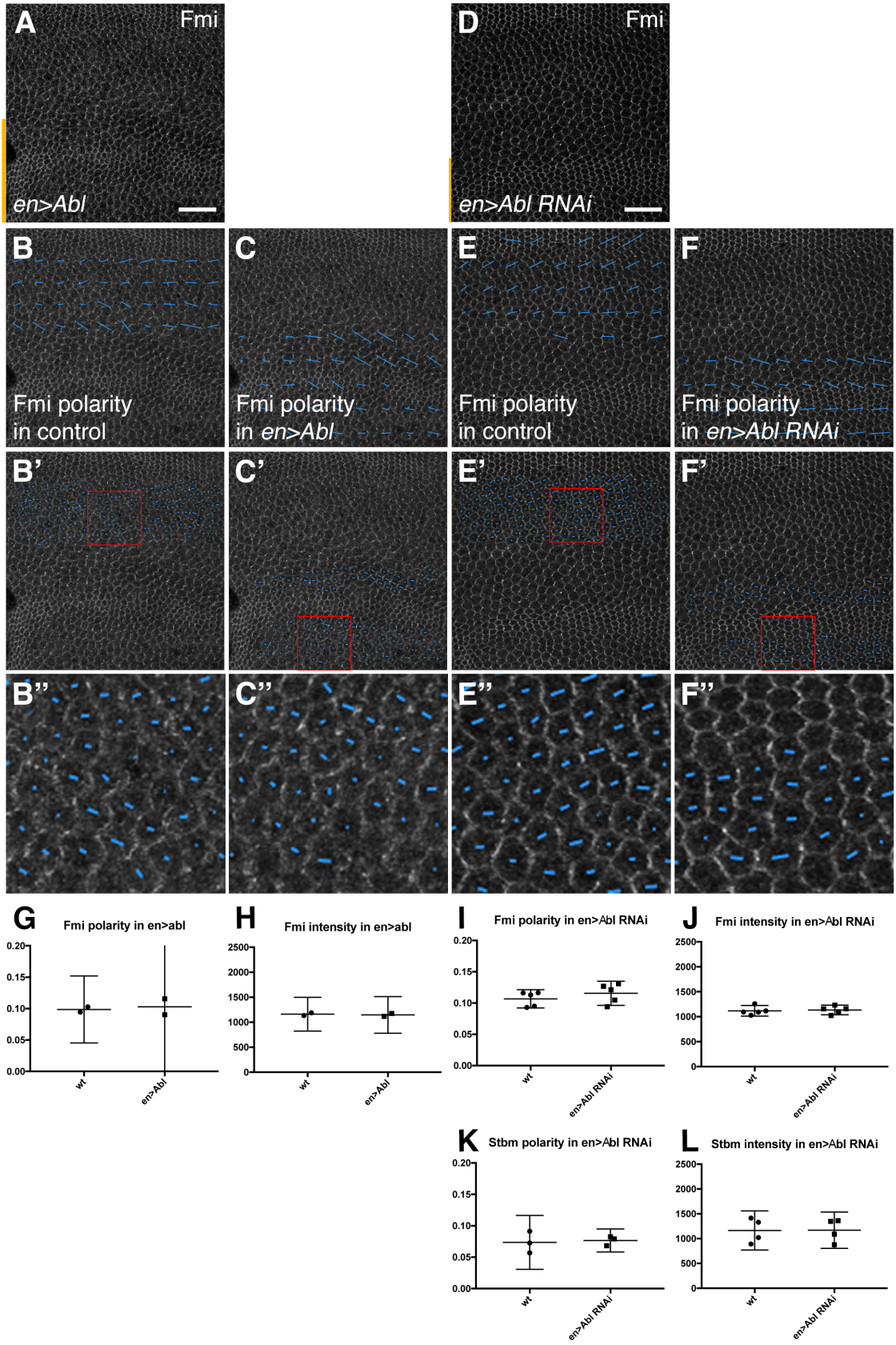

Figure 2.13 Core planar polarity protein polarity and intensity in *en>Abl* and *en>Abl RNAi* pupal wings Figure legends in next page

Figure 2.13 Core planar polarity protein polarity and intensity in *en>Abl* and *en>Abl RNAi* pupal wings

(A,D) *en>Abl* (A) or *en>Abl RNAi* (D) expressing 28h APF pupal wings. Fmi is immunolabelled in grey. The *en* expression region is indicated by the yellow line on the left. Scale bar 20 μm.

(B-C'') Blue lines represent polarity nematics of Fmi in panel A in control region without *en* expression (B) and *en* expression region (C). (B-C) Coarse-Grain polarity nematics averaged over a 3-cell size. (B'-C') Single cell polarity nematics (B''-C'') zoomed-in of red box region.

(E-F'') Blue lines represent polarity nematics of Fmi in panel D in control region (E) and *en* expression region (F). (E-F) Coarse-Grain polarity nematics averaged over a 3-cell size. (E'-F') Single cell polarity nematics (E''-F'') zoomed-in of red box region.

(G-H) Comparison of Fmi polarity (G) and membrane intensity (H) comparing *en>Abl* expressed tissue to control tissue. No significant difference in polarity (G, N = 2 wings, p-value = 0.6965) or membrane intensity (H, N = 2 wings, p-value = 0.0956) in two-tail two-sample Student's paired t-test. Error bar: 95% confidence interval.

(I-J) Comparison of Fmi polarity (I) and membrane intensity (J) comparing *en>Abl RNAi* expressed tissue to control tissue. No significant difference in polarity (I, N = 5 wings, p-value = 0.2693) or membrane intensity (J, N = 5 wings, p-value = 0.4737) in two-tail two-sample Student's paired t-test. Error bar: 95% confidence interval.

(K-L) Comparison of Stbm polarity (K) and membrane intensity (L) comparing *en>Abl RNAi* expressed tissue to control tissue. No significant difference in polarity (K, N = 3 wings, p-value = 0.6796) or membrane intensity (L, N = 4 wings, p-value = 0.8455) in two-tail two-sample Student's paired t-test. Error bar: 95% confidence interval.

2.2.3.4 short-term expression of Abl and Abl RNAi in clones

In the previous **Section 2.2.3.3**, it is noticed that cells near *ptc>Abl* expression region boundary are irregular and core protein puncta are mis-localised. However, the expression region can only be estimated in *ptc>* driven expression experiments as no expression region marker is used. To express Abl and Abl RNAi in tissue with a clear border, clones were generated.

By inserting an *FRT-STOP-FRT* sequence in between the *Act5C* promoter and the Gal4 sequence, the Gal4/UAS system is halted. When the FLP recombinase is induced to express under the *hsp70* promoter by 37°C heat-shock (Lindquist, 1980a; b; Velazquez et al., 1983), the *FRT-STOP-FRT* sequence gets flipped out and the *Act5C* promoter induces Gal4 expression. Thus, Abl or Abl RNAi is expressed in cells excise the cassette and their progeny inherit the excised state. *UAS-LacZ* is also expressed to mark the Gal4/UAS system activated cells (**Materials and Methods 6.1.4.2**).

Dsh was immunolabelled in this experiment as it is proposed to be the direct target of Abl phosphorylation. No significant difference in Dsh polarity magnitude and membrane intensity was detected between Abl RNAi expression clones and wild-type regions (Figure 2.14 G-H). As for Abl overexpression clones, may be due to a small sample size (N = 2), no significant difference in Dsh polarity magnitude is observed comparing Abl overexpression clones and wild-type regions (Figure 2.14 I-J). However, a noticeable change in polarity direction does appear in Abl overexpression clones (Figure 2.14 E-E'' compared to F-F''). As proposed above, the change in polarity direction can be indirect via effects on adherens junctions and cytoskeleton (Fox and Peifer, 2007; Grevengoed *et al.*, 2001). Indeed, cells were more irregular in Abl overexpressed clones (Figure 2.14 E-E'' compared to F-F'').

Thus, although still uncertain, the regulation of Abl on planar polarity is not supported based on the results shown here. Considering that the EGFP-Dsh[Y473>F] largely lost its membrane localisation, and the Y473 residue lies within the DEP domain, which is

crucial for the membrane recruitment of Dsh (Axelrod *et al.*, 1998; Gammons *et al.*, 2016; Tauriello *et al.*, 2012), the Y473 residue is important for Dsh been recruited to cell membrane. However, there is no evidence provided supporting the regulation of Abl kinase affects Dsh membrane recruitment. This may be due to the mutation on Y473 disrupting the conformation, or possibly there is another Tyr-kinase redundantly phosphorylates Y473. Thus, the importance of phosphorylation on DshY473 residue cannot be denied based on the data shown here.

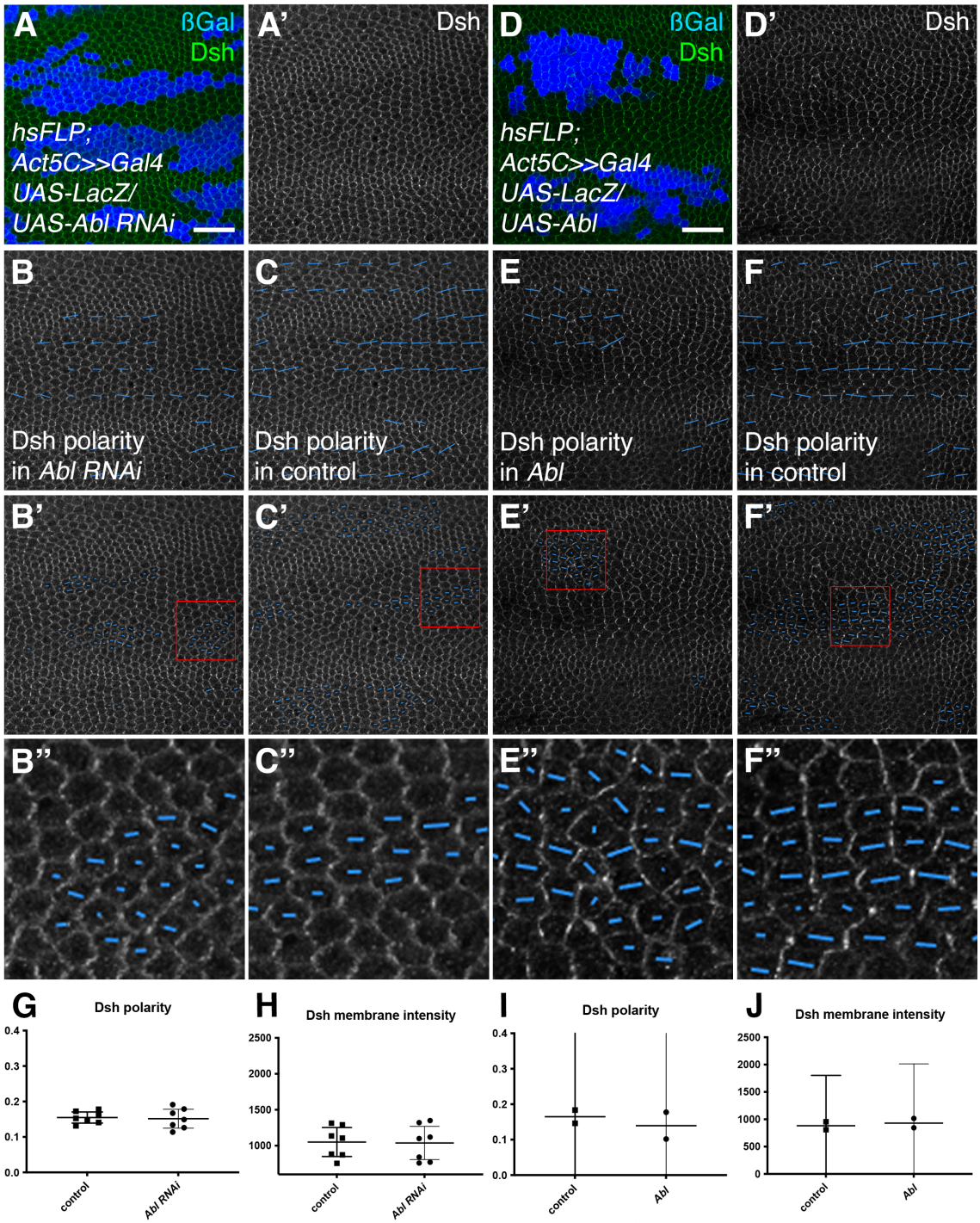

Figure 2.14 Core planar polarity protein polarity and intensity in pupal wings carrying clones expressing *UAS>Abl* and *UAS>Abl RNAi*

28 h APF pupal wing carrying clones expressing *Abl RNAi* (A-C'',G,H) or *Abl* (D-F'',I,J). Stop cassette in Act5C>>Gal4 in flipped out by hs-FLP to induce *UAS-Abl RNAi* or *UAS-Abl* expression.

(A) 28 h APF pupal wing carrying clones expressing *Abl RNAi. Abl RNAi* expressing tissue is indicated by the gain of blue β-gal immunolabelling. β-gal is immunolabelled in blue (A); Dsh is immunolabelled in green (A) or grey (A'). Scale bar 20 μm.

(B-C'') Blue lines represent polarity nematics of Dsh in panel A in *Abl RNAi* expressed tissue (B) or control tissue (C). (B-C) Coarse-Grain polarity nematics averaged over a 3-cell size. (B'-C') Single cell polarity nematics (B''-C'') zoomed-in of red box region.
(D) 28 h APF pupal wing carrying clones overexpressing *Abl. Abl o*verexpressing tissue is indicated by the gain of blue β-gal immunolabelling. β-gal is immunolabelled in blue (D); Dsh is immunolabelled in green (D) or grey (D'). Scale bar 20 μm.
(E-F'') Blue lines represent polarity nematics of Dsh in panel D in *Abl* overexpressed tissue (E) or control tissue (F). (E-F) Coarse-Grain polarity nematics averaged over a 3-cell size. (E'-F') Single cell polarity nematics (E''-F'') zoomed-in of red box region.
(G-H) Comparison of polarity (G) or membrane intensity (H) of Dsh, comparing *Abl RNAi* expressed tissue and control tissue. No significant difference in two-tail two-sample Student's paired t-test, (G) p-value = 0.7470; (H) p-value = 0.5228. N = 7 wings, error bar: 95% confidence interval.
(I-J) Comparison of polarity (I) or membrane intensity (J) of Dsh, comparing *Abl* overexpressed tissue and control tissue. No significant difference in two-tail two-sample Student's paired t-test, (I) p-value = 0.4117; (J) p-value = 0.1633. N = 2 wings, error bar: 95% confidence interval.

2.2.4 Kinases phosphorylating Pk

Msn (Daulat *et al.*, 2012; Paricio *et al.*, 1999) and Nmo (Choi and Benzer, 1994; Collu *et al.*, 2018; Mirkovic *et al.*, 2011) are both found to affect planar polarity in *Drosophila* eyes. In this section, I am going to examine whether pupal wing polarity is affected by them.

2.2.4.1 Msn allele clones

The *msn[172]* alleles carrying inversion breakpoints within the coding region were used to check the role of Msn in planar polarity in the *Drosophila* pupal wing (Figure 2.15).

The ideal experiment is to check immunolabelled Pk membrane localisation, but all the images stained for Pk are of poor quality as the example image shown in (Figure 2.15 F-F'). The only available images are of Dsh staining (Figure 2.15 A-A'), which would also reflect the localisation of Pk as overexpression of Pk leads to larger core protein puncta (Bastock 2003) and loss of Pk causes loss of core protein polarity (Bastock *et al.*, 2003; Strutt and Strutt, 2007; Tree *et al.*, 2002).

Homozygous *msn[172]* clones in *Drosophila* pupal wings have no obvious change in core protein membrane localisation level compared to control tissue (Figure 2.15 E, p-value = 0.2679, comparing B-B'' to C-C'').

When comparing Dsh polarity between inside and outside *msn[172]* clones, a weak but statistically significant decrease of polarity in *msn[172]* clones was noticed (Figure 2.15 D, p-value = 0.0164), suggesting Msn positively regulates planar polarity without affecting membrane intensity in pupal wing cells. However, whether such regulation is reproducible in other approaches, e.g., RNAi or other alleles, is worth testing.

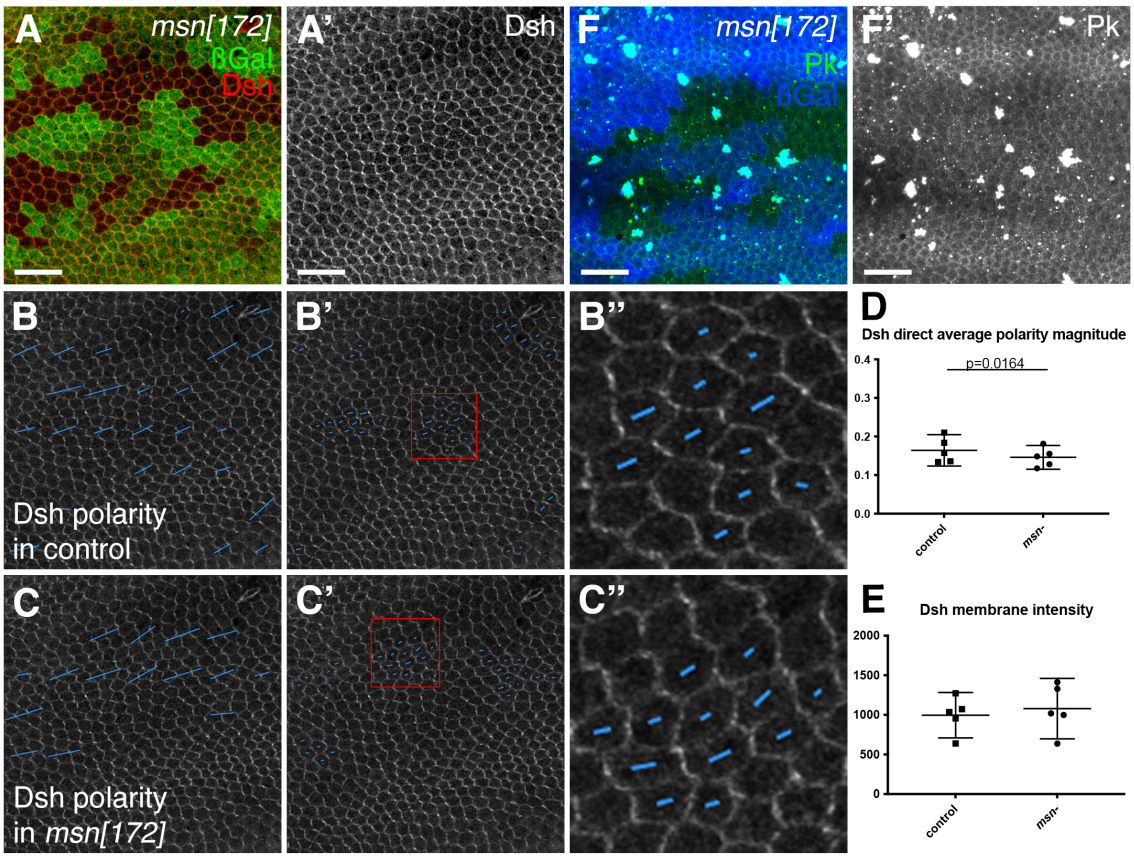

Figure 2.15 *msn[172]* allele clones affect core planar polarity protein polarity

(A) 28 h APF pupal wing, carrying twin clones of *msn[172]* (homozygous *msn[172]* tissue is indicated by the loss of green β-gal immunolabelling); Dsh is immunolabelled in red (A) or grey (A'). Scale bar 20 μm.

(B-C'') Blue lines represent polarity nematics of Dsh in panel A in *arm-LacZ/arm-LacZ* control tissue (B) and homozygous *msn[172]* tissue (C). (B-C) Coarse-Grain polarity nematics averaged over a 3-cell size. (B'-C') Single cell polarity nematics (B''-C'') zoomed-in of red box region.

(D-E) Comparison of polarity (D) and membrane intensity (E) of Dsh, comparing *msn[172]* clones to control tissue. Dsh polarity in *msn[172]* clones is lower than that in control tissue (D, p-value = 0.0164), but the membrane intensity of Dsh shows no change (E, p-value = 0.2679). N = 5 wings, statistical significance calculated by two-tail two-sample Student's paired t-test. Error bar: 95% confidence interval.

(F) Example image shows poor Pk staining in 28 h APF pupal wing carrying twin clones of *msn[172]* (homozygous *msn[172]* tissue is indicated by the loss of blue β-gal immunolabelling); Pk is immunolabelled in red (F) or grey (F'). Scale bar 20 μm.

2.2.4.2 Nmo phosphorylation sites mutations

In vitro kinase assay identified two clusters of Nmo phosphorylation sites on Pk: [S515, S519, S595, S599] and [T708, S725, T737, S762] (Collu *et al.*, 2018). To check the potential effect of Nmo phosphorylation in pupal wings, these two clusters of eight S/T residues were mutated to Ala or Glu to generate phosphomutant EGFP-pk[A] and phosphomimetic EGFP-pk[E] mutations. Mutations were expressed under *Act5C*-promoter. The polarity magnitudes are not significantly affected in EGFP-pk[A] and EGFP-pk[E] clones, compared to EGFP-pk wild-type clones (Figure 2.16 D), suggesting phosphorylation on these residues is not crucial for planar polarity in wings.

Another interesting statement worth checking is that Nmo phosphorylation on Pk promotes Pk isoform degradation in eyes (Collu *et al.*, 2018). Here I want to check if the Pk level is affected in wings as the Pk isoform is the dominant isoform in wings but not in eyes. If the phosphorylation on these two clusters of S/T residues promotes Pk degradation, a reduced EGFP-pk[E] level is expected. However, the phosphomimetic EGFP-pk[E] mutant shows significantly higher membrane (Figure 2.16 E, p-value = 0.0105) and cytoplasm protein levels (Figure 2.16 F, p-value = 0.0002) compared to the wild-type control. Nevertheless, phosphomutant EGFP-Pk[A] protein level shows no significant difference to EGFP-Pk[wt] (Figure 2.16 E-F). My results shown here contradicted the degradation model in (Collu *et al.*, 2018), but may, instead, suggest an opposite model in wings that phosphorylation on Pk prevents Pk isoform to be degraded.

Since my data are insufficient to determine whether reported phosphorylation sites regulate planar polarity in wings, the only conclusion I can draw here is that the protein level of phosphomimetic EGFP-pk[E] mutant is increased in pupal wing cells, and this does not affect planar polarity.

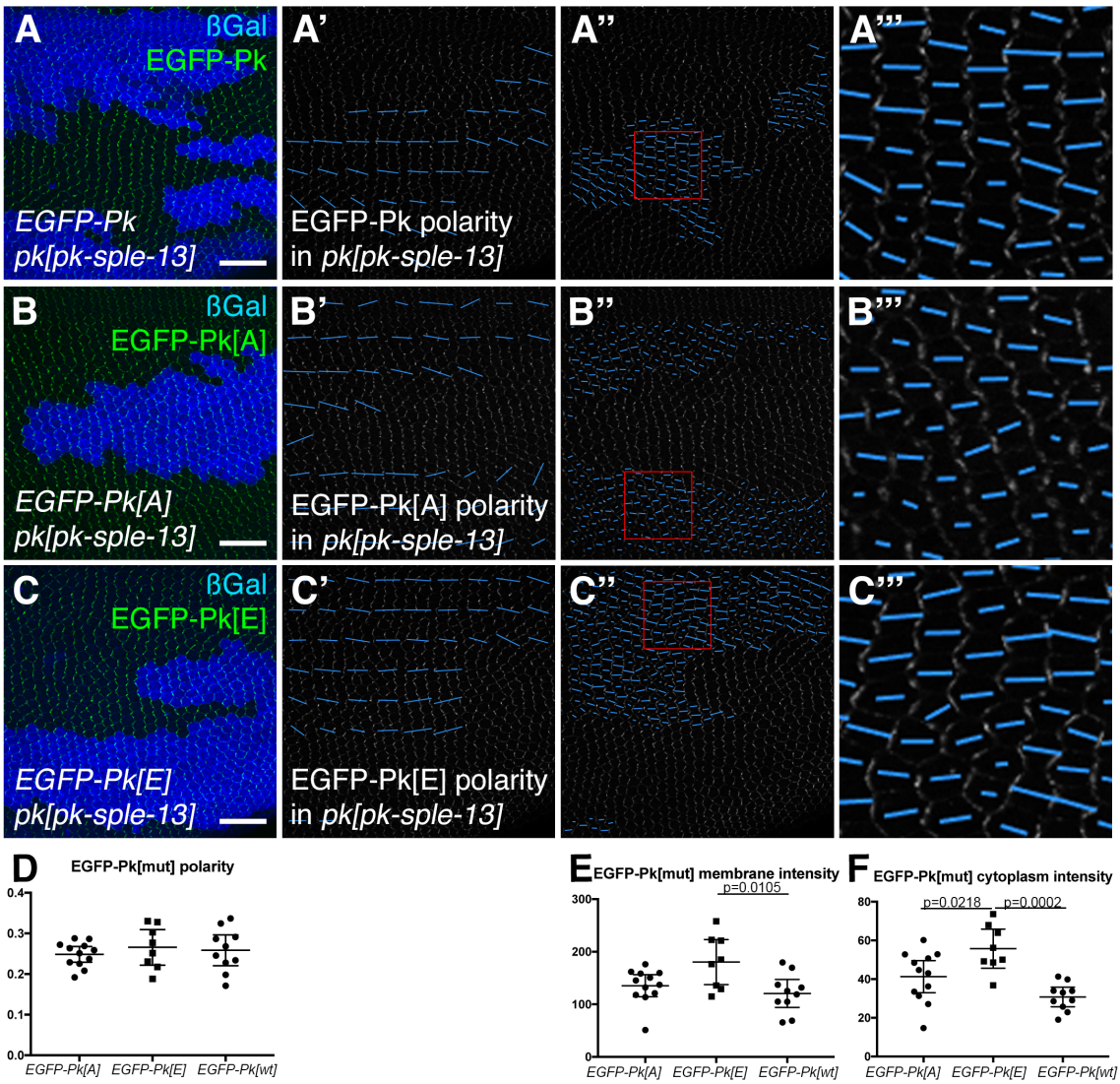

Figure 2.16 *EGFP-Pk[mut]* polarity and intensity in *pk[pk-sple-13]* clones

(A-C'') 28 h APF pupal wing carrying twin clones of *pk[pk-sple-13]* (homozygous *pk[pk-sple-13]* tissue is indicated by the loss of blue β-gal immunolabelling). EGFP-Pk (A), EGFP-Pk[A] (B), or EGFP-Pk[E] (C) is expressed in the whole wing. (A'-C') Blue lines represent Coarse-Grain polarity nematics averaged over a 3-cell size. (A''-C'') Single cell polarity nematics (A'''-C''') zoomed-in of red box region. Scale bar 20 μm.

(D-F) Comparison of polarity (D), membrane intensity (E), and cytoplasm intensity (F) among EGFP-Pk (N = 10 wings), EGFP-Pk[A] (N = 12 wings), and EGFP-Pk[E] (N = 8 wings) in *pk[pk-sple-13]* background.

(D) No significant difference in polarity is shown in the ANOVA test. p-value ANOVA results for comparisons between EGFP-Pk and EGFP-Pk[A] = 0.8636; EGFP-Pk and EGFP-Pk[E] = 0.9384; EGFP-Pk[A] and EGFP-Pk[E] = 0.6827. Error bar: 95% confidence interval.

(E) The membrane intensity of EGFP-Pk[E] is higher than that of EGFP-Pk, p-value ANOVA = 0.0105. No significant difference between EGFP-Pk and EGFP-Pk[A], p-

value ANOVA = 0.6680; and between EGFP-Pk[A] and EGFP-Pk[E], p-value ANOVA = 0.0508. Error bar: 95% confidence interval.

(F) The cytoplasm intensity of EGFP-Pk[E] is higher than that of EGFP-Pk (p-value ANOVA = 0.0002) and EGFP-Pk[A] (p-value ANOVA = 0.0218). No significant difference between EGFP-Pk[A] and EGFP-Pk[E], p-value ANOVA = 0.0870. Error bar: 95% confidence interval.

2.3 Discussion

2.3.1 aPKC Discussion

In this section, three approaches were used to attenuate aPKC activity. First, no adequate size clone was found in the amorphic *aPKC* mutant flies, so the polarity cannot be quantified. Then temperature-sensitive allele clones were generated but show no effect on planar polarity, presumably due to the insufficient inhibition of aPKC kinase activity. Finally, a more aggressive method was tried, in which expression of a dominant negative form of aPKC reorients core protein puncta and reduces the strength of the polarity (Figure 2.4 E,G, 2.5 F). Although *ptc>aPKC[DN]* affects the strength of planar polarity in the wing, there is only a slight (Figure 2.5 E) or no (Figure 2.4 F,H; Figure 2.5 G) change in membrane intensity, suggesting that the expression of aPKC is not or only weakly affects core protein membrane levels.

Here, evidence is provided supporting aPKC regulates planar polarity in *Drosophila* wings but does not support that core protein membrane levels is affected. Considering a previously published work shows that aPKC affects planar polarity in the eye via phosphorylating Fz in residues proposed to regulate Dsh recruitment (Djiane *et al.*, 2005; Strutt *et al.*, 2012; Umbhauer *et al.*, 2000; Wong *et al.*, 2003; Wu *et al.*, 2008), see **Introduction 1.3.1**. Whether aPKC affects core protein, especially Dsh, membrane localisation needs to be further confirmed.

It is also worth noticing that the dominant-negative form of proteins may cause off-target effects (Shen et al., 2013), so that results generated in aPKC[DN] expression experiments are needed to be tested by other approaches. Further experiments examine how aPKC affects planar polarity is described in **Chapter 4**.

2.3.2 Par-1 Discussion

As little is known on whether Par-1 regulates Dsh function in *Drosophila* pupal wings and how Par-1 regulates Dsh function remains unclear, I checked planar polarity in *par-1[k05603]* clones and Par-1 RNAi conditional expression in *Drosophila* pupal wings but found no obvious change in core protein puncta localisation. The negative results shown here lower our interest in Par-1.

In addition, the Dsh mutations experiment shows that the S/T236-247 residues are crucial for Dsh function in planar polarity. However, as phosphomutant and phosphomimetic Dsh show similar effects (Figure 2.8 and Figure 2.9), it is still unclear whether the phosphorylation event in the S/T236-247 residues regulates Dsh function. In the FRAP experiment, phosphomutant Dsh[S/T236-247>A]-GFP has increased mobility (Figure 2.9 C), which is consistent with the previous publication (Strutt *et al.*, 2019a). However, the mobility of the phosphomimetic form of Dsh was not examined in (Strutt *et al.*, 2019a), which is also found to increase in the experiment described here (Figure 2.9 C). This may be due to:

1) the mutations themselves affect Dsh conformation and function rather than the phosphorylation events. Supporting this, when only five rather than eight S/T residues were mutated to Ala, the wing hair phenotype of *dsh-* mutant was rescued (Strutt *et al.*, 2019a). These results suggest that the aggressive eight mutations disrupt the conformation of Dsh, thus, affecting its membrane localisation, polarity, and mobility. Or

2) the phosphorylation events are important, but the Glutamic acid is not sufficiently charged to mimic effects of the phosphorylated serine and threonine (Chen and Cole, 2015), thus, the 'phosphomimetic' Dsh may actually mimicking a hypo-phosphorylated status of Dsh. In this case, a stronger charged phosphomimetic mutations are required in future research examining the function of S/T236-247 residues.

In contrast to the less interested Par-1, solid evidence has been previously provided

to show Dco plays a role in planar polarity. Dco is proposed to also phosphorylate S/T236-247 residues (Klein *et al.*, 2006; Strutt *et al.*, 2006), and regulates planar polarity in *Drosophila* wings (Klein *et al.*, 2006; Strutt *et al.*, 2019a; Strutt *et al.*, 2006; Strutt and Strutt, 2020). More experiments to dissect the role of Dco are described in **Chapter 3**.

2.3.3 Abl Discussion

The EGFP-Dsh[Y473>F] mutant protein is hardly localised to the cell membrane (Figure 2.10 A-B). A similar result is also reported in 30 h APF pupal wing cells (Singh *et al.*, 2010). These results highlight that the Y473 residue is crucial for Dsh membrane localisation. Indeed, DshY473 residue lies within the DEP domain, which is found crucial for its membrane recruitment (Axelrod *et al.*, 1998; Gammons *et al.*, 2016; Tauriello *et al.*, 2012). It is also proposed that DEP domain interaction with negatively charged phospholipids regulating Dsh membrane localisation (Simons et al., 2009). Thus, the phosphorylation on Y473 residue, which affects protein charge, may be the mechanism for a decreased Dsh membrane localisation. So next, Abl was manipulated to check if the Dsh localisation is regulated by the phosphorylation of Abl. If Abl regulates planar polarity via phosphorylating Y473 residue, a lower membrane intensity in *abl*- mutant clones and *Abl RNAi* expression region is expected, which is not observed (Figure 2.11 E,G,I; Figure 2.12 J,K; Figure 2.13 J,L). These results indicate that decreased Abl activity does not significantly affect core protein membrane localisation in *Drosophila* wing cells.

Such a conflict may suggest: 1) a redundancy that other kinases may phosphorylate Y473 in compensating for Abl; or 2) Y473 disrupts the conformation (or charge status) of Dsh thus inhibiting its membrane binding and Abl does not regulate planar polarity via phosphorylation of Y473.

In addition, a noticeable change in polarity direction and cell shape is observed in Abl overexpression clones (Figure 2.12 B-C, Figure 2.14 E-F). Since Abl has been reported to regulate epithelial morphogenesis via regulating adherens junctions and cytoskeleton (Fox and Peifer, 2007; Grevengoed *et al.*, 2001), the change in polarity direction may be an indirect effect via cell shape change as cell packing has been proposed to affect planar polarity (Aigouy *et al.*, 2010; Classen *et al.*, 2005; Etournay *et al.*, 2015).

Here I provide evidence that compromised Abl activity does not affect planar polarity in wings; while the overexpression of Abl leads to polarity direction change but may be indirect via affecting cell shape. Further research is needed to obtain more evidence for whether Abl regulates planar polarity, but it is of low priority in this project.

2.3.4 Pk kinase Discussion

Data in **Section 2.2.4** show that *msn*- mutant decreases Dsh planar polarity but does not affect Dsh membrane intensity in pupal wings (Figure 2.15 D-E). However, as, Pk, the proposed direct substrate of Msn was not immunolabelled, whether Msn regulate planar polarity is still unclear. Indirect evidence was produced that Dsh membrane intensity is not affected (Figure 2.15 E), suggesting the formation of the core protein complex is not largely affected. Thus, Pk membrane localisation is unlikely to be affected by Msn in pupal wing cells.

In *Drosophila* eyes, loss-of-function alleles of *msn* suppress the Dsh overexpression phenotype (Paricio *et al.*, 1999), and *msn* RNAi knock-down enhances Pk[Sple] overexpression phenotype (Daulat *et al.*, 2012). These result suggest that Msn enhances Pk[Sple] activity in *Drosophila* eyes, possibly due to in promote Pk[Sple] membrane localisation as the PRICKLE1 membrane localisation is increased in MINK1 overexpressed HEK293T cells and decreased in morpholino oligonucleotide (MO)-

xMink1 knock-down in *Xenopus* embryos (Daulat *et al.*, 2012). However, Pk[Sple] is not the dominant isoform in *Drosophila* wings. Msn in *Drosophila* wing cells may only affect the submissive isoform Pk[Sple] and the dominant isoform Pk is not affected, thus, the core protein membrane localisation is not affected.

My result in planar polarity strength (Figure 2.15 D) does not agree with a previous publication where no canonical planar polarity defect is observed in *msn-* adult wings but missing wing hairs (Paricio *et al.*, 1999). This may be because the change in planar polarity strength is statistically significant but only mild, the orientation of the polarity is not obviously affected either (Figure 2.15 comparing B to C). Thus, the mild effect on planar polarity may be insufficient to affect adult wing phenotype.

Section 2.2.5 describes that the proposed Nmo phosphorylation sites are mutated and no change in polarity is observed (Figure 2.16 D). This result does not agree with (Collu *et al.*, 2018), where the expression of the phosphomutant Pk produce a more severe ommatidia rotation phenotype comparing to the overexpression of wild-type Pk. (Collu *et al.*, 2018) also suggest that Nmo regulates planar polarity in *Drosophila* eyes by phosphorylating Pk and increasing Pk degradation. In contrast, my result in (Figure 2.16 E-F) shows that the protein level of Pk[E] mutants is increased.

As stated in **Introduction 1.2.1**, Pk is the dominant isoform in the wing, while Pk[Sple] dominantly functions in the eye (Gubb *et al.*, 1999) and the balance of Pk/Sple isoform is crucial for planar polarity (Collu *et al.*, 2018; Gubb *et al.*, 1999). The contradicted results in eyes (Collu *et al.*, 2018) and wings (this work) may further suggest that Nmo promote planar polarity in both tissues by reducing the Pk isoform protein level in eyes and increasing the dominant Pk isoform protein level in wings. However, as EGFP-Pk[E] does not show any change in polarity strength, the evidence provided here is still insufficient for proving Nmo phosphorylation regulates planar polarity. There is a publication reports that *nmo-* mutant alleles producing truncated transcripts show adult

wing hair direction change (Verheyen *et al.*, 2001). However, as the adult wing hair phenotype is not observed in flies with amorphic allele *nmo[P]* (Verheyen *et al.*, 2001), the phenotype may not be due to loss of Nmo function but an unknown effect of the mutant alleles. Since the Nmo kinase is not directly manipulated in this Thesis, future experiment manipulating Nmo activity in wing cells is needed to examine the role of Nmo.

In summary, results in this chapter support the planar polarity regulation role of aPKC, partly support that of Abl, Msn, and Nmo, but not that of Par-1.

CHAPTER 3

Effects of acute manipulation of Dco on planar polarity

3.1 Introduction

In **Introduction 1.3.3** I described how Dco regulates planar polarity and affects the phosphorylation of Dsh and Stbm.

However, the research in previous publications was all carried out by long-term manipulation of Dco activity, e.g., *dco-* mutant, dominant-negative Dco expression, and dco RNAi expression, which may lead to indirect effects on core planar polarity. On the one hand, Dco has been reported to regulate the Wg signalling pathway (Bernatik *et al.*, 2014; Gao *et al.*, 2002; Kishida *et al.*, 2001; Klein *et al.*, 2006; McKay *et al.*, 2001; Peters *et al.*, 1999; Sakanaka *et al.*, 1999; Zhang *et al.*, 2006). Considering the core planar polarity pathway and the canonical Wg signalling pathway share components like Fz and Dsh, and Wnts is a possible upstream cue for planar polarity, where ectopic Wnts sources re-orient Vangl2/Prickle3 complex in *Xenopus* early ectoderm (Chu and Sokol, 2016); and even distribution disrupts planar polarity in mouse embryos (Minegishi *et al.*, 2017). The effect on Wg signalling might affect core planar polarity. On the other hand, Dco is reported to phosphorylate Ft (Feng and Irvine, 2009; Pan *et al.*, 2013; Sopko et al., 2009), which is a component of another possible upstream pathway, Ft/Ds (Strutt and Strutt, 2021). In addition, Ft is also a receptor for the Hippo signalling pathway which regulates tissue growth and cell proliferation (Bennett and Harvey, 2006; Cho et al., 2006; Silva et al., 2006; Tyler and Baker, 2007; Willecke et al., 2006). Another upstream regulator for Hippo signalling pathway Expanded (Ex)(Hamaratoglu et al., 2006) is also phosphorylated and regulated by CKI family kinases (Fulford et al., 2019). In addition, Hedgehog signalling is also affected by CKI family kinases (Jia et al., 2004; Jia et al., 2005; Price and Kalderon, 2002; Su et al., 2011). Thus, the effect of Dco on core planar polarity can be indirect via other signalling pathways. The first aim of this chapter is to provide evidence for whether Dco directly affects planar polarity protein localisation and stability by acutely manipulating Dco activity.

Another aim of this chapter is to test if Dsh and/or Stbm are the direct substrates of phosphorylation. Although evidence showing Dsh is a direct target is limited, the possibility cannot be eliminated that Dco directly phosphorylates Dsh and thus regulates Stbm polarity indirectly, or *vice versa*. Hence, separating the 'primary' substrates and the 'secondary' substrates is a crucial question in the field. Here, I will acutely manipulate Dco to examine its effects on Dsh and Stbm, expecting to visualise the most immediate effects, for instance, the effect on dynamics in the 'primary' substrate.

3.2 Nanobody-based acute knock-down of Dco

3.2.1 Acute knock-down of Dco-GFP affects planar polarity

The objective of this section is to find out if Dco affects the planar polarity acutely in a nanobody-based acute knockdown experiment.

In order to knock down Dco acutely, the NSlmb-vhhGFP fusion protein was used. In camelids, there are antibodies composed of heavy chains only and devoid of light chains (Hamers-Casterman et al., 1993). The antigen-binding domain of such heavy chain antibodies (vhh), also referred to as nanobody™ (a registered trademark of Ablynx), is a good alternative to conventional antibodies (van der Linden et al., 1999) due to their small size and single domain feature. The vhhGFP is a type of vhh binding to GFP specifically and efficiently (Saerens et al., 2005). The NSlmb-vhhGFP is generated by fusing the vhhGFP to the N-terminal part of Slmb, which is a *Drosophila* F-box protein (component of E3 enzymes SKP1–CUL1–F-box protein ligase complex). The NSlmb-vhhGFP deplete target GFP fusions in eukaryotic genetic system directly and rapidly (Caussinus et al., 2011). In this experiment, the NSlmb-vhhGFP were induced to express under control of the *hsp70* promoter in transgenic flies by heat-shocking at 37°C, similar to (Ressurreicao *et al.*, 2018).

A Fosmid transgene from FlyFos library was used to express GFP-tagged Dco in pupal wings cells. The Fosmid covers the Dco genomic region with superfolder-GFP (sfGFP) and other tags inserted into C-terminal of the Dco coding sequence (Sarov et al., 2016)(marked as Dco-GFP).

When both the Dco-GFP Fosmid transgene and the NSlmb-vhhGFP transgene are expressed in *dco-* mutant background, the vhhGFP nanobody specifically binds to Dco-GFP and the NSlmb motif induces the degradation of the complex. Thus, Dco is knocked down acutely (Figure 3.1 A). A decrease in Dsh (or Stbm) asymmetrical localisation is expected in this experiment, while other core proteins may remain unaffected or slowly affected if Dco directly phosphorylates and stabilises Dsh (or Stbm).

Note that the nanobody transgenic lines used in this experiment are not ideal. In pupal wings without heat-shock, there are some cells that show obviously lower Dco-GFP signals (Figure 3.1 B'', red dots indicate cells with low cytoplasmic GFP signal), suggesting a non-negligible leaky expression of NSlmb-vhhGFP. Also note that a previous publication has shown that heat-shock *per se* does not affect core protein polarity (Ressurreicao *et al.*, 2018), thus 2-hour heat-shocked pupal wings are directly compared to no heat-shock wings in this experiment.

Despite that the transgene insertion may express weakly without heat-shock, Dco-GFP is largely degraded after a 2-hour heat-shock compared to no heat-shock wings (Figure 3.1 E'' compared to B''), showing the NSlmb-vhhGFP functions as expected in degrading Dco-GFP. In this experiment, the Dsh significantly lost its proximodistal asymmetric localisation (Figure 3.1 G, comparing B' to E') and less aligned (Figure 3.1 C-C' compared to F-F') in 2-hour heat-shocked pupal wings compared to no heat-shock control wings. This result shows that acute knock-down of Dco-GFP decreases Dsh polarity, suggesting a direct role of Dco activity in Dsh asymmetrical localisation.

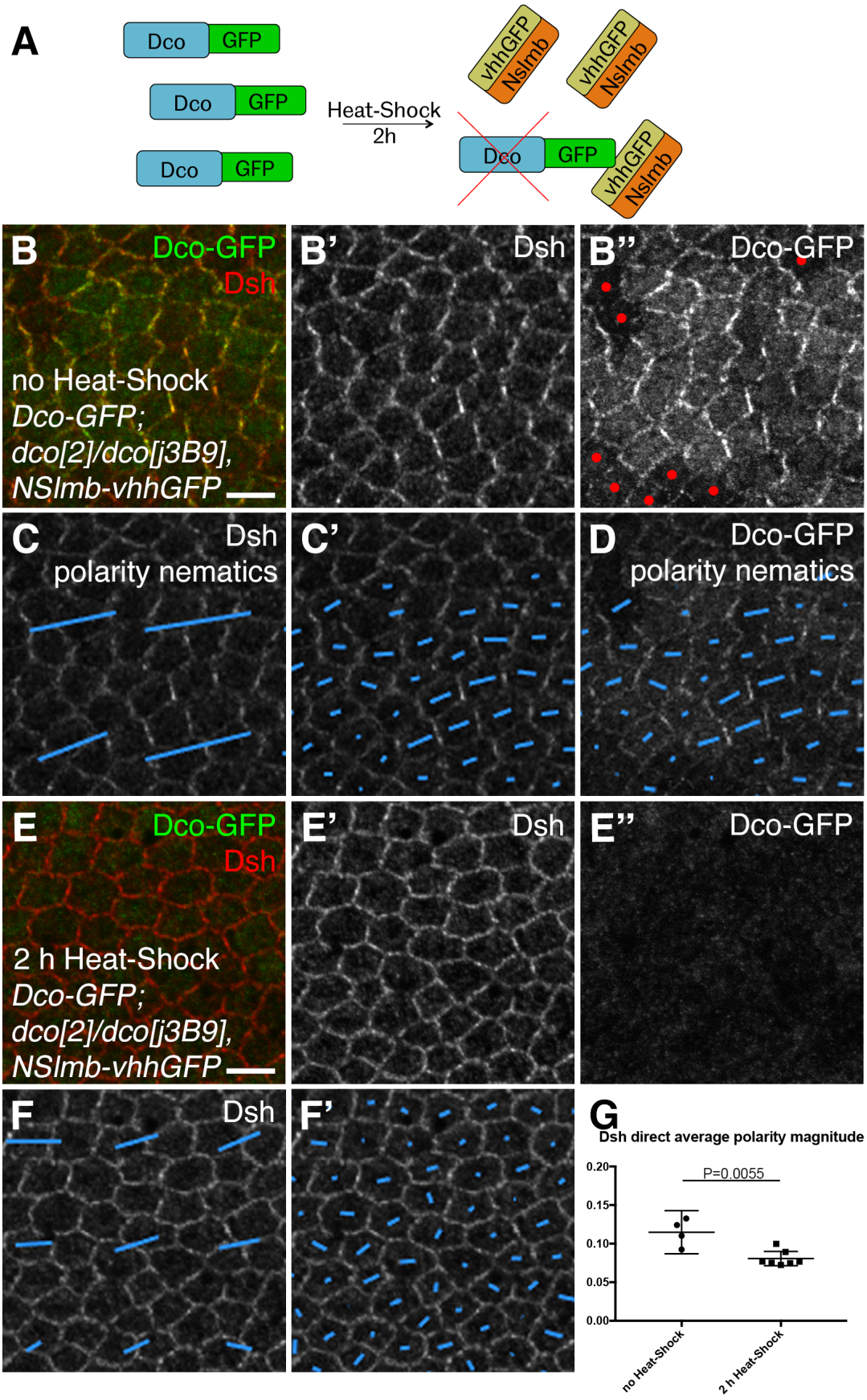

Figure 3.1 Nanobody-based Dco-GFP knock-down decreases Dsh polarity

Figure legends in next page

Figure 3.1 Nanobody-based Dco-GFP knock-down decreases Dsh polarity

(A) Schematic of nanobody-based acute knockdown experiment. Heat-shock induces expression of vhhGFP-NSlmb nanobody that driven Dco-GFP degradation.

(B-B'') 28 h APF pupal wing expressing Dco-GFP in *dco[2]/dco[j3B9]* background. NSlmb-vhhGFP nanobody is not expressed in the absence of heat-shock. Dsh was immunolabelled in red (B) or grey (B'). (B'') Dco-GFP fluorescence, red dots indicate cells with low Dco-GFP signals. Scale bar 5 μm.

(C-C') Blue lines represent polarity nematics of Dsh in panel B'. (C) Coarse-Grain polarity nematics averaged over a 3-cell size. (C') Single cell polarity nematics.

(D) Blue lines represent single cell polarity nematics of Dco-GFP in panel B''.

(E-E'') 28 h APF pupal wing expressing Dco-GFP and NSlmb-vhhGFP in *dco[2]/dco[j3B9]* background. NSlmb-vhhGFP nanobody was induced to express by a 2 h heat-shock. Dsh was immunolabelled in red (E) or grey (E'). (E'') Dco-GFP fluorescence is not detected on cell membranes. Scale bar 5 μm.

(F-F') Blue lines represent polarity nematics of Dsh in panel E'. (F) Coarse-Grain polarity nematics averaged over a 3-cell size. (F') Single cell polarity nematics

(F) Comparison of direct average polarity magnitudes of immunolabelled Dsh in Dco-sequestrated (2 h heat-shock, N = 7) pupal wings and control wings (no heat-shock, N = 4). Dsh polarity is lower in Dco-sequestrated pupal wing cells, p-value in a two-tail two-sample Student's paired t-test = 0.0055. Error bar: 95% confidence intervals.

3.2.2 Acute knock-down of Dco-HA

To confirm the role of Dco on planar polarity independent of GFP, the hemagglutinin (HA)-tagged Dco was also made. The FlyFos Fosmid covering the Dco genomic region was tagged with HA and SpotTag, with HA-SpotTag- sequence inserted into N-terminal (HA-SpotTag-Dco, marked as HA-Dco) or SpotTag-HA- sequence inserted into C-terminal (Dco-SpotTag-HA, marked as Dco-HA) of the Dco coding sequence, see **Materials and Methods 6.1.3**.

The HA-tagged protein can be bound and sequestrated to mitochondria using a *hsp70* promoter controlled Tom70-HAScFv nanobody (Ressurreicao *et al.*, 2018). The Tom70-HAScFv fusion protein was also tagged with Myc, which is immunolabelled to confirm the Tom70-HAScFv expression after heat-shock. However, as shown in (Figure 3.2 A-A'), the immunolabelled Myc is weakly detected in wings without heat-shock (Figure 3.2 A'), showing this transgene is also expressed leaky.

After two-hour heat-shock, Myc tagged Tom70-HAScFv is highly expressed (Figure 3.2 B-B'). Unlike the Dco-GFP knock-down results where Dsh-GFP localised symmetrically on cell membrane after two-hour heat-shock (Figure 3.1 C'), Dsh-HA immunolabelling is not obviously affected as puncta still localise on proximal and distal cell junctions (Figure 3.2 A'' compared to B''). This may be due to a fault of the Dco-HA transgene as the HA immunolabeling looks identical between heat-shocked and no heat-shock control wings (Compare Figure 3.2 A''' to B'''). Nevertheless, both C-terminal tagged Dco-GFP (Figure 3.1 B'') and immunolabelled N-terminal tagged HA-Dco (Figure 3.4 A) shows cell membrane localisation, suggesting the tagging site does not deplete the membrane localisation of Dco. Thus, the HA antibody, which succeed in detecting HA-Dco (Figure 3.4 A) did not detect Dco-HA, suggesting that HA-Dco is not expressed in this transgene. This may explain why Dsh localisation is not obviously affected (Compare Figure 3.2 A''' to B''').

As both nanobody transgenes used in Dco-GFP and Dco-HA knock-down are found express leaky, they may not be ideal tools. So I alternatively used another even more acute knock-down method, chemical inhibitors as a parallel approach.

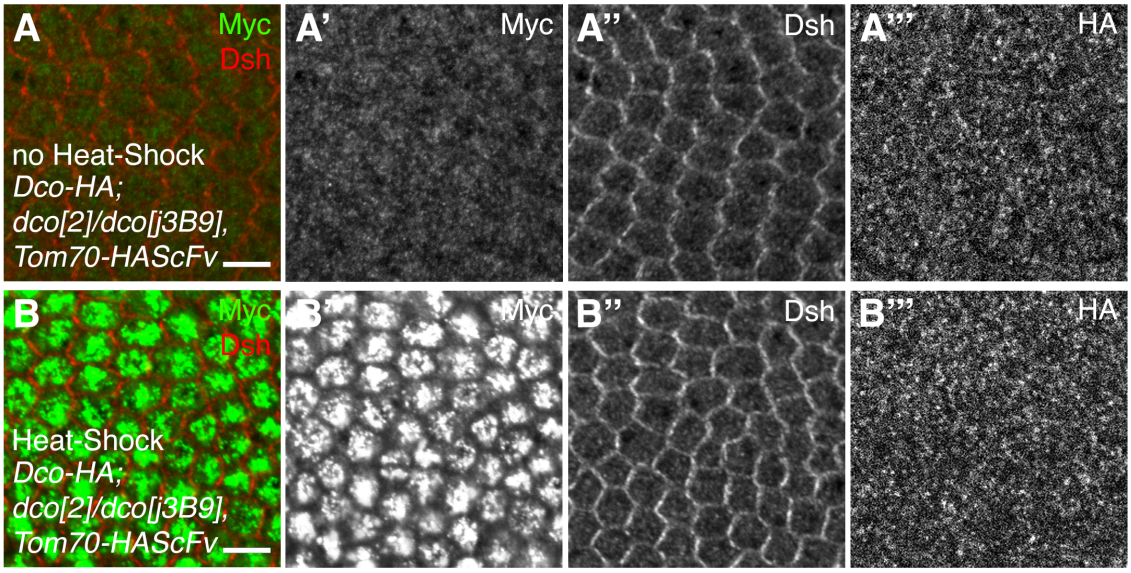

Figure 3.2 Nanobody-based Dco-HA knock-down failed

28 h APF pupal wing carrying *Dco-HA* transgene in *dco[2]/dco[j3B9]* background. Tom70-HAScFv nanobody was not expressed in the absence of heat-shock (A-A''); or was induced to express by a 2 h heat-shock (B-B''). Myc tag on Tom70-HAScFv nanobody was immunolabelled in green (A,B) or grey (A',B'); Dsh was immunolabelled in red (A,B) or grey (A'',B''). (A''',B''') No immunolabelled HA signal was detected on cell membrane. Scale bar 5 μm.

3.3 Chemical CKI inhibitor acutely affects Dsh and Stbm stability

The membrane localisation change of Dsh would ultimately affect other core protein localisation. For instance, the total amount and stable amount of Stbm is reduced in a planar polarity-specific *dsh[1]* mutant background (Strutt *et al.*, 2019a); and semi-acute (hours-scale) cleavage of Dsh reduces Stbm polarity and stable amount on cell junctions (Ressurreicao *et al.*, 2018). This means that the time window when only one member of the protein complex changes its localisation is narrow. Thus, to separate the 'primary' and 'secondary' substrate of Dco, a more acute approach is needed to check if the planar polarity of Stbm is affected more acutely or less acutely than Dsh, other than the hours-scale acute knock-down described above.

A broad-spectrum cell-permeant CKI inhibitor D4476 (4-[4-(2,3-dihydro-benzo[1,4]dioxin-6-yl)-5-pyridin-2-yl-1H-imidazol-2-yl]benzamide)(Rena *et al.*, 2004) was used to inhibit Dco activity acutely in the 'minutes' time scale. Note that D4476 inhibits Dco (CKIε) and other CKI isoforms, so the final result can be of collective effects. D4476 is also reported to inhibit activin receptor-like kinase 5 (ALK5, a member of the family of type-I TGF-β receptors)(Callahan et al., 2002; Rena *et al.*, 2004). As no direct cross-talk between the TGF-β signalling and the planar polarity has been found, the inhibition of D4476 on ALK5 is not a concern in this work. Also, there is a Dco (CKIε) specific inhibitor PF-4800567, which is reported to also inhibit EGFR (Walton et al., 2009). Because EGFR affects planar polarity in *Drosophila* eyes (Brown and Freeman, 2003; O'Keefe *et al.*, 2009; Strutt and Strutt, 2003; Weber *et al.*, 2008), PF-4800567 inhibitor is not preferred in this experiment.

As 28 h APF pupal wings are covered in cuticular membranes that prevent chemical accessibility, I used 6 h APF prepupal wings instead, where the pupal cuticle has not been secreted (Waddington, 1939). Core proteins are expressed and localised on cell membranes at 6 h APF, but their localisation is not obviously asymmetric in the majority

of wings cells (Classen *et al.*, 2005). Thus, in this system, only the mobility of Dsh and Stbm is examined. The mobility of EGFP-tagged Dsh or Stbm in membranes is measured by FRAP. Long-term expression of dominant-negative Dco has been reported to affect Dsh and Stbm membrane stability in pupal wings (Strutt *et al.*, 2019a) but it is unclear how rapid the effects are.

D4476 inhibits most of CKI activity at a concentration greater than 10 μM *in vitro* (Rena *et al.*, 2004), while 12 h 50 μM D4476 treatment exhibits cytotoxicity in cell culture (Hu et al., 2015). Thus, to maximise the inhibition and avoid the cytotoxicity of long inhibition, I first tried 30 min 50 μM D4476 treatment in 6 h APF prepupal wings. Although the apoptosis markers are not checked, cells in 6 h APF prepupal wings still maintain their normal morphology after 30 min D4476 treatment and about 6 min FRAP imaging (Figure 2.9 A-A''), so there is no instant cytotoxicity effect.

After 30-min inhibition, the fraction of EGFP-Dsh fluorescence that has recovered after photobleaching is increased compared to that of control wings treated with Dimethyl Sulfoxide (DMSO) only (Figure 3.3, A, p-value for plateaus < 0.0001) while that of Stbm-EGFP is decreased (Figure 3.3, B, p-value for plateaus < 0.0001). These results show that acute inhibition of CKI activity destabilises EGFP-Dsh and stabilises Stbm-EGFP on the cell membrane, suggesting Dco rapidly stabilises Dsh and destabilises Stbm acutely.

As previously stated, planar polarity-specific *dsh[1]* mutant background reduces Stbm total amount and stable amount (Strutt *et al.*, 2019a); semi-acute cleavage of Dsh reduces Stbm polarity and stable amount on cell junctions (Ressurreicao *et al.*, 2018). The 'primary' substrate cannot be distinguished in the 30 min inhibition experiments where both Dsh and Stbm changes their stability, as changes in their stability can be indirect.

To rule out the 'primary' substrate, 10 min inhibition experiments were then tried. After 10-min D4476 treatment, the stability of EGFP-Dsh decreases (Figure 3.3 C, p-value for plateaus = 0.0404) but it is not as mobile as the 30-min treatment group (Figure 3.3 C, p-value for plateaus = 0.0109). Note that due to technical limitations, it is impossible to stop the inhibition effect while imaging. To avoid damaging the fragile prepupal wings, wings were transferred with 1μL chemical treatment solution by pipetting into 4μL 2.5% methyl cellulose/Schneider's media for mounting (see **Materials and Methods 6.2.4**). Thus, after 10 min treatment in 50 μM D4476, prepupal wings were then still in 10 μM D4476 treatment during FRAP imaging, in which CKI is still inhibited *in vitro* (Rena *et al.*, 2004). So in this case, the actual inhibition time is longer than the time indicated, especially for the 10-min treatment in the Stbm-EGFP experiments where technical issue delays Stbm-EGFP sample imaging for about 15 mins. The estimated inhibition time for this experiment is 10-min 50 μM plus about 15-min 10μM D4476 treatment. This may be the reason why 10-min treatment gives a similar result to that of 30-min treatment (Figure 3.3, D, p-value for plateaus = 0.0873). Thus, in this stage, I still cannot identify the 'primary' substrate as both proteins show changes in 10-min treatments.

Another attempt to identify the 'primary' substrate is to FRAP Dsh or Stbm in absence of the other one. 30-min D4476 treatment in *stbm-* null mutant prepupal wings shows no change in the EGFP-Dsh recovery plateau compared to control wings lacking drug treatment (Figure 3.3, E), which might suggest that Dco stabilises Dsh in a Stbm-dependent manner. However, the plateau for EGFP-Dsh recovery reaches about 80%, and this may be the ceiling of the recovery. Instead, faster recovery is noticed in the first couple of minutes in this experiment (Figure 3.3, E, p-value for K (K_{fast} and K_{slow}) = 0.0006), suggesting EGFP-Dsh recovery is still affected by CKI inhibition in absence of Stbm. As for the Stbm-EGFP recovery in absence of Dsh, there is only one data point of DMSO control so the statistical analysis cannot be done. However, by eye, the recovery of the treated group seems to be lower than that of the control data point (Figure 3.3, H), suggesting the effect of Dco on Stbm mobility is independent of Dsh.

Another Dco inhibitor, PF-4800567, treated prepupal wing cells also exhibit higher EGFP-Dsh recovery compared to that of DMSO treatment prepupal wing cells (Figure 3.3 G, p-value = 0.0007), confirming the role of Dco in stabilising Dsh.

A EGFP-Dsh FRAP after 30min treatment

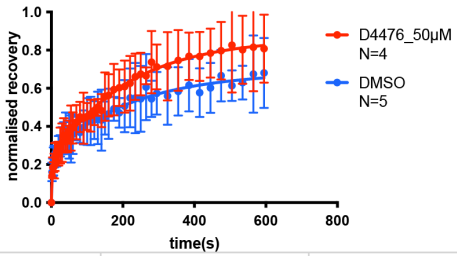

95% CI	D4476_50μM	DMSO
Plateau	0.8369 to 0.8965	0.6536 to 0.7313
PercentFast	23.74 to 27.71	34.86 to 40.16
KFast	0.2199 to 0.5363	0.2263 to 0.5119
KSlow	0.004124 to 0.005295	0.003421 to 0.005411
Fast HalfLife	1.293 to 3.152	1.354 to 3.063
Slow HalfLife	130.9 to 168.1	128.1 to 202.6

B Stbm-EGFP FRAP after 30min treatment

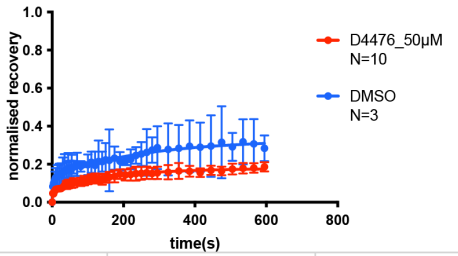

95% CI	D4476_50μM	DMSO
Plateau	0.1718 to 0.1852	0.3099 to 0.3602
PercentFast	32.34 to 38.43	38.66 to 44.61
KFast	0.2531 to 0.7507	0.2152 to 0.4666
KSlow	0.004915 to 0.007136	0.002747 to 0.004962
Fast HalfLife	0.9233 to 2.739	1.485 to 3.220
Slow HalfLife	97.13 to 141.0	139.7 to 252.3

C EGFP-Dsh FRAP after 10min treatment

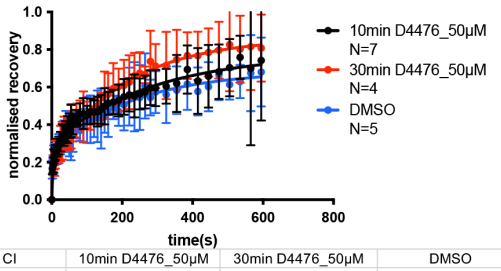

95% CI	10min D4476_50μM	30min D4476_50μM	DMSO
Plateau	0.7249 to 0.8674	0.8369 to 0.8965	0.6536 to 0.7313
PercentFast	35.71 to 41.33	23.74 to 27.71	34.86 to 40.16
KFast	0.1477 to 0.3218	0.2199 to 0.5363	0.2263 to 0.5119
KSlow	0.002444 to 0.004733	0.004124 to 0.005295	0.003421 to 0.005411
Fast HalfLife	2.154 to 4.692	1.293 to 3.152	1.354 to 3.063
Slow HalfLife	146.4 to 283.6	130.9 to 168.1	128.1 to 202.6

D Stbm-EGFP FRAP after 10min treatment

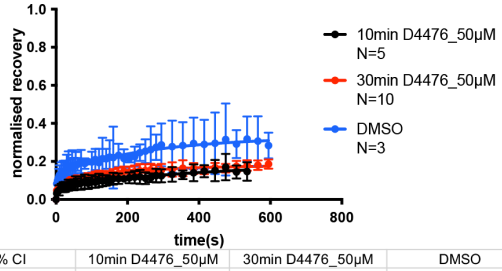

95% CI	10min D4476_50μM	30min D4476_50μM	DMSO
Plateau	0.1628 to 0.2652	0.1718 to 0.1852	0.3099 to 0.3602
PercentFast	25.80 to 38.11	32.34 to 38.43	38.66 to 44.61
KFast	0.1320 to 0.3021	0.2531 to 0.7507	0.2152 to 0.4666
KSlow	0.001172 to 0.003831	0.004915 to 0.007136	0.002747 to 0.004962
Fast HalfLife	2.294 to 5.251	0.9233 to 2.739	1.485 to 3.220
Slow HalfLife	180.9 to 591.5	97.13 to 141.0	139.7 to 252.3

E EGFP-Dsh in *stbm* FRAP after 30min treatment

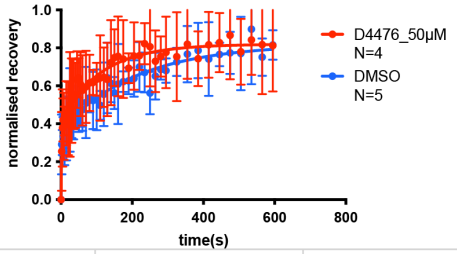

95% CI	D4476_50μM	DMSO
Plateau	0.7876 to 0.8438	0.7873 to 0.9679
PercentFast	46.25 to 56.24	40.19 to 48.20
KFast	0.2931 to 0.7700	0.2786 to 1.500
KSlow	0.006771 to 0.01219	0.002485 to 0.005854
Fast HalfLife	0.9002 to 2.365	0.4620 to 2.488
Slow HalfLife	56.86 to 102.4	118.4 to 278.9

F Stbm-EGFP in *dsh* FRAP after 30min treatment

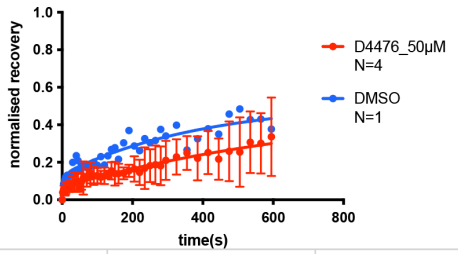

95% CI	D4476_50μM	DMSO
Plateau	(Very wide)	0.4151 to 1.149
PercentFast	???	14.06 to 33.12
KFast	???	0.07059 to 0.6518
KSlow	(Very wide)	0.0005985 to 0.004866
Fast HalfLife	???	1.063 to 9.819
Slow HalfLife	(Very wide)	142.5 to 1158

G EGFP-Dsh FRAP after 30min PF-4800567 treatment

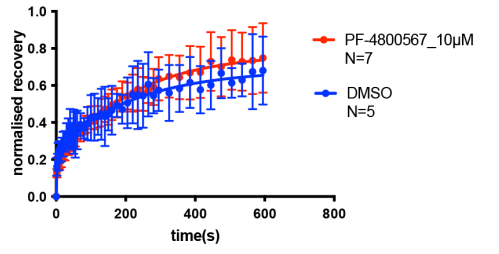

95% CI	PF4800567_10μM	DMSO
Plateau	0.7517 to 0.8007	0.6536 to 0.7313
PercentFast	21.21 to 24.49	34.86 to 40.16
KFast	0.2995 to 0.8444	0.2263 to 0.5119
KSlow	0.004184 to 0.005195	0.003421 to 0.005411
Fast HalfLife	0.8209 to 2.314	1.354 to 3.063
Slow HalfLife	133.4 to 165.7	128.1 to 202.6

Figure 3.3 CKI inhibitor regulates core planar polarity protein mobility

Figure legends in next page

Figure 3.3 CKI inhibitor regulates core planar polarity protein mobility

(A-B) FRAP analysis of EGFP-Dsh in *dsh[V26]* background (A) and Stbm-EGFP in *stbm[6]* background (B) in 6 h APF pupal wings after 30 min treatment of D4476 and DMSO control. Error bar: 95% confidence intervals. Curves are fitted in two-phase exponential association, parameters in fitted curves are summarised in the table on the bottom. Curves for D4476 treatment is in red, and for DMSO treatment control is in blue. (A) The recovery plateau of EGFP-Dsh increases significantly after 30-min D4476 treatment (N = 4 wings) compared to DMSO control (N = 5 wings), p-value < 0.0001. (B) Recovery plateau of Stbm-EGFP decreases significantly after 30-min D4476 treatment (N = 10 wings) compared to DMSO control (N = 3 wings), p-value < 0.0001. Statistical significance calculated by extra sum-of-squares F test.

(C-D) FRAP analysis of EGFP-Dsh in *dsh[V26]* background (C) and Stbm-EGFP in *stbm[6]* background (D) in 6 h APF pupal wings after 10 min treatment of D4476 and DMSO control. Error bar: 95% confidence intervals. Curves are fitted in two-phase exponential association, parameters in fitted curves are summarised in the table on the bottom. Curves for 10 min D4476 treatment is in red, for DMSO treatment control is in blue, and curve for 30 min D4476 treatment is also shown in red. (C) The recovery plateau of EGFP-Dsh after 10-min D4476 treatment (N = 10 wings) increases significantly compared to 30-min treatment of D4476 (N = 4 wings), p-value = 0.0109; and decreases significantly compared to DMSO control (N = 5 wings, p-value = 0.0404. (D) the recovery plateau of Stbm-EGFP after 10-min D4476 (N = 5 wings) show no significant change compared to 30 min treatment of D4476 (N = 10 wings)(p-value = 0.5007) and DMSO control (N = 3 wings)(p-value = 0.0873). Statistical significance calculated by extra sum-of-squares F test.

(E-F) FRAP analysis of EGFP-Dsh (E) and Stbm-EGFP (F) in *dsh[V26];stbm[6]* background in 6 h APF pupal wings after 30 min treatment of D4476 and DMSO control. Error bar: 95% confidence intervals. Curves are fitted in two-phase exponential association, parameters in fitted curves are summarised in the table on the bottom. Curves for 30 min D4476 treatment is in red, for DMSO treatment control is in blue. (E) The plateau of EGFP-Dsh after 30 min treatment of D4476 (N = 4 wings) has no significant change compared to DMSO control (N = 5 wings), p-value = 0.3237; while p-value for the rate of recovery [K_{fast} and K_{slow}] = 0.0006. (F) the recovery plateau of Stbm-EGFP (N = 4 wings) and DMSO control (N = 1 wing). Statistical significance calculated by extra sum-of-squares F test.

(G) FRAP analysis of EGFP-Dsh in *dsh[V26]* background in 6 h APF pupal wings after 30 min treatment of PF-4800567, and DMSO control. Error bar: 95% confidence intervals. Curves are fitted in two-phase exponential association, parameters in fitted curves are summarised in the table on the right. Curves for PF-4800567 treatment is

in red, and for DMSO treatment control is in blue. The recovery plateau of EGFP-Dsh increases significantly after 30-min PF-4800567 treatment (N = 7 wings) compared to DMSO control (N = 5 wings), p-value = 0.0007. Statistical significance calculated by extra sum-of-squares F test.

3.4 Dco asymmetric proximodistal subcellular localisation

An interesting observation in the nanobody-base Dco-GFP knock-down experiment shows that the GFP-tagged Dco is itself localised asymmetrically on the apicolateral junctions in the presence of the NSlmb-vhhGFP (Figure 3.1, B''). As pupae were aged at 25°C without heat-shock, the NSlmb-vhhGFP is not induced to express so that Dco-GFP is still retained.

To confirm that Dco is actually asymmetrically localised and the localisation is not due to the effect of the GFP tag, the localisation of Dco with HA-tagging is also checked. As shown in (Figure 3.4 B), the C-terminal tagged Dco-HA shows a poor HA immunolabelled signal, consistent with the Dco-HA staining in (Figure 3.2 A''' and B''). So, only the N-terminal tagged HA-Dco is examined for its asymmetric localisation (Figure 3.4 A-A''). Similar to the Dco-GFP in (Figure 3.1 B'' and D), HA-Dco shows weak proximodistal localisation (Figure 3.4 A''), and Coarse-Grain nematics indicate that the weak cellular proximodistal localisation coordinates into a tissue level proximodistal polarity (Figure 3.4 A').

The next question after observing the asymmetric localisation of Dco is it to ask whether it is selectively localised. Specifically, to find out which side of the cell is Dco localised to: distal cell ends, proximal cell ends, or both ends. Dco-GFP clones were generated in a heterozygous *dco-/+* background and a higher GFP intensity is observed at distal cell ends (Figure 3.4, D-E). This result shows that a greater amount of Dco localises on distal clone boundaries compared to proximal sides.

There is a previously published paper worth mentioning here where Dco-GFP was expressed under the *Act5C* promoter in the presence of endogenous Dco expression (Strutt *et al.*, 2006). Dco-GFP expressed in this condition is not observed to be asymmetric (Strutt *et al.*, 2006). Since the endogenous Dco is present in wing cells, it may compete with Dco-GFP for membrane localisation. To test this and to confirm the

asymmetric localisation of Dco, I repeated the *Act5C* driven Dco-GFP expression experiment in a *dco-* background. As expected, the *dco-* mutant background unmasks the asymmetric localisation of Dco-GFP (Figure 3.4 E-E' and F-F'). In (Figure 3.4 E'), the *Act5C* driven expressed Dco-GFP is strongly enriched at distal cell edges that large bright puncta are observed at the distal clone boundary (red arrows in Figure 3.4 E') but hardly observed at the proximal clone boundary (blue arrows in Figure 3.4 E').

The asymmetric localisation of the *Act5C* driven Dco-GFP shown in (Figure 3.4 E') is obviously stronger than that of the Dco-GFP expressed in Fosmid transgene shown in (Figure 3.4 C). This may be due to reduced competition with the endogenous Dco as stated above. Another explanation is that Dco-GFP may be expressed at higher levels under the *Act5C* promoter compared to the endogenous level in a Fosmid transgene, thus more GFP-tagged Dco was localised.

I also noticed a strong co-localisation between GFP-tagged Dco and core planar polarity proteins. First of all, the Dco-GFP is punctate in both Fosmid transgene expression (Figure 3.1 B') and *Act5C* driven expression (Figure 3.4 E'). Puncta of the Dco-GFP is found to co-localise with Dsh immunolabelling puncta (Figure 3.1 B-B'') and Fmi immunolabelling puncta (Figure 3.4 E-E''). These data suggest recruitment of Dco by core proteins.

In addition, the Fmi polarity increases in Dco-GFP expressing clones compared to *dco-* mutant tissue without Dco-GFP expression (Figure 3.4 G, p-value = 0.0025) This result supports the regulatory role of Dco on planar polarity, consistent to the observation in Dco knock-down experiment (Figure 3.1) and previous publications (Klein *et al.*, 2006; Strutt *et al.*, 2019a; Strutt *et al.*, 2006; Strutt and Strutt, 2020).

In summary, results in this section show that Dco is asymmetrically localised on distal cell ends and co-localises with core protein puncta in 28 h APF pupal wings.

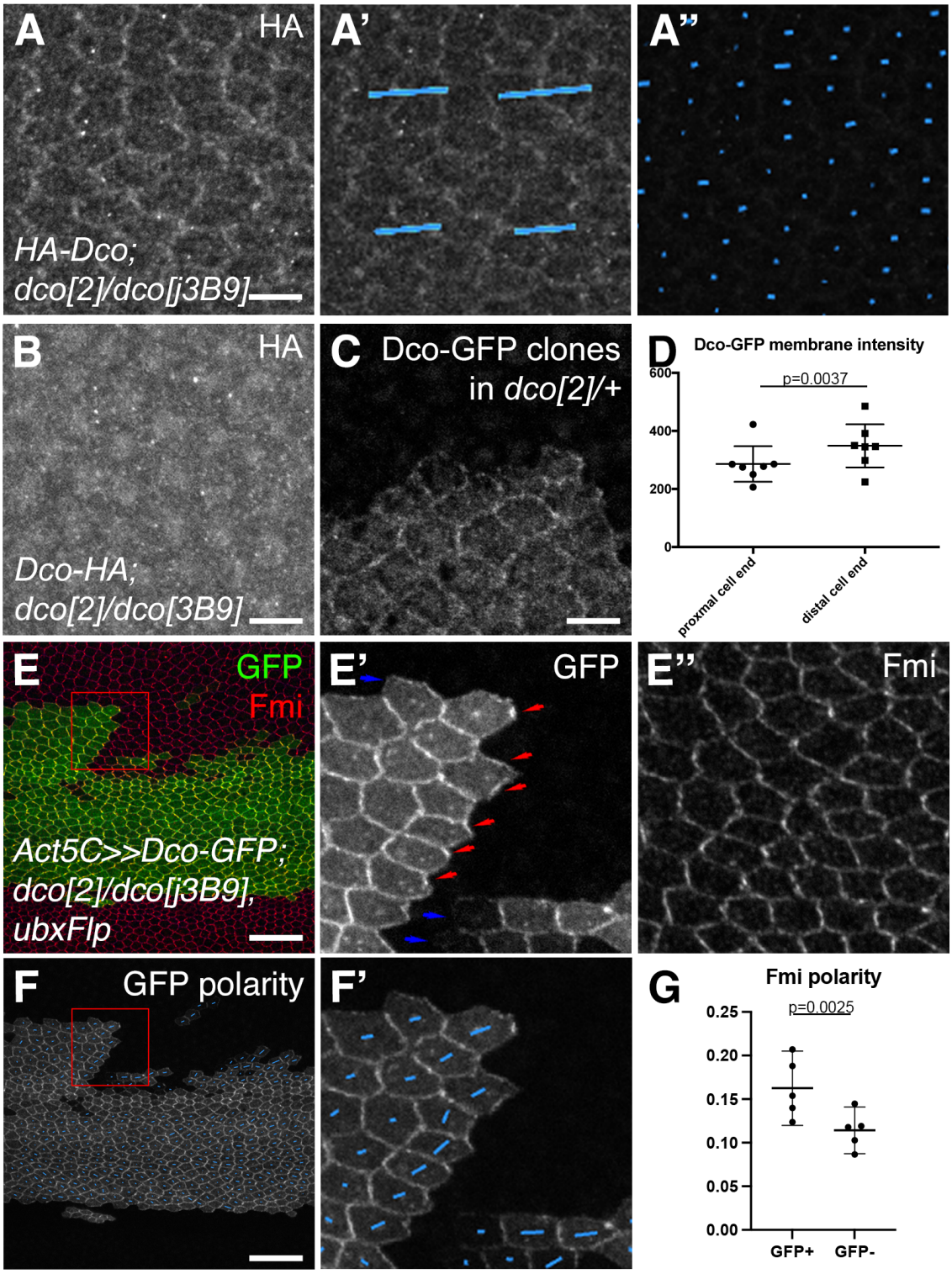

Figure 3.4 Dco-GFP localise asymmetrically

(A-A'') 28 h APF pupal wing expressing HA-Dco in *dco[2]/dco[j3B9]* background, immunolabelled for HA. Blue lines represent Coarse-Grain polarity nematics averaged over a 3-cell size (A'), and single cell polarity nematics (A''). Scale bar 5 μm.

(B) 28 h APF pupal wing carrying *Dco-HA* transgene in *dco[2]/dco[j3B9]* background. No immunolabelled HA signal was detected on cell membrane. Scale bar 5 μm.

(C) 28 h APF pupal wing carrying clones expressing Dco-GFP in *dco[2]/+* background. Scale bar 5 μm.

(D) Comparison of Dco-GFP intensity in Dco-GFP clones in *dco[2]/+* background. Dco-GFP intensity is higher distal clone boundaries compared to that on proximal clone boundaries, p-value = 0.0037, N = 7 wings. Statistical significance calculated by two-tail two-sample Student's paired t-test. Error bar: 95% confidence interval.

(E-E'') 28 h APF pupal wing carrying clones expressing Dco-GFP in *dco[2]/dco[j3B9]* background. GFP signal is shown in green (E) or grey (E'); Fmi is immunolabelled in red (E) or grey (E''). Region in red box is zoomed-in in panel (E'-E''), red arrows in panel E' indicate distal cell ends with high GFP signal; while blue arrows indicate proximal cell ends with low GFP signal. Scale bar 20 μm.

(F-F') Blue lines represent single cell polarity nematics of Fmi in panel E. Region in red box is zoomed-in in panel F'. Scale bar 5 μm.

(G) Comparison of Fmi polarity in Dco-GFP expressing clones (GFP+, *Act5C-Dco-GFP;dco[2]/dco[j3B9]*) and region without Dco-GFP expression (GFP-, *dco[2]/dco[j3B9]*). Fmi polarity is higher in Dco-GFP expressing clones, p-value = 0.0025, N = 5 wings. Statistical significance calculated by two-tail two-sample Student's paired t-test. Error bar: 95% confidence interval.

3.5 Discussion

3.5.1 Acute manipulations suggest a direct role of Dco on planar polarity

The first objective of this chapter is to provide evidence for whether Dco directly affects planar polarity protein localisation and stability by acutely manipulating Dco activity. My results in the 2-hour timescale Dco knock-down experiment (Figure 3.1) and 10-30 minutes timescale Dco inhibition experiment (Figure 3.3) support that a decreased Dco activity acutely regulates planar polarity and membrane mobility of core proteins Dsh and Stbm. These results consistent to results shown in **Section 2.2.2.3**, where the phosphomutant Dsh shows a decreased planar polarity (Figure 2.8) and Dsh mobility (Figure 2.9), supporting the importance of the S/T236-247 residues on Dsh and support that Dco directly regulates planar polarity.

The minutes-timescale Dco inhibition is relatively acute. A previous publication has shown that D4476 inhibitor inhibits the phosphorylation on ZRANB1 and decrases its deubiquitinase activity, in which obvious effect is only observable after 20-min inhibition (Feng et al., 2019). In light of this, the effect of the short 10-min and 30-min Dco inhibition (Figure 3.3) suggest that Dco directly regulates core protein membrane mobility. Thus, my results support that Dco directly regulates planar polarity via regulating core protein membrane mobility.

3.5.2 The ‘primary’ substrate

Another objective of this chapter is to identify which of Dsh or Stbm is the ‘primary’ or ‘direct’ substrate of Dco phosphorylation. While this question remains difficult to be definitively answered, my results in (Figure 3.3), which shows that Dco inhibition affects Dsh mobility in absence of Stbm and affects Stbm mobility in absence of Dsh, are consistent with the previous conclusion that Dco can act directly on both substrates

(Kelly *et al.*, 2016; Strutt *et al.*, 2019a; Strutt *et al.*, 2006). Thus, there might not be a primary substrate.

It is worth noticing that a reduced Dsh level on cell membrane reduces Stbm membrane localisation and stability (Ressurreicao *et al.*, 2018); and *stbm-* mutant decrease distal complex component Fz stability (Warrington *et al.*, 2017). These results suggest that a destabilised Dsh would ultimately destabilise Stbm and a stabilised Stbm would stabilise Dsh, which is not fully agreed with my results and results in (Strutt *et al.*, 2019a) where Dco exhibits opposite effects on the distal complex component Dsh and the proximal complex component Stbm. If the inhibition of Dco destabilise Dsh, how does Stbm get stabilised? Similarly, if the inhibition of Dco stabilise Stbm, how does Dsh get destabilised? Such a contradictory supports an independent regulation model:

> A reduction of Dsh leads to a reduced planar polarity and a reduce in core protein asymmetric localisation complexes (Bastock *et al.*, 2003; Feiguin *et al.*, 2001; Shimada *et al.*, 2001; Tree *et al.*, 2002; Usui *et al.*, 1999), suggesting that mixed-complexes are formed in this condition. In present of Dco, Dco destabilise Stbm in the mixed-complex, thus leading to a reduced stability (Ressurreicao *et al.*, 2018). However, in absence of Dco, Stbm in the mixed-complex cannot be destabilised, thus, the overall stability increases.

Another question needs to be answered is that whether Dco phosphorylates Dsh on S/T236-247 residues. An *in vitro* kinase assay shows that the mutation on residue S236 blocks the phosphorylation of Dsh by vertebrate Dco homologue CKIε (Klein *et al.*, 2006); and my results in (Figure 2.8) and (Figure 2.9) show that S/T236-247 residues are important for planar polarity, supporting S/T236-247 residues are Dco phosphorylation sites. However, an online tool NetPhos (Blom *et al.*, 1999) predicts that the S/T236-247 is phosphorylated by multiple serine/threonine protein kinases. Nevertheless, more than 100 S/T residues are present among 623 amino acids in *Drosophila* Dsh, hence hard to identify the functional phosphorylation sites of Dco on

Dsh. Thus, whether S/T236-247 residues on Dsh are phosphorylated by Dco is still unclear. Future identification of the phosphorylation sites can provide more evidence on this question by examining the phosphorylation status changes upon CKI inhibition. Such an experiment may also support a direct effect of Dco on regulating Dsh.

3.5.3 Subcellular localisation of Dco

In this chapter, I also describe a distal biased asymmetric localisation of Dco kinase. This result was first noticed in the nanobody-base Dco-GFP knock-down experiment (Figure 3.1) and further confirmed in HA-tagged Dco and Act5C-Dco-EGFP clonal experiment (Figure 3.3). To our knowledge, this is the first time Dco kinase has been observed to localise asymmetrically.

Considering the opposite effect of Dco on Dsh and Stbm stability, the asymmetric localisation of Dco lead to a model where Dco colocalises to distal complex, stabilises Dsh and destabilises Stbm on distal cell ends, thus promote planar polarity (Figure 3.5, and further discussed in **Discussion 5.2.1**). This model implies an assumption that 'mixed' complexes are present *in vivo*. Dco may function to stabilise Dsh in the 'mixed' complex and expel Stbm. It is worth noticing that mixed Dgo puncta are observed in a Stbm phosphomutant background (Strutt *et al.*, 2019a), suggesting phosphorylation of Stbm helps remove mis-localised proteins. Actually, before 24 h APF, the localisations of the core proteins are largely symmetric in pupal wing cells (Axelrod, 2001; Usui *et al.*, 1999), suggesting a 'mixed' status. Previous publications also suggest that the phosphorylation of Stbm is increased in distal cell ends: in an S2 cells co-transfection experiment, distal complex component Fz induces Stbm phosphorylation in a Dsh-independent manner (Kelly *et al.*, 2016); in pupal wings, the proximal complex component Pk negatively regulates Stbm phosphorylation (Strutt *et al.*, 2019a). Whether Fz and Pk regulates Stbm phosphorylation via affecting Dco localisation or

activation is unknown. Future study is required to determine the mechanism for Dco asymmetric localisation.

In addition, the density of Dco on proximal ends is not dramatically higher compared to the cytoplasm density (Figure 3.4 C,F'), so there may be a minor population of Dco on proximal cell ends. The proximal Dco can still be functional, which also fits the model as the major population is on the distal side, the function on the distal end can be dominant. Alternatively, the minor proximal population may not be functional as there might be an unknown mechanism inhibiting/activating Dco activity spatially.

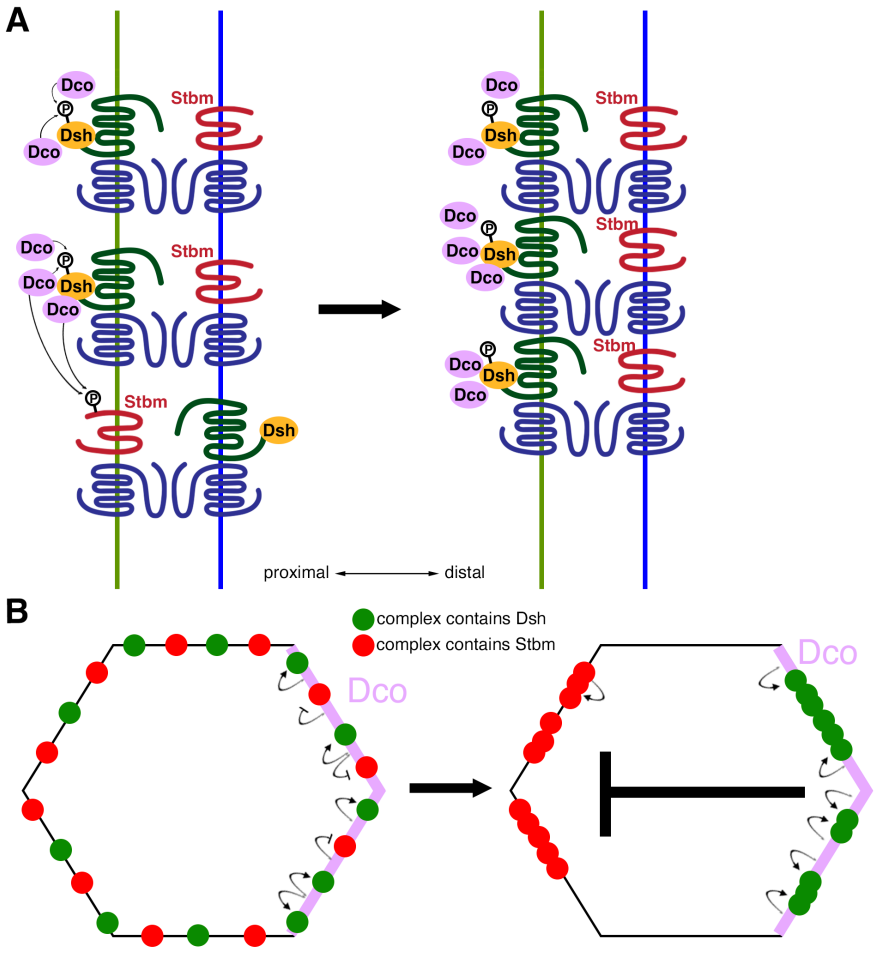

Figure 3.5 Distally localised Dco promote core pathway planar polarity

(A) Schematic showing model for distally localised Dco locally phosphorylates and stabilises Dsh in the distal complex. Dco phosphorylates the mis-localised Stbm and destabilises Stbm on distal cell junctions. Thus, Dsh promotes sorting.

(B) Schematic showing model for distally localised Dco promotes Dsh stabilising to distal cell ends and inhibits Stbm stabilising to distal cell ends. Stbm is removed from distal cell ends by Dco, and is stabilised to proximal junctions under other mechanisms. Thus, Dco promotes planar polarity in a cell-scale mechanism.

CHAPTER 4

Examination of aPKC function in core planar polarity establishment in Drosophila wings

4.1 Introduction

Atypical Protein Kinase C (aPKC) is a crucial apical-basal polarity regulator localised to the apical region (Goldstein and Macara, 2007; Suzuki and Ohno, 2006). It has been reported to genetically interact with Fz and regulate planar polarity in *Drosophila* eyes (Djiane *et al.*, 2005). My results in **Chapter 2** show that the expression of the dominant-negative form of aPKC leads to change in Fmi/Stbm protein distribution and polarity strength, supporting aPKC regulate planar polarity in *Drosophila* wings (Figure 2.4, Figure 2.5). However, the mechanism for aPKC regulating planar polarity is still unclear.

Djiane *et. al.* proposed that aPKC is recruited to Fz via another apicobasal polarity component dPatj thus phosphorylating Fz on S554 and 560 (Djiane *et al.*, 2005). These two phosphorylation residues lie in the cytoplasmic tail adjacent to the last transmembrane region (Figure 4.1 A). This region in the cytoplasmic tail is proposed to be crucial for Dsh recruitment to Fz as Fz[S554>F] mutant fails to recruit Dsh (Strutt *et al.*, 2012) and S560 lies within the conserved KTxxxW motif (Figure 4.1 A), which is also required for Dsh binding in *Xenopus* (Umbhauer *et al.*, 2000), *in vitro* (Wong *et al.*, 2003), and in *Drosophila* wing discs (Wu *et al.*, 2008). Given that reduced membrane localisation of Dsh decreases Fmi, Fz, and Stbm membrane protein levels in pupal wing cells (Ressurreicao *et al.*, 2018), if Dsh recruitment was regulated by phosphorylation of aPKC a change in core protein membrane intensity is expected. However, my results in **Chapter 2** show that the core protein Fmi and Stbm membrane intensity is not significantly affected simultaneously to the polarity change (Figure 2.4, Figure 2.5). Nonetheless, Djiane *et al*. reported that mutations in S554 and S560 residues on Fz cause no changes in Dsh recruitment in S2 cells and wing imaginal discs (Djiane *et al.*, 2005). Hence, it is still unclear whether aPKC regulates planar polarity in *Drosophila* wing cells via phosphorylating Fz on S554 and 560 and reducing Dsh recruitment.

To test this hypothesis and to examine the role of aPKC in pupal wings, multiple approaches were used in this chapter:

Firstly, whether the two reported phosphorylation sites of aPKC regulate Dsh recruitment is tested. The putative phosphorylation sites on Fz, S554 and S560, are mutated to examine their function in Dsh recruitment and planar polarity (**Section 4.2**).

Secondly, to test whether manipulating aPKC activity shows a similar phenotype of Fz S554 and S560 mutations. Approaches other than the previous dominant-negative form aPKC can be used, for instance, aPKC overexpression in pupal wings and ATP-analogue sensitive-based aPKC inhibition in prepupal wings (**Section 4.3**).

Finally, since an apical localised apicobasal polarity determinant, dPatj, physically interact with Fz (Djiane *et al.*, 2005), whether core proteins regulate aPKC membrane localisation is also tested (**Section 4.4**).

4.2 Candidate phosphorylation sites of aPKC on Fz proposed to be phosphorylated by aPKC

The phosphorylation of Fz by aPKC has been shown in *in vitro* kinase assays where two particular residues in the C-terminal of Fz (Figure 4.1 A) were shown to be essential for the phosphorylation by aPKC (Djiane *et al.*, 2005).

However, the evidence that aPKC phosphorylation of Fz is required for the establishment and maintenance of planar polarity has not been fully explored. Indeed, although Fz C-terminal is phosphorylated on specific residues *in vitro*, Djiane et al. reported that mutating S554 and S560 on Fz cause no changes in Dsh recruitment in S2 cells or in wing imaginal discs (Djiane *et al.*, 2005). However, Djiane et al. only tested these mutants in overexpression assays, the Dsh recruitment function of Fz intracellular loops (Cong *et al.*, 2004b; Strutt *et al.*, 2012; Tauriello *et al.*, 2012; Umbhauer *et al.*, 2000; Wong *et al.*, 2003) may be sufficient to recruit Dsh in

overexpression. Thus, whether S554 and S560 residues regulate Fz function by recruiting Dsh is tested in *Drosophila* pupal wings under conditions where Fz is not overexpressed.

To test whether these two putative phosphorylation sites are required *in vivo* in the *Drosophila* pupal wing to regulate Fz function, three constructs were created: an unmutated Fz-sfGFP, a phosphomutant Fz[A554,A560]-sfGFP (marked as Fz[A]-sfGFP) and a phosphomimetic Fz[E554,E560]-sfGFP (marked as Fz[E]-sfGFP)(Figure 4.1 B). Constructs are under the control of *Act5C*- promoter and sfGFP was tagged onto Fz to facilitate observation. Fz expressed under *Act5C*- promoter rescues *fz*- in pupal wings (Strutt, 2001). Constructs were introduced into *Drosophila* and recombined to a *fz*- mutant allele. Pupal wing twin-clones were generated to create an internal control to allow endogenous wild-type Fz expressing cells and Fz mutated cells to be compared within the same wing.

Firstly, wild-type tagged Fz-sfGFP was tested to see if it was correctly localised to the cell membrane in 28 h APF pupal wings. Twin-clones of endogenous Fz and Fz-sfGFP were created in pupal wings at 28 h APF to confirm that expression levels are in an appropriate range using the *Act5C* promoter in *attP2* site and sfGFP-tagging does not affect Fz localisation and polarity orientation. Wild-type Fz-sfGFP localised asymmetrically within the cells to the distal cell membranes (Figure 4.2 A). This can be seen at the clone borders where Fz-sfGFP in the clone is localised on the distal edges of the clone but not on the proximal edges (Figure 4.2 A', blue arrows in A' indicate distal Fz-sfGFP localisation). The orientation of polarity was also measured and shows that inside the *Fz-sfGFP* clones, polarity nematics were pointing in a proximal-distal orientation as seen in wild-type tissue (Figure 4.2 B-B').

In addition, the wild-type sfGFP-tagged Fz did not disrupt Dsh protein intensity in the cytoplasm (Figure 4.2 E) or the membrane intensity (Figure 4.2 F). The polarity strength of Dsh was also measured (Figure 4.2 G), where Dsh showed no difference

in polarity magnitude in Fz-sfGFP clones compared to control tissue. These results show that sfGFP-tagging of Fz and the expression under *Act5C* promoter do not disrupt the membrane localisation of Fz or Dsh.

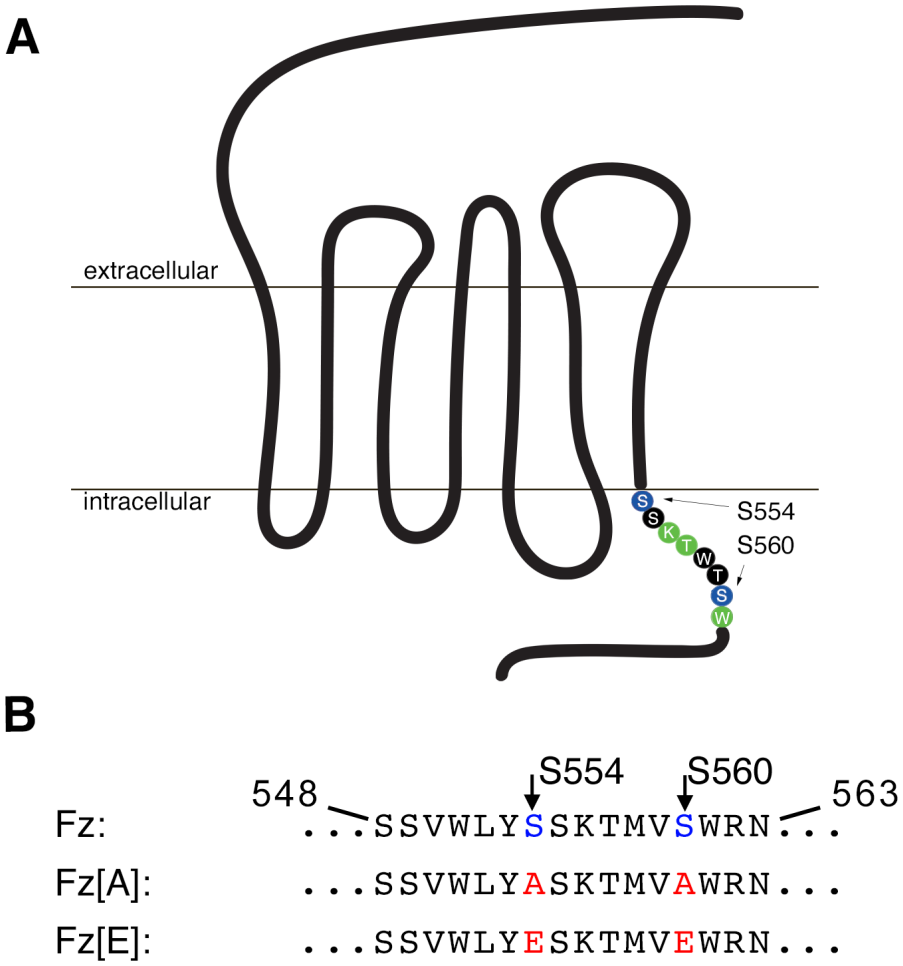

Figure 4.1 Fz C-terminal amino acid sequence

(A) Schematic showing the structure of Fz and amino acid sequence starting after the last transmembrane region. Fz is consisting of a N-terminal extracellular domain, three extracellular loops (on the top), seven transmembrane domains (in the middle, the region between two horizontal lines represents cell membrane), three intracellular loops, and a C-terminal intracellular tail (on the bottom). The KTxxxW motif is marked in green; S554 and S560 residues are marked in blue and are indicated by arrows.
(B) Schematic showing the Fz amino acid sequence starting from the last transmembrane region and extending towards the C-terminus. Two putative aPKC phosphorylation sites on Frizzled are the serines (S) at positions S554 and S560, marked in blue. Mutated amino acids to either alanine (A) or glutamic acid (E) are shown in red.

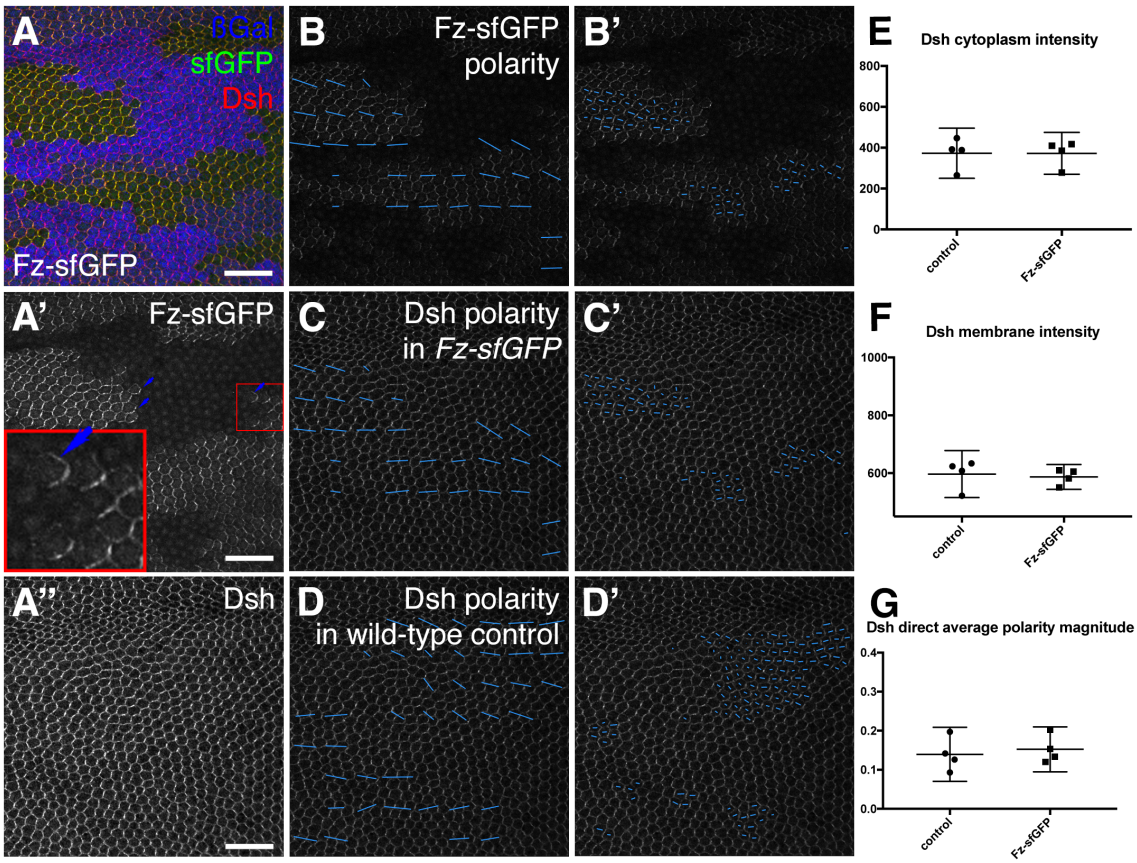

Figure 4.2 sfGFP-tag attached to Fz does not significantly change Dsh membrane intensity and polarity

(A-A'') 28 h APF pupal wing aged at 25°C carrying twin clones of *fz-sfGFP* (homozygous *fz-sfGFP* tissue is indicated by the loss of blue β-gal immunolabelling). β-gal is immunolabelled in blue, Fz-sfGFP signal shown in green (A) or grey (A'), Dsh is immunolabelled in red (A) or grey (A''); (A') sfGFP signal, blue arrows indicate cell junctions with distal sfGFP signal, a 20*20 μm^2 region marked in the red box is zoomed-in at the lower-left corner. Scale bar: 20 μm.

(B-D') Blue lines represent Coarse-Grain polarity nematics averaged over a 3-cell size (B-D) or single cell polarity nematics (B'-D') in 28 h APF pupal wings for (B) Fz-sfGFP shown in panel A', (C) Dsh in homozygous *fz-sfGFP* clone regions (shown by loss of β-gal immunolabelling in panel A), and (D) Dsh in wild-type Fz control tissue.

(E-F) Comparison of Dsh fluorescent intensity measurements in homozygous *fz-sfGFP* clone regions and homozygous wild-type Fz control regions, (E) No significant difference in the cytoplasm intensity, p = 0.9723. (F) No significant difference in the membrane intensity, p = 0.5645. N = 4 wings, a two-tail two sample Student's paired t-test was used. Error bar: 95% confidence intervals.

(G) Comparison of Direct average polarity nematics of Dsh. No significant difference in the cytoplasm intensity, p = 0.0798. N = 4 wings, a two-tail two sample Student's paired t-test was used. Error bar: 95% confidence intervals.

4.2.1 Phosphomutant and phosphomimetic versions of Fz-sfGFP exhibit disrupted polarity phenotypes

After confirming that sfGFP tagged Fz functions normally, the next step was to test whether the putative phosphorylation of these two residues affects Fz function.

Similar to the wild-type Fz-sfGFP, the phosphomutant Fz[A]-sfGFP did localise to the cell membrane and localise asymmetrically within the clones of cells (Figure 4.3 A-A'). However, on closer inspection, the Fz[A]-sfGFP did not localise to all of the distal cell membranes on the distal side of the clones as was observed in the wild-type Fz-sfGFP clones (compare Figure 4.2 A' and Figure 4.3 A', red arrows indicate distal cell membranes without Fz[A]-sfGFP localisation). This suggests that Fz[A]-sfGFP can localise to the cell membrane but is not able to redistribute to the distal end of the cell. In addition, the clones did not align their polarity along the proximodistal axis in the Fz[A]-sfGFP phosphomutant (compare Figure 4.2 B'-B' and Figure 4.3 B-B'), indicating that the polarity is not globally aligning across the wing cells.

Interestingly, in the phosphomimetic Fz[E]-sfGFP clones tagged Fz was localised to the cell membranes but showed greatly reduced asymmetric localisation within the clones (Figure 4.4 A). In addition, Fz[E]-sfGFP was not found at the clone boundary (Figure 4.4 A', red arrows indicate distal cell membranes without Fz[E]-sfGFP localisation). Polarity nematics also show a greatly reduced polarity (compare Figure 4.2 B-B' and Figure 4.4 B-B'). These results indicate that the phosphomimetic form of Fz was unable to form polarised asymmetric complexes.

Overall, the putative phosphorylation disrupted forms of Fz appear to be removed from the clone boundaries or unable to be stabilised there. So instead of a distal Fz containing complex forming on the distal side of the clone, the proximal complex forms there instead, thus inverting the local polarity.

It should be noted that the reduction in Fz protein level causes defects in Fz asymmetry and polarity alignment (Strutt *et al.*, 2016). Therefore, the change in membrane localisation and disrupted polarity in Fz[A]-sfGFP and Fz[E]-sfGFP clones could be due to an unequal expression level of the *Act5C* promoter driven expression compared to the endogenous Fz in the neighbouring control tissue. However, there is no significant difference in the intensity of the three Fz-sfGFP transgenes measured in the cytoplasm or at the membrane (Figure 4.4 H,I). This suggests that it is the disruption to the phosphorylation that leads to the changes in the distal Fz localisation and reduction of the polarity strength (Figure 4.4 J).

To summarise, the loss of cell junction localisation of the mutated Fz indicates a failure in forming or stabilising into intercellular complexes. Thus the Fz protein in the neighbouring wild-type cells accumulates on the clone boundary, resulting in proximal complexes accumulating inside the clone boundary and excluding the phosphor-disrupted Fz constructs. Consistent with this, the polarity strength is significantly lower in the mutated Fz (Figure 4.4 J, p-value comparing Fz[A]-sfGFP and Fz-sfGFP = 0.0148, comparing Fz[E]-sfGFP and Fz-sfGFP = 0.0001), showing a compromised function in planar polarity. Such an observation resembles the *fz-* mutant clones where planar polarity is disrupted in *fz-* clones and distal non-autonomy is shown (Adler *et al.*, 2000; Chen *et al.*, 2008; Gubb and Garcia-Bellido, 1982; Strutt and Strutt, 2007; Strutt, 2001; Vinson and Adler, 1987). Thus, mutations on S554 and S560 greatly disrupt Fz function. In the next section, I will examine whether the change in planar polarity is due to Fz being unable to recruit Dsh to the membrane and form stable complexes.

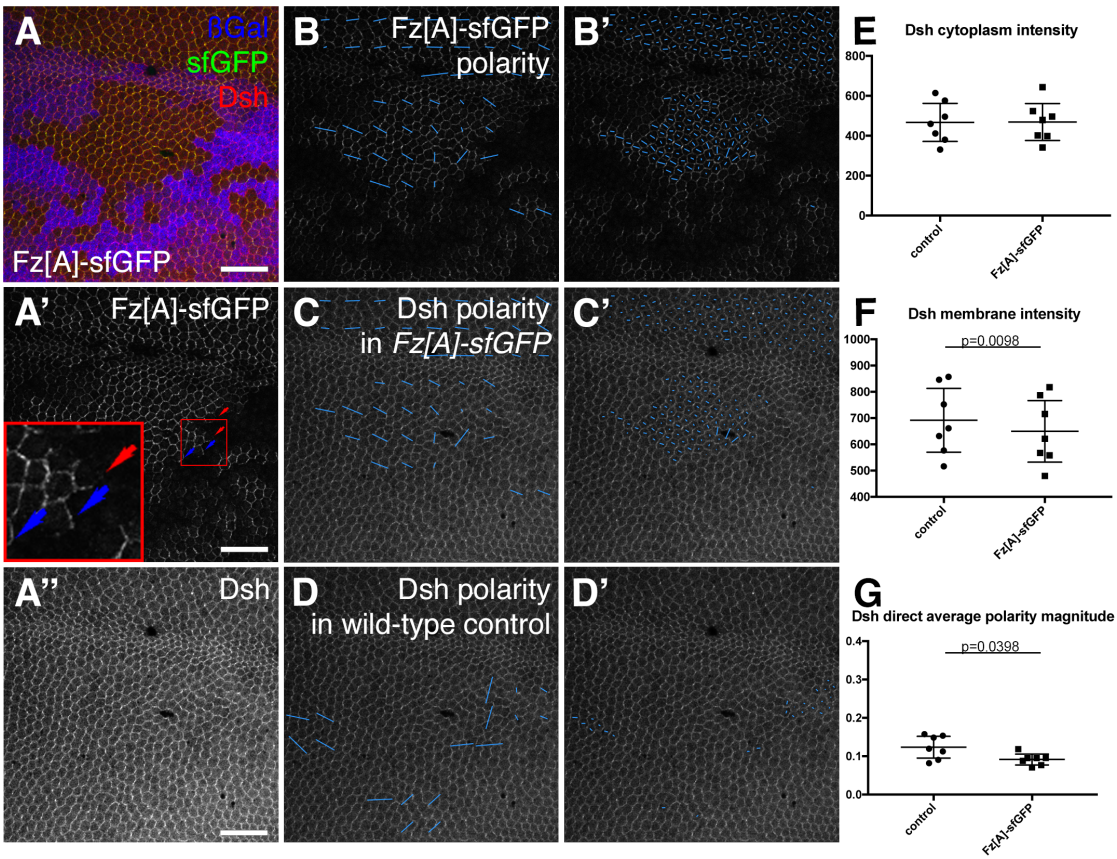

Figure 4.3 Mutation of Fz amino acids S554 and S560 to un-phosphorylatable Alanines affects Dsh cell membrane intensity and polarity

(A-A'') 28 h APF pupal wing aged at 25°C carrying twin clones of *fz[A]-sfGFP* (homozygous *fz[A]-sfGFP* tissue is indicated by the loss of blue β-gal immunolabelling). β-gal is immunolabelled in blue, Fz[A]-sfGFP signal shown in green (A) or grey (A'), Dsh is immunolabelled in red (A) or grey (A''); (A') sfGFP signal, blue arrows indicate cell junctions with distal sfGFP signal, a 20*20 μm^2 region marked in the red box is zoomed-in at the lower-left corner. Scale bar: 20 μm.

(B-D') Blue lines represent Coarse-Grain polarity nematics averaged over a 3-cell size (B-D) or single cell polarity nematics (B'-D') in 28 h APF pupal wings for (B) Fz[A]-sfGFP shown in panel A', (C) Dsh in homozygous *fz[A]-sfGFP* clone regions (shown by loss of β-gal immunolabelling in panel A), and (D) Dsh in wild-type Fz control tissue.

(E-F) Comparison of Dsh fluorescent intensity measurements in homozygous *fz[A]-sfGFP* and homozygous wild-type Fz clone regions. (E) No significant difference in the cytoplasm intensity, p = 0.9093. (F) Dsh membrane intensity is lower in homozygous *fz[A]-sfGFP* clones, p=0.0098. N = 7 wings, a two-tail two sample Student's paired t-test was used. Error bar: 95% confidence intervals.

(G) Direct average polarity nematics of Dsh. Dsh polarity is lower in homozygous *fz[A]-sfGFP* clones, p=0.0398. N = 7, a two-tail two sample Student's paired t-test was used. Error bar: 95% confidence intervals.

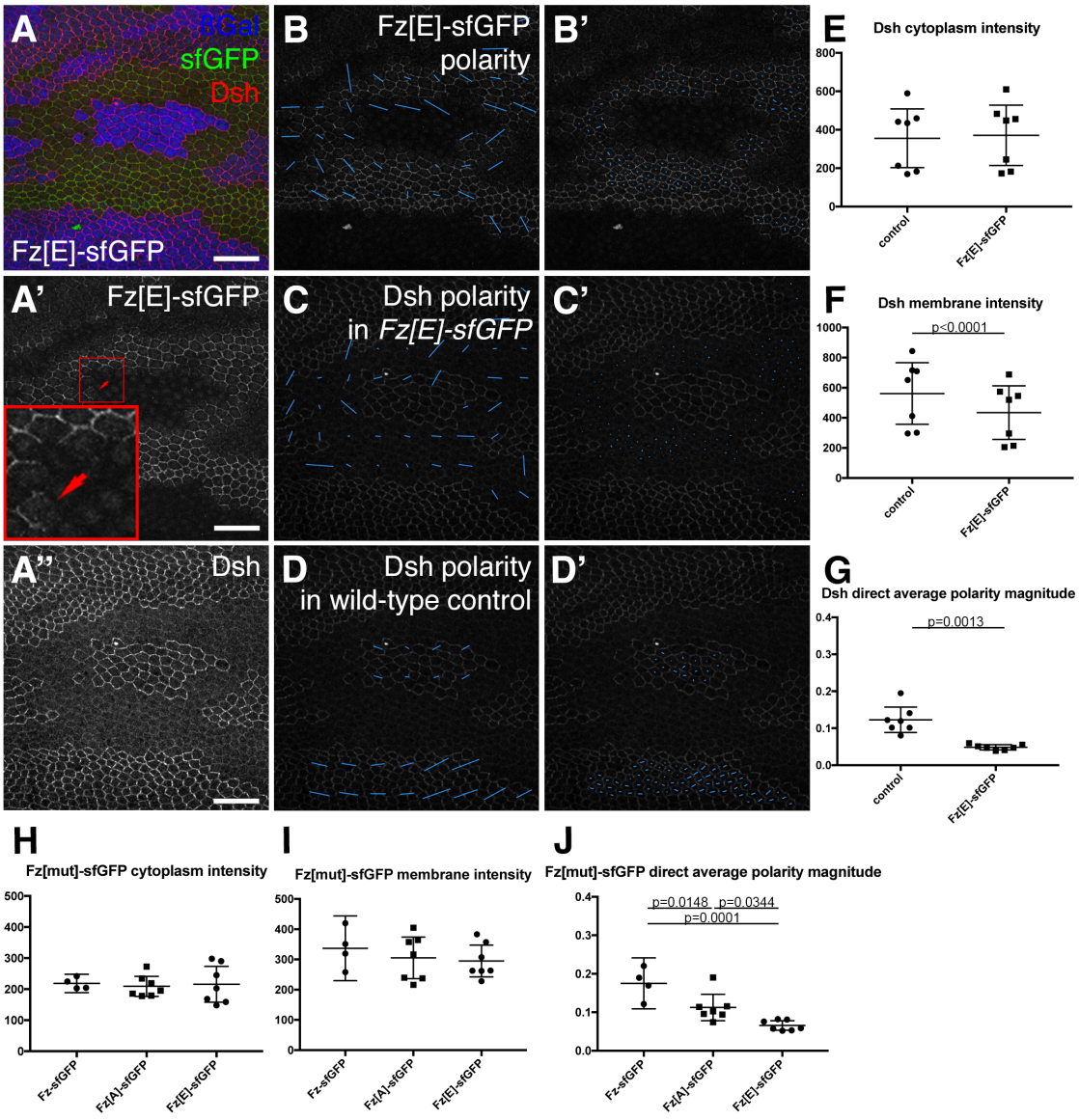

Figure 4.4 Mutation of Fz amino acids S554 and S560 to simulated phosphorylated Glutamic acid affects Dsh cell membrane intensity and polarity

(A-A'') 28 h APF pupal wing aged at 25°C carrying twin clones of *fz[E]-sfGFP* (homozygous *fz[E]-sfGFP* tissue is indicated by the loss of blue β-gal immunolabelling). β-gal is immunolabelled in blue, Fz[E]-sfGFP signal shown in green (A) or grey (A'), Dsh is immunolabelled in red (A) or grey (A''); (A') sfGFP signal, blue arrows indicate cell junctions with distal sfGFP signal, a 20*20 μm^2 region marked in the red box is zoomed-in at the lower-left corner. Scale bar: 20 μm.

(B-D') Blue lines represent Coarse-Grain polarity nematics averaged over a 3-cell size (B-D) or single cell polarity nematics (B'-D') in 28 h APF pupal wings for (B) Fz[E]-sfGFP shown in panel A', (C) Dsh in homozygous *fz[E]-sfGFP* clone regions (shown by loss of β-gal immunolabelling in panel A), and (D) Dsh in homozygous wild-type Fz control tissue.

(E-F) Comparison of Dsh fluorescent intensity measurements in homozygous Fz[E]-sfGFP and homozygous wild-type Fz clone regions. (E) No significant difference in the cytoplasm intensity, p = 0.0718. (F) Dsh membrane intensity is lower in homozygous *fz[E]-sfGFP* clones, p <0.0001. N = 7 wings, a two-tail two sample Student's paired t-test was used. Error bar: 95% confidence intervals.

(G) Direct average polarity nematics of Dsh. Dsh polarity is lower in homozygous *fz[E]-sfGFP* clones, p=0.0013. N = 7, a two-tail two sample Student's paired t-test was used. Error bar: 95% confidence intervals.

(H-I) Comparison of sfGFP fluorescent intensity measurements from Fz-sfGFP (N=4), Fz[A]-sfGFP (N=7) and Fz[E]-sfGFP (N=7) in homozygous clones (H) in the cytoplasm, no significant difference is shown in the ANOVA test, p-value ANOVA results for comparisons between Fz-sfGFP and Fz[A]-sfGFP = 0.9447; Fz-sfGFP and Fz[E]-sfGFP = 0.9957; Fz[A]-sfGFP to Fz[E]-sfGFP = 0.9596; or (I) in membrane regions, no significant difference is shown in the ANOVA test, , p-value ANOVA results for comparisons between Fz-sfGFP and Fz[A]-sfGFP = 0.7301; Fz-sfGFP and Fz[E]-sfGFP = 0.5797; Fz[A]-sfGFP and Fz[E]-sfGFP = 0.9538. Error bar: 95% confidence intervals.

(J) Comparison of direct average polarity nematics of sfGFP among Fz-sfGFP (N=4), Fz[A]-sfGFP (N=7) and Fz[E]-sfGFP (N=7). p-value ANOVA results for comparisons between Fz-sfGFP and Fz[A]-sfGFP = 0.0148; Fz-sfGFP and Fz[E]-sfGFP = 0.0001; Fz[A]-sfGFP to Fz[E]-sfGFP = 0.0344. Error bar: 95% confidence intervals.

4.2.2 The phosphomutant and phosphomimetic Fz-sfGFP constructs disrupt Dsh recruitment, but unclear whether phosphorylation is involved

The effect of phosphomutant and phosphomimetic Fz-sfGFP constructs on the asymmetric localisation of Dsh could be due to the inhibition of Dsh recruitment to the membrane, as stated above (Strutt *et al.*, 2012; Umbhauer *et al.*, 2000; Wong *et al.*, 2003; Wu *et al.*, 2008). Dsh recruitment may be altered by the change in the phosphorylation state of Fz, which in turn decreases the asymmetric localisation of core polarity complexes as the loss of Dsh in *Drosophila* pupal wing cells is known to disrupt the formation of stable core protein complexes (Bastock *et al.*, 2003; Feiguin *et al.*, 2001; Shimada *et al.*, 2001; Tree *et al.*, 2002; Usui *et al.*, 1999; Warrington *et al.*, 2017).

To test the hypothesis that the phosphorylation disrupted constructs inhibit Dsh recruitment to the membrane, immunolabelled Dsh in Fz-sfGFP (Figure 4.2 C-C'), Fz[A]-sfGFP (Figure 4.3 C-C'), and Fz[E]-sfGFP (Figure 4.4 C-C') twin clones is compared to that in control clones (Figure 4.2 D-D'; Figure 4.3 D-D'; Figure 4.4 D-D') in the same wings.

In the Fz[A]-sfGFP clones Dsh was retained at the membrane (Figure 4.3 A'') but was statistically weaker in intensity than that in control tissue (Figure 4.3 F, p-value = 0.0098), the measured intensity of Dsh in the cytoplasm was not significantly different (Figure 4.3 E). However, although Dsh asymmetry was also observed (Figure 4.3 A'',C-D'), the polarity magnitude was reduced (Figure 4.3, G p-value = 0.0398), suggesting the polarity of Dsh was disrupted by phosphomutant sfGFP-Fz[A].

In Fz[E]-sfGFP clones, Dsh intensity was also unchanged in the cytoplasm (Figure 4.4 A'',E) but significantly reduced at the cell boundary (Figure 4.4 A'',F p-value < 0.0001). The polarity of Dsh in Fz[E]-sfGFP clones is also weaker compared to control tissue (Figure 4.4, G p-value = 0.0013). These results show that changes to the

phosphorylation state of the residues S554 and S560 in Fz affect the recruitment of Dsh to the cell membrane.

However, it is still unclear whether Dsh recruitment is directly related to the phosphorylation on S554 and S560 in Fz. It would be strong evidence supporting this if opposite effects were observed, for instance, the phosphomimetic mutant increases membrane localised Dsh while the phosphomutant mutant has the opposite effect, but this was not observed. Instead, both phosphomutant (Fz[A]-sfGFP) and phosphomimetic (Fz[E]-sfGFP) clones have weaker Dsh membrane localisation compared to the unmutated Fz-sfGFP (Figure 4.4 J). So, the conclusion drawn in this stage is that S554 and S560 residues on Fz are crucial for Dsh recruitment, but whether the phosphorylation is involved is still unclear.

4.3 Manipulation of aPKC activity

4.3.1 Overexpression of wild-type aPKC induces cell-death-like phenotype

In the previous section, the S554 and S560 phosphorylation sites of Fz in its C terminus were shown to have a role in regulating Dsh recruitment to the cell membrane. Serines to alanine mutations on these residues reduce Fz phosphorylation by human aPKC (PKCζ) in an *in vitro* kinase assay (Djiane *et al.*, 2005), showing these sites can be phosphorylated by aPKC. Therefore, I wanted to know, does increasing aPKC expression alter Dsh recruitment to the membrane? An aPKC overexpression experiment was performed.

The kinase aPKC plays a significant role in apicobasal polarity (Sotillos *et al.*, 2004; Ventura *et al.*, 2020), reviewed in (Tepass, 2012). The apical membrane localisation of aPKC is regulated by other apicobasal polarity components, for instance, Dlg and Scrib (Ventura *et al.*, 2020). To ensure the overexpressed aPKC localised on the cell

membrane, a membrane-targeting CaaX motif (Gao *et al.*, 2009) was fused to a wild-type aPKC to make the aPKC$^{CaaX\ WT}$ construct (Sotillos *et al.*, 2004) (marked as aPKC[wt] in this Thesis).

The aPKC[wt] construct was overexpressed in *Drosophila* pupal wings using the *patched (ptc)-Gal4* driver so that only a stripe of known expression region was created across the centre of the wing. Fmi was immunolabelled in this experiment as it reflects Dsh membrane localisation as acutely decreased Dsh protein level decreases the membrane localisation and polarity of Fmi, Fz, and Stbm (Ressurreicao *et al.*, 2018).

Initially, wings containing the *ptc-Gal4* induced UAS-aPKC[wt] construct were cultured at 29°C and aged until the equivalent of 28 h APF when aged at 25°C. Under this condition, large cells were observed in the *ptc* expression region and the epithelium appears disrupted (Figure 4.5, D). This phenotype was most likely to be due to cell death leaving holes in the wing, making it impossible to quantify the intensity of the cell membranes. Previously published work also described similar phenotypes when overexpressing aPKC[wt], where wings show integrity defect and aPKC is shown to phosphorylate and stabilise Crb (Sotillos *et al.*, 2004). My large-cell-like morphology results shown here agrees with the Crb overexpression phenotype in adult wings where holes are found in overexpression region (Sotillos *et al.*, 2004), which can be rescued by dominant-negative aPKC (Sotillos *et al.*, 2004).

Ageing pupae at 29°C disrupts morphology which may mask defects in polarity orientation caused by aPKC overexpression. To find out if there are any potential more subtle polarity changes caused by aPKC overexpression, pupae were aged at 25°C and then shifted to 29°C for either 3.5 h or 4.75 h to increase the expression of aPKC[wt] transiently (see **Materials and Methods 6.2.1**). The pupae aged at 25°C for 28 h did not show any strong differences in the morphology of the cells (Figure 4.5, A), pupal wings raised at 25°C and shifted to 29°C for 3.5 h or 4.75 h showed mild differences in the morphology of the cells and the cells were less well packed (Figure 4.5, B-C

compared to A and D), showing aPKC still affects apical cell morphology. Since the morphology is not strongly disrupted, the planar polarity was then examined.

The pupae aged at 25°C for 28 h were first checked, in which the immunolabelled core polarity protein Fmi shows proximodistally aligned polarity nematics (Figure 4.5, A-A"'). Pupal wings in this condition are used as the control for comparison.

Pupal wings raised at 25°C and shifted to 29°C for 4.75 h showed an increase in the magnitude of polarity compared to control wings raised at 25°C (p-value = 0.0377) or to wings raised at 25°C and shifted to 29°C for 3.5 h (p-value = 0.0115)(Figure 4.5, E). This suggests that these wings were more polarised. Curiously, for the wings raised at 25°C and shifted to 29°C for 4.75 h, the Fmi membrane intensity was not changed (Figure 4.5 G), while the cytoplasm intensity is significantly reduced compared to wings raised at 25°C (p-value = 0.0300) or to wings raised at 25°C and shifted to 29°C for 3.5 h (p-value = 0.0056)(Figure 4.5, F). This may be evidence of the beginning of the disruption in cell morphology.

Results here show that polarity strength increases with the overexpression of aPKC (Figure 4.5 E) and Fmi membrane intensity is not reduced as if Dsh membrane localisation is affected (Figure 4.5 G). Results in **Section 2.2.1.1** show that reducing aPKC activity using a dominant negative aPKC reduces polarity strength (Figure 2.4, E, Figure 2.5, D) and the Fmi membrane intensity is not significantly increased (Figure 2.4, F, Figure 2.5, E). These data suggest a positive role of aPKC in planar polarity, but core protein level Fmi is not affected at the membrane.

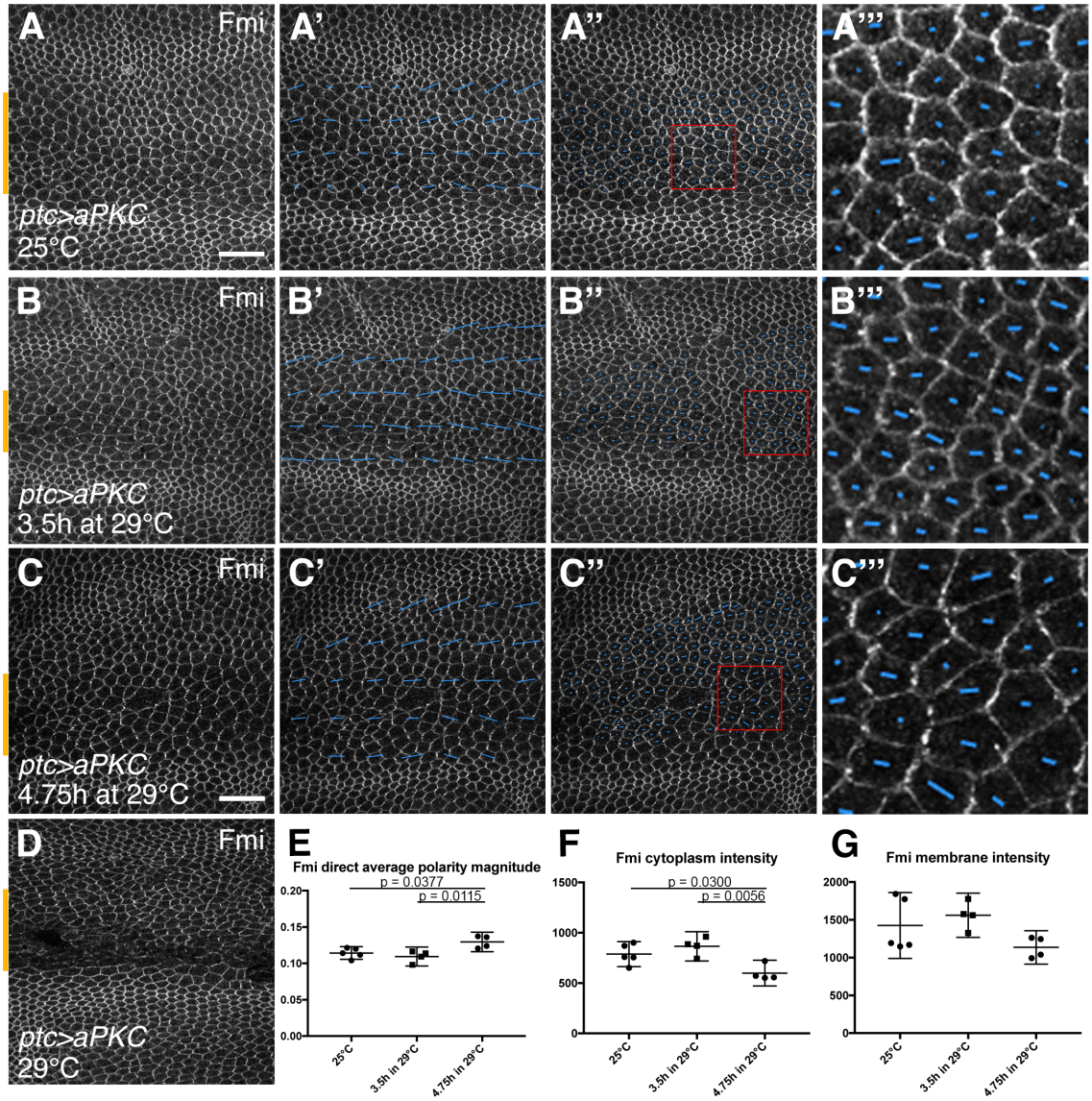

Figure 4.5 Fmi immunolabelling in ptc>aPKC pupal wings

Fmi immunolabelling in 28 h APF aPKC overexpression in the *patched(ptc)* expression domain in pupal wings cultured at different temperatures to vary aPKC expression.

(A-A'') Control *ptc>aPKC* pupal wings aged at 25°C. Blue lines represent Coarse-Grain polarity nematics averaged over a 3-cell size (A'), Single cell polarity nematics (A''), Zoomed-in of red box region (A'''). Scale bar: 20 μm.

(B-B'') 28 h APF *ptc>aPKC* pupal wings cultured in 25°C for 24 h then move to 29°C for 3.5 h. Blue lines represent Coarse-Grain polarity nematics averaged over a 3-cell size (B'), Single cell polarity nematics (B''), Zoomed-in of red box region (B'''). Scale bar: 20 μm.

(C-C'') 28 h APF *ptc>aPKC* pupal wings cultured in 25°C for 22.5 h then move to 29°C for 4.75 h. Blue lines represent Coarse-Grain polarity nematics averaged over a 3-cell size (C'), Single cell polarity nematics (C''), Zoomed-in of red box region (C'''). Scale bar: 20 μm.

(D) 28 h APF *ptc>aPKC* pupal wings cultured in 29°C for 24 h. Scale bar: 20 μm.
(E) Comparison of direct average polarity nematics of immunolabelled Fmi in 28 h APF pupal wings with different 29°C culture time. p-value ANOVA results for comparisons between wings aged at 25°C to wings shifted to 29°C for 4.75 h = 0.0377; between wings shifted to 29°C for 3.5 h to wings shifted to 29°C for 4.75 h = 0.0115. No significant difference is shown in the ANOVA test between wings aged at 25°C to wings shifted to 29°C for 3.5 h, p-value = 0.6368. N = 5 wings for wings aged at 25°C; N = 4 wings for wings shifted to 29°C for 3.5 h; N = 4 wings for wings shifted to 29°C for 4.75 h. Error bar: 95% confidence interval.
(F-G) Comparison of immunolabelled Fmi intensity in 28 h APF pupal wings with different 29°C culture time (F) in the cytoplasm, p-value ANOVA results for comparisons between wings aged at 25°C to wings shifted to 29°C for 4.75 h = 0.0300; between wings shifted to 29°C for 3.5 h to wings shifted to 29°C for 4.75 h = 0.0935. No significant difference is shown in the ANOVA test between wings aged at 25°C to wings shifted to 29°C for 3.5 h, p-value = 0.4490; or (G) in membrane regions, no significant difference is shown in the ANOVA test. p-value ANOVA results for comparisons between wings aged at 25°C to wings shifted to 29°C for 3.5 h = 0.7182; between wings aged at 25°C to wings shifted to 29°C for 4.75 h = 0.2548; between wings shifted to 29°C for 3.5 h to wings shifted to 29°C for 4.75 h = 0.0935. N = 5 wings for wings aged at 25°C; N = 4 wings for wings shifted to 29°C for 3.5 h; N = 4 wings for wings shifted to 29°C for 4.75 h. Error bar: 95% confidence intervals.

4.3.2 Inhibiting analogue sensitive form of aPKC affects cell size

Attempting to avoid disruption of the epithelium and associated changes in cell shape and size, I used an ATP analogue-sensitive form of aPKC to manipulate aPKC activity. This form of aPKC is called aPKC[as4], which is specifically inhibited in the presence of an ATP analogue 1NA-PP1 (Hannaford et al., 2019). 1NA-PP1 specifically inhibits the kinase activity of aPKC[as4] with the IC50 of ~0.1μM, *in vitro* (Hannaford *et al.*, 2019). As for *in vivo* aPKC[as4] inhibition, 5-min 20 μM 1NA-PP1 treatment significantly reduces Par-6 apical localisation in *Drosophila* follicle cells; and 110-min 10 μM 1NA-PP1 treatment also significantly affects Baz apical localisation in egg chambers (Hannaford *et al.*, 2019). In this experiment, 30-min 10 μM 1NA-PP1 treatment was performed.

To address whether aPKC kinase activity alters Dsh recruitment to the membrane, twin-clones of aPKC[as4] were generated in the prepupal wing to directly compare the Dsh intensity and cell polarity in control cells and aPKC disrupted cells. Six hour APF prepupal wings were used, where core planar polarity proteins, especially Dsh, were found to localise to apical cell junction (Axelrod, 2001; Classen *et al.*, 2005; Tree *et al.*, 2002) and the pupal cuticle has not been secreted (Waddington, 1939) thus chemicals can access the cells, which is not possible if using pupal wings. The 6 h APF prepupal wings were placed into the 1NA-PP1 10 μM drug for a 30-min treatment prior to fixing and immunostaining.

Endogenous E-cad was immunolabelled and found that the cell apical area is significantly decreased (Figure 4.6 D p-value = 0.0083), consistent with a recent publication showing that acute optogenetic perturbation and chemical inhibition of aPKC in the *Drosophila* follicular epithelium increases apical constriction and disrupts epithelial architecture (Osswald et al., 2022). This result confirms that aPKC was inhibited successfully in this approach as the cell shape was affected acutely. However, the attempt to avoid cell shape change failed.

Immunolabelled Dsh was examined despite the change in cell apical area. In prepupal wings treated with 1NA-PP1 for 30min, no change in Dsh membrane intensity (Figure 4.6, A',F) or in polarity magnitude (Figure 4.6, E) was observed when comparing the wild-type control tissue and the *aPKC[as4]* clones (Figure 4.6, E-G). Therefore, these results suggest that acutely disrupting aPKC in this manner does not affect Dsh membrane localisation or asymmetric localisation.

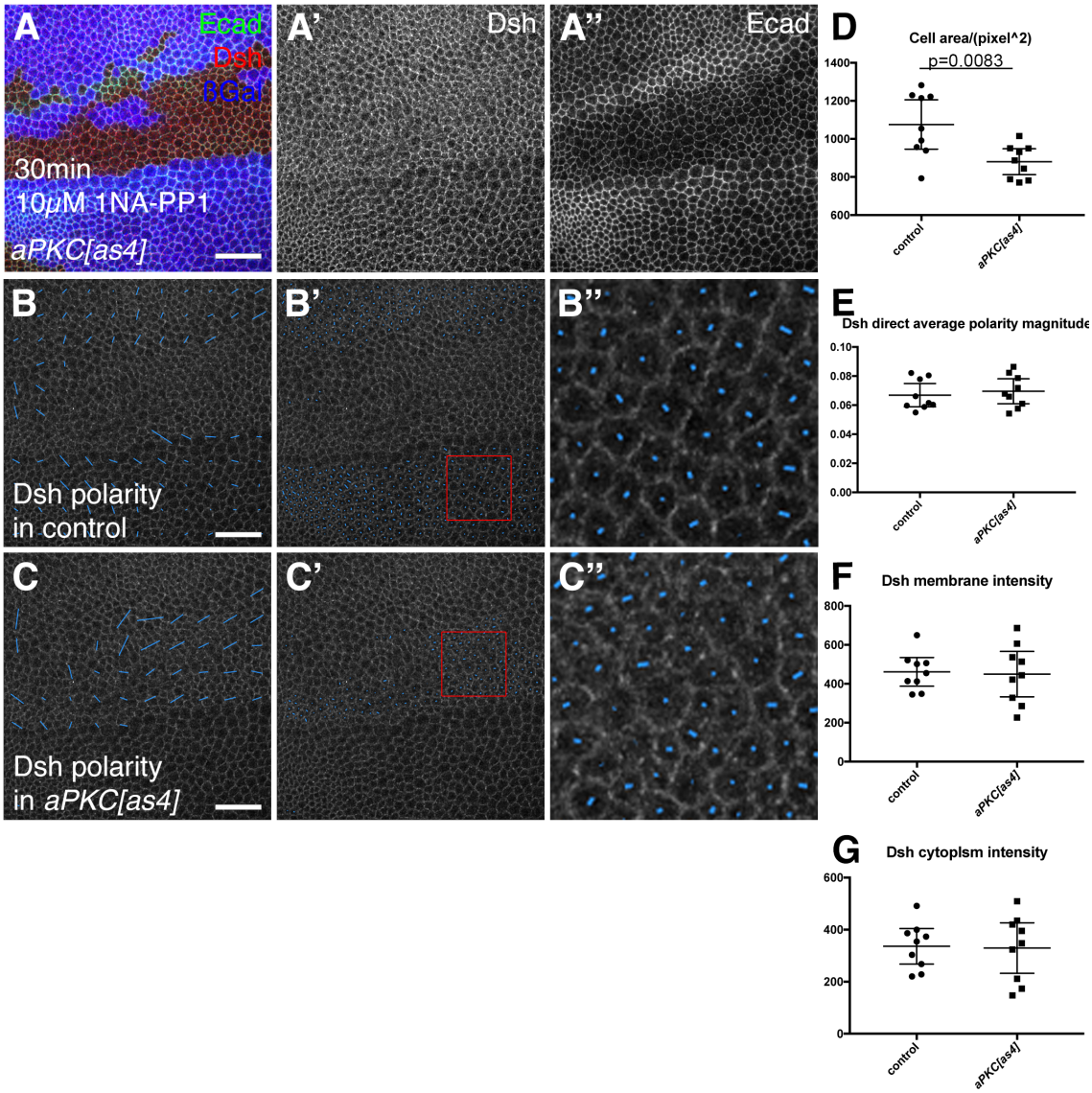

Figure 4.6 Inhibition of analogue sensitive form of aPKC

Figure legends in next page

Figure 4.6 Inhibition of analogue sensitive form of aPKC

(A) 6 h APF prepupal wing aged at 25°C carrying twin clones of *aPKC[as4]* (homozygous *aPKC[as4]* tissue is indicated by the loss of blue β-gal immunolabelling). aPKC[as4] was inhibited by adding the drug 1NA-PP1 for 30 min at a concentration of 10μM; (A') immunolabelled Dsh; (A'') immunolabelled E-cad. Scale bar: 20 μm.

(B-C') Blue lines represent polarity nematics of the immunolabelled Dsh in panel A' in 6 h APF *arm-LacZ* control prepupal wings tissue (B-B') or homozygous *aPKC[as4]* prepupal wings tissue (C-C'). (B,C) Coarse-Grain polarity nematics averaged over a 3-cell size (B',C') Single cell polarity nematics (B'',C'') Zoomed-in of red box region. Scale bar: 20 μm.

(D) Comparison of cell area in control tissue and homozygous *aPKC[as4]* tissue in 6 h APF prepupal wings. Cell area is smaller in homozygous *aPKC[as4]* tissue, $p = 0.0083$, statistical significance calculated by a two-tail two-sample Student's paired t-test. N = 9 wings. Error bar: 95% confidence intervals.

(E) Comparison of direct average polarity nematics of immunolabelled Dsh in control tissue and homozygous *aPKC[as4]* tissue in 6 h APF prepupal wings. No significant difference is shown in a two-tail two-sample Student's paired t-test, $p = 0.6100$, N = 9 wings. Error bar: 95% confidence intervals.

(F-G) Comparison of immunolabelled Dsh intensity in control tissue and homozygous *aPKC[as4]* tissue in 6 h APF prepupal wings. No significant difference is shown (F) in the membrane intensity, $p = 0.8317$; or (G) in the cytoplasm intensity, $p = 0.8785$. N = 9 wings, a two-tail two sample Student's paired t-test was used. Error bar: 95% confidence intervals.

4.4 Core planar polarity protein Fmi regulates aPKC level

Fz physically interacts with dPatj, which also regulates planar polarity and genetically interacts with aPKC in the *Drosophila* eye (Djiane *et al.*, 2005). Since the apical localised apicobasal polarity determinants act in mutual interaction network (reviewed in (Tepass, 2012)), I hypothesise that the subcellular localisation of aPKC is also regulated by Fz or other core planar polarity proteins. To test this hypothesis, aPKC immunofluorescent signal was checked in *fmi[E59]* null mutant clones in 28 h APF pupal wings (Figure 4.7 A-A'). In *fmi-* mutant tissue, all other five core proteins loss cell junctional localisation (Axelrod, 2001; Bastock *et al.*, 2003; Feiguin *et al.*, 2001; Shimada *et al.*, 2001; Strutt, 2001; Tree *et al.*, 2002).

A slight but statistically significant increase in both cytoplasmic intensity (p-value = 0.0067) and membrane intensity (p-value = 0.0327) of aPKC is noticed in *fmi[E59]* mutant clones compared to control tissue (Figure 4.7, F). This suggests that core planar polarity proteins affect the overall protein level of aPKC. Interestingly, aPKC immunolabelling in *fmi-* clones appears hazy (Figure 4.7 A', comparing zoomed-in regions in B'' to C''), indicating the cytoplasm population is increased to a larger extent. This may suggest that aPKC is less tightly localised to the junctions in *fmi-* clones. Thus, Fmi or possibly other core proteins may play a role in localising aPKC to the apical membrane.

Since *fmi-* mutant affects aPKC membrane level, whether aPKC localises asymmetrically is also checked. As shown in (Figure 4.7 B-B'' and C-C''), aPKC is not strongly asymmetrically localised and polarity nematics are not aligned. The strength of asymmetric localisation also shows no difference (Figure 4.7 D). Therefore, no strong evidence supporting aPKC asymmetric localisation in pupal wings was obtained.

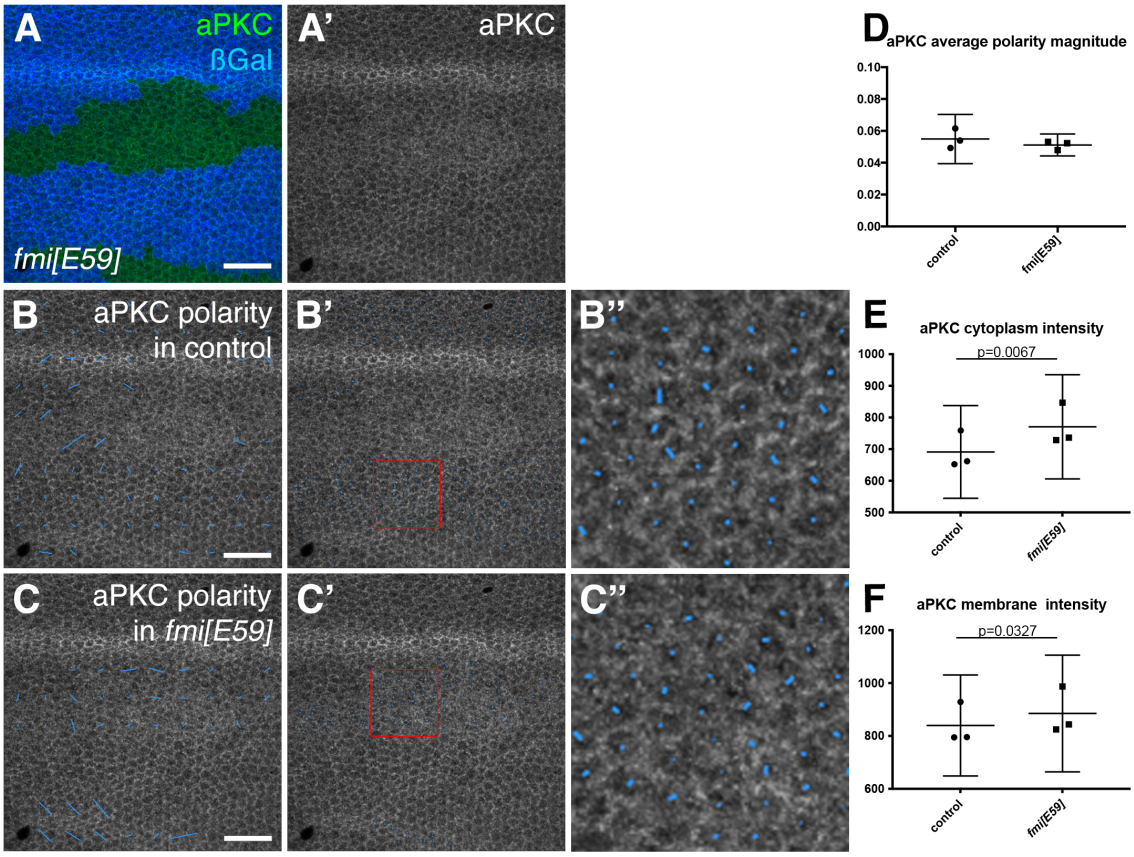

Figure 4.7 aPKC immunolabelling in pupal wings carrying *fmi[E59]* mutant clones

(A-A'') 28 h APF pupal wing aged at 25°C carrying twin clones of *fmi[E59]* (homozygous *fmi[E59]* tissue is indicated by the loss of blue β-gal immunolabelling); β-gal is immunolabelled in blue; aPKC is immunolabelled in green (A) or grey (A'). Scale bar: 20 μm.

(B-C') Blue lines represent polarity nematics in 28 h APF *arm-LacZ* control pupal wings tissue (B-B') or homozygous *fmi[E59]* pupal wings tissue (C-C'). (B,C) Coarse-Grain polarity nematics averaged over a 3-cell size (B',C') Single cell polarity nematics (B'',C'') Zoomed-in of red box region. Scale bar: 20 μm.

(D) Comparison of direct average polarity nematics of immunolabelled aPKC in control tissue and homozygous *fmi[E59]* tissue in 28 h APF pupal wings. N = 3 wings, p = 0.2474, statistical significance calculated by two-tail two-sample Student's paired t-test. Error bar: 95% confidence intervals.

(E-F) Comparison of immunolabelled aPKC intensity in control tissue and homozygous *fmi[E59]* tissue in 28 h APF pupal wings. (F) The cytoplasm intensity is higher in homozygous *fmi[E59]* tissue, p = 0.0067. (G) The membrane intensity is higher in homozygous *fmi[E59]* tissue, p = 0.0327. N = 3 wings, a two-tail two sample Student's paired t-test was used. Error bar: 95% confidence intervals.

4.5 Discussion

4.5.1 The proposed aPKC phosphorylation sites on the Fz C-terminal tail are required for planar polarity in the *Drosophila* wing

In this chapter, the two reported phosphorylation sites of aPKC, S554 and S560, on Fz were mutated to test whether they regulate Dsh recruitment. By mutating these two residues, aside from changes in Dsh recruitment, it is found that both phosphomutant and phosphomimetic forms of Fz show decreased polarity (Figure 4.4 J), showing the S554 and S560 residues are required for Fz polarity.

However, the (Djiane *et al.*, 2005) data suggests that aPKC-mediated Fz phosphorylation results in planar polarity defects in the *Drosophila* eye, but but only when the phosphomutant form of Fz (Fz[A]) were overexpressed. They found that the overexpressed phosphomimetic version (Fz[E]) did not cause ommatidial polarity defects. These contradict the result in the wing shown in (Figure 4.4 J)(**Section 4.2.1**), albeit the ommatidial polarity is a less sensitive assay than core protein asymmetry. Similar mutants were checked in wings and found no clone boundary localisation can be observed in Fz[E]-sfGFP clones, suggesting Fz[E] fails in its competition with endogenous Fz. This can be the reason why Djiane *et al.,* did not see phenotype in Fz[E] expressed eyes as Fz[E] may not stabilise to cell junction in the presence of endogenous Fz, thus, cannot interfere with the polarity establishment.

4.5.2 Mutating S554 and S560 of Fz affects Dsh recruitment to the cell membrane in the wing

Dsh membrane intensity is decreased in both phosphomutant and phosphomimetic Fz clones compared to control tissue (Figure 4.3 F; Figure 4.4 F), suggesting Dsh membrane recruitment is regulated by S554 and S560 residues. This is contradicted by (Djiane *et al.*, 2005), where Fz[A] and Fz[E] recruits Dsh-GFP in overexpression wing imaginal discs and transfected S2 cells, resembling wild-type Fz (Djiane *et al.*,

2005). This may be because Fz[E] contains weak Dsh recruitment ability on its intracellular loops (Cong *et al.*, 2004b; Strutt *et al.*, 2012; Tauriello *et al.*, 2012; Umbhauer *et al.*, 2000; Wong *et al.*, 2003), which may be sufficient to recruit Dsh in overexpression. As shown in (Figure 4.4 A''), physiological level Fz[E]-sfGFP expression still weakly recruits Dsh to cell membranes.

My results from these mutants further confirm the importance of the cytoplasmic tail region, which is adjacent to the last transmembrane region, in recruiting Dsh (Strutt *et al.*, 2012; Umbhauer *et al.*, 2000; Wong *et al.*, 2003; Wu *et al.*, 2008). However, as no opposite effects on phosphomutant and phosphomimetic Fz-sfGFP were observed, it is still hard to conclude whether the effect is due to the phosphorylation status of S554 and S560.

4.5.3 aPKC positively regulates planar polarity but the core protein level is not affected

In **Section 4.3.1**, I described an aPKC overexpression experiment showing a positive regulatory role of aPKC in planar polarity but no change in core protein level was observed (Figure 4.5). This is consistent with the aPKC[DN] expression result in **Section 2.2.1.1**, in which the dominant-negative aPKC expression region exhibits a weaker polarity strength while the membrane intensity is unchanged (Figure 2.4 and 2.1.5). These results show the opposite effects on planar polarity strength between the expression of the dominant-negative form of aPKC and the overexpression of aPKC, supporting the view that aPKC positively regulates planar polarity while it does not affect core protein membrane intensity.

In aPKC overexpressed tissue, in which Fz is expected to be hyper-phosphorylated, planar polarity strength increases (Figure 4.5 E). This does not mimic the phenotype of the phosphomimetic form of Fz, where polarity strength and Dsh recruitment are

decreased (Figure 4.4 F,G,J). Conversely, a reduced Dsh membrane level leads to a reduced Fmi membrane localisation and polarity (Ressurreicao *et al.*, 2018), which is not observed in aPKC overexpression tissue (Figure 2.4 and Figure 2.5), suggesting aPKC does not affect Dsh recruitment. Thus, an increased aPKC level does not mimic the phosphomimetic Fz phenotype, suggesting S554 and S560 are not functional phosphorylation sites of aPKC, or alternatively, the Glutamic acid phosphomimetics are not charged enough (Chen and Cole, 2015). A insufficient negative charge phosphomimetic mutant may actually mimicking a hypo-phosphorylated status of Fz, thus, phosphomutant and phosphomimetic mutant produce similar phenotype. It is also possible that mutations on Fz disrupt its conformation and reduce its function in Dsh recruitment and planar polarity.

4.5.4 Acute inhibiting aPKC activity leads to cell area decrease

The Dsh membrane localisation is not changed by the acute inhibition of aPKC (Figure 4.6 F). This also suggests that Dsh recruitment is not regulated by the phosphorylation of aPKC. Instead, the cell apical area was found to be smaller after 30-min 1NA-PP1 inhibition on aPKC[as4] (Figure 4.6 D), suggesting that the effect of aPKC on regulating cell shape is more acute than on planar polarity. This result is consistent with a recent publication that acute inhibition of aPKC in the *Drosophila* follicular epithelium increases apical constriction (Osswald *et al.*, 2022). This paper proposed that the effect of aPKC on apical constriction is via actomyosin; and the apical constriction applies pulling forces on neighbouring cells (Osswald *et al.*, 2022).

Thus, besides the Dsh recruitment hypothesis, I will propose a theoretical possibility where aPKC indirectly affects planar polarity via affecting actomyosin.

On the one hand, as an apicobasal polarity component, aPKC regulates the apicobasal subcellular distribution of non-muscle myosin II proteins (Reviewed in (Carmena,

2021)), which is an essential component of actomyosin network that direct epithelial rearrangements (Bertet et al., 2004; Rauzi et al., 2010; Sawyer et al., 2011; Skoglund et al., 2008). On the other hand, wing cells rearrange their shape and cell junctions in the hinge contraction process in which mechanical tension guides the reorientation of core planar polarity proteins (Aigouy *et al.*, 2010; Etournay *et al.*, 2015). These results link aPKC to tension in hinge contraction. This model will be further discussed in **Discussion 5.2.2**.

4.5.5 Do the core proteins affect the levels of aPKC?

The result in **Section 4.3** shows that in the absence of Fmi, aPKC protein level is increased in pupal wing cells, showing a negative regulatory role of Fmi on aPKC (Figure 4.7). It is unclear how Fmi regulates aPKC intensity. Since both membrane and cytoplasm intensity is found to increase in *fmi-* clones, core planar polarity proteins may affect the overall protein level. Or as suggested by the hazy immunolabelled aPKC in *fmi-* clones (Figure 4.7 C''), core proteins may play a role in localising aPKC to the apical membrane.

Given that core proteins localise asymmetrically, if core proteins regulate aPKC localisation, would aPKC be localised asymmetrically? There is a previous publication reporting aPKC planar anisotropic subcellular localisation in *Drosophila* salivary glands during tubulogenesis (Roper, 2012). Other apicobasal polarity components are also reported to localise asymmetrically in the tissue plane. For instance, Par-1 is found asymmetrically localised in pupal wings (Harumoto et al., 2010); Baz is also asymmetrically localised in *Drosophila* eye cone cells (Aigouy and Le Bivic, 2016) and in *Drosophila* embryos (Simoes Sde et al., 2010). In light of these results, asymmetric localisation of aPKC in pupal wings is expected as aPKC mutually interacts with other apicobasal polarity determinants (reviewed in (Tepass, 2012)).

However, there is not an obvious asymmetry of aPKC in the pupal wing at 28 h APF. As measured in (Figure 4.7 D), the polarity magnitude of aPKC in wild-type tissue is lower than 0.08, while the other measurements of core protein polarity magnitudes in wild-type control tissue in this Thesis are generally above 0.10. Also, polarity nematics in (Figure 4.7 B-B'' and C-C'') show that aPKC is not strongly asymmetrically localised. Therefore, no strong evidence supporting aPKC asymmetric localisation in pupal wings so far. Future experiment confirming whether aPKC is asymmetrically localised in planar plain in *Drosophila* wings is needed.

CHAPTER 5

General Discussion

The aim of this project was to systematically assess the role of kinases in core planar polarity in the *Drosophila* wing model. This aim can be broken into two major objectives:

1) To test whether kinases on the candidate list (**Introduction 1.3**) play a role in planar polarity establishment in the *Drosophila* wing.
2) To examine the mechanism of how these kinases regulate planar polarity in the *Drosophila* wing.

5.1 Which kinases play a role in planar polarity establishment in *Drosophila* wing

Testing candidate kinases in a systematic manner in a simple model system is crucial in the field. Multiple kinases have been proposed to regulate planar polarity in different contexts (**Introduction 1.3**, and reviewed in (Harrison *et al.*, 2020)), e.g., vertebrates or *Drosophila* eyes. Compared to vertebrates and *Drosophila* eyes, the *Drosophila* wing has its unique advantages. First of all, the planar polarity is most well-studied in *Drosophila* wings (Goodrich and Strutt, 2011; Maung and Jenny, 2011; Strutt and Strutt, 2021; Thomas and Strutt, 2012). Secondly, the readout of the planar polarity is clear and simple in *Drosophila* pupal wing cells, which establishes the asymmetrical proximodistal localisation of core planar polarity proteins after 24 h APF (Aigouy *et al.*, 2010; Axelrod, 2001; Bastock *et al.*, 2003; Strutt, 2001; Tree *et al.*, 2002; Usui *et al.*, 1999). The asymmetric localisation of core proteins is easily accessible in the flat monolayer epithelium pupal wings.

Among kinases, aPKC, Par-1, Dco, Abl, Msn, and Nmo were picked as our candidate kinases and their function in planar polarity were checked in the *Drosophila* wing model.

aPKC

Results in **Chapter 2** and **Chapter 4** show that aPKC positively regulates planar polarity in wings (Figure 2.4; Figure 2.5; Figure 4.5). It was hypothesised that aPKC regulates Dsh recruitment via phosphorylating Fz on S554 and S560 residues. My results confirm the importance of these two residues in the KTxxxW region in recruiting Dsh (Strutt *et al.*, 2012; Umbhauer *et al.*, 2000; Wong *et al.*, 2003; Wu *et al.*, 2008). However, it is still hard to conclude whether the effect is due to the phosphorylation status of S554 and S560. Hence, the mechanism of the regulation of aPKC on planar polarity is still unclear. The possible mechanism for aPKC regulating planar polarity is discussed below (**Discussion 5.2.1**).

Par-1 and Dco

Par-1 is unlikely to regulate planar polarity in wings as the hypomorphic allele (Figure 2.6) or RNAi (Figure 2.7) of Par-1 does not induce planar polarity change. Although mutations on the putative phosphorylation sites of Par-1 in S/T236-247 residues in Dsh (Penton *et al.*, 2002) do affect Dsh polarity, membrane level, and stability, S/T236-247 residues are also putative phosphorylation sites of other serine/threonine kinases, e.g., Dco (Klein *et al.*, 2006; Strutt *et al.*, 2006).

Previous publications in the *Drosophila* wing have shown a role of Dco in regulating planar polarity (Klein *et al.*, 2006; Strutt *et al.*, 2019a; Strutt *et al.*, 2006), but the mechanism is yet to be examined. My results in Chapter 3 provide some lines of evidence supporting that Dco regulates planar polarity via promoting core protein sorting. Detail is discussed below (**Discussion 5.2.2**).

Abl

Abl is also unlikely to regulate planar polarity in wings. The mutation on the reported phosphorylation site DshY473 reduces Dsh membrane targeting (Figure 2.10 A-B), but the *abl*- amorphic allele clones (Figure 2.11) or *Abl RNAi* expressing tissue (Figure

2.12; Figure 2.13; Figure 2.14) does not show Dsh localisation change, not mimicking the DshY473 phonotype. This may be due to redundancy with other kinases that phosphorylate Y473 in compensating for Abl or Y473 disrupts the conformation (or charge status) of Dsh thus inhibiting its membrane binding. Hence, Abl is not essential in regulating planar polarity or localising Dsh to the membrane. Whether Abl has a regulatory role in planar polarity is still an unsolved question.

Besides, cells in the Abl overexpression tissue appear to be irregular (Figure 2.12; Figure 2.13; Figure 2.14). This agrees with previous publications that Abl regulates epithelial morphogenesis via regulating adherens junctions and cytoskeleton (Fox and Peifer, 2007; Grevengoed *et al.*, 2001). The change in polarity direction may be an indirect effect via cell shape change as cell packing has been proposed to affect planar polarity (Aigouy *et al.*, 2010; Classen *et al.*, 2005; Etournay *et al.*, 2015).

Msn

Dsh polarity decreases in *msn-* clones (Figure 2.15), suggesting Msn regulates planar polarity in *Drosophila* wings. In *Drosophila* eyes, loss-of-function alleles of *msn* suppress the Dsh overexpression phenotype (Paricio *et al.*, 1999), and *msn* RNAi knock-down enhances Pk[Sple] overexpression phenotype (Daulat *et al.*, 2012). These results suggest that Msn enhances Pk[Sple] activity in *Drosophila* eyes, possibly due to promoting Pk[Sple] membrane localisation as PRICKLE1 membrane localisation is increased in MINK1 overexpressed HEK293T cells and decreased in morpholino oligonucleotide (MO)-xMink1 knock-down in *Xenopus* embryos (Daulat *et al.*, 2012). However, Pk[Sple] is not the dominant isoform in *Drosophila* wings (Gubb *et al.*, 1999). Msn in *Drosophila* wing cells may only affect the isoform Pk[Sple] while the dominant isoform Pk is not affected, thus, the core protein membrane localisation is not affected.

Nmo

The Nmo kinase is not directly manipulated in this Thesis. Instead, the proposed Nmo phosphorylation sites are mutated. The protein level of the phosphomimetic Pk mutant is increased (Figure 2.16 E-F) while no change in polarity is observed (Figure 2.16 D). This does not agree with (Collu *et al.*, 2018), where Nmo is suggested to regulate planar polarity in *Drosophila* eyes by phosphorylating Pk and increasing Pk degradation. The contradiction may suggest that Nmo promotes planar polarity by decreasing the Pk isoform protein level in *Drosophila* eyes, while functioning oppositely in wings to increase the Pk protein level in wing cells, thus, also promoting planar polarity.

5.2 How do kinases regulate planar polarity in the *Drosophila* wing

5.2.1 Dco: local and cellular sorting

In this Thesis, the acute manipulation of Dco activity supports a direct regulatory role of Dco in planar polarity. Chemical inhibition experiments of Dco show that Dco acutely stabilises Dsh to cell junctions while destabilises Stbm from cell junctions (Figure 3.3). This agrees with a previous publication showing that long-term expression of dominant-negative Dco stabilises Dsh and destabilises Stbm (Strutt *et al.*, 2019a). Also, Dco itself is observed to be localised asymmetrically to the distal cell junction and colocalise with core protein puncta (Figure 3.4).

As stated in **Introduction 1.2.3.3**, a cell-scale mechanism is needed in the establishment process of planar polarity (Fischer *et al.*, 2013). My results in **Chapter 3** suggest an asymmetrically localised Dco-mediated cellular sorting mechanism of planar polarity establishment, in which the local stabilising and destabilising of the core proteins Dsh and Stbm can be amplified into a cell scale (Figure 3.5).

On the one hand, Dco localises distally and stabilises Dsh locally on the distal cell junction. This also means that Dco has no/weak stabilisation on Dsh on proximal cell junctions, thus the proximally mis-localised Dsh cannot get stabilised into core protein complexes. The free Dsh diffuses (or gets transported (Matis et al., 2014)) to the distal cell junctions and gets stabilised there after meeting Dco.

On the other hand, Dco destabilises the mis-localised Stbm on the distal cell junction. Evidence supporting this is that Fz promotes Stbm phosphorylation, suggesting Stbm phosphorylation happens in distal junctions (Kelly *et al.*, 2016). Also, mixed Dgo puncta are observed in a Stbm phosphomutants background (Strutt *et al.*, 2019a), suggesting phosphorylation of Stbm helps remove mis-localised proteins. The destabilised Stbm may move to and get stabilised onto proximal junctions, the proximal cytoplasmic core

protein Pk may participate in stabilising Stbm (Strutt *et al.*, 2019a).

If Dco asymmetric localisation can be important for planar polarity establishment, what regulates the asymmetric localisation of Dco? So far, there is no direct evidence for identifying the regulator for Dco membrane localisation. Indirect evidence can be provided here as Dco is observed to be colocalised with core protein puncta (Figure 3.4), suggesting core proteins recruit Dco. This is supported by the discovery that Dsh physically interacts with Dco vertebrate homologue CKIε (Gao *et al.*, 2002; Klein *et al.*, 2006), and Stbm co-immunoprecipitate Dco (Kelly *et al.*, 2016). In addition, Dsh phosphorylation requires Fz (Klein *et al.*, 2006; Strutt *et al.*, 2006) and is stimulated by Dgo (Jenny *et al.*, 2005), suggesting that the distal core planar polarity proteins may recruit Dco. Besides, Ft, a component in Ft/Ds polarity and Hippo signalling pathway, is also found to co-immunoprecipitate Dco (Feng and Irvine, 2009; Pan *et al.*, 2013; Sopko *et al.*, 2009). However, as Ft localise anteroposteriorly in 28 h APF pupal wings (Brittle *et al.*, 2022; Merkel et al., 2014), the regulatory effect for Dco localisation, if there is any, would be negative.

Whether the asymmetric distribution of Dco is crucial for its function in planar polarity is also unclear. As there is a cytoplasm population of Dco, Dsh and Stbm may get phosphorylated when they are not localised in complexes at junctions, followed by stabilising onto opposite junctions. However, this is unlikely. There are some lines of evidence suggesting that the cell membrane localisation of Dsh and Stbm is important for their phosphorylation. Mutations disrupting Stbm membrane localisation reduce its phosphorylation level in S2 cells (Kelly *et al.*, 2016). Besides, Fz recruits Dsh to the cell membrane (Axelrod, 2001) and the phosphorylation level of Dsh is reduced in fz-mutants (Shimada *et al.*, 2001), suggesting that Fz recruits Dsh and induces Dsh phosphorylation. Thus, Dco may regulate planar polarity only when recruited to cell membranes.

Future experiments to identify Dco membrane localisation regulators can be done. For

instance, to check Dco localisation in a core protein mutant background. If Dco asymmetric localisation is regulated by core planar polarity proteins, a new feedback mechanism is suggested, where core proteins localise Dco to the distal cell end and Dco stabilise Dsh distally. Also, the cell-scale sorting model is needed to be tested, for example, forcing Dco ectopic localisation to proximal junctions to examine whether the (cellular-scale) polarity is reversed. This experiment would also provide evidence for whether the asymmetric distribution of Dco is crucial for planar polarity.

5.2.2 aPKC: cross-talk between apicobasal polarity and planar polarity?

The apicobasal polarity component aPKC kinase affects planar polarity, as shown in **Section 2.2.1.1** and **Section 4.3.1** (Figure 2.4; 2.5; Figure 4.5). The acute chemical aPKC inhibition result (Figure 4.6 D) suggests that the effect of aPKC on actomyosin-mediated apical constriction is more acute than on planar polarity. Consistently, aPKC negatively regulates actomyosin in *Drosophila* ((Osswald *et al.*, 2022; Roper, 2012), reviewed in (Carmena, 2021)). Thus, the regulatory role of aPKC on the actomyosin network suggests that aPKC plays a role in wing cell tensions.

Myosin II localisation is positively regulated by tension (Fernandez-Gonzalez et al., 2009). In the process of the planar polarity establishment between 24 h and 30 h APF, forces are applied on pupal wing cells due to hinge contraction. In this process, Myosin II is observed to accumulate to anteroposterior cell junctions most likely to counter that tension (Sugimura and Ishihara, 2013). Since wing cells rearrange their shape and cell junctions in the hinge contraction process and the mechanical tension guides the reorientation of core planar polarity proteins (Aigouy *et al.*, 2010; Etournay *et al.*, 2015), aPKC may regulate planar polarity via regulating tensions.

This mechanism may also explain the cell-death-like phenotype in aPKC overexpression experiment (Figure 4.5). In this condition, the overexpressed aPKC

reduces Myosin II accumulation on the anteroposterior junctions, which makes cells less intolerant to tensions, thus, disrupts cell shape and tissue morphology.

In addition, not only aPKC, but other apicobasal polarity components also regulate actomyosin (Lecuit and Yap, 2015; Mack and Georgiou, 2014; Silver et al., 2019). For instance, Baz regulates the planar polarized distribution of myosin II and adherens junction proteins in *Drosophila* embryos (Simoes Sde *et al.*, 2010). Thus, other apicobasal polarity components may also regulate planar polarity in a similar mechanism.

Interestingly, cross-talks between the apicobasal polarity pathway and the planar polarity pathways have been reported:

On the one hand, apicobasal polarity regulates core planar polarity. For instance, aPKC regulates planar polarity in *Drosophila* eyes (Djiane *et al.*, 2005) and in wings (this work). Also, the loss or gain of Baz function leads to planar polarity defects in eyes (Djiane *et al.*, 2005), and the overexpression of Baz disrupts Fmi membrane localisation in wings (Wasserscheid *et al.*, 2007). Wasserscheid *et al*. also showed that Baz binds to the Stan isoform of Fmi which contains a PDZ-binding motif in pull-down assays (Wasserscheid *et al.*, 2007), suggesting a physical binding between apicobasal polarity determinants and core planar polarity proteins, consistent with the binding between Fz and dPatj yeast two hybrid assays (Djiane *et al.*, 2005). In addition, the overexpression of Par-1 leads to Fmi mis-localisation in *Drosophila* wing cells (Harumoto *et al.*, 2010).

On the other hand, planar polarity regulates the planar localisation of apicobasal polarity components. In the fly notum, sensory organ precursors at mitosis localise the Par complex components (Garg et al., 2017; Goldstein and Macara, 2007; Suzuki and Ohno, 2006) to the posterior side colocalise to Fz, while Stbm recruits basolateral polarity components to the anterior side (Bellaiche et al., 2004; Bellaiche et al., 2001a;

Bellaiche et al., 2001b; Besson et al., 2015; Gho and Schweisguth, 1998; Lu et al., 1999). In eyes, the localisation of Baz (a member of the Par complex) largely overlaps with that of Stbm in adult cone cells (Aigouy and Le Bivic, 2016); while Baz localises to the Fz side in the third instar developing eye discs (Djiane *et al.*, 2005); in *Drosophila* embryos, Baz is also asymmetrically localised (Simoes Sde *et al.*, 2010). In Zebrafish embryos, *Vangl2* mutants affect Par-3/Baz clustering and Par-3/Baz cluster position (Donati et al., 2021). The asymmetric localisation of Baz is regulated by core planar polarity proteins as the asymmetry localisation of Baz in eye cone cells is lost in *fmi*- cells but not in Crumbs, a main Baz regulator, mutant cells (Aigouy and Le Bivic, 2016). However, as Baz and Stbm or Baz and Fz is not strongly interacting in yeast two hybrid assays (Courbard et al., 2009; Djiane *et al.*, 2005), the colocalisation may be mediated by other apicobasal polarity or planar polarity factors. For instance, Dsh is also reported to recruit Baz in sensory organ precursors (Garg *et al.*, 2017).

My results in (Figure 4.7) show a negative regulatory role of Fmi on aPKC protein level but show no clear evidence supporting aPKC is asymmetrically localised in *Drosophila* pupal wing cells. In fact, not all apicobasal polarity components are symmetrically localised in the systems listed above. For instance, Par-6 is not asymmetrically localised in cone cells where Baz is observed to localise asymmetrically (Aigouy and Le Bivic, 2016). Thus, future experiments confirming whether aPKC or other apicobasal polarity components are asymmetrically localised in the plane in *Drosophila* wings is needed.

Evidence provided here suggests a model where core planar polarity proteins regulate the subcellular planar localisation of apicobasal polarity components, which regulates the distribution of actomyosin and cell tension, thus, in turn, regulates planar polarity establishment.

5.3 Summary

The main goals of the project were largely achieved. Kinases were screened in *Drosophila* pupal wings and evidence was provided to support or deny a role of candidate kinases in core planar polarity (**Chapter 2**). Two kinases, Dco and aPKC, were picked for further testing. Dco regulates planar polarity in *Drosophila* pupal wings by acutely affecting core protein stability. Dco was also observed to localise asymmetrically on the distal cell end, suggesting a cell-scale sorting mechanism such that distal localised Dco stabilises distal complex component Dsh and destabilises proximal component Stbm locally to promote planar polarity (**Chapter 3**). aPKC also regulates planar polarity in *Drosophila* pupal wings, but the mechanism is still unclear, only a possible model is provided here (**Chapter 4**).

CHAPTER 6

Materials and Methods

6.1 Materials

6.1.1 Antibodies

Table 6.1 List of antibodies used

Antibody used	Sources	Concentration used
Primary antibodies used in immunolabelling		
Rabbit anti-β-gal	Cappel: cat#55976	1:4000
Mouse monoclonal anti-β-gal	Promega: cat#Z3783	1:500
Rat monoclonal anti-DE-CAD (DCAD2)	Developmental Studies Hybridoma Bank: AB_528120; (Oda et al., 1994)	1:20
Rabbit anti-Stbm	(Bastock *et al.*, 2003)	1:1000
Rabbit anti-Dsh	(Strutt *et al.*, 2013a)	1:1000 IF
Rabbit anti-Fz, affinity purified	(Bastock and Strutt, 2007)	1:300
Rat anti-Pk, affinity purified	(Strutt *et al.*, 2013a)	1:25
Mouse monoclonal anti-Fmi #74	Developmental Studies Hybridoma Bank: AB_2619583; (Usui *et al.*, 1999)	1:2000 IF
Rabbit polyclonal anti-PKC ζ	Santa Cruz: sc-216	1:250
Mouse monoclonal anti-Myc 9E10	Sheffield BioServe	1:25
HA-Tag (6E2) Mouse monoclonal Antibody (Alexa Fluor® 647 Conjugate)	Cell Signalling: #3444	1:100
Secondary antibodies used in immunolabelling		
Goat anti-Mouse Cy2	Jackson 115-225-146	1:1000
Goat anti-mouse Cy5	Jackson 115-175-146	1:1000

Antibody used	**Sources**	**Concentration used**
Goat anti-Rabbit RRX	Jackson 111-295-003	1:1000
Donkey anti-Rat Cy2	Jackson 712-225-150	1:1000
Goat anti-Rat Cy5	Jackson 112-175-102	1:1000
Antibodies used in Western blot		
Rabbit anti-Dsh, affinity purified	(Strutt *et al.*, 2006)	1:250
Mouse monoclonal anti-Actin AC-40	Sigma cat#A4700	1:1000
Goat anti-Mouse-HRP	Dako: P044701-2	1:5000
Goat anti-Rabbit-HRP	Dako: P044801-2	1:5000

Fmi: Flamingo

Fz: Frizzled

Stbm: Strabismus

Dsh: Dishevelled

Pk: Prickle

β-gal: β-Galactosidase

HRP: Horseradish peroxidase

6.1.2 *Drosophila* stocks used

Table 6.2 Full genotypes used in each experiment

Experiment	Genotype
Figure 2.1	*w/y,w,Ubx-FLP1; FRT42B aPKC[k06403]/FRT42B arm-LacZ*
Figure 2.2	*w/y,w,Ubx-FLP1; FRT42B aPKC[ts]/FRT42B arm-lacZ*
Figure 2.3	*w[1118]*
Figure 2.4	*w; UAS-DaPKC.DN.CAAX(6)/en-Gal4*
Figure 2.5	*w; UAS-DaPKC.DN.CAAX(6)/ptc-Gal4*
Figure 2.6	*w/y,w,Ubx-FLP1; FRT42 par-1[k05603]/FRT42 arm-LacZ*
Figure 2.7	*y sc v/w; TRiP.HMS00405[attP2]/en-Gal4*
Figure 2.8 & Figure 2.9	*w dsh[V26] FRT19A/ y w dsh[V26] FRT18; P[acman]-EGFP-dsh[attP40]/+* *w dsh[V26] FRT19A/ y w dsh[V26] FRT18; P[acman]-EGFP-dsh[S/T236-247>A][attP40]/+* *w dsh[V26] FRT19A/ y w dsh[V26] FRT18; P[acman]-EGFP-dsh[S/T236-247>A] [attP40]/+*
Figure 2.10	*y w dsh[V26] FRT18; P[acman]-EGFP-Dsh[attP40]* *Ubi-mRFP[nls], hs-FLP1 FRT19A/ w dsh[V26] FRT19A; Ubx-FLP3/P[acman]-EGFP-dsh[attP40]* *Ubi-mRFP[nls], hs-FLP1 FRT19A/ w dsh[V26] FRT19A; Ubx-FLP3/P[acman]-EGFP-dsh[Y473>F][attP40]* *w[1118]* *w dsh[1]/Y; P[acman]-EGFP-dsh[attP40]/+* *w dsh[1]/Y; P[acman]-EGFP-dsh[Y473>F][attP40]/+* *w dsh[1]*
Figure 2.11	*w/y w Ubx-FLP1; arm-lacZ FRT80/Abl[2] FRT80*
Figure 2.12	*w; UAS-Abl/ptc-Gal4* *y v/w; TRiP.JF02960[attP2]/ptc-Gal4*
Figure 2.13	*w; UAS-Abl/en-Gal4*

Experiment	Genotype
	y v/w; TRiP.JF02960[attP2]/en-Gal4
Figure 2.14	*w/y w hsFLP1; Act5C>y+>GAL4, UAS-lacZ/UAS-Abl* *w/y w hsFLP1; Act5C>y+>GAL4, UAS-lacZ/ TRiP.JF02960[attP2]*
Figure 2.15	*w/y w Ubx-FLP1; arm-lacZ FRT80/msn[172] FRT80*
Figure 2.16	*w/y, w, Ubx-FLP1; FRT42 pk-sple[13] cn[1]/ FRT42 arm-LacZ; Act5C>>EGFP-Pk[attP2]/+* *w/y, w, Ubx-FLP1; FRT42 pk-sple[13] cn[1]/ FRT42 arm-LacZ; Act5C>>EGFP-Pk[A][attP2]/+* *w/y, w, Ubx-FLP1; FRT42 pk-sple[13] cn[1]/ FRT42 arm-LacZ; Act5C>>EGFP-Pk[E][attP2]/+*
Figure 3.1	*w; fTRG01037.sfGFP-TVPTBF[VK02]/+; hsP70-NSlmb-vhhGFP4, FRT82B dco[j3B9]/FRT82 dco[2]*
Figure 3.2	*w; FlyFos020844-dco-SpotTag-HA[VK31] FRT82 dco[2]/ hsP-Tom70-HAScFv[attP2] FRT82B dco[j3B9]*
Figure 3.3	*y w dsh[V26] FRT18; P[acman]-EGFP-Dsh[attP40]* *w; P[acman]-Stbm-EGFP-LoxP[attP40] FRT40 stbm[6]* *y w dsh[V26] FRT19A/+; P[acman]-EGFP-Dsh[attP40] stbm[6]* *w dsh[V26] FRT19A/ dsh[1]; P[acman]-Stbm-EGFP-LoxP[attP40] FRT40 stbm[6]/+*
Figure 3.4	*w; FlyFos020844-dco-SpotTag-HA[VK31] FRT82 dco[2]/ FRT82B dco[j3B9]* *w; FlyFos020844-HA-SpotTag-dco[VK31] FRT82 dco[2]/ FRT82B dco[j3B9]* *w; fTRG01037.sfGFP-TVPTBF[VK02] FRT40/FRT40; FRT82 dco[2]/+* *w; Act5C>>Dco-GFP FRT82 dco[2]/ Ubx-FLP3 FRT82B dco[j3B9]*
Figure 4.2	*w/ y w Ubx-FLP1; Act5C-Fz-sfGFP[attP2] fz[P21] FRT80/ arm-lacZ FRT80*

Experiment	**Genotype**
Figure 4.3	*w/ y w Ubx-FLP1;Act5C-Fz[A554,A560]-sfGFP[attP2] fz[P21] FRT80/ arm-lacZ FRT80*
Figure 4.4	*w/ y w Ubx-FLP1;Act5C-Fz-sfGFP[attP2] fz[P21] FRT80/ arm-lacZ FRT80* *w/ y w Ubx-FLP1;Act5C-Fz[A554,A560]-sfGFP[attP2] fz[P21] FRT80/ arm-lacZ FRT80* *w/ y w Ubx-FLP1;Act5C-Fz[E554,E560]-sfGFP[attP2] fz[P21] FRT80/ arm-lacZ FRT80*
Figure 4.5	*w; ptc-Gal4/+; UAS-DaPKC.WT.CAAX(5)/+*
Figure 4.6	*w/y, w, Ubx-FLP1; FRT42 aPKC[as4]#3/FRT42 arm-LacZ*
Figure 4.7	*w/y, w, Ubx-FLP1; FRT42 fmi[E59]/FRT42 arm-LacZ*
Table 2.1	*dsh[1]/Y* *dsh[1]/Y; P[acman]-EGFP-dsh[attP40]* *dsh[1]/Y; P[acman]-EGFP-dsh[S/T236-247>A][attP40]* *dsh[1]/Y; P[acman]-EGFP-dsh[S/T236-247>E][attP40]* *dsh[1]/Y; P[acman]-EGFP-dsh[Y473>F][attP40]* *w dsh[V26] FRT19A/ Y; P[acman]-EGFP-dsh[S/T236-247>A][attP40]* *w dsh[V26] FRT19A/ Y; P[acman]-EGFP-dsh[Y473>F][attP40]*

Table 6.3 Transgenes and mutation alleles information

Name	Description	Flybase ID
w[1118]	Used as wild-type	FBal0018186
Core planar polarity protein mutation alleles		
fmi[E59]	(Usui *et al.*, 1999)	FBal0101421
fz[P21]	(Jones *et al.*, 1996)	FBal0004937
stbm[6]	(Wolff and Rubin, 1998)	FBal0062423
dsh[1]	a planar polarity-specific mutant allele	FBal0003138
dsh[V26]	amorphic allele (Perrimon and Mahowald, 1987)	FBal0003140
pk-sple[13]	(Gubb *et al.*, 1999)	FBal0060943
Core planar polarity proteins transgenes		
P[acman]-Stbm-EGFP-LoxP	(Strutt *et al.*, 2016)	
P[acman]-EGFP-dsh	(Strutt *et al.*, 2016)	
EGFP-Pk	(Strutt *et al.*, 2013b)	
Kinase mutation alleles		
aPKC[k06403]	amorphic allele	FBal0064438
aPKC[as4]	*aPKC[I342A,T405A]*; (Hannaford *et al.*, 2019)	FBal0346247
aPKC[ts]	*aPKC[F532L]*; (Guilgur *et al.*, 2012)	FBal0277054
dco[2]	hypomorphic allele	FBal0032015
dco[j3B9]	loss of function allele	FBal0010937
abl[2]	amorphic allele	FBal0339087
par-1[k05603]	hypomorphic allele	FBal0117402
msn[172]	Inversion breakpoint within the coding region	FBal0061020

Name	Description	Flybase ID
Kinase transgenes		
UAS-DaPKC.DN.CAAX(6)	*aPKC[K293W]-CaaX*; (Sotillos *et al.*, 2004)	FBal0189627
UAS-DaPKC.WT.CAAX(5)	(Sotillos *et al.*, 2004)	FBal0192028
fTRG01037.sfGFP-TVPTBF	*2XTY1-SGFP-V5-preTEV-BLRP-3XFLAG* sequence inserted into C-terminal of Dco coding region in *FlyFos020844*; (Sarov *et al.*, 2016)	FBal0339087
Act5C>>Dco-GFP	(Strutt *et al.*, 2006)	FBal0194122
TRiP.HMS00405	RNAi against Par-1; (Ni et al., 2011)	FBal0248166
TRiP.JF02960	RNAi against Abl; (Perkins *et al.*, 2015)	FBal0239462
UAS-Abl	(Singh *et al.*, 2010)	FBal0095895
Other transgenes		
hs-FLP1	Bloomington *Drosophila* Stock Center: 6; (Golic and Lindquist, 1989)	FBti0002044
Ubx-FLP1	Bloomington *Drosophila* Stock Center: 42718; (Emery et al., 2005)	FBti0150334
Ubx-FLP3	Bloomington *Drosophila* Stock Center: 42719; (Emery *et al.*, 2005)	FBti0150356
ptc-GAL4	Bloomington *Drosophila* Stock Center: 2017; (Hinz *et al.*, 1994)	FBti0002124
en-GAL4	Bloomington Drosophila Stock Center: 30564; (Johnson *et al.*, 1995)	FBti0003572
Act5C>y+>GAL4	Also marked as Act5C>>GAL4 in this Thesis	FBtp0001405
Ubi-mRFP-nls	Marked as mRFP[nls] in this Thesis	FBti0129785
FRT18		FBti0002070

Name	Description	Flybase ID
FRT19A		FBti0000870
FRT40		FBti0002071
FRT42B		FBti0001247
FRT42		FBti0141188
FRT80		FBti0002073
FRT82		FBti0002074
hsP-Tom70-HAScFv	This work	
hsP70-NSlmb-vhhGFP4	This work	
arm-LacZ	On 2R, 51 D	FBti0023289
	P[w+, arm-lacZ]AZE16.3 On 3L	FBti0018347
	P[w+, Act5C>y+>GAL4]25, P[w+, UAS-lacZ]	Homemade, similar to FBst0004410

6.1.3 *Drosophila* transgenes generated in this work

Fz[S554,S560] mutations

pAttB-Act5C>>Fz-sfGFP was generated as the map shown below, sfGFP was inserted with a VDPPVAT linker sequence at the C-terminal of the Fz coding sequence (CDS):

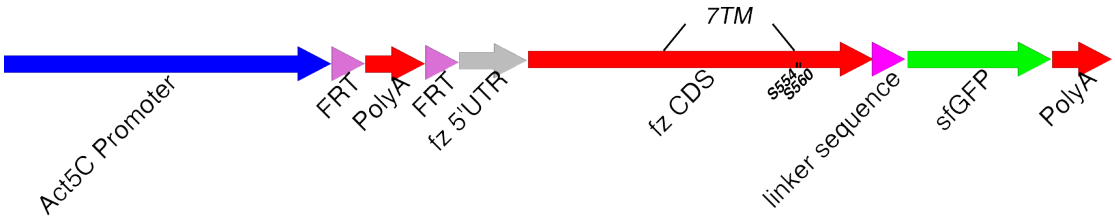

pAttB-Act5C>>Fz-sfGFP was digested with AgeI (A^CCGGT) and BglII (A^GATCT), and ligated to AgeI and BglII digested:

5'-GATCTTTATGGTGAAGTATTTGTGCTCCATGCTGGTCGGCGTGACAAGTTCC
GTTTGGTTGTACGCCAGTAAAACGATGGTGGCATGGCGTAACTTTGTCGAGCGT
TTGCAGGGTAAAGAGCCACGGACCAGGGCGCAGGCGTATGTCGATCCACCGG^
T-3'

or:

5'-GATCTTTATGGTGAAATATCTCTGTTCGATGTTGGTAGGAGTCACCTCGTCGG
TGTGGCTGTACGAGTCCAAAACTATGGTAGAGTGGCGGAATTTTGTCGAACGCC
TCCAGGGCAAAGAACCTCGAACGCGAGCGCAGGCGTACGTCGATCCACCGG^T
-3'

to generate *pAttB-Act5C>>Fz[A554,A560]* or *pAttB-Act5C>>Fz[E554,E560]*, respectively. The *FRT-PolyA-FRT* sequence was then Flipped-out by crossing to *hs-FLP1* and heat-shock. Thus, *pAttB-Act5C-Fz-sfGFP*, *pAttB-Act5C-Fz[A554,A560]*, and *pAttB-Act5C-Fz[E554,E560]* were made.

Dsh[S/T236-247] and Dsh[Y473] mutations

P[acman]-EGFP-dsh (Strutt *et al.*, 2016) bacterial artificial chromosome (BAC) construct was used to generate *P[acman]-EGFP-dsh[S/T236-247>A], P[acman]-EGFP-dsh[S/T236-247>E],* and *P[acman]-EGFP-dsh[Y473>F]*, map for construct shown below:

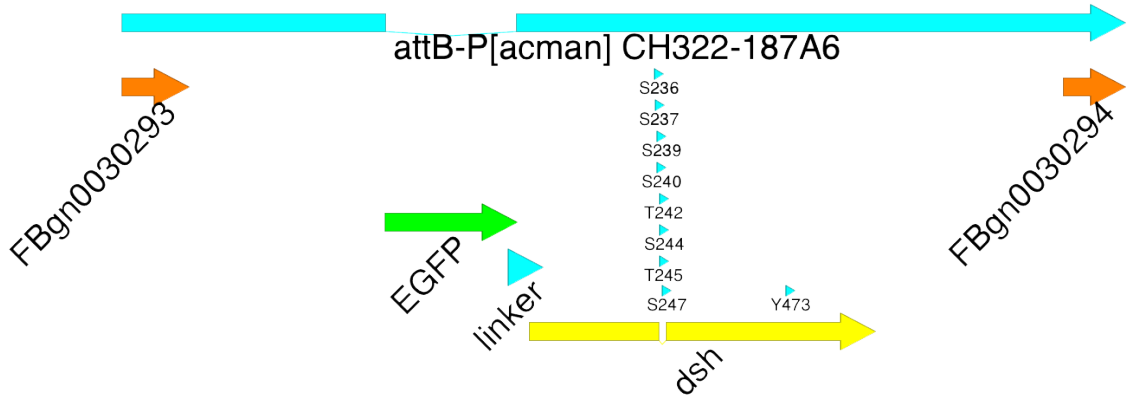

KanaRpsL strategy was used. The target sequence to be mutated in *P[acman]-EGFP-dsh* construct was firstly replaced by KanaRpsL cassette in the recombinase containing SW106 strain *E. coli* by electroporating, which increases the resistance to Kanamycin and sensitivity to Streptomycin. The Kanamycin resistant *E. coli* were then selected, and the repair sequence was electroporated. Streptomycin tolerated *E. coli* contains the repair sequence replacing the original sequence.

5’-GCAAGAAGCCGCAGAGGCGCAAAAAACGGGCGCCCAGCATGTCGCGCACCt
cctcgtacagctccataaccgactcgaccatgtccCTAAATATCATTACCGTCTCCATCAACATGG
AGGCGGTCAACTTTCTGGG-3’

sequence in Dsh coding sequence in *P[acman]-EGFP-dsh* were replaced by:

5’-GCAAGAAGCCGCAGAGGCGCAAAAAACGGGCGCCCAGCATGTCGCGCACC
GCCGCCtacGCCGCCataGCCgacGCCGCCatgGCCCTAAATATCATTACCGTCTCC
ATCAACATGGAGGCGGTCAACTTTCTGGG-3’

to generate *P[acman]-EGFP-dsh[S/T236-247>A]*, or by:

5’-GCAAGAAGCCGCAGAGGCGCAAAAAACGGGCGCCCAGCATGTCGCGCACC
GAGGAGtacGAGGAGataGAGgacGAGGAGatgGAGCTAAATATCATTACCGTCTCC
ATCAACATGGAGGCGGTCAACTTTCTGGG-3’

to generate *P[acman]-EGFP-dsh[S/T236-247>E]*.

P[acman]-EGFP-dsh[T473>F] was made by replacing:

5'-GCAATTACATCAAGCATACGGTCAATAAGTTGACCTTCTCGGAGCAGTGCTAC
TACGTGGTGAACGAGGAGCGCAATCCCAATCTGTTGGGCCGAGGACATCT-3'

in *P[acman]-EGFP-dsh* by:

5'-GCAATTACATCAAGCATACGGTCAATAAGTTGACCTTCTCGGAGCAGTGCTTC
TACGTGGTGAACGAGGAGCGCAATCCCAATCTGTTGGGCCGAGGACATCT-3'

Pk mutations

pAttB-Act5C>STOP>EGFP-Pk (Strutt *et al.*, 2013b) were used to make *pAttB-Act5C>STOP>EGFP-Pk[A]* and *pAttB-Act5C>STOP>EGFP-Pk[E].*

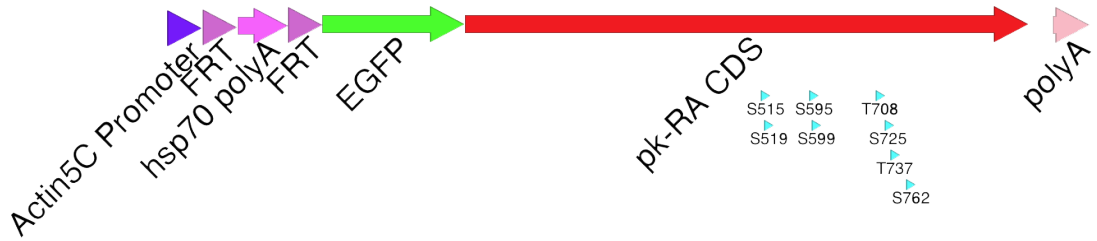

T708, S725, T737, S762 were mutated to Alanine or Glutamic acid by ligating SphI and EcoRI digested *pAttB-Act5C>STOP>EGFP-Pk* to SphI and EcoRI digested:

5'-CACACCGCCAGCATGCCGGAATTGGCAGGAAAGTTGGTGGCTCCCCCTGCC
CACATGCAACACCTCAGCCAACTCCACGCAGTATCCAGTCACCAATTCCAGCAA
CATGAGTATGCCGACATATTGCATCCTCCACCCCCACCGCCGGGTGAAATCCC
CGAGCTCCCAGCCCCGAATCTCTCGGTCGCCAGCACAGCTCTCCCTCCGGAGC
TCATGGGAGCGCCTACACATTCCGCCGGTGATCGGTCCCTCAATGCACCAATG
TCCACGCAAAGTGCCAGCCACGCTCCGCCTCACCCCGTGTCGATACTGAGCGG
AGCATCGTCGAGCGCGCCAATGAGTGGAGAACCTGCTAAGAAAAAAGGTGTTC
GCTTTGAGGGAATTCCGGACACACT-3' (for Alanine mutation),

or

5'-CACACCGCCAGCATGCCGGAATTGGCAGGAAAGTTGGTGGCTCCCCCTGCC
CACATGCAACACCTCAGCCAACTCCACGCAGTATCCAGTCACCAATTCCAGCAA

CATGAGTATGCCGACATATTGCATCCTCCACCCCCACCGCCGGGTGAAATCCC
CGAGCTCCCAGAGCCGAATCTCTCGGTCGCCAGCACAGCTCTCCCTCCGGAGC
TCATGGGAGAGCCTACACATTCCGCCGGTGATCGGTCCCTCAATGAGCCAATG
TCCACGCAAAGTGCCAGCCACGCTCCGCCTCACCCCGTGTCGATACTGAGCGG
AGCATCGTCGAGCGAGCCAATGAGTGGAGAACCTGCTAAGAAAAAAGGTGTTC
GCTTTGAGGGAATTCCGGACACACT-3' (for Glutamic acid mutation)

S515,S519,S595,S599 mutated sequences were generated by overlap PCR (Polymerase Chain Reaction). The overlapped mutation sequences are listed below:

S515A S519A:

5'-GCCACGCCTCCAGCGCCCCGCCTATGGCCCCGCAACAGCAGCAGC-3'

S515E S519E:

5'-GCCACGCCTCCAGCGAGCCGCCTATGGAGCCGCAACAGCAGCAGC-3'

S595A S599A:

5'-GCACCTCGCAGAACCTAGCCCCTCTGAACGCCCCCGGCGACTTCCAGCCC-3'

S595E S599E:

5'-GCACCTCGCAGAACCTAGAGCCTCTGAACGAGCCCGGCGACTTCCAGCCC-3'

Overlap PCR products were also cloned into *pAttB-Act5C>STOP>EGFP-Pk* construct on ApaI/NdeI (for S515,S519 mutations) or NdeI/SphI (for S595,S599 mutations) sites.

HA-tagging on Dco

FlyFos020844 Fosmid containing Dco coding region was used to make *FlyFos020844-HA-SpotTag-dco* and *FlyFos020844-dco-SpotTag-HA* using KanaRpsL strategy, whose maps are shown below.

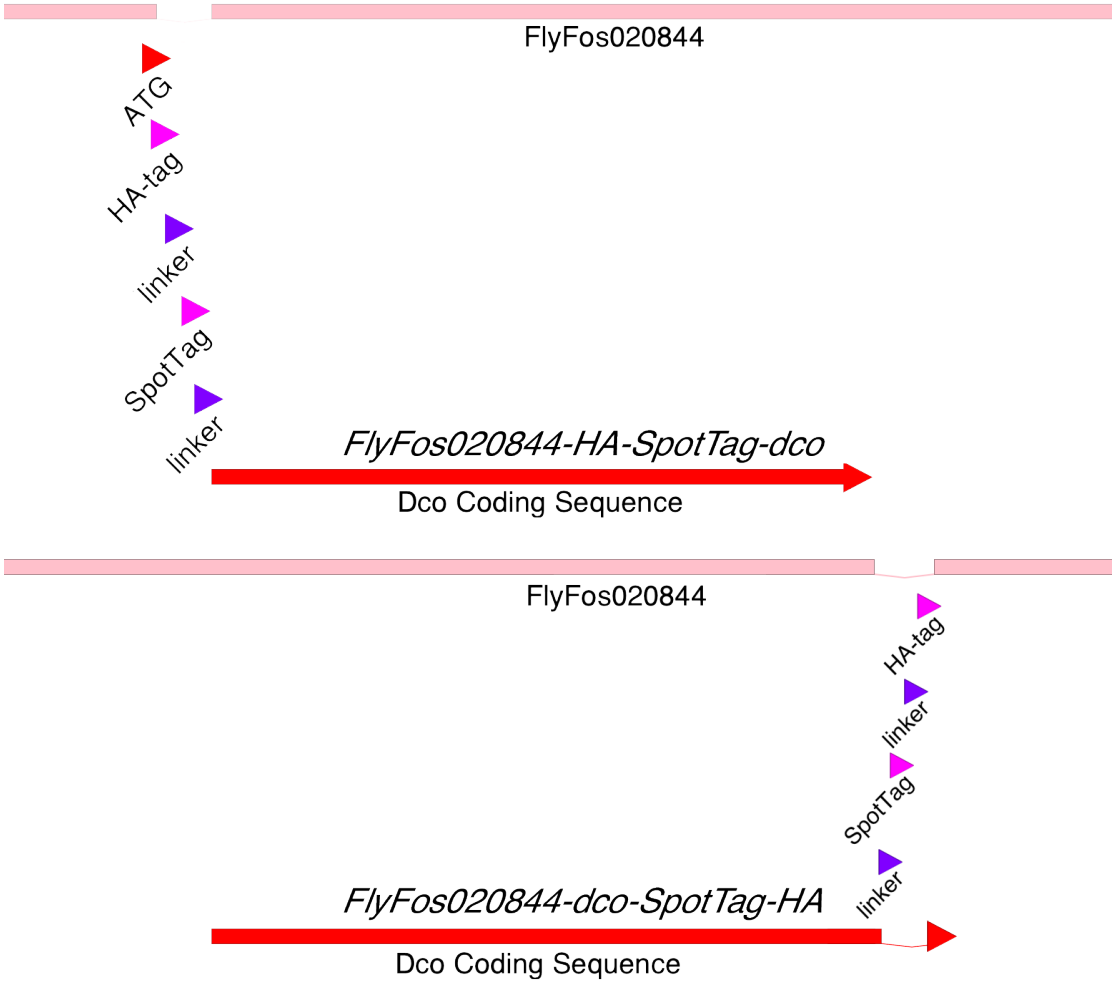

HA-SpotTag- sequence was inserted into the N-terminal of the Dco coding sequence in FlyFos020844 Fosmid by replacing:

5'-GAGGAGTCCGAACTCTACCACACAGAAACCCACAGAAACAGACGTAACAAAA TGGAGCTGCGCGTGGGTAACAAATATCGCCTGGGCCGCAAGATAGGATCGGGA TC-3'

by:

5'-GAGGAGTCCGAACTCTACCACACAGAAACCCACAGAAACAGACGTAACAAAA TGTACCCTTATGATGTCCCGGATTATGCCAGCGGCGGCGGTGGATCGGGAGGC GGAGGAAGCCCCGATCGCGTTCGAGCTGTAAGCCACTGGTCCTCCGGCTCCG CCGGATCCATGGAGCTGCGCGTGGGTAACAAATATCGCCTGGGCCGCAAGATA GGATCGGGATC-3'.

The -*SpotTag-HA* sequence was inserted into the C-terminal of the Dco coding sequence in FlyFos020844 Fosmid by replacing:

5'-TTCGATACGGATGCGGCAGGGAGGCGGTGGTGGCGGCGGTGGAGTGGGCG
TAGGCGGTATGCCGAGCGGCGGAGGGGGCGGTGGCGTGGGGAACGCCAAAT
AATATTTTATCGTTTAGGTTGCGACGCTGGACACGACACAGTAGACAAAC-3'

by:

5'-TTCGATACGGATGCGGCAGGGAGGCGGTGGTGGCGGCGGTGGAGTGGGCG
TAGGCGGTATGCCGAGCGGCGGAGGGGGCGGTGGCGTGGGGAACGCCAAAG
GCTCCGCCGGATCCCCCGATCGCGTTCGAGCTGTAAGCCACTGGTCCTCCAGC
GGCGGCGGTGGATCGGGAGGCGGAGGAAGCTACCCTTATGATGTCCCGGATT
ATGCCTAATATTTTATCGTTTAGGTTGCGACGCTGGACACGACACAGTAGACAA
AC-3'.

All constructed transgenes were injected by GenetiVision Corporation.

6.1.4 *Drosophila* genetics

6.1.4.1 UAS-GAL4 binary expression system

The Gal4/UAS system (Brand *et al.*, 1994; Brand and Perrimon, 1993) was used to temporospatially express target genes. When Gal4 coding sequence is inserted downstream of either *engrailed(en)* or *patched(ptc)* promoter, the yeast transcriptional activator GAL4 can be expressed in the posterior region of the pupal wing (*en*-expression region) or in a stripe region between veins 3-4 of the pupal wing (*ptc*-expression region)(Hinz *et al.*, 1994; Johnson *et al.*, 1995).

GAL4 activity is enhanced in high temperatures (e.g., 29°C) compared to lower temperatures (e.g., RT) (Brand *et al.*, 1994). Thus, fly crosses for Gal4/UAS expression experiments were kept at RT before pupae collection to reduce the effects before pupae formation.

6.1.4.2 Mitotic clones generation using FLP/FRT

Twin-clones in wings were generated using the FLP/FRT system (Xu and Rubin, 1993). FLP is a recombinase inducing recombination mitosis. The recombination induced by FLP recombinase occurs between *FRT* elements on two chromosomes in heterogeneous genotype cells to generate homozygous genotype cells after mitosis. The FLP recombinase expression was induced under either *Ubx* promoter (*Ubx-FLP* (Emery *et al.*, 2005)) or *hsP70* promoter (*hs-FLP1* (Golic and Lindquist, 1989)). The *hsP70* promoter induces expression at 37°C (Lindquist, 1980a; b) but not at 25°C (Velazquez *et al.*, 1983).

In the clonal Abl or Abl RNAi expression experiments (Figure 2.14), clonal EGFP-Pk expression experiments (Figure 2.16), and clonal Dco-GFP expression experiments (Figure 3.4 E-F), clones were generated by inserting *Act5C>STOP>GAL4* (*Act5C promoter-FRT-STOP-FRT-Gal4*) into the genome. When the FLP recombinase induced the expression, the recombination stochastically flipped out the STOP codon in some cells and excise the cassette. Only these cells and their progenies inherit the excised state expressed Gal4 and triggered the target gene expression.

Specifically, in the clonal Abl or Abl RNAi expression experiments (Figure 2.14), the FLP expression was induced under *hs-FLP*. In this experiment, adult flies were transferred to fresh vials at 24 h after cross set up. Vials containing eggs or larvae were heat-shock at 48 h and 72 h after cross set up to induce FLP expression. In these experiments, the *UAS-LacZ* transgene was also inserted to mark Gal4-expressing cells with β-gal immunolabelling.

6.1.5 Chemical inhibitors used

Table 6.4 List of chemical inhibitors used

Chemicals	Description	CAS number	Supplier
D4476	Broad-spectrum CKI inhibitor	301836-43-1	AOBIOUS
PF-4800567	Dco (CKIε) specific inhibitor	1188296-52-7	Cayman
1NA-PP1	ATP analogue	221243-82-9	Cayman

6.1.5.1 Software used

Table 6.5 List of software used

NIS Elements AR version 4.60-5.21	Nikon
Image Lab version 4.1	BioRad Laboratories
ImageJ version 2.9.0	https://fiji.sc
MATLAB_R2022b	Mathworks
GraphPad Prism version 9.4.1	GraphPad Software, Inc.
Tissue Analyzer	(Aigouy *et al.*, 2010; Aigouy et al., 2016)
Membrane intensity scripts	(Strutt *et al.*, 2016)
QuantifyPolarity	(Tan *et al.*, 2021)

6.2 Methods

6.2.1 Fly culture and pupae ageing

All fly work was performed in the *Drosophila* Facility at the University of Sheffield (https://www.sheffield.ac.uk/flyfacility/drosophila). Stable stocks were cultured at 19°C (room-temperature, RT) and kept in plastic vials with fly food on the bottom. Flies for experimental use were cultured in plastic vials, plastic straight sided bottles, or ICRF bottles.

To set up crossings, virgin females and males of desired genotypes were collected and mated in plastic vials or straight sided bottles. Crosses were kept at RT or 25°C. Adult flies in crossings were changed to a fresh vial or bottle every 2-4 days. Genotypes of progenies from crossings for each experiment are listed in **Table 6.2**

Prepupae (when the pupal cuticle was still white) were collected onto the wall of plastic vials for ageing. The plastic vial used for ageing also has food on the bottom to keep the ageing environment damp. The time of collection was marked as 0 h after puparium formation (APF). At the time of collection, the sex of prepupae can be checked under a dissecting microscope if certain sex pupal is desired. Males have two more transparent genital discs embedded in fat, and lie at about 2/3 of body length from the anterior.

Pupae were aged at 25°C for 6 h for prepupal wings and 28 h for pupal wings experiments, except the ones listed below:

In the *aPKC[temperature-sensitive]* inhibition experiment (Figure 2.2 F-J), pupae were aged at 29°C for 24 h.

In the *hsP70-* driven nanobody expression experiment (Figure 3.1 C-D; Figure 3.2 B), pupae were aged at 25°C for 28 h. Vials containing pupae were then put into a 37°C water-bath tank for 2-hour heat-shock before dissection.

In the aPKC[wt] overexpression experiment in (Figure 4.5), pupae were either: aged at 25°C for 24h then switch to 29°C for 3.5 h (3 hours and 30 mins)(Figure 4.5 B); aged at 25°C for 22.5 h (22 hours and 30 mins) then switch to 29°C for 4.75 h (4 hours and 45 mins)(Figure 4.5 C); or aged at 29°C for 24 h (Figure 4.5 D).

6.2.2 Pupal wing dissection

Pupae aged to 28 h APF at 25°C (or other conditions indicated above) were dissected out from the pupal cuticle and transferred to a drop of 4% paraformaldehyde in PBS (phosphate buffered saline) for fixation. The fixation time varies depending on the antibody used. Fixation time for pupae was normally 20 mins, except for Rabbit anti-Dsh (5 mins) and Rabbit anti-Fz (60 mins). Pupal wings were then dissected out from fixed pupae by pulling the wing on its hinge region and transferred into a fresh drop of 4% paraformaldehyde in PBS for second round fixation for 5 mins.

Wings at this stage are surrounded by transparent pupal cuticles. Pupal cuticles were removed after two rounds of fixation and the wings were transferred to a blocking solution (900µL [PBS + 0.2% Trition X-100 (VWR)] + 100µL Normal Goat Serum) for a 1-hour blocking at RT.

6.2.3 Pupal wing dissection for FRAP

FRAP was done in live imaging, thus the pupae used were not fixed. Instead of been dissected out from the pupal cuticle, 28 h APF pupal wings were exposed by cutting a small region on the pupal cuticle, but not removed from the pupal cuticle. Exposed wings were then stuck to glass bottom dishes (Iwaki) coated with heptane glue (made by diluting glue from sticky tape (Sellotape) in heptane) and rested for 5-10 min before FRAP. Detailed protocol can be found in (Warrington et al., 2022)

6.2.4 Prepupal wing dissection and chemical treatment

Unlike 28 h APF pupal wings, 6 h APF prepupal wings are attached to the trachea, like wing imaginal discs. Pupae were cut into half on its anteroposterior midline. To liberate prepupal wings, the trachea was Then cut by cutting the anterior spiracles. A drop of Schneider's Medium was immediately dropped on pupae to avoid dehydration. The anterior part of pupae was then transferred to 1 mL Schneider's Medium without serum to avoid effects of factors in serum. Pupae were then dissected out from the anterior cuticle by pulling the pupae body, wings were now exposed on the anterior side. Chemicals in stock concentration (D4476: 50 mM, PF-4800567: 10 mM, and 1NA-PP1: 50 mM) in Dimethyl Sulfoxide (DMSO) were added into Schneider's Medium to achieve the desired concentration in experiments.

Prepupal wings were dissected out from pupae during chemical treatment by pulling the most proximal hinge part and left in the chemical treatment solution. After the treatment time, prepupal wings were immediately transferred for the next step experiment by gently pipetting.

For fixed sample experiments, prepupal wings were then transferred into 4% paraformaldehyde in PBS for a 5-min fixation before immunolabelling.

For FRAP experiments, the imaging chamber for live imaging was firstly made by sticking Sellotape Super Clear tape on a microscope slide. An approximately 7 x 7 mm^2 square hole on the tape was cut out and coated with 4 µL [Schneider's medium + 1.25 % methyl cellulose]. Prepupal wings were transferred by gently pipetting together with 1 µL chemical treatment medium into the imaging chamber. Coverslip was then put on the chamber and sealed with nail polish.

6.2.5 Fixed pupal wings and prepupal wings immunostaining

The immunostaining process is identical between pupal wings and prepupal wings. Fixed wings were transferred to Nunclon™ plates (Thermo Scientific) by pipetting with blocking solution. The blocking solution in wells was replaced by 15 µL primary antibodies solution in blocking solution (concentration in **Table 6.1**). The plate was then sealed with parafilm (Bemis) and left at 4°C in fridge for incubation overnight.

After the primary antibody incubation, wings were washed with 12 µL [PBS + 0.2% TX-100] each well for 12 times in one hour at RT. Then the final wash was replaced by the secondary antibody mix. The plate was sealed with parafilm and left at 4°C in fridge for incubation overnight.

After the secondary antibody incubation, wings were again washed with 12 µL [PBS + 0.2% TX-100] each well for 12 times in one hour at RT. Then the final wash was replaced by 15 µL [4% paraformaldehyde in PBS] for a 10-min fixation. Another three washes with about 12 µL [PBS + 0.2% TX-100] were performed and then replaced by about 12 µL PBS.

25 µL [PBS + 10% glycerol + 2.5% DABCO (1,4-diazabicyclo [2.2.2] octane, an antifade), pH7.5] mount solution was added at the middle of a microscope slide. Wings were then transferred into the mounting solution using forceps (or by gentle pipetting for prepupal wings) and then covered with a coverslip. Slides were kept at 4°C in fridge and sealed with nail polish before imaging.

6.2.6 Fixed sample imaging and image processing

The image process was similar to that in (Strutt *et al.*, 2019a). Immunostained wings were imaged on a Nikon GaAsP A1R microscope in the Wolfson Light Microscopy Facility at the University of Sheffield. Nikon 60x NA = 1.4 apochromatic objective lens was used, and the pinhole size was set to 1.2 AU (35.8 µm). Wings without clones

were imaged with vein 4 on the lower-middle, covering the cross vein to ensure all images were taken in a similar region in the wing. Wings with clones were imaged covering clones. Z-stacks of 9 slices covering adherens junctions region with the highest Ecad or core protein immunolabelling signal were imaged with 0.15 μm intervals. Each stack was imaged with 8 seconds/frame scan speed and in 1024 x 1024 pixels in a 2x zoomed-in sight fields (pixel size = 0.1μM). 3 slices with the highest signal were selected and averaged using ImageJ(Fiji).

Cells in images were segmented by generating membrane masks using Tissue Analyzer (Fiji plugin (Aigouy *et al.*, 2010; Aigouy *et al.*, 2016)). Since the core proteins on clone edges affect the adjacent cells, the first row of cells on clone boundaries were not included for quantification, except those in the *aPKC[k06403]* twin-clone experiment (Figure 2.1) where homozygous *aPKC[k06403]* clones were in small size. A MATLAB script was used to calculate membrane and cytoplasm intensity on segmented images (Strutt *et al.*, 2016). Cell areas were calculated using QuantifyPolarity (Tan *et al.*, 2021). Data acquired were compared using Student's paired t-test in Microsoft Excel or using ANOVA in GraphPad Prism.

Polarity nematics and magnitudes were also calculated using QuantifyPolarity in a Principal Component Analysis (PCA) based method (Tan *et al.*, 2021). In general, the PCA-based method compresses cells into regular shapes and normalises intensities. The angle with the largest variance of normalised intensities is defined as the angle of single cell polarity, and the extent of the variance is defined as the polarity magnitude (strength of polarity). The single cell polarity quantified was then averaged over a three-cell size to generate the Coarse-Grain polarity, which reflects the polarity strength and alignment at the tissue level.

6.2.7 Fluorescence Recovery After Photobleaching (FRAP) experiments and data process

Live-imaging samples mounted as described above were used for FRAP experiments. Nikon GaAsP A1R microscope was used and FRAP was performed with Nikon 60x NA = 1.4 apochromatic objective lens and 1.2 AU (35.8 μm) pinhole size. Given that photo-bleaching strongly affects live imaging, the laser power was reduced, and the resolution has to be decreased compared to fixed sample imaging. The flattest region with a bright fluorescent signal was imaged with 0.5 seconds/frame scan speed and in 256x256 pixels in an 8x zoomed-in fields (pixel size = 0.1μM).

The FRAP experiments were performed as described in (Warrington *et al.*, 2022). In each wing, four “hub-and-spoke” regions covering half of all vertical and horizontal cell junctions (Strutt *et al.*, 2011) were chosen as regions of interest (ROI)(example image shown in Figure 2.9). Three images were taken before bleach to measure the fluorescence before bleach, and then a strong laser with 80% of the available laser power was applied to all four ROIs. Images after bleach were taken in a time series listed in **Table 6.6.** After all the imaging, the laser was then turned off to take a ‘background’ image, for measuring background fluorescence.

Table 6.6 Time series of image taking in FRAP

Number of images taken	Time intervals	Description
3	No delay	Before bleach
No image taken	0.115 seconds	Bleaching
5	2 seconds	After bleach
10	5 seconds	After bleach
10	10 seconds	After bleach
10	15 seconds	After bleach
10	30 seconds	After bleach

Fluorescence recovery data were collected in ImageJ(Fiji). The background fluorescence was measured by averaging the fluorescent intensity in the laser-off background image. The average fluorescent intensity in four bleached hub-and-spoke regions and in four unbleached hub-and-spoke regions was also measured and the laser-off background fluorescent intensity was subtracted.

Data processing was performed in Microsoft Excel. The fluorescent intensity in unbleached hub-and-spoke regions was used to adjust the fluorescent intensity in each bleach ROI for acquisition bleaching:

$$I_n = \frac{\overline{I[no\ bleach]_{prebleach}}}{I[no\ bleach]_n} \times I[bleach]_n$$

where $I[no\ bleach]_{prebleach}$ is the averaged intensity of the four unbleached ROIs before bleach, $I[no\ bleach]_n$ is the intensity of the unbleached region at timepoint n, $I[bleach]_n$ is the intensity of the bleached ROI at timepoint n, and I_n is the adjusted fluorescent intensity of the bleached ROI at timepoint n. All the intensity numbers here were with background fluorescent intensity subtracted.

The normalised recovery ratios of each ROI were then calculated as:

$$normalised\ recovery = \frac{I_n - I_0}{\overline{I_{prebleach}} - I_0}$$

where I_n is the acquisition bleaching-adjusted fluorescent intensity of the bleached ROI at timepoint n, I_0 is the acquisition bleaching adjusted-intensity of the first timepoint after the bleach (taken immediately after bleaching), and $\overline{I_{prebleach}}$ is the averaged acquisition bleaching-adjusted intensity of the four bleach ROI before bleach.

The normalised recovery ratios of four bleached ROI in each FRAP experimental sample were then averaged and transferred into GraphPad Prism for curve fitting. Each column in GraphPad Prism represents one experimental sample in one wing.

Two-phase exponential association were used to fit data sets of multiple time series into one final curve and 95% confidence intervals were calculated. The two-phase exponential association was calculated as below:

$$Y = \mathrm{Y}_0 + Span_{fast} \times \left(1 - e^{-K_{fast} \times X}\right) + Span_{slow} \times \left(1 - e^{-K_{slow} \times X}\right)$$

$$Span_{fast} = (\text{platuau} - \mathrm{Y}_0) \times Percent_{fast} \times 0.1$$

$$Span_{slow} = (\text{platuau} - \mathrm{Y}_0) \times Percent_{slow} \times 0.1$$

Where Y starts at Y0 and ascends to $Y_0 + Span_{fast} + Span_{slow}$ with two phases, Y0 here is a constant 0 as recovery ratio was normalised to start at 0, K_{fast} and K_{slow} are rate constants, $Percent_{fast}$ is the percentage of the signal due to the fast phase.

Two or more curves were compared using the Extra sum-of-squares F test in GraphPad Prism, which determines if there is a significant difference between the curve plateau and the rates of recovery (K).

6.2.8 Adult wings and legs imaging

Adult flies were anaesthetised on a carbon-dioxide plate. Wings and the middle legs were dissected by pulling the most proximal region of the hinge near body walls. Wings and legs dissected out were transferred onto microscope slides with drops of isopropanol. Coverslips coated with 12 µl of GMM (Gary's Magic Mountant, [50% Canada balsam, 50% methyl salicylate]) were covered onto microscope slides when isopropanol dried. Mounted samples were left on the hot block at 60 °C overnight, then kept in RT before imaging. Adult samples were imaged on a Leica compound microscope with Jenoptik C14 using the Jenoptik software ProgRes® CapturePro.

6.2.9 Western blots

28 h pupal wings were dissected out from the pupal cuticle and transferred to a drop of PBS. Wings were then directly dissected into 2x NuPAGE (Novex) sample buffer with 200mM DTT. Samples were then boiled for 10 min and centrifuged in max speed for 5 min before loading or being kept in -20°C. Samples were run on a pre-cast NuPage 4-12% Bis-Tris gel (Invitrogen, NP0323BOX) in 1X NuPAGE MOPS SDS Running Buffer (novex, NP0001) at 200V for 60 min. Gels were cut out and be assembled into Electroblotting cassette together with Nitrocellulose Blotting Membrane (Amersham, 10600003). Transfer was run in 1X Western transfer buffer (100 mL 10X transfer buffer (2.9 g Glycine, 5.8 g Tris, 0.37 g SDS), 700 mL distilled water, 200 mL methanol) at 50 V for 2 hours. Following transfer, the membrane was rinsed briefly with PBST (0.1% Tween-20 in PBS) and blocked with freshly prepared Blocking Solution (5% Marvel milk powder in PBST) for 1 hour on a shaking platform at room temperature.

Western blots were probed with antibodies listed in **Table 6.1**. Primary antibodies diluted in Blocking Solution were incubated overnight at 4°C on a roller. Membrane was then washed with PBST for 5 times within 30 mins. Secondary antibodies diluted in Blocking Solution were incubated for 2 hours at room temperature on a roller, followed by another 5 times PBST wash within 30 mins. Western blots were detected using SuperSignal West Dura Extended Duration Substrate (Thermo Scientific) and imaged in BioRad ChemiDoc XRS +.

Bibliography

Adler, P.N., Taylor, J., and Charlton, J. (2000). The domineering non-autonomy of frizzled and van Gogh clones in the Drosophila wing is a consequence of a disruption in local signaling. Mech Dev *96*, 197-207. 10.1016/s0925-4773(00)00392-0.

Adler, P.N., Zhu, C., and Stone, D. (2004). Inturned localizes to the proximal side of wing cells under the instruction of upstream planar polarity proteins. Curr Biol *14*, 2046-2051. 10.1016/j.cub.2004.11.007.

Aigouy, B., Farhadifar, R., Staple, D.B., Sagner, A., Roper, J.C., Julicher, F., and Eaton, S. (2010). Cell flow reorients the axis of planar polarity in the wing epithelium of Drosophila. Cell *142*, 773-786. 10.1016/j.cell.2010.07.042.

Aigouy, B., and Le Bivic, A. (2016). The PCP pathway regulates Baz planar distribution in epithelial cells. Sci Rep *6*, 33420. 10.1038/srep33420.

Aigouy, B., Umetsu, D., and Eaton, S. (2016). Segmentation and Quantitative Analysis of Epithelial Tissues. Methods Mol Biol *1478*, 227-239. 10.1007/978-1-4939-6371-3_13.

Aldaz, S., Escudero, L.M., and Freeman, M. (2010). Live imaging of Drosophila imaginal disc development. Proc Natl Acad Sci U S A *107*, 14217-14222. 10.1073/pnas.1008623107.

Aldaz, S., Escudero, L.M., and Freeman, M. (2013). Dual role of myosin II during Drosophila imaginal disc metamorphosis. Nat Commun *4*, 1761. 10.1038/ncomms2763.

Ambegaonkar, A.A., Pan, G., Mani, M., Feng, Y., and Irvine, K.D. (2012). Propagation of Dachsous-Fat planar cell polarity. Curr Biol *22*, 1302-1308. 10.1016/j.cub.2012.05.049.

Amonlirdviman, K., Khare, N.A., Tree, D.R., Chen, W.S., Axelrod, J.D., and Tomlin, C.J. (2005). Mathematical modeling of planar cell polarity to understand domineering nonautonomy. Science *307*, 423-426. 10.1126/science.1105471.

Angers, S., Thorpe, C.J., Biechele, T.L., Goldenberg, S.J., Zheng, N., MacCoss, M.J., and Moon, R.T. (2006). The KLHL12-Cullin-3 ubiquitin ligase negatively regulates the Wnt-beta-catenin pathway by targeting Dishevelled for degradation. Nat Cell Biol *8*, 348-357. 10.1038/ncb1381.

Axelrod, J.D. (2001). Unipolar membrane association of Dishevelled mediates Frizzled planar cell polarity signaling. Genes Dev *15*, 1182-1187. 10.1101/gad.890501.

Axelrod, J.D., Miller, J.R., Shulman, J.M., Moon, R.T., and Perrimon, N. (1998). Differential recruitment of Dishevelled provides signaling specificity in the planar cell polarity and Wingless signaling pathways. Gene Dev *12*, 2610-2622. DOI 10.1101/gad.12.16.2610.

Bastock, R., and Strutt, D. (2007). The planar polarity pathway promotes coordinated cell migration during Drosophila oogenesis. Development *134*, 3055-3064. 10.1242/dev.010447.

Bastock, R., Strutt, H., and Strutt, D. (2003). Strabismus is asymmetrically localised and binds to Prickle and Dishevelled during Drosophila planar polarity patterning. Development *130*, 3007-3014. 10.1242/dev.00526.

Bellaiche, Y., Beaudoin-Massiani, O., Stuttem, I., and Schweisguth, F. (2004). The planar cell polarity protein Strabismus promotes Pins anterior localization during asymmetric division of sensory organ precursor cells in Drosophila. Development *131*, 469-478. 10.1242/dev.00928.

Bellaiche, Y., Gho, M., Kaltschmidt, J.A., Brand, A.H., and Schweisguth, F. (2001a). Frizzled regulates localization of cell-fate determinants and mitotic spindle rotation during asymmetric cell division. Nat Cell Biol *3*, 50-57. 10.1038/35050558.

Bellaiche, Y., Radovic, A., Woods, D.F., Hough, C.D., Parmentier, M.L., O'Kane, C.J., Bryant, P.J., and Schweisguth, F. (2001b). The Partner of Inscuteable/Discs-large complex is required to establish planar polarity during asymmetric cell division in Drosophila. Cell *106*, 355-366. 10.1016/s0092-8674(01)00444-5.

Belotti, E., Puvirajesinghe, T.M., Audebert, S., Baudelet, E., Camoin, L., Pierres, M., Lasvaux, L., Ferracci, G., Montcouquiol, M., and Borg, J.P. (2012). Molecular characterisation of endogenous Vangl2/Vangl1 heteromeric protein complexes. PLoS One *7*, e46213. 10.1371/journal.pone.0046213.

Bennett, F.C., and Harvey, K.F. (2006). Fat cadherin modulates organ size in Drosophila via the Salvador/Warts/Hippo signaling pathway. Curr Biol *16*, 2101-2110. 10.1016/j.cub.2006.09.045.

Benton, R., and St Johnston, D. (2003). Drosophila PAR-1 and 14-3-3 inhibit Bazooka/PAR-3 to establish complementary cortical domains in polarized cells. Cell *115*, 691-704. 10.1016/s0092-8674(03)00938-3.

Bernatik, O., Sedova, K., Schille, C., Ganji, R.S., Cervenka, I., Trantirek, L., Schambony, A., Zdrahal, Z., and Bryja, V. (2014). Functional analysis of dishevelled-3 phosphorylation identifies distinct mechanisms driven by casein kinase 1ϵ and frizzled5. J Biol Chem *289*, 23520-23533. 10.1074/jbc.M114.590638.

Bertet, C., Sulak, L., and Lecuit, T. (2004). Myosin-dependent junction remodelling controls planar cell intercalation and axis elongation. Nature *429*, 667-671. 10.1038/nature02590.

Besson, C., Bernard, F., Corson, F., Rouault, H., Reynaud, E., Keder, A., Mazouni, K., and Schweisguth, F. (2015). Planar Cell Polarity Breaks the Symmetry of PAR Protein Distribution prior to Mitosis in Drosophila Sensory Organ Precursor Cells. Current Biology *25*, 1104-1110. 10.1016/j.cub.2015.02.073.

Bhanot, P., Brink, M., Samos, C.H., Hsieh, J.C., Wang, Y., Macke, J.P., Andrew, D., Nathans, J., and Nusse, R. (1996). A new member of the frizzled family from Drosophila functions as a Wingless receptor. Nature *382*, 225-230. 10.1038/382225a0.

Bhanot, P., Fish, M., Jemison, J.A., Nusse, R., Nathans, J., and Cadigan, K.M. (1999). Frizzled and DFrizzled-2 function as redundant receptors for Wingless during Drosophila embryonic development. Development *126*, 4175-4186.

Bhat, K.M. (1998). frizzled and frizzled 2 play a partially redundant role in wingless signaling and have similar requirements to wingless in neurogenesis. Cell *95*, 1027-1036. 10.1016/s0092-8674(00)81726-2.

Bhat, M.A., Izaddoost, S., Lu, Y., Cho, K.O., Choi, K.W., and Bellen, H.J. (1999). Discs Lost, a novel multi-PDZ domain protein, establishes and maintains epithelial polarity. Cell *96*, 833-845. 10.1016/s0092-8674(00)80593-0.

Bilder, D., Schober, M., and Perrimon, N. (2003). Integrated activity of PDZ protein complexes regulates epithelial polarity. Nat Cell Biol *5*, 53-58. 10.1038/ncb897.

Blom, N., Gammeltoft, S., and Brunak, S. (1999). Sequence and structure-based prediction of eukaryotic protein phosphorylation sites. J Mol Biol *294*, 1351-1362. 10.1006/jmbi.1999.3310.

Boggon, T.J., Murray, J., Chappuis-Flament, S., Wong, E., Gumbiner, B.M., and Shapiro, L. (2002). C-cadherin ectodomain structure and implications for cell adhesion mechanisms. Science *296*, 1308-1313. 10.1126/science.1071559.

Borghi, N., Sorokina, M., Shcherbakova, O.G., Weis, W.I., Pruitt, B.L., Nelson, W.J., and Dunn, A.R. (2012). E-cadherin is under constitutive actomyosin-generated tension that is increased

at cell-cell contacts upon externally applied stretch (vol 109, 12568, 2012). P Natl Acad Sci USA *109*, 19034-19034. 10.1073/pnas.1217417109.
Boutros, M., Mihaly, J., Bouwmeester, T., and Mlodzik, M. (2000). Signaling specificity by Frizzled receptors in Drosophila. Science *288*, 1825-1828. 10.1126/science.288.5472.1825.
Boutros, M., and Mlodzik, M. (1999). Dishevelled: at the crossroads of divergent intracellular signaling pathways. Mech Develop *83*, 27-37. Doi 10.1016/S0925-4773(99)00046-5.
Boutros, M., Paricio, N., Strutt, D.I., and Mlodzik, M. (1998). Dishevelled activates JNK and discriminates between JNK pathways in planar polarity and wingless signaling. Cell *94*, 109-118. Doi 10.1016/S0092-8674(00)81226-X.
Brand, A.H., Manoukian, A.S., and Perrimon, N. (1994). Ectopic expression in Drosophila. Methods Cell Biol *44*, 635-654. 10.1016/s0091-679x(08)60936-x.
Brand, A.H., and Perrimon, N. (1993). Targeted gene expression as a means of altering cell fates and generating dominant phenotypes. Development *118*, 401-415. 10.1242/dev.118.2.401.
Brittle, A., Thomas, C., and Strutt, D. (2012). Planar polarity specification through asymmetric subcellular localization of Fat and Dachsous. Curr Biol *22*, 907-914. 10.1016/j.cub.2012.03.053.
Brittle, A., Warrington, S.J., Strutt, H., Manning, E., Tan, S.E., and Strutt, D. (2022). Distinct mechanisms of planar polarization by the core and Fat-Dachsous planar polarity pathways in the Drosophila wing. Cell Rep *40*, 111419. 10.1016/j.celrep.2022.111419.
Brittle, A.L., Repiso, A., Casal, J., Lawrence, P.A., and Strutt, D. (2010). Four-jointed modulates growth and planar polarity by reducing the affinity of dachsous for fat. Curr Biol *20*, 803-810. 10.1016/j.cub.2010.03.056.
Brodsky, M.H., and Steller, H. (1996). Positional information along the dorsal-ventral axis of the Drosophila eye: graded expression of the four-jointed gene. Dev Biol *173*, 428-446. 10.1006/dbio.1996.0038.
Brown, K.E., and Freeman, M. (2003). Egfr signalling defines a protective function for ommatidial orientation in the Drosophila eye. Development *130*, 5401-5412. 10.1242/dev.00773.
Bryant, D.M., and Mostov, K.E. (2008). From cells to organs: building polarized tissue. Nat Rev Mol Cell Biol *9*, 887-901. 10.1038/nrm2523.
Buckley, C.E., and St Johnston, D. (2022). Apical-basal polarity and the control of epithelial form and function. Nat Rev Mol Cell Biol *23*, 559-577. 10.1038/s41580-022-00465-y.
Burak, Y., and Shraiman, B.I. (2009). Order and stochastic dynamics in Drosophila planar cell polarity. Plos Comput Biol *5*, e1000628. 10.1371/journal.pcbi.1000628.
Butler, M.T., and Wallingford, J.B. (2017). Planar cell polarity in development and disease. Nat Rev Mol Cell Biol *18*, 375-388. 10.1038/nrm.2017.11.
Callahan, J.F., Burgess, J.L., Fornwald, J.A., Gaster, L.M., Harling, J.D., Harrington, F.P., Heer, J., Kwon, C., Lehr, R., Mathur, A., et al. (2002). Identification of novel inhibitors of the transforming growth factor beta1 (TGF-beta1) type 1 receptor (ALK5). J Med Chem *45*, 999-1001. 10.1021/jm010493y.
Carmena, A. (2020). The Case of the Scribble Polarity Module in Asymmetric Neuroblast Division in Development and Tumorigenesis. Int J Mol Sci *21*. 10.3390/ijms21082865.
Carmena, A. (2021). Non-muscle myosin II activation: adding a classical touch to ROCK. Small GTPases *12*, 161-166. 10.1080/21541248.2019.1671148.

Caussinus, E., Kanca, O., and Affolter, M. (2011). Fluorescent fusion protein knockout mediated by anti-GFP nanobody. Nat Struct Mol Biol *19*, 117-121. 10.1038/nsmb.2180.
Chae, J., Kim, M.J., Goo, J.H., Collier, S., Gubb, D., Charlton, J., Adler, P.N., and Park, W.J. (1999). The Drosophila tissue polarity gene starry night encodes a member of the protocadherin family. Development *126*, 5421-5429. 10.1242/dev.126.23.5421.
Chartier, F.J., Hardy, E.J., and Laprise, P. (2011). Crumbs controls epithelial integrity by inhibiting Rac1 and PI3K. J Cell Sci *124*, 3393-3398. 10.1242/jcs.092601.
Chen, C.M., and Struhl, G. (1999). Wingless transduction by the Frizzled and Frizzled2 proteins of Drosophila. Development *126*, 5441-5452. 10.1242/dev.126.23.5441.
Chen, W.S., Antic, D., Matis, M., Logan, C.Y., Povelones, M., Anderson, G.A., Nusse, R., and Axelrod, J.D. (2008). Asymmetric homotypic interactions of the atypical cadherin flamingo mediate intercellular polarity signaling. Cell *133*, 1093-1105. 10.1016/j.cell.2008.04.048.
Chen, Z., and Cole, P.A. (2015). Synthetic approaches to protein phosphorylation. Curr Opin Chem Biol *28*, 115-122. 10.1016/j.cbpa.2015.07.001.
Cho, B., Pierre-Louis, G., Sagner, A., Eaton, S., and Axelrod, J.D. (2015a). Clustering and negative feedback by endocytosis in planar cell polarity signaling is modulated by ubiquitinylation of prickle. Plos Genet *11*, e1005259. 10.1371/journal.pgen.1005259.
Cho, B., Pierre-Louis, G., Sagner, A., Eaton, S., and Axelrod, J.D. (2015b). Clustering and Negative Feedback by Endocytosis in Planar Cell Polarity Signaling Is Modulated by Ubiquitinylation of Prickle. Plos Genet *11*. ARTN e1005259
10.1371/journal.pgen.1005259.
Cho, E., Feng, Y., Rauskolb, C., Maitra, S., Fehon, R., and Irvine, K.D. (2006). Delineation of a Fat tumor suppressor pathway. Nat Genet *38*, 1142-1150. 10.1038/ng1887.
Choi, K.W., and Benzer, S. (1994). Rotation of photoreceptor clusters in the developing Drosophila eye requires the nemo gene. Cell *78*, 125-136. 10.1016/0092-8674(94)90579-7.
Chu, C.W., and Sokol, S.Y. (2016). Wnt proteins can direct planar cell polarity in vertebrate ectoderm. Elife *5*. 10.7554/eLife.16463.
Clark, H.F., Brentrup, D., Schneitz, K., Bieber, A., Goodman, C., and Noll, M. (1995). Dachsous encodes a member of the cadherin superfamily that controls imaginal disc morphogenesis in Drosophila. Genes Dev *9*, 1530-1542. 10.1101/gad.9.12.1530.
Classen, A.K., Anderson, K.I., Marois, E., and Eaton, S. (2005). Hexagonal packing of Drosophila wing epithelial cells by the planar cell polarity pathway. Dev Cell *9*, 805-817. 10.1016/j.devcel.2005.10.016.
Collier, S., and Gubb, D. (1997). Drosophila tissue polarity requires the cell-autonomous activity of the fuzzy gene, which encodes a novel transmembrane protein. Development *124*, 4029-4037. 10.1242/dev.124.20.4029.
Collier, S., Lee, H., Burgess, R., and Adler, P. (2005). The WD40 repeat protein fritz links cytoskeletal planar polarity to frizzled subcellular localization in the Drosophila epidermis. Genetics *169*, 2035-2045. 10.1534/genetics.104.033381.
Collu, G.M., Jenny, A., Gaengel, K., Mirkovic, I., Chin, M.L., Weber, U., Smith, M.J., and Mlodzik, M. (2018). Prickle is phosphorylated by Nemo and targeted for degradation to maintain Prickle/Spiny-legs isoform balance during planar cell polarity establishment. Plos Genet *14*, e1007391. 10.1371/journal.pgen.1007391.
Cong, F., Schweizer, L., and Varmus, H. (2004a). Casein kinase Iepsilon modulates the

signaling specificities of dishevelled. Mol Cell Biol *24*, 2000-2011. 10.1128/MCB.24.5.2000-2011.2004.

Cong, F., Schweizer, L., and Varmus, H. (2004b). Wnt signals across the plasma membrane to activate the beta-catenin pathway by forming oligomers containing its receptors, Frizzled and LRP. Development *131*, 5103-5115. 10.1242/dev.01318.

Copley, C.O., Duncan, J.S., Liu, C., Cheng, H.X., and Deans, M.R. (2013). Postnatal Refinement of Auditory Hair Cell Planar Polarity Deficits Occurs in the Absence of Vangl2. Journal of Neuroscience *33*, 14001-14016. 10.1523/Jneurosci.1307-13.2013.

Courbard, J.R., Djiane, A., Wu, J., and Mlodzik, M. (2009). The apical/basal-polarity determinant Scribble cooperates with the PCP core factor Stbm/Vang and functions as one of its effectors. Dev Biol *333*, 67-77. 10.1016/j.ydbio.2009.06.024.

Couto, A., Mack, N.A., Favia, L., and Georgiou, M. (2017). An apicobasal gradient of Rac activity determines protrusion form and position. Nat Commun *8*, 15385. 10.1038/ncomms15385.

Curtin, J.A., Quint, E., Tsipouri, V., Arkell, R.M., Cattanach, B., Copp, A.J., Henderson, D.J., Spurr, N., Stanier, P., Fisher, E.M., et al. (2003). Mutation of Celsr1 disrupts planar polarity of inner ear hair cells and causes severe neural tube defects in the mouse. Curr Biol *13*, 1129-1133. 10.1016/s0960-9822(03)00374-9.

Das, G., Jenny, A., Klein, T.J., Eaton, S., and Mlodzik, M. (2004). Diego interacts with Prickle and Strabismus/Van Gogh to localize planar cell polarity complexes. Development *131*, 4467-4476. 10.1242/dev.01317.

Das, G., Reynolds-Kenneally, J., and Mlodzik, M. (2002). The atypical cadherin Flamingo links Frizzled and Notch signaling in planar polarity establishment in the Drosophila eye. Dev Cell *2*, 655-666. 10.1016/s1534-5807(02)00147-8.

Daulat, A.M., Luu, O., Sing, A., Zhang, L., Wrana, J.L., McNeill, H., Winklbauer, R., and Angers, S. (2012). Mink1 regulates beta-catenin-independent Wnt signaling via Prickle phosphorylation. Mol Cell Biol *32*, 173-185. 10.1128/MCB.06320-11.

Desai, R., Sarpal, R., Ishiyama, N., Pellikka, M., Ikura, M., and Tepass, U. (2013). Monomeric alpha-catenin links cadherin to the actin cytoskeleton. Nat Cell Biol *15*, 261-273. 10.1038/ncb2685.

Devenport, D. (2014). The cell biology of planar cell polarity. J Cell Biol *207*, 171-179. 10.1083/jcb.201408039.

Devenport, D., and Fuchs, E. (2008). Planar polarization in embryonic epidermis orchestrates global asymmetric morphogenesis of hair follicles. Nat Cell Biol *10*, 1257-1268. 10.1038/ncb1784.

Djiane, A., Yogev, S., and Mlodzik, M. (2005). The apical determinants aPKC and dPatj regulate Frizzled-dependent planar cell polarity in the Drosophila eye. Cell *121*, 621-631. 10.1016/j.cell.2005.03.014.

Donati, A., Anselme, I., Schneider-Maunoury, S., and Vesque, C. (2021). Planar polarization of cilia in the zebrafish floor-plate involves Par3-mediated posterior localization of highly motile basal bodies. Development *148*. 10.1242/dev.196386.

Emery, G., Hutterer, A., Berdnik, D., Mayer, B., Wirtz-Peitz, F., Gaitan, M.G., and Knoblich, J.A. (2005). Asymmetric Rab 11 endosomes regulate delta recycling and specify cell fate in the Drosophila nervous system. Cell *122*, 763-773. 10.1016/j.cell.2005.08.017.

Etheridge, S.L., Ray, S., Li, S., Hamblet, N.S., Lijam, N., Tsang, M., Greer, J., Kardos, N., Wang, J., Sussman, D.J., et al. (2008). Murine dishevelled 3 functions in redundant pathways with dishevelled 1 and 2 in normal cardiac outflow tract, cochlea, and neural tube development. Plos Genet *4*, e1000259. 10.1371/journal.pgen.1000259.

Etournay, R., Popovic, M., Merkel, M., Nandi, A., Blasse, C., Aigouy, B., Brandl, H., Myers, G., Salbreux, G., Julicher, F., and Eaton, S. (2015). Interplay of cell dynamics and epithelial tension during morphogenesis of the Drosophila pupal wing. Elife *4*, e07090. 10.7554/eLife.07090.

Ewen-Campen, B., Comyn, T., Vogt, E., and Perrimon, N. (2020). No Evidence that Wnt Ligands Are Required for Planar Cell Polarity in Drosophila. Cell Rep *32*, 108121. 10.1016/j.celrep.2020.108121.

Feiguin, F., Hannus, M., Mlodzik, M., and Eaton, S. (2001). The ankyrin repeat protein Diego mediates Frizzled-dependent planar polarization. Dev Cell *1*, 93-101. 10.1016/s1534-5807(01)00010-7.

Feng, X., Jia, Y., Zhang, Y., Ma, F., Zhu, Y., Hong, X., Zhou, Q., He, R., Zhang, H., Jin, J., et al. (2019). Ubiquitination of UVRAG by SMURF1 promotes autophagosome maturation and inhibits hepatocellular carcinoma growth. Autophagy *15*, 1130-1149. 10.1080/15548627.2019.1570063.

Feng, Y., and Irvine, K.D. (2007). Fat and expanded act in parallel to regulate growth through warts. Proc Natl Acad Sci U S A *104*, 20362-20367. 10.1073/pnas.0706722105.

Feng, Y., and Irvine, K.D. (2009). Processing and phosphorylation of the Fat receptor. Proc Natl Acad Sci U S A *106*, 11989-11994. 10.1073/pnas.0811540106.

Fernandez-Gonzalez, R., Simoes Sde, M., Roper, J.C., Eaton, S., and Zallen, J.A. (2009). Myosin II dynamics are regulated by tension in intercalating cells. Dev Cell *17*, 736-743. 10.1016/j.devcel.2009.09.003.

Fischer, S., Houston, P., Monk, N.A., and Owen, M.R. (2013). Is a persistent global bias necessary for the establishment of planar cell polarity? PLoS One *8*, e60064. 10.1371/journal.pone.0060064.

Fisher, K.H., and Strutt, D. (2019). A theoretical framework for planar polarity establishment through interpretation of graded cues by molecular bridges. Development *146*. 10.1242/dev.168955.

Flores-Benitez, D., and Knust, E. (2016). Dynamics of epithelial cell polarity in Drosophila: how to regulate the regulators? Curr Opin Cell Biol *42*, 13-21. 10.1016/j.ceb.2016.03.018.

Fox, D.T., and Peifer, M. (2007). Abelson kinase (Abl) and RhoGEF2 regulate actin organization during cell constriction in Drosophila. Development *134*, 567-578. 10.1242/dev.02748.

Fristrom, D., Wilcox, M., and Fristrom, J. (1993). The distribution of PS integrins, laminin A and F-actin during key stages in Drosophila wing development. Development *117*, 509-523. 10.1242/dev.117.2.509.

Fulford, A.D., Holder, M.V., Frith, D., Snijders, A.P., Tapon, N., and Ribeiro, P.S. (2019). Casein kinase 1 family proteins promote Slimb-dependent Expanded degradation. Elife *8*. 10.7554/eLife.46592.

Gammons, M.V., Renko, M., Johnson, C.M., Rutherford, T.J., and Bienz, M. (2016). Wnt Signalosome Assembly by DEP Domain Swapping of Dishevelled. Molecular Cell *64*, 92-104. 10.1016/j.molcel.2016.08.026.

Gao, B., Song, H., Bishop, K., Elliot, G., Garrett, L., English, M.A., Andre, P., Robinson, J., Sood,

R., Minami, Y., et al. (2011). Wnt signaling gradients establish planar cell polarity by inducing Vangl2 phosphorylation through Ror2. Dev Cell *20*, 163-176. 10.1016/j.devcel.2011.01.001.
Gao, B., and Yang, Y. (2013). Planar cell polarity in vertebrate limb morphogenesis. Curr Opin Genet Dev *23*, 438-444. 10.1016/j.gde.2013.05.003.
Gao, J., Liao, J., and Yang, G.Y. (2009). CAAX-box protein, prenylation process and carcinogenesis. Am J Transl Res *1*, 312-325.
Gao, Z.H., Seeling, J.M., Hill, V., Yochum, A., and Virshup, D.M. (2002). Casein kinase I phosphorylates and destabilizes the beta-catenin degradation complex. Proc Natl Acad Sci U S A *99*, 1182-1187. 10.1073/pnas.032468199.
Garg, B., Giri, B., Majumder, K., Dudeja, V., Banerjee, S., and Saluja, A. (2017). Modulation of post-translational modifications in beta-catenin and LRP6 inhibits Wnt signaling pathway in pancreatic cancer. Cancer Lett *388*, 64-72. 10.1016/j.canlet.2016.11.026.
Gerondopoulos, A., Strutt, H., Stevenson, N.L., Sobajima, T., Levine, T.P., Stephens, D.J., Strutt, D., and Barr, F.A. (2019). Planar Cell Polarity Effector Proteins Inturned and Fuzzy Form a Rab23 GEF Complex. Curr Biol *29*, 3323-3330 e3328. 10.1016/j.cub.2019.07.090.
Gho, M., and Schweisguth, F. (1998). Frizzled signalling controls orientation of asymmetric sense organ precursor cell divisions in Drosophila. Nature *393*, 178-181. 10.1038/30265.
Goldstein, B., and Macara, I.G. (2007). The PAR proteins: fundamental players in animal cell polarization. Dev Cell *13*, 609-622. 10.1016/j.devcel.2007.10.007.
Golic, K.G., and Lindquist, S. (1989). The FLP recombinase of yeast catalyzes site-specific recombination in the Drosophila genome. Cell *59*, 499-509. 10.1016/0092-8674(89)90033-0.
Goodrich, L.V., and Strutt, D. (2011). Principles of planar polarity in animal development. Development *138*, 1877-1892. 10.1242/dev.054080.
Grevengoed, E.E., Loureiro, J.J., Jesse, T.L., and Peifer, M. (2001). Abelson kinase regulates epithelial morphogenesis in Drosophila. J Cell Biol *155*, 1185-1198. 10.1083/jcb.200105102.
Gros, J., Serralbo, O., and Marcelle, C. (2009). WNT11 acts as a directional cue to organize the elongation of early muscle fibres. Nature *457*, 589-593. 10.1038/nature07564.
Gubb, D., and Garcia-Bellido, A. (1982). A genetic analysis of the determination of cuticular polarity during development in Drosophila melanogaster. J Embryol Exp Morphol *68*, 37-57.
Gubb, D., Green, C., Huen, D., Coulson, D., Johnson, G., Tree, D., Collier, S., and Roote, J. (1999). The balance between isoforms of the prickle LIM domain protein is critical for planar polarity in Drosophila imaginal discs. Genes Dev *13*, 2315-2327. 10.1101/gad.13.17.2315.
Guilgur, L.G., Prudencio, P., Ferreira, T., Pimenta-Marques, A.R., and Martinho, R.G. (2012). Drosophila aPKC is required for mitotic spindle orientation during symmetric division of epithelial cells. Development *139*, 503-513. 10.1242/dev.071027.
Guo, N., Hawkins, C., and Nathans, J. (2004). Frizzled6 controls hair patterning in mice. Proc Natl Acad Sci U S A *101*, 9277-9281. 10.1073/pnas.0402802101.
Hafen, E. (1997). Fly pushing: The theory and practice of Drosophila genetics - Greenspan,RJ. Nature *389*, 559-560.
Hale, R., Brittle, A.L., Fisher, K.H., Monk, N.A., and Strutt, D. (2015). Cellular interpretation of the long-range gradient of Four-jointed activity in the Drosophila wing. Elife *4*. 10.7554/eLife.05789.
Hales, K.G., Korey, C.A., Larracuente, A.M., and Roberts, D.M. (2015). Genetics on the Fly: A Primer on the Drosophila Model System. Genetics *201*, 815-842. 10.1534/genetics.115.183392.

Hamaratoglu, F., Willecke, M., Kango-Singh, M., Nolo, R., Hyun, E., Tao, C., Jafar-Nejad, H., and Halder, G. (2006). The tumour-suppressor genes NF2/Merlin and Expanded act through Hippo signalling to regulate cell proliferation and apoptosis. Nat Cell Biol *8*, 27-36. 10.1038/ncb1339.

Hamers-Casterman, C., Atarhouch, T., Muyldermans, S., Robinson, G., Hamers, C., Songa, E.B., Bendahman, N., and Hamers, R. (1993). Naturally occurring antibodies devoid of light chains. Nature *363*, 446-448. 10.1038/363446a0.

Hannaford, M., Loyer, N., Tonelli, F., Zoltner, M., and Januschke, J. (2019). A chemical-genetics approach to study the role of atypical Protein Kinase C in Drosophila. Development *146*. 10.1242/dev.170589.

Harnos, J., Canizal, M.C.A., Jurasek, M., Kumar, J., Holler, C., Schambony, A., Hanakova, K., Bernatik, O., Zdrahal, Z., Gomoryova, K., et al. (2019). Dishevelled-3 conformation dynamics analyzed by FRET-based biosensors reveals a key role of casein kinase 1. Nat Commun *10*, 1804. 10.1038/s41467-019-09651-7.

Harris, T.J., and Peifer, M. (2004). Adherens junction-dependent and -independent steps in the establishment of epithelial cell polarity in Drosophila. J Cell Biol *167*, 135-147. 10.1083/jcb.200406024.

Harris, T.J., and Peifer, M. (2005). The positioning and segregation of apical cues during epithelial polarity establishment in Drosophila. J Cell Biol *170*, 813-823. 10.1083/jcb.200505127.

Harrison, C., Shao, H., Strutt, H., and Strutt, D. (2020). Molecular mechanisms mediating asymmetric subcellular localisation of the core planar polarity pathway proteins. Biochem Soc Trans *48*, 1297-1308. 10.1042/BST20190404.

Harumoto, T., Ito, M., Shimada, Y., Kobayashi, T.J., Ueda, H.R., Lu, B., and Uemura, T. (2010). Atypical cadherins Dachsous and Fat control dynamics of noncentrosomal microtubules in planar cell polarity. Dev Cell *19*, 389-401. 10.1016/j.devcel.2010.08.004.

Heisenberg, C.P., Tada, M., Rauch, G.J., Saude, L., Concha, M.L., Geisler, R., Stemple, D.L., Smith, J.C., and Wilson, S.W. (2000). Silberblick/Wnt11 mediates convergent extension movements during zebrafish gastrulation. Nature *405*, 76-81. 10.1038/35011068.

Hinz, U., Giebel, B., and Campos-Ortega, J.A. (1994). The basic-helix-loop-helix domain of Drosophila lethal of scute protein is sufficient for proneural function and activates neurogenic genes. Cell *76*, 77-87. 10.1016/0092-8674(94)90174-0.

Hsieh, J.C., Rattner, A., Smallwood, P.M., and Nathans, J. (1999). Biochemical characterization of Wnt-frizzled interactions using a soluble, biologically active vertebrate Wnt protein. Proc Natl Acad Sci U S A *96*, 3546-3551. 10.1073/pnas.96.7.3546.

Hu, Y., Song, W., Cirstea, D., Lu, D., Munshi, N.C., and Anderson, K.C. (2015). CSNK1alpha1 mediates malignant plasma cell survival. Leukemia *29*, 474-482. 10.1038/leu.2014.202.

Hutterer, A., Betschinger, J., Petronczki, M., and Knoblich, J.A. (2004). Sequential roles of Cdc42, Par-6, aPKC, and Lgl in the establishment of epithelial polarity during Drosophila embryogenesis. Dev Cell *6*, 845-854. 10.1016/j.devcel.2004.05.003.

Ishikawa, H.O., Takeuchi, H., Haltiwanger, R.S., and Irvine, K.D. (2008). Four-jointed is a Golgi kinase that phosphorylates a subset of cadherin domains. Science *321*, 401-404. 10.1126/science.1158159.

Jenny, A., Darken, R.S., Wilson, P.A., and Mlodzik, M. (2003). Prickle and Strabismus form a functional complex to generate a correct axis during planar cell polarity signaling. EMBO J *22*,

4409-4420. 10.1093/emboj/cdg424.
Jenny, A., Reynolds-Kenneally, J., Das, G., Burnett, M., and Mlodzik, M. (2005). Diego and Prickle regulate Frizzled planar cell polarity signalling by competing for Dishevelled binding. Nat Cell Biol *7*, 691-697. 10.1038/ncb1271.
Jessen, J.R., Topczewski, J., Bingham, S., Sepich, D.S., Marlow, F., Chandrasekhar, A., and Solnica-Krezel, L. (2002). Zebrafish trilobite identifies new roles for Strabismus in gastrulation and neuronal movements. Nat Cell Biol *4*, 610-615. 10.1038/ncb828.
Jia, J., Tong, C., Wang, B., Luo, L., and Jiang, J. (2004). Hedgehog signalling activity of Smoothened requires phosphorylation by protein kinase A and casein kinase I. Nature *432*, 1045-1050. 10.1038/nature03179.
Jia, J., Zhang, L., Zhang, Q., Tong, C., Wang, B., Hou, F., Amanai, K., and Jiang, J. (2005). Phosphorylation by double-time/CKIepsilon and CKIalpha targets cubitus interruptus for Slimb/beta-TRCP-mediated proteolytic processing. Dev Cell *9*, 819-830. 10.1016/j.devcel.2005.10.006.
Johnson, R.L., Grenier, J.K., and Scott, M.P. (1995). patched overexpression alters wing disc size and pattern: transcriptional and post-transcriptional effects on hedgehog targets. Development *121*, 4161-4170. 10.1242/dev.121.12.4161.
Johnson, S.A., and Milner, M.J. (1987). The final stages of wing development in Drosophila melanogaster. Tissue Cell *19*, 505-513. 10.1016/0040-8166(87)90044-9.
Jones, K.H., Liu, J., and Adler, P.N. (1996). Molecular analysis of EMS-induced frizzled mutations in Drosophila melanogaster. Genetics *142*, 205-215. 10.1093/genetics/142.1.205.
Kelly, L.K., Wu, J., Yanfeng, W.A., and Mlodzik, M. (2016). Frizzled-Induced Van Gogh Phosphorylation by CK1epsilon Promotes Asymmetric Localization of Core PCP Factors in Drosophila. Cell Rep *16*, 344-356. 10.1016/j.celrep.2016.06.010.
Kibar, Z., Vogan, K.J., Groulx, N., Justice, M.J., Underhill, D.A., and Gros, P. (2001). Ltap, a mammalian homolog of Drosophila Strabismus/Van Gogh, is altered in the mouse neural tube mutant Loop-tail. Nat Genet *28*, 251-255. Doi 10.1038/90081.
Kishida, M., Hino, S., Michiue, T., Yamamoto, H., Kishida, S., Fukui, A., Asashima, M., and Kikuchi, A. (2001). Synergistic activation of the Wnt signaling pathway by Dvl and casein kinase Iepsilon. J Biol Chem *276*, 33147-33155. 10.1074/jbc.M103555200.
Klein, T.J., Jenny, A., Djiane, A., and Mlodzik, M. (2006). CKI epsilon/discs overgrown promotes both Wnt-Fz/beta-catenin and Fz/PCP signaling in Drosophila. Current Biology *16*, 1337-1343. 10.1016/j.cub.2006.06.030.
Kloss, B., Price, J.L., Saez, L., Blau, J., Rothenfluh, A., Wesley, C.S., and Young, M.W. (1998). The Drosophila clock gene double-time encodes a protein closely related to human casein kinase Iepsilon. Cell *94*, 97-107. 10.1016/s0092-8674(00)81225-8.
Klunder, L.J., Faber, K.N., Dijkstra, G., and van, I.S.C.D. (2017). Mechanisms of Cell Polarity-Controlled Epithelial Homeostasis and Immunity in the Intestine. Cold Spring Harb Perspect Biol *9*. 10.1101/cshperspect.a027888.
Ko, H.W., Jiang, J., and Edery, I. (2002). Role for Slimb in the degradation of Drosophila Period protein phosphorylated by Doubletime. Nature *420*, 673-678. 10.1038/nature01272.
Krahn, M.P., Buckers, J., Kastrup, L., and Wodarz, A. (2010). Formation of a Bazooka-Stardust complex is essential for plasma membrane polarity in epithelia. Journal of Cell Biology *190*, 751-760. 10.1083/jcb.201006029.

Laprise, P., Lau, K.M., Harris, K.P., Silva-Gagliardi, N.F., Paul, S.M., Beronja, S., Beitel, G.J., McGlade, C.J., and Tepass, U. (2009). Yurt, Coracle, Neurexin IV and the Na(+),K(+)-ATPase form a novel group of epithelial polarity proteins. Nature *459*, 1141-1145. 10.1038/nature08067.
Lawrence, P.A., Casal, J., and Struhl, G. (2004). Cell interactions and planar polarity in the abdominal epidermis of Drosophila. Development *131*, 4651-4664. 10.1242/dev.01351.
Le Garrec, J.F., Lopez, P., and Kerszberg, M. (2006). Establishment and maintenance of planar epithelial cell polarity by asymmetric cadherin bridges: a computer model. Dev Dyn *235*, 235-246. 10.1002/dvdy.20617.
Lecuit, T., and Yap, A.S. (2015). E-cadherin junctions as active mechanical integrators in tissue dynamics. Nat Cell Biol *17*, 533-539. 10.1038/ncb3136.
Lele, Z., Bakkers, J., and Hammerschmidt, M. (2001). Morpholino phenocopies of the swirl, snailhouse, somitabun, minifin, silberblick, and pipetail mutations. Genesis *30*, 190-194. 10.1002/gene.1063.
Leys, S.P., and Hill, A. (2012). The Physiology and Molecular Biology of Sponge Tissues. Adv Mar Biol *62*, 1-56. 10.1016/B978-0-12-394283-8.00001-1.
Li, D., Angermeier, A., and Wang, J. (2019). Planar cell polarity signaling regulates polarized second heart field morphogenesis to promote both arterial and venous pole septation. Development *146*. 10.1242/dev.181719.
Li, R., and Gundersen, G.G. (2008). Beyond polymer polarity: how the cytoskeleton builds a polarized cell. Nat Rev Mol Cell Biol *9*, 860-873. 10.1038/nrm2522.
Lin, Y.Y., and Gubb, D. (2009). Molecular dissection of Drosophila Prickle isoforms distinguishes their essential and overlapping roles in planar cell polarity. Dev Biol *325*, 386-399. 10.1016/j.ydbio.2008.10.042.
Lindquist, S. (1980a). Translational efficiency of heat-induced messages in Drosophila melanogaster cells. J Mol Biol *137*, 151-158. 10.1016/0022-2836(80)90322-8.
Lindquist, S. (1980b). Varying patterns of protein synthesis in Drosophila during heat shock: implications for regulation. Dev Biol *77*, 463-479. 10.1016/0012-1606(80)90488-1.
Lu, B., Usui, T., Uemura, T., Jan, L., and Jan, Y.N. (1999). Flamingo controls the planar polarity of sensory bristles and asymmetric division of sensory organ precursors in Drosophila. Curr Biol *9*, 1247-1250. 10.1016/s0960-9822(99)80505-3.
Lu, Q., Schafer, D.A., and Adler, P.N. (2015). The Drosophila planar polarity gene multiple wing hairs directly regulates the actin cytoskeleton. Development *142*, 2478-2486. 10.1242/dev.122119.
Lu, Q., Yan, J., and Adler, P.N. (2010). The Drosophila planar polarity proteins inturned and multiple wing hairs interact physically and function together. Genetics *185*, 549-558. 10.1534/genetics.110.114066.
Ma, D., Amonlirdviman, K., Raffard, R.L., Abate, A., Tomlin, C.J., and Axelrod, J.D. (2008). Cell packing influences planar cell polarity signaling. Proc Natl Acad Sci U S A *105*, 18800-18805. 10.1073/pnas.0808868105.
Ma, D., Yang, C.H., McNeill, H., Simon, M.A., and Axelrod, J.D. (2003). Fidelity in planar cell polarity signalling. Nature *421*, 543-547. 10.1038/nature01366.
MacDonald, B.T., Tamai, K., and He, X. (2009). Wnt/beta-catenin signaling: components, mechanisms, and diseases. Dev Cell *17*, 9-26. 10.1016/j.devcel.2009.06.016.
Mack, N.A., and Georgiou, M. (2014). The interdependence of the Rho GTPases and

apicobasal cell polarity. Small GTPases *5*, 10. 10.4161/21541248.2014.973768.
Mahoney, P.A., Weber, U., Onofrechuk, P., Biessmann, H., Bryant, P.J., and Goodman, C.S. (1991). The fat tumor suppressor gene in Drosophila encodes a novel member of the cadherin gene superfamily. Cell *67*, 853-868. 10.1016/0092-8674(91)90359-7.
Mao, Y., Rauskolb, C., Cho, E., Hu, W.L., Hayter, H., Minihan, G., Katz, F.N., and Irvine, K.D. (2006). Dachs: an unconventional myosin that functions downstream of Fat to regulate growth, affinity and gene expression in Drosophila. Development *133*, 2539-2551. 10.1242/dev.02427.
Matakatsu, H., and Blair, S.S. (2004). Interactions between Fat and Dachsous and the regulation of planar cell polarity in the Drosophila wing. Development *131*, 3785-3794. 10.1242/dev.01254.
Matakatsu, H., and Blair, S.S. (2006). Separating the adhesive and signaling functions of the Fat and Dachsous protocadherins. Development *133*, 2315-2324. 10.1242/dev.02401.
Matakatsu, H., and Blair, S.S. (2012). Separating planar cell polarity and Hippo pathway activities of the protocadherins Fat and Dachsous. Development *139*, 1498-1508. 10.1242/dev.070367.
Matis, M., Russler-Germain, D.A., Hu, Q., Tomlin, C.J., and Axelrod, J.D. (2014). Microtubules provide directional information for core PCP function. Elife *3*, e02893. 10.7554/eLife.02893.
Maung, S.M., and Jenny, A. (2011). Planar cell polarity in Drosophila. Organogenesis *7*, 165-179. 10.4161/org.7.3.18143.
Maurer-Stroh, S., Koranda, M., Benetka, W., Schneider, G., Sirota, F.L., and Eisenhaber, F. (2007). Towards complete sets of farnesylated and geranylgeranylated proteins. Plos Comput Biol *3*, 634-648. ARTN e66
10.1371/journal.pcbi.0030066.
McKay, R.M., Peters, J.M., and Graff, J.M. (2001). The casein kinase I family in Wnt signaling. Dev Biol *235*, 388-396. 10.1006/dbio.2001.0308.
Mellman, I., and Nelson, W.J. (2008). Coordinated protein sorting, targeting and distribution in polarized cells. Nat Rev Mol Cell Biol *9*, 833-845. 10.1038/nrm2525.
Merkel, M., Sagner, A., Gruber, F.S., Etournay, R., Blasse, C., Myers, E., Eaton, S., and Julicher, F. (2014). The Balance of Prickle/Spiny-Legs Isoforms Controls the Amount of Coupling between Core and Fat PCP Systems. Current Biology *24*, 2111-2123. 10.1016/j.cub.2014.08.005.
Mieszczanek, J., Strutt, H., Rutherford, T.J., Strutt, D., Bienz, M., and Gammons, M.V. (2022). Selective function of the PDZ domain of Dishevelled in noncanonical Wnt signalling. J Cell Sci *135*. 10.1242/jcs.259547.
Minegishi, K., Hashimoto, M., Ajima, R., Takaoka, K., Shinohara, K., Ikawa, Y., Nishimura, H., McMahon, A.P., Willert, K., Okada, Y., et al. (2017). A Wnt5 Activity Asymmetry and Intercellular Signaling via PCP Proteins Polarize Node Cells for Left-Right Symmetry Breaking. Dev Cell *40*, 439-452 e434. 10.1016/j.devcel.2017.02.010.
Mirkovic, I., Gault, W.J., Rahnama, M., Jenny, A., Gaengel, K., Bessette, D., Gottardi, C.J., Verheyen, E.M., and Mlodzik, M. (2011). Nemo kinase phosphorylates beta-catenin to promote ommatidial rotation and connects core PCP factors to E-cadherin-beta-catenin. Nat Struct Mol Biol *18*, 665-672. 10.1038/nsmb.2049.
Montcouquiol, M., Sans, N., Huss, D., Kach, J., Dickman, J.D., Forge, A., Rachel, R.A., Copeland, N.G., Jenkins, N.A., Bogani, D., et al. (2006). Asymmetric localization of Vangl2 and

Fz3 indicate novel mechanisms for planar cell polarity in mammals. J Neurosci *26*, 5265-5275. 10.1523/JNEUROSCI.4680-05.2006.

Morais-de-Sa, E., Mirouse, V., and St Johnston, D. (2010). aPKC phosphorylation of Bazooka defines the apical/lateral border in Drosophila epithelial cells. Cell *141*, 509-523. 10.1016/j.cell.2010.02.040.

Mottola, G., Classen, A.K., Gonzalez-Gaitan, M., Eaton, S., and Zerial, M. (2010). A novel function for the Rab5 effector Rabenosyn-5 in planar cell polarity. Development *137*, 2353-2364. 10.1242/dev.048413.

Murdoch, J.N., Doudney, K., Paternotte, C., Copp, A.J., and Stanier, P. (2001). Severe neural tube defects in the loop-tail mouse result from mutation of Lpp1, a novel gene involved in floor plate specification. Hum Mol Genet *10*, 2593-2601. DOI 10.1093/hmg/10.22.2593.

Nagaoka, T., Furuse, M., Ohtsuka, T., Tsuchida, K., and Kishi, M. (2019). Vangl2 interaction plays a role in the proteasomal degradation of Prickle2. Sci Rep *9*, 2912. 10.1038/s41598-019-39642-z.

Nelson, W.J. (2003). Adaptation of core mechanisms to generate cell polarity. Nature *422*, 766-774. 10.1038/nature01602.

Ni, J.Q., Zhou, R., Czech, B., Liu, L.P., Holderbaum, L., Yang-Zhou, D., Shim, H.S., Tao, R., Handler, D., Karpowicz, P., et al. (2011). A genome-scale shRNA resource for transgenic RNAi in Drosophila. Nat Methods *8*, 405-407. 10.1038/nmeth.1592.

O'Keefe, D.D., Gonzalez-Nino, E., Burnett, M., Dylla, L., Lambeth, S.M., Licon, E., Amesoli, C., Edgar, B.A., and Curtiss, J. (2009). Rap1 maintains adhesion between cells to affect Egfr signaling and planar cell polarity in Drosophila. Dev Biol *333*, 143-160. 10.1016/j.ydbio.2009.06.032.

Oda, H., Uemura, T., Harada, Y., Iwai, Y., and Takeichi, M. (1994). A Drosophila homolog of cadherin associated with armadillo and essential for embryonic cell-cell adhesion. Dev Biol *165*, 716-726. 10.1006/dbio.1994.1287.

Ossipova, O., Dhawan, S., Sokol, S., and Green, J.B. (2005). Distinct PAR-1 proteins function in different branches of Wnt signaling during vertebrate development. Dev Cell *8*, 829-841. 10.1016/j.devcel.2005.04.011.

Osswald, M., Barros-Carvalho, A., Carmo, A.M., Loyer, N., Gracio, P.C., Sunkel, C.E., Homem, C.C.F., Januschke, J., and Morais-de-Sa, E. (2022). aPKC regulates apical constriction to prevent tissue rupture in the Drosophila follicular epithelium. Curr Biol *32*, 4411-4427 e4418. 10.1016/j.cub.2022.08.063.

Pan, G., Feng, Y., Ambegaonkar, A.A., Sun, G., Huff, M., Rauskolb, C., and Irvine, K.D. (2013). Signal transduction by the Fat cytoplasmic domain. Development *140*, 831-842. 10.1242/dev.088534.

Pannekoek, W.J., de Rooij, J., and Gloerich, M. (2019). Force transduction by cadherin adhesions in morphogenesis. F1000Res *8*. 10.12688/f1000research.18779.1.

Paricio, N., Feiguin, F., Boutros, M., Eaton, S., and Mlodzik, M. (1999). The Drosophila STE20-like kinase misshapen is required downstream of the Frizzled receptor in planar polarity signaling. EMBO J *18*, 4669-4678. 10.1093/emboj/18.17.4669.

Park, W.J., Liu, J., Sharp, E.J., and Adler, P.N. (1996). The Drosophila tissue polarity gene inturned acts cell autonomously and encodes a novel protein. Development *122*, 961-969. 10.1242/dev.122.3.961.

Penton, A., Wodarz, A., and Nusse, R. (2002). A mutational analysis of dishevelled in Drosophila defines novel domains in the dishevelled protein as well as novel suppressing alleles of axin. Genetics *161*, 747-762. 10.1093/genetics/161.2.747.

Perkins, L.A., Holderbaum, L., Tao, R., Hu, Y., Sopko, R., McCall, K., Yang-Zhou, D., Flockhart, I., Binari, R., Shim, H.S., et al. (2015). The Transgenic RNAi Project at Harvard Medical School: Resources and Validation. Genetics *201*, 843-852. 10.1534/genetics.115.180208.

Perrimon, N., and Mahowald, A.P. (1987). Multiple functions of segment polarity genes in Drosophila. Dev Biol *119*, 587-600. 10.1016/0012-1606(87)90061-3.

Peters, J.M., McKay, R.M., McKay, J.P., and Graff, J.M. (1999). Casein kinase I transduces Wnt signals. Nature *401*, 345-350. 10.1038/43830.

Pielage, J., Stork, T., Bunse, I., and Klambt, C. (2003). The Drosophila cell survival gene discs lost encodes a cytoplasmic Codanin-1-like protein, not a homolog of tight junction PDZ protein Patj. Dev Cell *5*, 841-851. 10.1016/s1534-5807(03)00358-7.

Pieters, T., van Roy, F., and van Hengel, J. (2012). Functions of p120ctn isoforms in cell-cell adhesion and intracellular signaling. Front Biosci (Landmark Ed) *17*, 1669-1694. 10.2741/4012.

Povelones, M., Howes, R., Fish, M., and Nusse, R. (2005). Genetic evidence that Drosophila frizzled controls planar cell polarity and Armadillo signaling by a common mechanism. Genetics *171*, 1643-1654. 10.1534/genetics.105.045245.

Price, M.A., and Kalderon, D. (2002). Proteolysis of the Hedgehog signaling effector Cubitus interruptus requires phosphorylation by Glycogen Synthase Kinase 3 and Casein Kinase 1. Cell *108*, 823-835. 10.1016/s0092-8674(02)00664-5.

Rauzi, M., Lenne, P.F., and Lecuit, T. (2010). Planar polarized actomyosin contractile flows control epithelial junction remodelling. Nature *468*, 1110-1114. 10.1038/nature09566.

Rawls, A.S., and Wolff, T. (2003). Strabismus requires Flamingo and Prickle function to regulate tissue polarity in the Drosophila eye. Development *130*, 1877-1887. 10.1242/dev.00411.

Ray, R.P., Matamoro-Vidal, A., Ribeiro, P.S., Tapon, N., Houle, D., Salazar-Ciudad, I., and Thompson, B.J. (2015). Patterned Anchorage to the Apical Extracellular Matrix Defines Tissue Shape in the Developing Appendages of Drosophila. Dev Cell *34*, 310-322. 10.1016/j.devcel.2015.06.019.

Rena, G., Bain, J., Elliott, M., and Cohen, P. (2004). D4476, a cell-permeant inhibitor of CK1, suppresses the site-specific phosphorylation and nuclear exclusion of FOXO1a. EMBO Rep *5*, 60-65. 10.1038/sj.embor.7400048.

Ressurreicao, M., Warrington, S., and Strutt, D. (2018). Rapid Disruption of Dishevelled Activity Uncovers an Intercellular Role in Maintenance of Prickle in Core Planar Polarity Protein Complexes. Cell Rep *25*, 1415-1424 e1416. 10.1016/j.celrep.2018.10.039.

Rimm, D.L., Koslov, E.R., Kebriaei, P., Cianci, C.D., and Morrow, J.S. (1995). Alpha 1(E)-catenin is an actin-binding and -bundling protein mediating the attachment of F-actin to the membrane adhesion complex. Proc Natl Acad Sci U S A *92*, 8813-8817. 10.1073/pnas.92.19.8813.

Rogers, S., and Scholpp, S. (2022). Vertebrate Wnt5a - At the crossroads of cellular signalling. Semin Cell Dev Biol *125*, 3-10. 10.1016/j.semcdb.2021.10.002.

Rolls, M.M., Albertson, R., Shih, H.P., Lee, C.Y., and Doe, C.Q. (2003). Drosophila aPKC regulates cell polarity and cell proliferation in neuroblasts and epithelia. J Cell Biol *163*, 1089-1098. 10.1083/jcb.200306079.

Roper, K. (2012). Anisotropy of Crumbs and aPKC drives myosin cable assembly during tube formation. Dev Cell *23*, 939-953. 10.1016/j.devcel.2012.09.013.
Saerens, D., Pellis, M., Loris, R., Pardon, E., Dumoulin, M., Matagne, A., Wyns, L., Muyldermans, S., and Conrath, K. (2005). Identification of a universal VHH framework to graft non-canonical antigen-binding loops of camel single-domain antibodies. J Mol Biol *352*, 597-607. 10.1016/j.jmb.2005.07.038.
Sagner, A., Merkel, M., Aigouy, B., Gaebel, J., Brankatschk, M., Julicher, F., and Eaton, S. (2012). Establishment of global patterns of planar polarity during growth of the Drosophila wing epithelium. Curr Biol *22*, 1296-1301. 10.1016/j.cub.2012.04.066.
Sakanaka, C., Leong, P., Xu, L., Harrison, S.D., and Williams, L.T. (1999). Casein kinase iepsilon in the wnt pathway: regulation of beta-catenin function. Proc Natl Acad Sci U S A *96*, 12548-12552. 10.1073/pnas.96.22.12548.
Sarov, M., Barz, C., Jambor, H., Hein, M.Y., Schmied, C., Suchold, D., Stender, B., Janosch, S., K, J.V., Krishnan, R.T., et al. (2016). A genome-wide resource for the analysis of protein localisation in Drosophila. Elife *5*, e12068. 10.7554/eLife.12068.
Sawyer, J.K., Choi, W., Jung, K.C., He, L., Harris, N.J., and Peifer, M. (2011). A contractile actomyosin network linked to adherens junctions by Canoe/afadin helps drive convergent extension. Mol Biol Cell *22*, 2491-2508. 10.1091/mbc.E11-05-0411.
Schamberg, S., Houston, P., Monk, N.A., and Owen, M.R. (2010). Modelling and analysis of planar cell polarity. Bull Math Biol *72*, 645-680. 10.1007/s11538-009-9464-0.
Schwarz-Romond, T., Fiedler, M., Shibata, N., Butler, P.J.G., Kikuchi, A., Higuchi, Y., and Bienz, M. (2007). The DIX domain of Dishevelled confers Wnt signaling by dynamic polymerization. Nat Struct Mol Biol *14*, 484-492. 10.1038/nsmb1247.
Segalen, M., Johnston, C.A., Martin, C.A., Dumortier, J.G., Prehoda, K.E., David, N.B., Doe, C.Q., and Bellaiche, Y. (2010). The Fz-Dsh planar cell polarity pathway induces oriented cell division via Mud/NuMA in Drosophila and zebrafish. Dev Cell *19*, 740-752. 10.1016/j.devcel.2010.10.004.
Seifert, J.R., and Mlodzik, M. (2007). Frizzled/PCP signalling: a conserved mechanism regulating cell polarity and directed motility. Nat Rev Genet *8*, 126-138. 10.1038/nrg2042.
Shapiro, L., and Weis, W.I. (2009). Structure and biochemistry of cadherins and catenins. Cold Spring Harb Perspect Biol *1*, a003053. 10.1101/cshperspect.a003053.
Shen, S.P., Aleksic, J., and Russell, S. (2013). Identifying targets of the Sox domain protein Dichaete in the Drosophila CNS via targeted expression of dominant negative proteins. BMC Dev Biol *13*, 1. 10.1186/1471-213X-13-1.
Shimada, Y., Usui, T., Yanagawa, S., Takeichi, M., and Uemura, T. (2001). Asymmetric colocalization of Flamingo, a seven-pass transmembrane cadherin, and Dishevelled in planar cell polarization. Curr Biol *11*, 859-863. 10.1016/s0960-9822(01)00233-0.
Shulman, J.M., Benton, R., and St Johnston, D. (2000). The Drosophila homolog of C. elegans PAR-1 organizes the oocyte cytoskeleton and directs oskar mRNA localization to the posterior pole. Cell *101*, 377-388. 10.1016/s0092-8674(00)80848-x.
Silva, E., Tsatskis, Y., Gardano, L., Tapon, N., and McNeill, H. (2006). The tumor-suppressor gene fat controls tissue growth upstream of expanded in the hippo signaling pathway. Curr Biol *16*, 2081-2089. 10.1016/j.cub.2006.09.004.
Silver, J.T., Wirtz-Peitz, F., Simoes, S., Pellikka, M., Yan, D., Binari, R., Nishimura, T., Li, Y.,

Harris, T.J.C., Perrimon, N., and Tepass, U. (2019). Apical polarity proteins recruit the RhoGEF Cysts to promote junctional myosin assembly. J Cell Biol *218*, 3397-3414. 10.1083/jcb.201807106.

Simoes Sde, M., Blankenship, J.T., Weitz, O., Farrell, D.L., Tamada, M., Fernandez-Gonzalez, R., and Zallen, J.A. (2010). Rho-kinase directs Bazooka/Par-3 planar polarity during Drosophila axis elongation. Dev Cell *19*, 377-388. 10.1016/j.devcel.2010.08.011.

Simon, M.A. (2004). Planar cell polarity in the Drosophila eye is directed by graded Four-jointed and Dachsous expression. Development *131*, 6175-6184. 10.1242/dev.01550.

Simon, M.A., Xu, A., Ishikawa, H.O., and Irvine, K.D. (2010). Modulation of fat:dachsous binding by the cadherin domain kinase four-jointed. Curr Biol *20*, 811-817. 10.1016/j.cub.2010.04.016.

Simons, M., Gault, W.J., Gotthardt, D., Rohatgi, R., Klein, T.J., Shao, Y., Lee, H.J., Wu, A.L., Fang, Y., Satlin, L.M., et al. (2009). Electrochemical cues regulate assembly of the Frizzled/Dishevelled complex at the plasma membrane during planar epithelial polarization. Nat Cell Biol *11*, 286-294. 10.1038/ncb1836.

Singh, J., Yanfeng, W.A., Grumolato, L., Aaronson, S.A., and Mlodzik, M. (2010). Abelson family kinases regulate Frizzled planar cell polarity signaling via Dsh phosphorylation. Genes Dev *24*, 2157-2168. 10.1101/gad.1961010.

Skoglund, P., Rolo, A., Chen, X., Gumbiner, B.M., and Keller, R. (2008). Convergence and extension at gastrulation require a myosin IIB-dependent cortical actin network. Development *135*, 2435-2444. 10.1242/dev.014704.

Smith, J.A., and Liebl, E.C. (2005). Identification of the molecular lesions in alleles of the Drosophila Abelson tyrosine kinase. Drosophila Information Service *88*, 20-22.

Song, H., Hu, J., Chen, W., Elliott, G., Andre, P., Gao, B., and Yang, Y. (2010). Planar cell polarity breaks bilateral symmetry by controlling ciliary positioning. Nature *466*, 378-382. 10.1038/nature09129.

Sopko, R., Silva, E., Clayton, L., Gardano, L., Barrios-Rodiles, M., Wrana, J., Varelas, X., Arbouzova, N.I., Shaw, S., Saburi, S., et al. (2009). Phosphorylation of the tumor suppressor fat is regulated by its ligand Dachsous and the kinase discs overgrown. Curr Biol *19*, 1112-1117. 10.1016/j.cub.2009.05.049.

Sotillos, S., Diaz-Meco, M.T., Caminero, E., Moscat, J., and Campuzano, S. (2004). DaPKC-dependent phosphorylation of Crumbs is required for epithelial cell polarity in Drosophila. J Cell Biol *166*, 549-557. 10.1083/jcb.200311031.

Struhl, G., Casal, J., and Lawrence, P.A. (2012). Dissecting the molecular bridges that mediate the function of Frizzled in planar cell polarity. Development *139*, 3665-3674. 10.1242/dev.083550.

Strutt, D., Madder, D., Chaudhary, V., and Artymiuk, P.J. (2012). Structure-function dissection of the frizzled receptor in Drosophila melanogaster suggests different mechanisms of action in planar polarity and canonical Wnt signaling. Genetics *192*, 1295-1313. 10.1534/genetics.112.144592.

Strutt, D., and Strutt, H. (2007). Differential activities of the core planar polarity proteins during Drosophila wing patterning. Dev Biol *302*, 181-194. 10.1016/j.ydbio.2006.09.026.

Strutt, D., and Warrington, S.J. (2008). Planar polarity genes in the Drosophila wing regulate the localisation of the FH3-domain protein Multiple Wing Hairs to control the site of hair production. Development *135*, 3103-3111. 10.1242/dev.025205.

Strutt, D.I. (2001). Asymmetric localization of frizzled and the establishment of cell polarity in the Drosophila wing. Mol Cell *7*, 367-375. 10.1016/s1097-2765(01)00184-8.
Strutt, H., Gamage, J., and Strutt, D. (2016). Robust Asymmetric Localization of Planar Polarity Proteins Is Associated with Organization into Signalosome-like Domains of Variable Stoichiometry. Cell Rep *17*, 2660-2671. 10.1016/j.celrep.2016.11.021.
Strutt, H., Gamage, J., and Strutt, D. (2019a). Reciprocal action of Casein Kinase Iepsilon on core planar polarity proteins regulates clustering and asymmetric localisation. Elife *8*. 10.7554/eLife.45107.
Strutt, H., Langton, P.F., Pearson, N., McMillan, K.J., Strutt, D., and Cullen, P.J. (2019b). Retromer Controls Planar Polarity Protein Levels and Asymmetric Localization at Intercellular Junctions. Curr Biol *29*, 484-491 e486. 10.1016/j.cub.2018.12.027.
Strutt, H., Mundy, J., Hofstra, K., and Strutt, D. (2004). Cleavage and secretion is not required for Four-jointed function in Drosophila patterning. Development *131*, 881-890. 10.1242/dev.00996.
Strutt, H., Price, M.A., and Strutt, D. (2006). Planar polarity is positively regulated by casein kinase Iepsilon in Drosophila. Curr Biol *16*, 1329-1336. 10.1016/j.cub.2006.04.041.
Strutt, H., Searle, E., Thomas-Macarthur, V., Brookfield, R., and Strutt, D. (2013a). A Cul-3-BTB ubiquitylation pathway regulates junctional levels and asymmetry of core planar polarity proteins. Development *140*, 1693-1702. 10.1242/dev.089656.
Strutt, H., and Strutt, D. (2002). Nonautonomous planar polarity patterning in Drosophila: dishevelled-independent functions of frizzled. Dev Cell *3*, 851-863. 10.1016/s1534-5807(02)00363-5.
Strutt, H., and Strutt, D. (2003). EGF signaling and ommatidial rotation in the Drosophila eye. Curr Biol *13*, 1451-1457. 10.1016/s0960-9822(03)00545-1.
Strutt, H., and Strutt, D. (2008). Differential stability of flamingo protein complexes underlies the establishment of planar polarity. Curr Biol *18*, 1555-1564. 10.1016/j.cub.2008.08.063.
Strutt, H., and Strutt, D. (2020). DAnkrd49 and Bdbt act via Casein kinase Iepsilon to regulate planar polarity in Drosophila. Plos Genet *16*, e1008820. 10.1371/journal.pgen.1008820.
Strutt, H., and Strutt, D. (2021). How do the Fat-Dachsous and core planar polarity pathways act together and independently to coordinate polarized cell behaviours? Open Biol *11*, 200356. 10.1098/rsob.200356.
Strutt, H., Thomas-MacArthur, V., and Strutt, D. (2013b). Strabismus promotes recruitment and degradation of farnesylated prickle in Drosophila melanogaster planar polarity specification. Plos Genet *9*, e1003654. 10.1371/journal.pgen.1003654.
Strutt, H., Warrington, S.J., and Strutt, D. (2011). Dynamics of core planar polarity protein turnover and stable assembly into discrete membrane subdomains. Dev Cell *20*, 511-525. 10.1016/j.devcel.2011.03.018.
Su, Y., Ospina, J.K., Zhang, J., Michelson, A.P., Schoen, A.M., and Zhu, A.J. (2011). Sequential phosphorylation of smoothened transduces graded hedgehog signaling. Sci Signal *4*, ra43. 10.1126/scisignal.2001747.
Sugimura, K., and Ishihara, S. (2013). The mechanical anisotropy in a tissue promotes ordering in hexagonal cell packing. Development *140*, 4091-4101. 10.1242/dev.094060.
Sun, T.Q., Lu, B., Feng, J.J., Reinhard, C., Jan, Y.N., Fantl, W.J., and Williams, L.T. (2001). PAR-1 is a Dishevelled-associated kinase and a positive regulator of Wnt signalling. Nat Cell

Biol *3*, 628-636. 10.1038/35083016.
Suzuki, A., and Ohno, S. (2006). The PAR-aPKC system: lessons in polarity. J Cell Sci *119*, 979-987. 10.1242/jcs.02898.
Tada, M., Concha, M.L., and Heisenberg, C.P. (2002). Non-canonical Wnt signalling and regulation of gastrulation movements. Semin Cell Dev Biol *13*, 251-260. 10.1016/s1084-9521(02)00052-6.
Tada, M., and Smith, J.C. (2000). Xwnt11 is a target of Xenopus Brachyury: regulation of gastrulation movements via Dishevelled, but not through the canonical Wnt pathway. Development *127*, 2227-2238. 10.1242/dev.127.10.2227.
Tan, S.E., Tan, W., Fisher, K.H., and Strutt, D. (2021). QuantifyPolarity, a new tool-kit for measuring planar polarized protein distributions and cell properties in developing tissues. Development *148*. 10.1242/dev.198952.
Tanentzapf, G., and Tepass, U. (2003). Interactions between the crumbs, lethal giant larvae and bazooka pathways in epithelial polarization. Nature Cell Biology *5*, 46-52. 10.1038/ncb896.
Tauriello, D.V., Jordens, I., Kirchner, K., Slootstra, J.W., Kruitwagen, T., Bouwman, B.A., Noutsou, M., Rudiger, S.G., Schwamborn, K., Schambony, A., and Maurice, M.M. (2012). Wnt/beta-catenin signaling requires interaction of the Dishevelled DEP domain and C terminus with a discontinuous motif in Frizzled. Proc Natl Acad Sci U S A *109*, E812-820. 10.1073/pnas.1114802109.
Taylor, J., Abramova, N., Charlton, J., and Adler, P.N. (1998). Van Gogh: a new Drosophila tissue polarity gene. Genetics *150*, 199-210. 10.1093/genetics/150.1.199.
Tepass, U. (1996). Crumbs, a component of the apical membrane, is required for zonula adherens formation in primary epithelia of Drosophila. Dev Biol *177*, 217-225. 10.1006/dbio.1996.0157.
Tepass, U. (2012). The apical polarity protein network in Drosophila epithelial cells: regulation of polarity, junctions, morphogenesis, cell growth, and survival. Annu Rev Cell Dev Biol *28*, 655-685. 10.1146/annurev-cellbio-092910-154033.
Tepass, U., and Knust, E. (1993). Crumbs and stardust act in a genetic pathway that controls the organization of epithelia in Drosophila melanogaster. Dev Biol *159*, 311-326. 10.1006/dbio.1993.1243.
Thomas, C., and Strutt, D. (2012). The roles of the cadherins Fat and Dachsous in planar polarity specification in Drosophila. Dev Dyn *241*, 27-39. 10.1002/dvdy.22736.
Togel, M., Pass, G., and Paululat, A. (2008). The Drosophila wing hearts originate from pericardial cells and are essential for wing maturation. Dev Biol *318*, 29-37. 10.1016/j.ydbio.2008.02.043.
Tomancak, P., Piano, F., Riechmann, V., Gunsalus, K.C., Kemphues, K.J., and Ephrussi, A. (2000). A Drosophila melanogaster homologue of Caenorhabditis elegans par-1 acts at an early step in embryonic-axis formation. Nat Cell Biol *2*, 458-460. 10.1038/35017101.
Tree, D.R., Shulman, J.M., Rousset, R., Scott, M.P., Gubb, D., and Axelrod, J.D. (2002). Prickle mediates feedback amplification to generate asymmetric planar cell polarity signaling. Cell *109*, 371-381. 10.1016/s0092-8674(02)00715-8.
Tyler, D.M., and Baker, N.E. (2007). Expanded and fat regulate growth and differentiation in the Drosophila eye through multiple signaling pathways. Dev Biol *305*, 187-201. 10.1016/j.ydbio.2007.02.004.

Umbhauer, M., Djiane, A., Goisset, C., Penzo-Mendez, A., Riou, J.F., Boucaut, J.C., and Shi, D.L. (2000). The C-terminal cytoplasmic Lys-thr-X-X-X-Trp motif in frizzled receptors mediates Wnt/beta-catenin signalling. EMBO J *19*, 4944-4954. 10.1093/emboj/19.18.4944.

Usui, T., Shima, Y., Shimada, Y., Hirano, S., Burgess, R.W., Schwarz, T.L., Takeichi, M., and Uemura, T. (1999). Flamingo, a seven-pass transmembrane cadherin, regulates planar cell polarity under the control of Frizzled. Cell *98*, 585-595. 10.1016/s0092-8674(00)80046-x.

van der Linden, R.H., Frenken, L.G., de Geus, B., Harmsen, M.M., Ruuls, R.C., Stok, W., de Ron, L., Wilson, S., Davis, P., and Verrips, C.T. (1999). Comparison of physical chemical properties of llama VHH antibody fragments and mouse monoclonal antibodies. Biochim Biophys Acta *1431*, 37-46. 10.1016/s0167-4838(99)00030-8.

Veeman, M.T., Slusarski, D.C., Kaykas, A., Louie, S.H., and Moon, R.T. (2003). Zebrafish prickle, a modulator of noncanonical Wnt/Fz signaling, regulates gastrulation movements. Curr Biol *13*, 680-685. 10.1016/s0960-9822(03)00240-9.

Velazquez, J.M., Sonoda, S., Bugaisky, G., and Lindquist, S. (1983). Is the major Drosophila heat shock protein present in cells that have not been heat shocked? J Cell Biol *96*, 286-290. 10.1083/jcb.96.1.286.

Venken, K.J., Carlson, J.W., Schulze, K.L., Pan, H., He, Y., Spokony, R., Wan, K.H., Koriabine, M., de Jong, P.J., White, K.P., et al. (2009). Versatile P[acman] BAC libraries for transgenesis studies in Drosophila melanogaster. Nat Methods *6*, 431-434. 10.1038/nmeth.1331.

Ventura, G., Moreira, S., Barros-Carvalho, A., Osswald, M., and Morais-de-Sa, E. (2020). Lgl cortical dynamics are independent of binding to the Scrib-Dlg complex but require Dlg-dependent restriction of aPKC. Development *147*. 10.1242/dev.186593.

Verheyen, E.M., Mirkovic, I., MacLean, S.J., Langmann, C., Andrews, B.C., and MacKinnon, C. (2001). The tissue polarity gene nemo carries out multiple roles in patterning during Drosophila development. Mech Dev *101*, 119-132. 10.1016/s0925-4773(00)00574-8.

Villano, J.L., and Katz, F.N. (1995). four-jointed is required for intermediate growth in the proximal-distal axis in Drosophila. Development *121*, 2767-2777. 10.1242/dev.121.9.2767.

Vinson, C.R., and Adler, P.N. (1987). Directional non-cell autonomy and the transmission of polarity information by the frizzled gene of Drosophila. Nature *329*, 549-551. 10.1038/329549a0.

Waddington, C.H. (1939). Preliminary Notes on the Development of the Wings in Normal and Mutant Strains of Drosophila. Proc Natl Acad Sci U S A *25*, 299-307. 10.1073/pnas.25.7.299.

Wallingford, J.B., and Habas, R. (2005). The developmental biology of Dishevelled: an enilgmatic protein governing cell fate and cell polarity. Development *132*, 4421-4436. 10.1242/dev.02068.

Wallingford, J.B., Rowning, B.A., Vogeli, K.M., Rothbacher, U., Fraser, S.E., and Harland, R.M. (2000). Dishevelled controls cell polarity during Xenopus gastrulation. Nature *405*, 81-85. 10.1038/35011077.

Walther, R.F., and Pichaud, F. (2010). Crumbs/DaPKC-dependent apical exclusion of Bazooka promotes photoreceptor polarity remodeling. Curr Biol *20*, 1065-1074. 10.1016/j.cub.2010.04.049.

Walton, K.M., Fisher, K., Rubitski, D., Marconi, M., Meng, Q.J., Sladek, M., Adams, J., Bass, M., Chandrasekaran, R., Butler, T., et al. (2009). Selective inhibition of casein kinase 1 epsilon minimally alters circadian clock period. J Pharmacol Exp Ther *330*, 430-439. 10.1124/jpet.109.151415.

Wang, J., Hamblet, N.S., Mark, S., Dickinson, M.E., Brinkman, B.C., Segil, N., Fraser, S.E., Chen, P., Wallingford, J.B., and Wynshaw-Boris, A. (2006a). Dishevelled genes mediate a conserved mammalian PCP pathway to regulate convergent extension during neurulation. Development *133*, 1767-1778. 10.1242/dev.02347.

Wang, J., Mark, S., Zhang, X., Qian, D., Yoo, S.J., Radde-Gallwitz, K., Zhang, Y., Lin, X., Collazo, A., Wynshaw-Boris, A., and Chen, P. (2005). Regulation of polarized extension and planar cell polarity in the cochlea by the vertebrate PCP pathway. Nat Genet *37*, 980-985. 10.1038/ng1622.

Wang, Y., Badea, T., and Nathans, J. (2006b). Order from disorder: Self-organization in mammalian hair patterning. Proc Natl Acad Sci U S A *103*, 19800-19805. 10.1073/pnas.0609712104.

Wang, Y., Guo, N., and Nathans, J. (2006c). The role of Frizzled3 and Frizzled6 in neural tube closure and in the planar polarity of inner-ear sensory hair cells. J Neurosci *26*, 2147-2156. 10.1523/JNEUROSCI.4698-05.2005.

Warrington, S.J., Strutt, H., Fisher, K.H., and Strutt, D. (2017). A Dual Function for Prickle in Regulating Frizzled Stability during Feedback-Dependent Amplification of Planar Polarity. Curr Biol *27*, 2784-2797 e2783. 10.1016/j.cub.2017.08.016.

Warrington, S.J., Strutt, H., and Strutt, D. (2022). Use of Fluorescence Recovery After Photobleaching (FRAP) to Measure In Vivo Dynamics of Cell Junction-Associated Polarity Proteins. Methods Mol Biol *2438*, 1-30. 10.1007/978-1-0716-2035-9_1.

Wasserscheid, I., Thomas, U., and Knust, E. (2007). Isoform-specific interaction of Flamingo/Starry Night with excess Bazooka affects planar cell polarity in the Drosophila wing. Dev Dyn *236*, 1064-1071. 10.1002/dvdy.21089.

Weber, U., Pataki, C., Mihaly, J., and Mlodzik, M. (2008). Combinatorial signaling by the Frizzled/PCP and Egfr pathways during planar cell polarity establishment in the Drosophila eye. Dev Biol *316*, 110-123. 10.1016/j.ydbio.2008.01.016.

Westfall, T.A., Brimeyer, R., Twedt, J., Gladon, J., Olberding, A., Furutani-Seiki, M., and Slusarski, D.C. (2003). Wnt-5/pipetail functions in vertebrate axis formation as a negative regulator of Wnt/beta-catenin activity. J Cell Biol *162*, 889-898. 10.1083/jcb.200303107.

Willecke, M., Hamaratoglu, F., Kango-Singh, M., Udan, R., Chen, C.L., Tao, C., Zhang, X., and Halder, G. (2006). The fat cadherin acts through the hippo tumor-suppressor pathway to regulate tissue size. Curr Biol *16*, 2090-2100. 10.1016/j.cub.2006.09.005.

Wodarz, A., Ramrath, A., Grimm, A., and Knust, E. (2000). Drosophila atypical protein kinase C associates with Bazooka and controls polarity of epithelia and neuroblasts. J Cell Biol *150*, 1361-1374. 10.1083/jcb.150.6.1361.

Wolff, T., and Rubin, G.M. (1998). Strabismus, a novel gene that regulates tissue polarity and cell fate decisions in Drosophila. Development *125*, 1149-1159. 10.1242/dev.125.6.1149.

Wong, H.C., Bourdelas, A., Krauss, A., Lee, H.J., Shao, Y., Wu, D., Mlodzik, M., Shi, D.L., and Zheng, J. (2003). Direct binding of the PDZ domain of Dishevelled to a conserved internal sequence in the C-terminal region of Frizzled. Mol Cell *12*, 1251-1260. 10.1016/s1097-2765(03)00427-1.

Wong, L.L., and Adler, P.N. (1993). Tissue polarity genes of Drosophila regulate the subcellular location for prehair initiation in pupal wing cells. J Cell Biol *123*, 209-221. 10.1083/jcb.123.1.209.

Wu, J., Jenny, A., Mirkovic, L., and Mlodzik, M. (2008). Frizzled-Dishevelled signaling specificity

outcome can be modulated by Diego in Drosophila. Mech Develop *125*, 30-42. 10.1016/j.mod.2007.10.006.

Wu, J., Klein, T.J., and Mlodzik, M. (2004). Subcellular localization of frizzled receptors, mediated by their cytoplasmic tails, regulates signaling pathway specificity. PLoS Biol *2*, E158. 10.1371/journal.pbio.0020158.

Wu, J., and Mlodzik, M. (2008). The frizzled extracellular domain is a ligand for Van Gogh/Stbm during nonautonomous planar cell polarity signaling. Developmental Cell *15*, 462-469. 10.1016/j.devcel.2008.08.004.

Xu, T., and Rubin, G.M. (1993). Analysis of genetic mosaics in developing and adult Drosophila tissues. Development *117*, 1223-1237. 10.1242/dev.117.4.1223.

Yanfeng, W.A., Berhane, H., Mola, M., Singh, J., Jenny, A., and Mlodzik, M. (2011). Functional dissection of phosphorylation of Disheveled in Drosophila. Dev Biol *360*, 132-142. 10.1016/j.ydbio.2011.09.017.

Yang, W., Garrett, L., Feng, D., Elliott, G., Liu, X., Wang, N., Wong, Y.M., Choi, N.T., Yang, Y., and Gao, B. (2017). Wnt-induced Vangl2 phosphorylation is dose-dependently required for planar cell polarity in mammalian development. Cell Res *27*, 1466-1484. 10.1038/cr.2017.127.

Yates, L.L., Papakrivopoulou, J., Long, D.A., Goggolidou, P., Connolly, J.O., Woolf, A.S., and Dean, C.H. (2010a). The planar cell polarity gene Vangl2 is required for mammalian kidney-branching morphogenesis and glomerular maturation. Hum Mol Genet *19*, 4663-4676. 10.1093/hmg/ddq397.

Yates, L.L., Schnatwinkel, C., Murdoch, J.N., Bogani, D., Formstone, C.J., Townsend, S., Greenfield, A., Niswander, L.A., and Dean, C.H. (2010b). The PCP genes Celsr1 and Vangl2 are required for normal lung branching morphogenesis. Hum Mol Genet *19*, 2251-2267. 10.1093/hmg/ddq104.

Yin, C., Kiskowski, M., Pouille, P.A., Farge, E., and Solnica-Krezel, L. (2008). Cooperation of polarized cell intercalations drives convergence and extension of presomitic mesoderm during zebrafish gastrulation. J Cell Biol *180*, 221-232. 10.1083/jcb.200704150.

Yonemura, S., Wada, Y., Watanabe, T., Nagafuchi, A., and Shibata, M. (2010). alpha-Catenin as a tension transducer that induces adherens junction development. Nat Cell Biol *12*, 533-542. 10.1038/ncb2055.

Yu, J.J.S., Maugarny-Cales, A., Pelletier, S., Alexandre, C., Bellaiche, Y., Vincent, J.P., and McGough, I.J. (2020). Frizzled-Dependent Planar Cell Polarity without Secreted Wnt Ligands. Dev Cell *54*, 583-592 e585. 10.1016/j.devcel.2020.08.004.

Zallen, J.A. (2007). Planar polarity and tissue morphogenesis. Cell *129*, 1051-1063. 10.1016/j.cell.2007.05.050.

Zhang, K., Yao, E., Lin, C., Chou, Y.T., Wong, J., Li, J., Wolters, P.J., and Chuang, P.T. (2020). A mammalian Wnt5a-Ror2-Vangl2 axis controls the cytoskeleton and confers cellular properties required for alveologenesis. Elife *9*. 10.7554/eLife.53688.

Zhang, L., Jia, J., Wang, B., Amanai, K., Wharton, K.A., Jr., and Jiang, J. (2006). Regulation of wingless signaling by the CKI family in Drosophila limb development. Dev Biol *299*, 221-237. 10.1016/j.ydbio.2006.07.025.

Zhou, W.K., and Hong, Y. (2012). Drosophila Patj plays a supporting role in apical-basal polarity but is essential for viability. Development *139*, 2891-2896. 10.1242/dev.083162.